Nonlinear Analysis of Reinforced Concrete Frames and Panels

By

Herbert Alexander Franklin

B.Eng. (University of New Zealand) 1957
M.A.Sc. (University of British Columbia) 1962

DISSERTATION

Submitted in partial satisfaction of the requirements for the degree of

DOCTOR OF PHILOSOPHY

in

Engineering

in the

GRADUATE DIVISION

of the

UNIVERSITY OF CALIFORNIA, BERKELEY

Approved:

A. C. Scordelis

E. L. Wilson

Frank E. Hauser

Committee in Charge

Degree conferred....DEGREE CONFERRED JUNE 10, 1970
Date

TABLE OF CONTENTS

LIST OF TABLES

LIST OF FIGURES

LIST OF SYMBOLS

A	cross-section of rod elements; plan area of quadrilateral elements.
[a]	transformation matrix of direction cosines; displacement transformation array.
[b]	displacement transformation array.
[C]	matrix of material constitutive coefficients for plane stress elements.
C	used for cos θ.
D	greatest difference between node numbers of an element.
d	depth of a frame element.
$\{dr_i\}$	vector of changes in global node displacements after iteration i.
d.o.f.	abbreviation for degrees of freedom.
E_i	Young's Modulus for material in direction i.
$\pm$ e	eccentricity of centroidal axis from reference axis for frame elements.
$\{e_i\}$	vector of strains at point i.
$\{e_p\}$	vector of principal strains.
F_i	element node forces in element coordinates.
F_s	shear strength of tielinks (force units).
F_t	tensile strength of tielinks (force units).
$\pm$ f	material stresses
f'_c	6" X 12" cylinder strength of concrete.
f'_r	modulus of rupture of concrete.
f'_s	shear strength of materials.
f'_t	tensile strength of concrete.
G_{ij}	shear modulus in coordinates i-j.

I	unit matrix with 1's on the diagonal; moment of inertia of flexural member transformed cross-section.
$[K_{xy}]$	global stiffness array referred to global Cartesian coordinates x-y.
K^*	true global stiffness after iteration i.
$[k_{mn}]$	element stiffness array referred to coordinates m-n.
k_h	horizontal component, tielink stiffness.
k_v	vertical component, tielink stiffness.
L	length of frame elements and rod elements.
M	moment in flexural members.
n	number of degrees of freedom per node; transformation ratios of moduli for flexural sections.
$\{P\}$	vector of section forces, frame elements.
$\{R_{xy}\}$	structure load vector referred to Cartesian coordinates x-y.
$\{R_F\}$	vector of node fracture forces.
R_i^*	unbalanced node forces after iteration i
$\{r\}$	node displacement vector for structure.
S	used for sin θ
$\{S\}$	element node force vector.
S_i	tributary length for tielink i.
$[\ ]^T$	suffix T means transpose of matrix or vector.
t	thickness of finite elements.
U	total strain energy scalar.
$[UV]$	array developed during derivation of element strain-displacement matrices.
$\{u\}$	horizontal displacements in finite elements.
$\{v\}$	vertical displacements in finite elements; vector of element node displacements.

W	virtual work scalar quantity.
$\{\delta_n\}$	unit node displacements.
δ	prefix for a small virtual quantity.
∂	prefix for partial derivatives
$[\lambda]$	transformation matrix for frame elements.
ν_i	Poisson Ratio for direction i from a uniaxial test.
θ_p	rotation to principal strain axes from global Cartesian axes.
φ	curvature of flexural members.
$\{\varphi\}$	vector of interpolation functions.
$\{\sigma_i\}$	vector of element stresses at point i.
$\{\sigma_p\}$	vector of principal stresses at a point.
$\{\xi\}$	vector of homogeneous triangular coordinates of a point.

NONLINEAR ANALYSIS OF REINFORCED CONCRETE
FRAMES AND PANELS

PH.D. H.A. FRANKLIN ENGINEERING

ABSTRACT

An analytical procedure is developed which utilizes quadrilateral, linear strain finite elements, special frame elements, axial force rod elements, and bi-directional tielink elements in order to study two-dimensional reinforced concrete frames with attached shear panels which are subjected to large lateral forces.

During the incremental loading procedure, allowance is made for the cracking and destruction of concrete elements with redistribution of stresses in the surrounding structure by iterating the solution within each load increment. The tielinks are used to connect the shear panels to the frame so that cracking can be included at the panel boundaries. The nonlinear material properties require the plane stress elements to have induced anisotropy under a general biaxial stress field. The method used here includes anisotropy for describing cracked elements, but assumes the uncracked elements to be isotropic. Material constitutive relations are not modified for the biaxial stress state. This method of analysis is applied to a set of test examples and to frame-and-panel models. Predictions of cracking, stress patterns, and deformations are compared to experimental results where possible.

A. C. Scordelis

Chairman, Thesis Committee

ACKNOWLEDGMENTS

The research reported herein was carried out during the author's graduate study for the Ph.D. degree in Civil Engineering at the University of California, Berkeley.

The author wishes to express his deep appreciation to Professor A. C. Scordelis for the direction and critical supervision he gave to completing this work; and to Professor E. L. Wilson for his suggestions and encouragement in the difficult early stages of development. He is also grateful to Professor F. E. Hauser, member of the thesis committee, for helpful comments; to Professors B. Bresler and V. Bertero for comments and suggestions; and to Mr. S. Mahin, Graduate Student in Civil Engineering, for his willing assistance with an ultimate strength analysis.

This work was sponsored by the National Science Foundation by Grant GK-1809. The University Computer Center, Berkeley Campus, provided their facilities for the computer work.

The author must also express deep appreciation to his wife Mary for her encouragement and determination during this long task, and for many hours of direct assistance given with her characteristic enthusiasm.

Special thanks go to Mrs. D. Aoki for her concerned work when typing the final copy.

1. INTRODUCTION

1.1 General Remarks

Destructive earthquakes have been observed for several decades which have caused millions of dollars of property damage, sometimes serious loss of life, and often great disruption of society in the affected areas. Structural engineers involved in aseismic designs carry a burden of responsibility that has provoked intensive professional and academic interest in the response of structures to earthquakes (30, 31). Any structure located in an active seismic area must be designed and constructed to safely resist the expected ground motions at that site. Adequate resistance is generally defined as the need to resist moderate earthquakes without unsightly damage and to resist severe earthquakes without collapse of the structure and danger of loss of life. To satisfy these requirements the structure must be analyzed to determine the stresses and deformations that may develop when ground motions occur.

Three types of analysis are presently used for this problem. The first approach applies a set of static lateral loads to the structure to represent the inertia forces that are developed by the motion of the structure. This procedure is described in code specifications but it is known to have only an elementary relationship to the actual forces that are generated in the structure (28). Furthermore, there are few guidelines available for the designer who must work with an unusual structural configuration. It has been observed that earthquakes produce deflections that depend on the dynamic response of the structure. As a result, the second approach to the structural problem has been

to apply a dynamic elastic analysis (32). This is known to generally predict story shear forces much in excess of those derived by Code procedures (35). This is particularly evident in rigid buildings, such as those with shear walls and panels, or in buildings with low damping. Structural designs based on a dynamic elastic analysis would become uneconomic in comparison with many successful designs that have been made under Code procedures. It has been necessary to invoke the idea of energy dissipation by inelastic behavior of sections of the structure. Hence the third approach in deriving the system response is to apply a dynamic inelastic analysis (28,30,33,34). This requires that the inelastic behavior be specified in terms of the shear force-lateral deflection behavior of each story. This is given as either an elastic-perfectly plastic response or as a bi-linear elastic response (36). Hysteretic behavior is usually defined so as to account for load reversals and to provide a realistic model for the energy dissipation process. This can also be augmented by dissipation through viscous damping effects.

It is important for the designer to know how an entire structure or subassembly will behave up until collapse occurs. Ideally this would mean being able to analyze the total response to arbitrary and reversed loads.

In the non-linear analysis of reinforced concrete framed structures the significant features are the formation of yield mechanisms, yield and collapse loads and deflections, locations of critical regions for hinge formation, changes in system stiffness, details of member cracking, the redistribution of internal forces that occurs

in the system, and overall energy absorption. When the system includes masonry or reinforced concrete panels or shear walls the requirements are the same but a more complex situation exists.

A non-linear analysis which traces the response of the structure through its entire load range is required for two main purposes. Firstly it gives the necessary nonlinear stiffness description for the inelastic dynamic analysis so that proper response displacements will be generated. Secondly, it provides the designer with the basis for deciding whether member sizes and details are adequate to withstand the generated displacements.

1.2 Previous Studies

Experimental testing of structures and structural elements have given the most information about behavior to failure and strength properties of reinforced concrete systems. This has successfully been generalized for simpler members (beams and columns) and their assemblages (trusses and frames). The predominance of the empirical expressions is being challenged by direct analysis, exemplified in recent work by Selna (6,37), which assumes linear elastic materials either up to tensile cracking or to a perfectly plastic yield condition, and includes shrinkage and creep effects. Wall and panel structures have been explored experimentally for some time (38,39,40, 41,42), but results are difficult to generalize (43). Analytical methods assume added significance in this area of interest and are being advanced. Recent work by Rashid et al. (44,45), Pope (52), or Zienkiewiecz et al. (46,47,48), assumes linear elastic materials up to either tensile cracking or to a perfectly plastic yield region,

and uses the finite element method to analyze two and three-dimensional continua. Attempts to analyze combinations of frames and walls or panels are yet restricted to linear elastic, non-failure problems (49). None of the above procedures include reversal loadings on the selected structures. The effects of bond interaction between concrete and its steel reinforcement have been explored by Scordelis, Ngo, and Nilson (8,9), by creating special two-dimensional finite element bond linkages to connect the steel to the concrete. These were non-linear linkages which connected linear elastic materials and gave valuable insight into the influence of reinforcement details on force transfers between the connected materials.

1.3 Scope of Present Investigation

This dissertation represents an attempt to advance the capability of present analytical methods by developing a non-linear analysis of reinforced concrete frames alone, or in combination with masonry or reinforced concrete shear walls or panels, or for these shear walls or panels alone. The process developed models a system whose stiffness deteriorates because of nonlinear material properties and the onset of tensile cracking or compression failures. The separations of panels or walls from the frames is also included if the force system requires this. The ability to handle load reversals (and so generate hysteresis loops of system response) was not included since this required information regarding cyclic stress-strain behavior of materials that is only gradually becoming available (50,51).

The analytical model used in this investigation permits the following types of elements to be used in assembling a structural

system:

(1) Quadrilateral finite elements for two dimensional panels and walls;

(2) Axial force rod elements for trusses or reinforcement;

(3) Frame elements that can be used to represent a reinforced concrete frame member subject to axial force, shear force, and bending moment.

(4) Special rigid tielink elements that are used to connect wall or panel elements to frame elements.

Nonlinear material properties, tensile cracking, and compressive failures in the elements are incorporated so that the assemblage of elements may be used to perform a nonlinear analysis of any two-dimensional, planar structure subjected to monotonically increasing, but variable, load patterns. Small displacement theory is assumed throughout the analysis.

The procedure developed is demonstrated by analyzing several examples of increasing complexity. The behavior to failure of a reinforced concrete one-story frame and a two-story frame are first studied with no infilled panels. These results are then compared to those obtained when weak, unreinforced infilled panels are added to each frame. The change in behavior is significant and agrees with experimental observations.

2. STRUCTURAL IDEALIZATION AND ANALYSIS

Structural idealization is the process of formulating a discrete element model of the structural system so that a finite number of degrees of freedom are defined. Discretization is particularly useful with regard to a material continuum which has an infinite number of degrees of freedom. The idealization leads directly to a finite number of algebraic equations (relating externally applied forces and structure displacements) which are usually best solved by using matrix algebra methods. This powerful approach to structural analysis is commonly referred to as "matrix analysis" or "using matrix methods" (2).

In analyzing frame structures a preliminary idealization is commonly made by the analyst. This is to regard one-dimensional members as line elements. For detailing their geometry, these elements are represented by their centroidal lines and joints between members are condensed to points where centroidal lines intersect. Formation of the discrete element model is then made by making cuts in the line elements. Since these discrete elements are already attached to neighbors at single points then the structural approximation is direct and such elements give exact representations of the original structure. Exact, that is, within the context of being able to derive accurate element stiffnesses or flexibilities.

Discrete elements of this type are familiar to the analyst as axially loaded rods joined at the ends to form trusses, or as primarily flexural members connected to form rigid frames. On the other hand, plates, panels, slabs and shell structures are examples of the

continuum-type systems which cannot have a preliminary idealization to line elements. The formation of discrete elements by cutting the original structure now implies line-cuts rather than joint separations. Such cutting removes the real, continuous edge connections between elements so one must substitute discrete joint (or node) connections to represent them. Clearly the inter-element forces at these artificial joints or nodes do not exist in reality and so further fictitious stress or displacement patterns over the element field must be introduced which can be related to the node forces or displacements. This causes the discrete element to become an approximation to the original structure. These special elements are called finite elements and their application for the discretization and analysis of a structural continuum is known as the finite element method (3,1). Considerable research effort continues to be exerted to explore the characteristics of finite elements in order to ensure reliable analytical solutions from their use (5).

The final step in the structural idealization requires that the internal and external forces be transformed into a statically equivalent set of concentrated forces acting at the appropriate nodal points. The array of discrete elements that represent the actual structure and the array of nodal forces that represent the applied forces together comprise the idealized structure to be analyzed.

2.1 The Selection of Discrete Elements

The first problem of this research was to define the necessary features of the structure to be analyzed and then to explore the corresponding structural idealizations. The specification was for a

planar, reinforced concrete, multi-story frame, with non-linear material properties loaded by vertical and lateral forces, and allowing for cracking, yielding or local failures in the members. Furthermore, the specification included for the provision of shear panels, consisting of two-dimensional concrete elements, with or without reinforcement, which could be attached to the frame in such a way that separations would occur where fractures between panels and frame were the natural result of the given loading. The idealization of the structure which satisfied this specification was achieved by means of four types of discrete elements, two of which were finite elements.

2.1.1 Shear Panels and Reinforcement

The loading of the shear panels is by interaction of the panel edges with the frame members. The force system is in the plane of the panel and includes no forces normal to that plane. Consequently the analysis of a shear panel becomes a two-dimensional plane-stress problem. The choice of a finite element for idealizing the panels is thus immediately simplified. Whereas triangular finite elements have some advantages when applied to irregularly bounded regions, their combination into quadrilateral finite elements has significant advantages. These are a reduction in mesh details, improved stress values that may be recovered by averaging over the sub-triangles, and the reduction of element connectivity by nodal condensation which reduces the computational effort. Also a quadrilateral finite element composed of two sub-triangles still maintains a capability for handling irregular boundaries depending on the sequence used in the nodal description. Some illustrations of the versatility of the quadrilateral element are given in Figure 2-2. The recommended finite

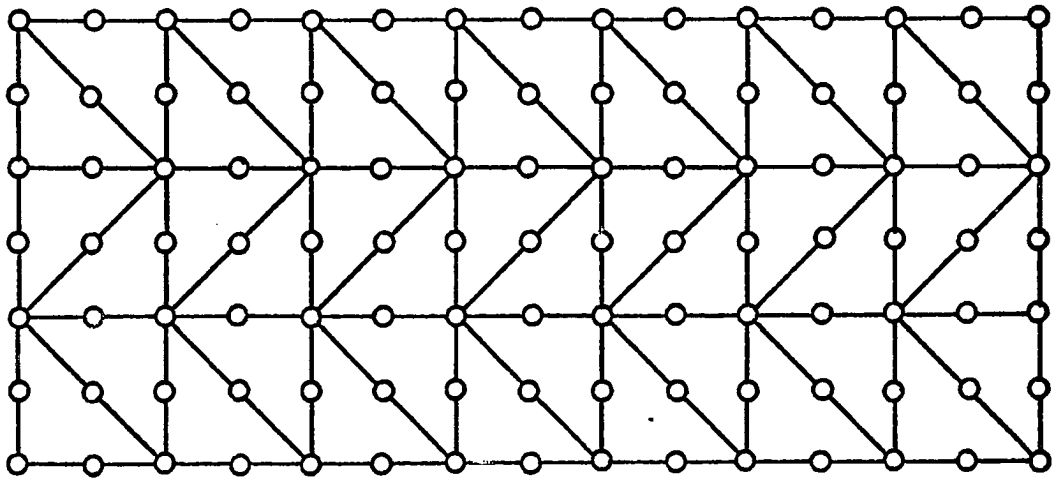

42 linear strain triangles require 105 nodes.

21 linear strain quadrilaterals require 32 nodes.

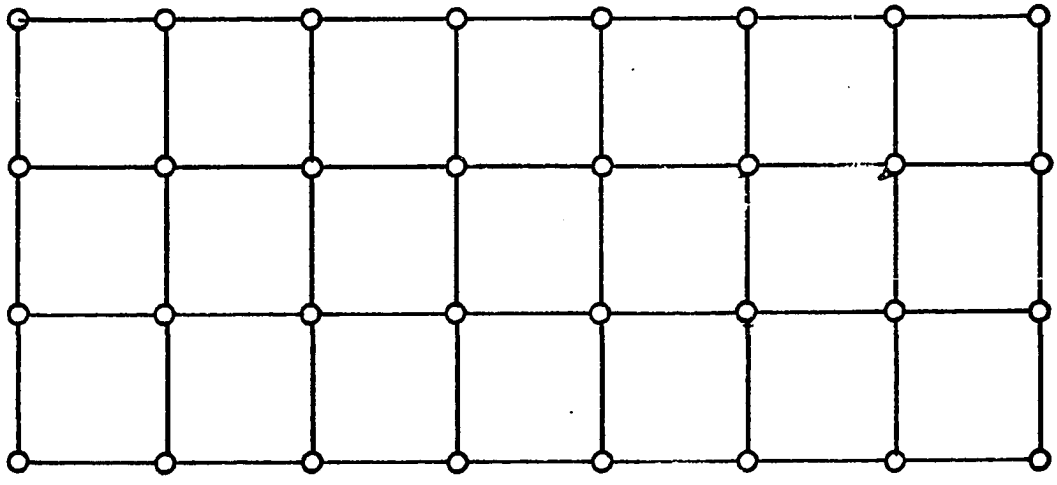

FIGURE 2.1

DISCRETIZATION NEEDED FOR TWO PLANE STRESS FINITE ELEMENTS.

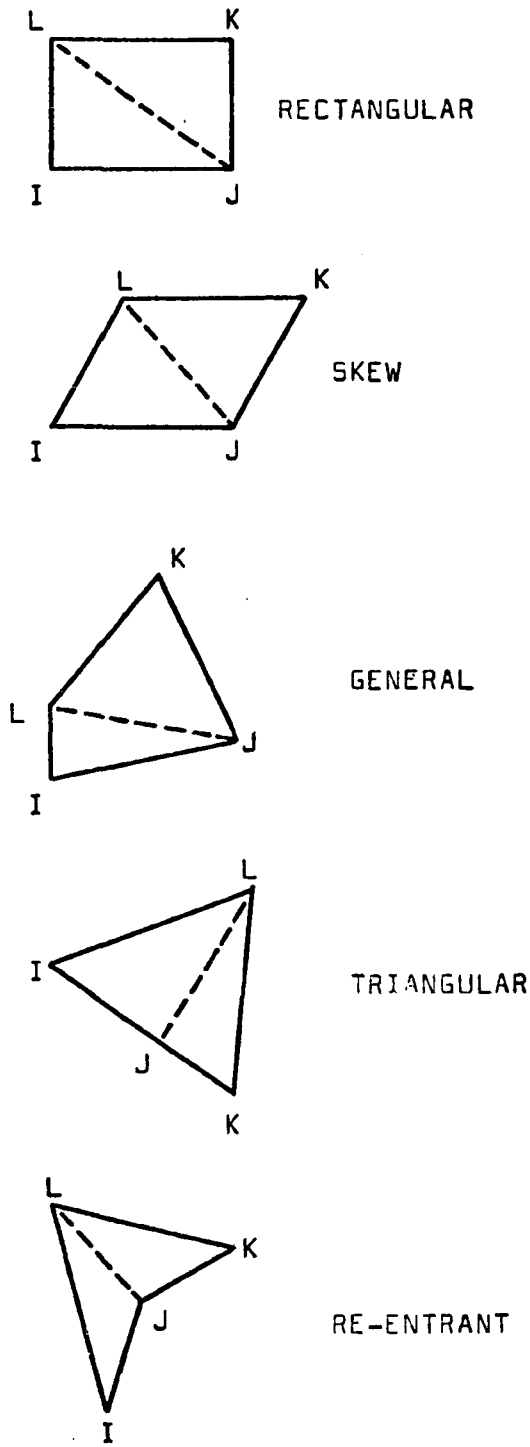

FIGURE 2.2 VERSATILITY OF QUADRILATERAL ELEMENTS.

element for the two-dimensional shear panel analysis was thus chosen as a 4-nodal point quadrilateral composed of two, linear strain, 4-nodal point triangles (5).

Reinforcement for the shear panels was represented by including axially-loaded, pin-jointed rods that acted as discrete elements between the nodes defining the quadrilateral element mesh. This particular combination of elements has previously been successfully applied to the analysis of reinforced concrete members (8,9).

2.1.2 Reinforced Concrete Frame Members

If the frame members could be regarded as line elements, in the conventional manner, then the discretization would be simple and direct. However, it was clear that the geometric width would be important for considering their interaction with connected shear panels. The connecting nodes transmit in-plane forces corresponding to two degrees of freedom, one force normal to the frame member axis or panel edge, and the other force parallel to that line or tangential to the panel edge. The normal force components produce the usual bending moments and shears in the frame members. The parallel components not only produce axial forces in the frame, but since their lines of action are located at the outer fibers of frame members, they transmit additional moments into the frame. This alone need not prevent idealizing the frame members as line elements. Systems of frame analysis are available that regard members as wide as shear walls as flexural line elements and then compensate for the actual width of the walls when forming stiffness coefficients for the connected beams (12). The controlling criterion was the need to include nonlinear material

properties and variable cracking in frame members subjected to axial, shear and moment forces. Thus some kind of discrete element idealization, other than a line element, was needed.

A combination of quadrilateral finite elements and rod-type discrete elements could be used for frame members that would be very good for the analysis of reinforced concrete. If these are used to represent the frame members with nonlinear material properties over the member cross-section, then the required array of elements would automatically define a very fine mesh over the adjacent shear panel. Conversely, an adequate mesh of elements for a shear panel would define far too coarse a mesh for the adjacent frame member.

The answer was to devise special frame elements that used a presentation by Selna (6) as a basis for their development. This finite element is capable of including nonlinear material properties across the section of a frame member and has a size which is compatible with adjacent quadrilateral finite elements. Furthermore, the depth of cracking that occurs is allowed for in each element and can be obtained with the data from the analysis.

2.1.3 Panel-To-Frame Connections

The special releasing connections between shear panels and frame members were solved by using discrete element tie-links that were an adaption of the bond-link concept introduced by Ngo and Scordelis (8) and further demonstrated by Nilson (9). These tie-links enable two specified nodes to be locked together or released according to prevailing conditions. Whereas the original bond-links were devised as discrete-elements representing the connection

between embedded steel and surrounding concrete, the present tie-links are used only to represent the edge connection between adjacent concrete elements; in particular between shear panels and frame members.

The details of the mathematical formulations for deriving various element stiffness are given in Chapter 3.

2.2 The Displacement Method of Analysis

The idealization of the two-dimensional structure produces a highly indeterminate system of discrete elements. By evaluating the stiffness of each element then the stiffness characteristics of the entire structure may be constructed. Finally a system of linear equations is produced which relate nodal point loads and displacements. This system of equations has a size determined by the total number of degrees of freedom of the idealized structure. Until the advent of the electronic digital computer the solution of very large arrays of equations was difficult and this approach to structural analysis was impractical. In present methods, displacement modes are used to evaluate element stiffnesses, which are then combined in a direct stiffness procedure to give compacted arrays of equations that are finally solved by taking advantage of their banded nature. The result is a versatile and powerful method of analysis of complex structures.

This process can be outlined for the elastic analysis of an idealized structure according to the following basic steps:

a. Derive element stiffnesses $[k_{mn}]$ in element coordinate system m-n.

b. Assemble the structure stiffness $[K_{xy}]$ and the load vector $\{R_{xy}\}$ in the global coordinate system.

c. Solve the equilibrium equations $\{R\} = [K]\{r\}$ for node displacements.

d. Recover the selected element stresses $\{\sigma\}$ or forces $\{S\}$ in the desired coordinate system.

2.2.1 Element Stiffness Arrays

The derivation of element stiffness is left until the next chapter and the appendices. At this stage assume that each element stiffness array is numerically available. For each element a matrix set relating nodal forces and displacements in the element coordinate system m-n can be stated as

$$\{S_{mn}\} = [k_{mn}]\{r_{mn}\} \tag{2.1}$$

where a stiffness influence coefficient k_{ij} is the force at, and in the direction of degree of displacement freedom i (abbreviated from now on as d.o.f. i) due to a unit displacement at the location, and in the direction of d.o.f. j. Figure 2-3 illustrates the standard number system for the d.o.f. of the general quadrilateral element. The number of degrees of freedom specifies the size of array $[k_{mn}]$. For the various elements to be used in this idealization this gives the maximum basic 8 X 8 element array as follows:

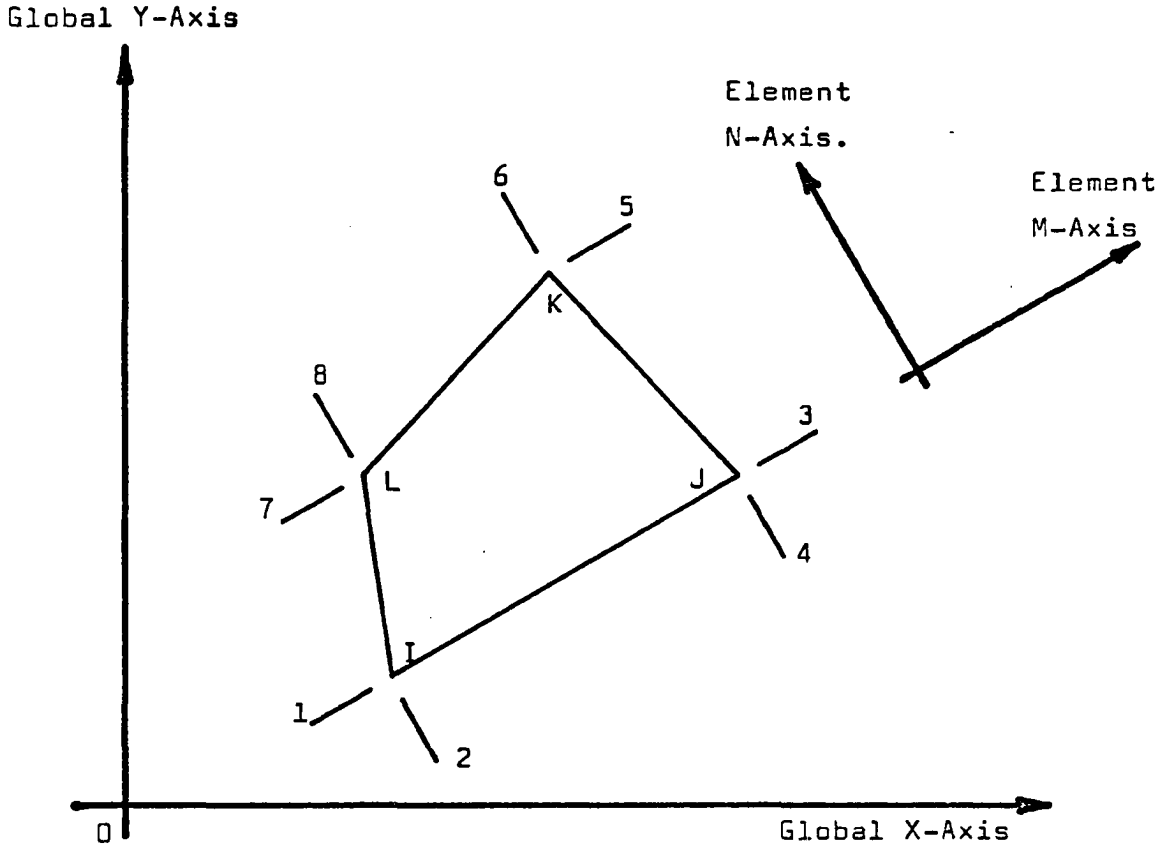

FIGURE 2.3

QUADRILATERAL ELEMENT DEGREES OF FREEDOM.

$$\begin{Bmatrix} S_1 \\ S_2 \\ \vdots \\ S_7 \\ S_8 \end{Bmatrix} = \begin{bmatrix} k_{11} & k_{12} & k_{13} & \cdots & k_{18} \\ & k_{22} & k_{23} & \cdots & k_{28} \\ & & \ddots & & \\ \text{Symm.} & & & k_{77} & k_{78} \\ & & & & k_{88} \end{bmatrix} \begin{Bmatrix} r_1 \\ r_2 \\ \vdots \\ r_7 \\ r_8 \end{Bmatrix} \tag{2.2}$$

This maximum size is obtained for the quadrilateral plane stress elements and for the frame elements. The rod and linkage elements each give only a 4 X 4 stiffness array and thus only the appropriate terms are loaded in the basic 8 X 8 array.

Transformation to the global coordinate system is necessary before assembly into the global stiffness array $[K_{xy}]$. This is a standard orthogonal transformation derived from the following basis. Let [a] be the array of direction cosines such that

$$r_{mn} = a\ r_{xy} \tag{2.3}$$

Alternatively each a_{ij} may be regarded to be the element displacement at i due to a unit global displacement at j. Permit a small virtual displacement to occur, then

$$\delta\ r_{mn} = a\ \delta\ r_{xy} \tag{2.4}$$

Let S_{xy} = node forces in the global system corresponding to displacements r_{xy}, S_{mn} = node forces in the element system corresponding to displacements r_{mn}, and let superscript T indicate the transposed vector or matrix. Virtual work is invariant for the system so

$$\delta\, r_{xy}^{T}\, S_{xy} = \delta\, r_{mn}^{T}\, S_{mn} \tag{2.5}$$

Substitute from Eq. (2.4) to get

$$\begin{aligned} S_{xy} &= a^{T}\, S_{mn} = a^{T}\, k_{mn}\, r_{mn} \\ &= a^{T}\, k_{mn}\, a\, r_{xy} \end{aligned} \tag{2.6}$$

Hence the global stiffness K_{xy} is obtained by the transformation

$$K_{xy} = a^{T}\, k_{mn}\, a \tag{2.7}$$

2.2.2 Structure Matrix Assembly

So far the element stiffness has been developed by considering the element nodes to be cyclically ordered irrespective of their assigned node number. In this way every element has stiffnesses loaded into an 8 X 8 array. However, the global $[K_{xy}]$ matrix is ordered according to the true node numbers. Element arrays are disintegrated and reassembled into $[K_{xy}]$, overlapping coefficients are added and the final result is a banded, usually sparse, symmetrical matrix. In a similar fashion the element $\{S_{xy}\}$ forces are assembled into the structure load vector $\{R_{xy}\}$. This method of processing produces a matrix array that is singular since rigid body degrees of freedom are included.

$$R_{o} = K_{o}\, r_{o} \tag{2.8}$$

Partition this array to account for boundary restraint conditions

$$\begin{Bmatrix} R_{a} \\ R_{s} \end{Bmatrix} = \left[\begin{array}{c|c} K_{aa} & K_{as} \\ \hline K_{sa} & K_{ss} \end{array}\right] \begin{Bmatrix} r_{a} \\ r_{s} \end{Bmatrix} \tag{2.9}$$

where r_a = unknown node displacements

R_a = known or equivalent node forces

r_s = known boundary constraints necessary to prevent rigid body motion = zero reference displacements

R_s = unknown reaction forces that equilibrate R_a

Expand and substitute $r_s = R_s$ = zero and an equivalent array can be used for solution

$$\begin{Bmatrix} R_a \\ \hline 0 \end{Bmatrix} = \left[\begin{array}{c|c} K_{aa} & 0 \\ \hline 0 & I \end{array}\right] \begin{Bmatrix} r_a \\ \hline 0 \end{Bmatrix} \tag{2.10}$$

This allows the entire array to be solved without actual reordering when the specified reference displacements occur at random points in the sequence.

With rigid body motions removed, any further displacement boundary conditions must be included. Partition the nontrivial portion again

$$R_a = \begin{Bmatrix} R_f \\ \hline R_d \end{Bmatrix} = \left[\begin{array}{c|c} K_{ff} & K_{fd} \\ \hline K_{df} & K_{dd} \end{array}\right] \begin{Bmatrix} r_f \\ \hline r_d \end{Bmatrix} \tag{2.11}$$

where r_f = unknown node displacements

R_f = known nodal forces

r_d = known boundary displacements

R_d = unknown boundary forces

Expand and modify the applied load vector

$$\begin{aligned} R_f &= K_{ff}\, r_f + K_{fd}\, r_d \\ R_f &= R_f - K_{fd}\, r_d = K_{ff}\, r_f \end{aligned} \tag{2.12}$$

This final set is solved for r_f displacements from the modified system

$$\begin{Bmatrix} R_f^* \\ \hline 0 \\ \hline 0 \end{Bmatrix} = \left[\begin{array}{c|c|c} K_{ff} & 0 & 0 \\ \hline 0 & I & 0 \\ \hline 0 & 0 & I \end{array}\right] \begin{Bmatrix} r_f \\ \hline 0 \\ \hline 0 \end{Bmatrix} \tag{2.13}$$

2.2.3 Solution of the Equilibrium Equations

Some special features of the global [K] matrix are advantageous for the solution process. These arrays are:

a. banded and sparse

b. symmetric about the diagonal, and

c. positive definite and diagonally dominant.

Figures 2-4(a) and (b) show that orderly numbering systems for nodes and elements produce a concentration of nonzero coefficients in a diagonal band. If D is the greatest difference between node numbers for any element, and n is the number of d.o.f. per node, then the half band width is (D+1) n. Since this gives a sparse array, storage processes and computing algorithms have been written to take advantage of these properties. Symmetry of the matrix can often be useful when constructing the arrays, particularly at the level of deriving element stiffnesses [k].

The work U done by forces $\{S\}$ gradually applied to a system of stiffness [K] will be

$$U = \tfrac{1}{2}\, S^T r \tag{2.14}$$

where displacements r occur. Since $S^T = r^T K$ (for symmetric K) then

$$U = \tfrac{1}{2}\, r^T K\, r > 0 \tag{2.15}$$

U is a scalar quantity always greater than zero for any vector r. This defines K as positive definite and establishes iteration as a

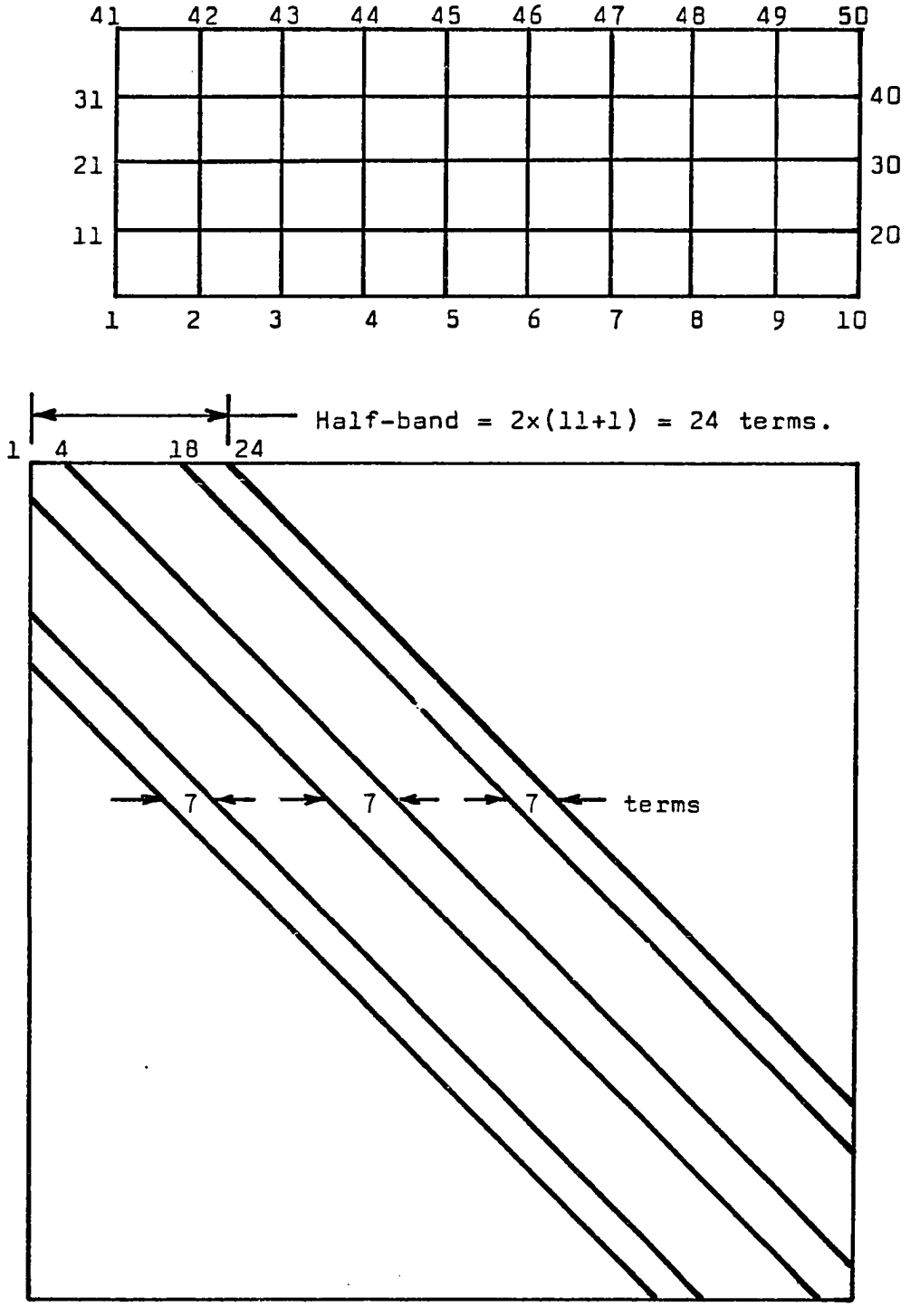

FIGURE 2.4(A) STIFFNESS MATRIX BAND EFFECT.

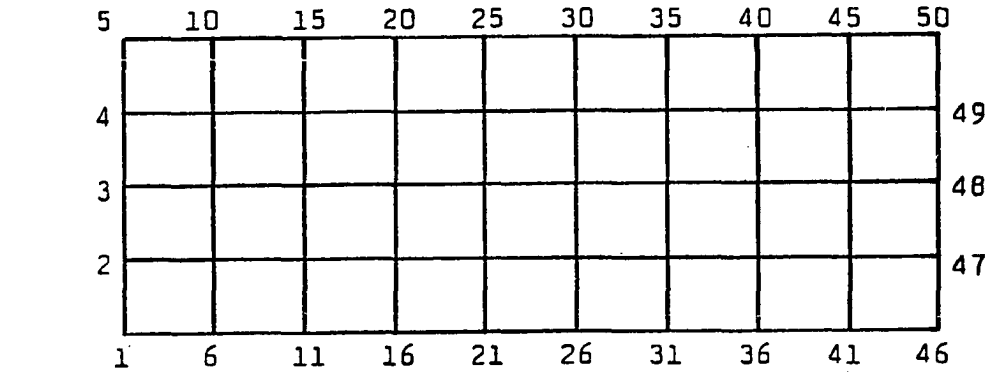

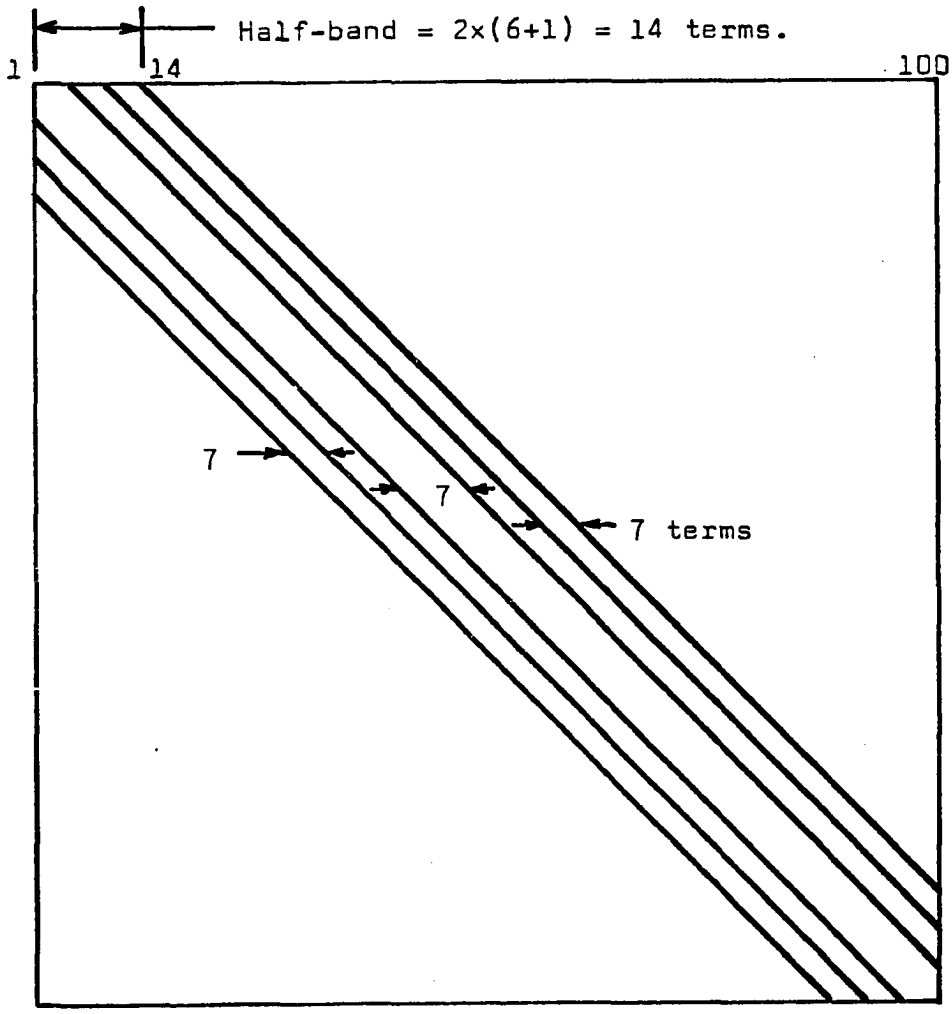

FIGURE 2.4'B) STIFFNESS MATRIX BAND EFFECT.

convergent method of solution (13). Structural changes might occur in a system to cause K to become singular or negative definite and this corresponds to the onset of structural instability. This idea may be used for stability analysis (1). Iteration has generally been superseded by direct methods of solving the equilibrium equations and the present investigation uses Gaussian elimination with back-substitution for solving the equilibrium equations (2,13).

2.2.4 Element Strains and Stresses

Having solved the structure node displacements $\{r\}$ then element node displacements $\{v\}$ may be constructed. In the usual procedure, strain-displacement or stress-displacement transformations are introduced and node displacements are converted into element principal strains or stresses. However, some elaboration must occur because of the nonlinear material properties and the changing structural topology. This will be developed in detail in the following chapters which discuss element matrices, material properties, and the nonlinear analysis procedure.

3. COMPUTATION OF ELEMENT STIFFNESSES

The stiffness relationships, which are the force per unit displacement coefficients at specified coordinates for each discrete structural element, must be calculated in order to construct the stiffness array of the complete assemblage. Several methods are used for determining element stiffnesses. Most of these methods are in the general classification of energy methods of analysis. It is possible to express the strain energy of the element in terms of the selected node displacements. By applying Castigliano's Theorem (Part I) the corresponding node forces can be computed. As alternative approaches variational methods or the virtual work theorems can be used to derive relations between node forces and node displacements.

If differential equations are available to relate forces and displacements for the member then a set of solutions may be obtained by integrating with suitable displacement boundary conditions. This approach is usually only suitable for the simplest situations. Some of these methods may yield flexibility coefficients more easily than stiffness relations, so that inversion of a flexibility array may be necessary. However, the rigid body motions will be missing from such a stiffness matrix and it must be modified before assembly into the global stiffness array. The method used in this research was to derive stiffnesses directly by application of unit displacements. This is equivalent to using the principle of virtual displacements. The elements will be discussed separately in the next sections.

3.1 The Quadrilateral Plane Stress Element

This element is constructed from two linear-strain triangles each

of which is modified from 6 nodes (12 d.o.f.) to 4 nodes (8 d.o.f.) by imposing a linear displacement variation on two sides of the triangle. This satisfies the displacement compatibility with adjacent elements in the assembled array. After connecting two triangles to give a 5-node quadrilateral (10 d.o.f.), then the common center node is eliminated by condensation to yield the final linear strain quadrilateral with 4 corner nodes (8 d.o.f.). This is shown schematically in Figure 3-1. Since these computations are shown in detail in other references (5,10), only the essential matrix operations will be outlined herein according to the scheme of Figure 3-2. For completeness and convenience of the reader, most of the matrix expansions are given in the above references.

Displacement fields are defined over the element in terms of unit displacements at each node by using homogeneous triangular coordinates $\{\xi\}$ and constructing interpolation functions $\{\varphi\}$ from them. Let the displacements u, v of a point i be $\{v_i\}$ and, at a node $\{v_n\}$. Then

$$\underset{2X1}{\{v_i\}} = \underset{2Xm}{[\varphi_{in}]} \quad \underset{mX1}{\{v_n\}} \tag{3.1}$$

where $[\varphi_{in}]$ is constructed by assembling suitably specialized forms of $\{\varphi\}$ and where m = 8 when the triangle is reduced to 4 nodes. For small deflections, strains $e_{jk} = \frac{1}{2}(v_{j,k} + v_{k,j})$ where the subscripts represent the appropriate partial derivatives. Applying this differentiation to the displacement field, for the set of strains at some point i

$$\underset{3X1}{\{e_i\}} = \underset{3X2}{[\partial]} \underset{2X1}{\{v_i\}} = \underset{3X2}{[\partial]} \underset{2X8}{[\varphi_{in}]} \underset{8X1}{\{v_n\}} \tag{3.2}$$

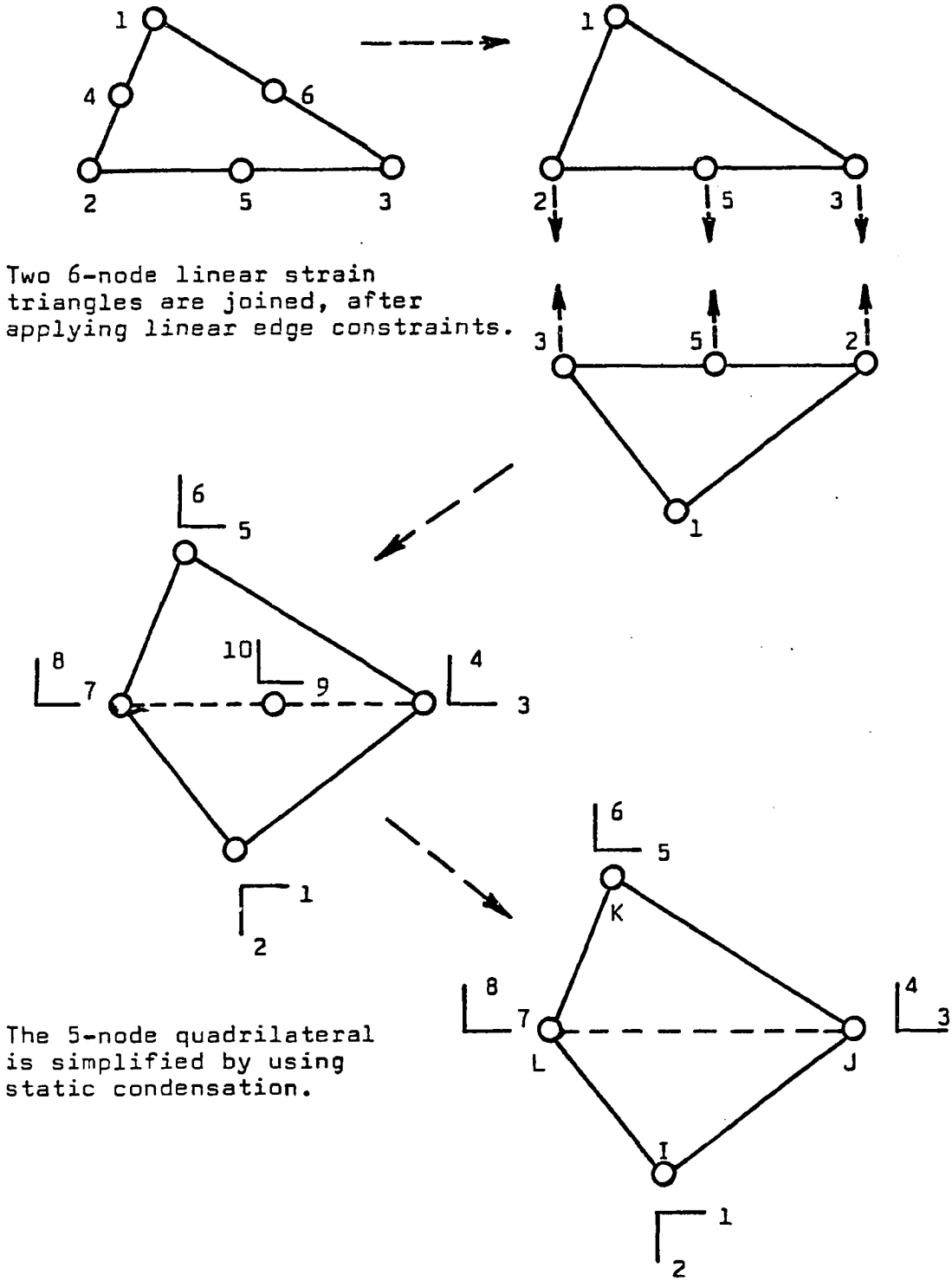

FIGURE 3.1 ASSEMBLY OF PLANE STRESS ELEMENTS.

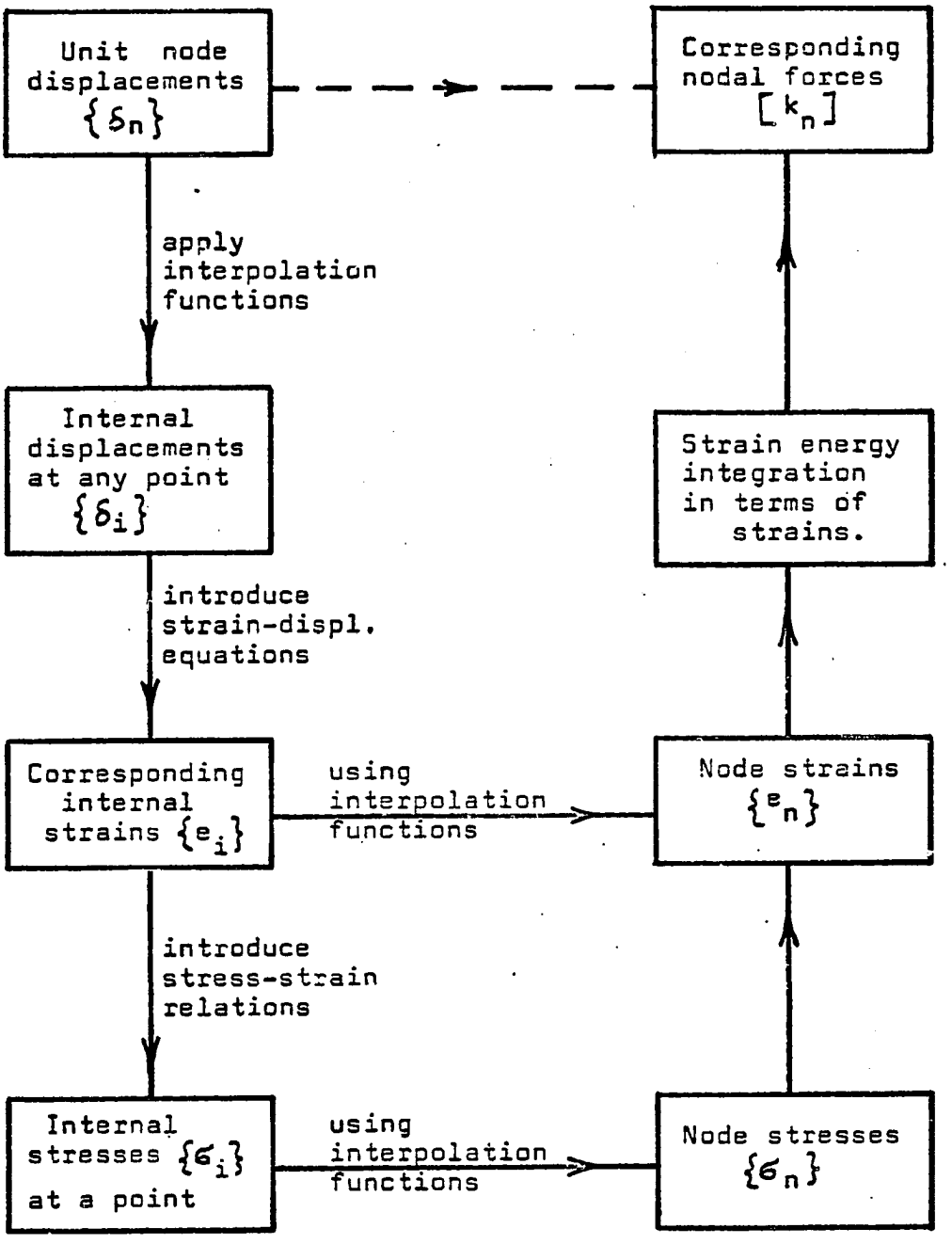

FIGURE 3.2 DEVELOPING THE PLANE STRESS ELEMENT STIFFNESS.

If the differentiation is carried out, and the expressions expanded and specialized for the set of strains at the 3 corner nodes, then the strain-displacement equations become

$$\underset{9X1}{\{e_n\}} = \underset{9X8}{\begin{bmatrix} U & 0 \\ 0 & V \\ V & U \end{bmatrix}} \underset{8X1}{\{v_n\}} = [UV]\{v_n\} \tag{3.3}$$

where arrays [U] and [V] (each being 3 X 4) are conveniently derived directly from the node Cartesian coordinates. At this stage note that the requirement of a linear strain field over the element suggests simple interpolations for the strains at a point in terms of the strains at the 3 corner nodes. Consequently, if

$$\underset{1X1}{\{e_x\}} = \underset{1X3}{\{\xi_e\}^T} \underset{3X1}{\{e_{xn}\}}$$

where $\{e_{xn}\}$ = values of e_x at each corner node, then any set of strains is given by

$$\underset{3X1}{\{e_i\}} = \underset{3X9}{[\varphi_e]} \underset{9X1}{\{e_n\}}$$

where

$$[\varphi_e] = \begin{bmatrix} \xi_e^T & 0 & 0 \\ 0 & \xi_e^T & 0 \\ 0 & 0 & \xi_e^T \end{bmatrix}$$

$$\underset{3X1}{\{e_i\}} = \underset{3X9}{[\varphi_e]} \underset{9X8}{[UV]} \underset{8X1}{\{v_n\}} \tag{3.4}$$

This transformation is used to derive the strains at the location of the eliminated center node by specializing the coordinates to give

$$\underset{3X1}{\{e_c\}} = \underset{3X9}{[\varphi_c]} \underset{9X1}{\{e_n\}} = \underset{3X9}{[\varphi_c]} \underset{9X8}{[UV]} \underset{8X1}{\{V_n\}} \tag{3.5}$$

In this work it is assumed that the material constitutive relations are constant over the element and that the stresses at any point may be expressed as

$$\underset{3X1}{\{\sigma_i\}} = \underset{3X3}{[C]} \underset{3X1}{\{e_i\}} = \underset{3X3}{[C]} \underset{3X9}{[\varphi_e]} \underset{9X1}{\{e_n\}} \tag{3.6}$$

or

$$\underset{3X1}{\{\sigma\}} = \underset{3X3}{[C]} \underset{3X9}{[\varphi_e]} \underset{9X8}{[UV]} \underset{8X1}{\{V_n\}} \tag{3.7}$$

Now the material properties have been introduced into the solution process. The selection of [C] can be used to reflect the characteristics of the material state, for example [C] can be specialized to solve either plane stress or plane strain problems, or another kind of specialization will represent anisotropic materials. The definition of the values of material moduli E_i used to construct [C] will be left for later discussion and for the present it will be assumed that [C] can be defined appropriately for each element.

Now the principle of virtual work will be introduced. If a system of real nodal forces $\{S_n\}$ is in equilibrium with a set of real internal stresses $\{\sigma_i\}$, and the system is subjected to a set of compatible virtual node displacements $\{V_n^*\}$, then the external virtual work W_E done by the real forces $\{S_n\}$ is equal to the internal virtual work W_I done by the real stresses $\{\sigma_i\}$ acted on by the virtual strain field $\{e_i^*\}$

$$W_E = \{V_n^*\}^T \{S_n\}$$
$$W_I = t \int_A \{e_i^*\} \{\sigma_i\} \, dA \tag{3.8}$$

A constant element thickness t has been assumed for the integral expression. Substituting from Eqs. (3.4) and (3.7), and equating the work expressions,

$$\{V_n^*\}^T \{S_n\} = t \int_A \{V_n^*\}^T [UV]^T [\varphi_e]^T [C] [\varphi_e] [UV] \{V_n\} \, dA$$

or

$$\{S_n\} = t \, [UV]^T \int_A [\varphi_e]^T [C] [\varphi_e] \, dA \, [UV] \{V_n\} \tag{3.9}$$

By setting $[N] = \int_A [\varphi_e]^T [C] [\varphi_e] \, dA$, this can be evaluated from tables (5). If a set of unit displacements are successively applied to the nodes, then $\{V_n\}$ is replaced by $[I]$ and the set of node force vectors represents the triangular element stiffness $[k]$

$$[k] = t \, [UV]^T [N] [UV] \tag{3.10}$$

These operations are performed for each triangular element, and then the two 8 X 8 arrays $[k_1]$ and $[k_2]$ are combined by direct superposition to give a single 10 X 10 stiffness array $[k]$ for the quadrilateral element. The center node degrees of freedom are removed by the usual condensation process. Partitioning and expanding

$$\begin{Bmatrix} S_a \\ S_b \end{Bmatrix} = \left[\begin{array}{c|c} k_{aa} & k_{ab} \\ \hline k_{ba} & k_{bb} \end{array}\right] \begin{Bmatrix} V_a \\ V_b \end{Bmatrix}$$

Omitting brackets, $S_b = k_{ba} \; V_a + k_{bb} \; V_b$

whence $V_b = K_{bb} (S_b - k_{ba} V_a)$

since $S_a = k_{aa} V_a + k_{ab} V_b$

then $S_a = k_{aa} v_a + k_{ab} (k_{bb}^{-1} S_b - k_{bb}^{-1} k_{ba} V_a)$

Finally $(S_a - k_{ab} k_{bb}^{-1} S_b) = (k_{aa} - k_{ab} k_{bb}^{-1} k_{ba}) V_a$

Since no external loads are allowed at the center node and since thermal forces and body forces are distributed directly to the corner nodes, then $S_b = 0$.

Finally
$$\underset{8X1}{\{S_a\}} = \underset{8 \times 8}{[k_{aa} - k_{ab} k_{bb}^{-1} k_{ba}]} \underset{8X1}{\{V_a\}} \qquad (3.11)$$

This is the completed stiffness relationship for the quadrilateral plane stress finite element. The global stiffness [k] is given by

$$[k] = [k_{aa} - k_{ab} k_{bb}^{-1} k_{ba}] \qquad (3.12)$$

It may be noted that the quadrilateral plane stress element has no naturally related 'element coordinate system.' The rod element has an element coordinate system that is oriented by the longitudinal axis and the frame element has a centroidal axis that can be used as a reference axis. In the present case the entire stiffness computation is conveniently carried out in the global coordinates and the resulting element stiffness [k] automatically refers to the global axes.

Assembling the structure stiffness matrix [K] and solving for the node displacements {r}, the node displacements {V} are recovered for each element and the set of strains $\{e_c\}$ is computed for the center node from the strain-displacement Eqs. (3.5). Since these are for global coordinates, they are transformed to give the magnitude and direction of the principal strains $\{e_p\}$. The material stress-strain

relation is used to convert $\{e_p\}$ into principal stress $\{\sigma_p\}$. These are then rotated back to the global coordinates to give the global stresses $\{\sigma_c\}$ at the center node. This last step depends on the assumption that the direction of principal strains coincides with the direction of principal stresses i.e., creep and shrinkage effects are absent.

3.2 The Frame Elements

The reinforced concrete frame members were assumed to have their lengths cut to form discrete segments joined together by corner nodes in a manner similar to the quadrilateral plane stress elements. Figure 3.3 shows this discretization for some beams and columns. The segments are of any length so that the analyst can select shorter segments where steeper force gradients are expected. Each segment is regarded as having top and bottom faces, with the bottom defined by the nodes I-J in the segment nodal description. With this feature, forces and displacements may be related to the left or right faces of a segment, and top or bottom concrete fiber stresses, or stresses in the bottom or other reinforcement layers may be specifically located. Such a description is then unique for each segment and is independent of the actual member orientation where difficulty would be otherwise experienced, for example, in identifying "top" or "bottom" faces of a column.

The geometric properties of a segment are assumed to be constant along its length so that the real cross section is constant and rectangular, and the transformed section is prismatic. The material properties are also assumed constant along any level in the segment

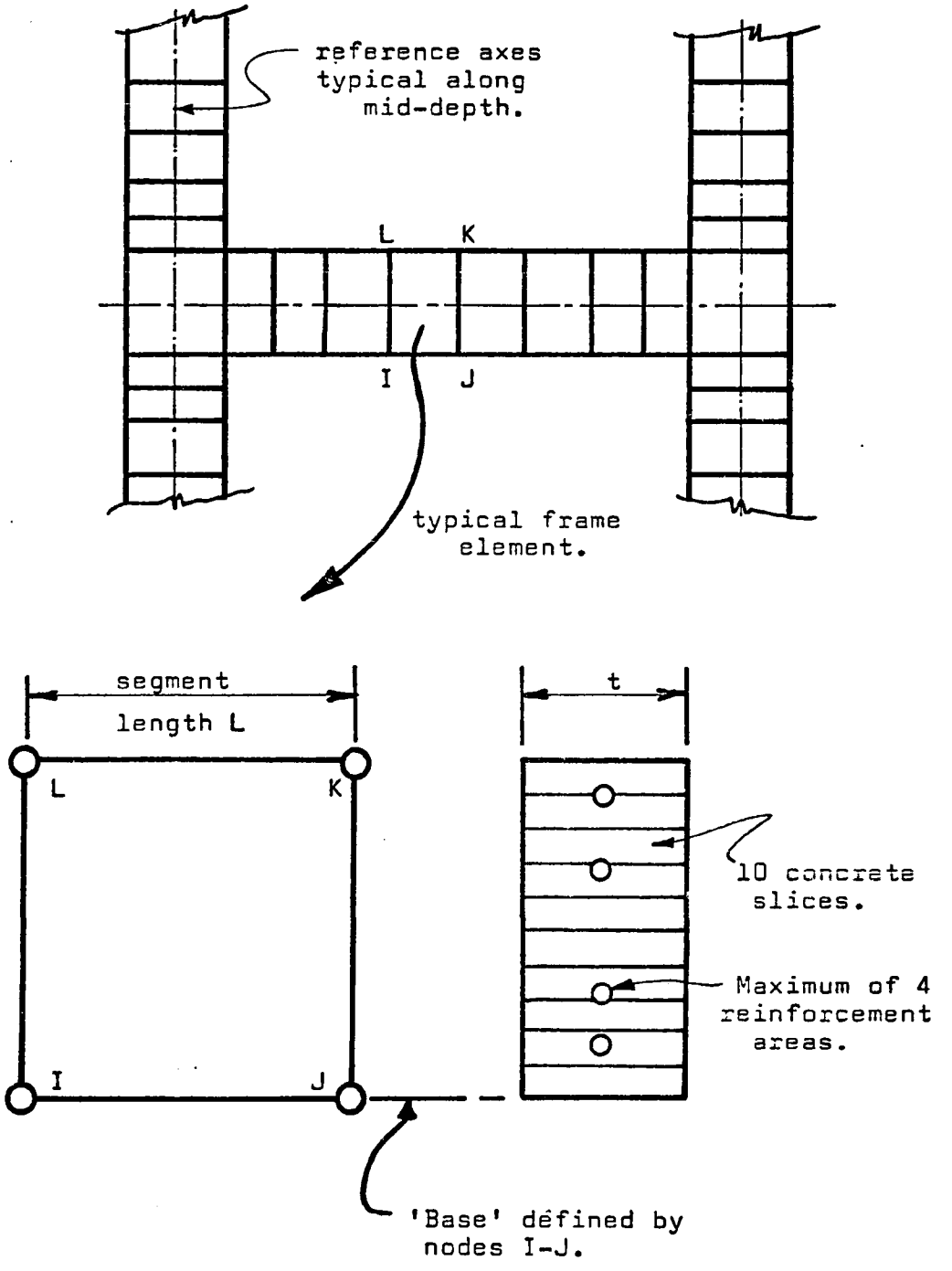

FIGURE 3.3 REINFORCED CONCRETE FRAME ELEMENTS.

length. This assumption is directly related to the assumption of constant strain along any level in the segment and the derived transformed section is prismatic. The transformed section properties of a segment are derived by regarding the concrete to be sliced into 10 layers from bottom to top and by including up to 4 discrete reinforcement areas at arbitrary distances from the bottom fiber. The strain intensity in each slice or reinforcement layer is derived by assuming that segment end sections remain plane during the deformations.

In this study, the constant strain along the mid-level of each slice is derived only from the displacements of the two end faces of the segment. Variable strains could be defined by including nodes at interior sections of the segment or by attempting to utilize the displacement patterns of adjacent segment end sections.

The process of computing the segment stiffness begins by considering the displacements and forces defined in Figure 3-4, which include axial forces, shear forces and moments. The corresponding standard 6 X 6 stiffness array $[k_g]$ is assembled and subscripted to show that it is implicitly referenced to the segment centroidal axis. Shear stiffness corrections were omitted for this development by recognizing that the primary force actions in the assembled frame members are flexural and axial rather than predominantly shear. The preliminary array therefore has the following form.

(a) Preliminary flexural degrees of freedom.

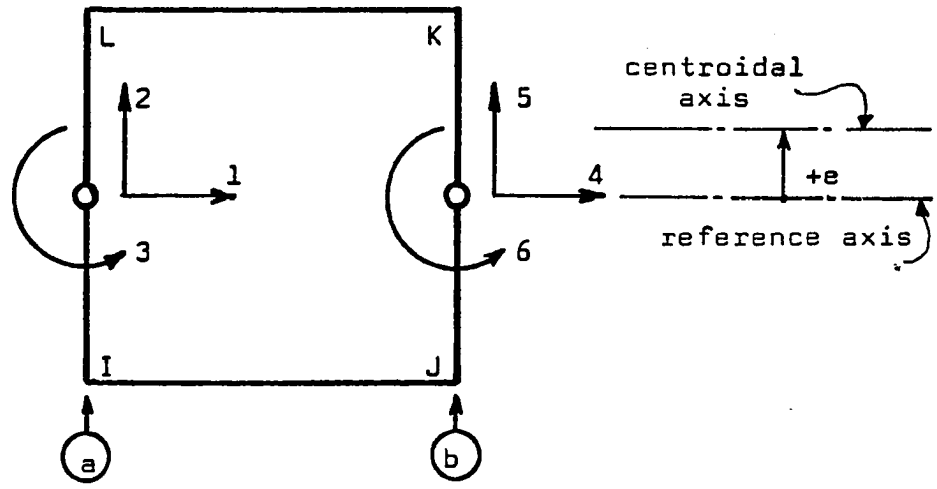

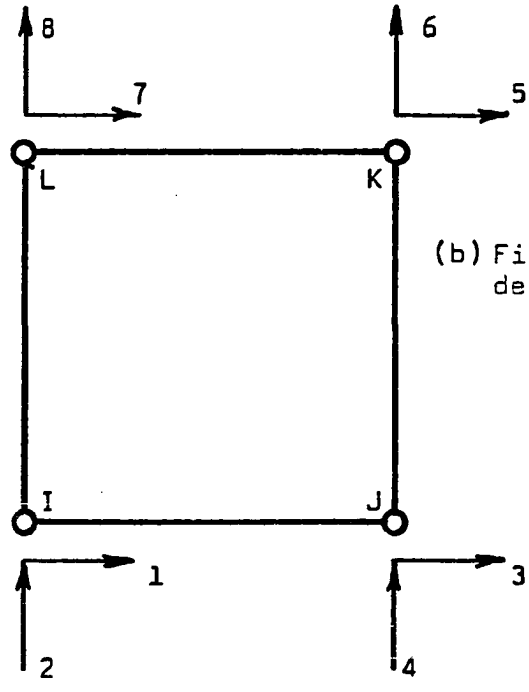

(b) Final quadrilateral degrees of freedom.

FIGURE 3.4 FRAME ELEMENT GENERALIZED COORDINATES.

$$[k_g] = \begin{bmatrix} \frac{AE}{L} & 0 & & & & \\ 0 & \frac{12EI}{L^3} & & & & \\ 0 & \frac{6EI}{L^2} & \frac{4EI}{L} & \text{(symm.)} & & \\ \frac{-AE}{L} & 0 & 0 & \frac{AE}{L} & & \\ 0 & \frac{-12EI}{L^3} & \frac{-6EI}{L^2} & 0 & \frac{12EI}{L^3} & \\ 0 & \frac{6EI}{L^2} & \frac{2EI}{L} & 0 & \frac{-6EI}{L^2} & \frac{4EI}{L} \end{bmatrix} \tag{3.13}$$

The array variables are:

L = Length of the segment

A = Transformed area of the cross-section

E = Reference Young's Modulus of the material, selected as the initial uniaxial modulus of the segment concrete

I = The moment of inertia of the transformed cross-section about the neutral axis.

The longitudinal strain is computed in each slice or reinforced layer, then the corresponding material modulus E_i is recovered from the stress-strain curves, and finally each slice or discrete area is transformed and summed to give the total transformed area A,

$$A = \underbrace{\sum_{i=1}^{10} n_i A_i}_{\text{concrete}} + \underbrace{\sum_{j=1}^{4} n_j A_j}_{\text{reinforcement}} \quad \text{where} \begin{cases} n_i = E_i/E \\ n_j = (E_j/E) - 1 \end{cases}$$

The location of the neutral axis and the related section I are computed by taking first and second area-moments. Cracked or crushed slices are automatically excluded from these summations to give the reduced section properties. This completes the computation of cross-section properties of a segment to construct the element $[k_g]$.

Variations of strains along the complete frame members causes variations in the transformed properties from segment to segment such that the centroidal axes do not necesarily coincide. The mid-depth axis is taken as the common reference line. Referring to Figure 3-4, let $\{V_r\}$ be displacements at the reference axis, and $\{V_g\}$ be displacements at the centroidal axis.

Let $\{V_g\} = [\lambda]\{V_r\}$ which requires that

$$[\lambda] = \begin{bmatrix} 1 & 0 & -e & 0 & 0 & 0 \\ & 1 & 0 & 0 & 0 & 0 \\ & & 1 & 0 & 0 & 0 \\ & & & 1 & 0 & -e \\ & \text{zero} & & & 1 & 0 \\ & & & & & 1 \end{bmatrix}$$

Eccentricity e is the distance from the reference axis to the centroidal axis.

Segment stiffnesss at the reference axis is then given by

$$[k_r] = [\lambda^T][k_g][\lambda] \qquad (3.14)$$

Now it is necessary to expand from the 6 X 6 array $[k_r]$ related to the median line of each segment, to the 8 X 8 array $[k_o]$ related to the 4 corner nodes, since it is at these nodes that external forces

are applied and internal connections completed for the structural idealization. Consider that

$$\underset{6X1}{\{V_r\}} = \underset{6X8}{[a_{rq}]} \underset{8X1}{\{V_q\}} \tag{3.15}$$

where subscript r relates variables to the median reference axis, subscript q relates them to the corner nodes of the quadrilateral segment, and the displacement transformation $[a_{rq}]$ has terms with dimensions "reference axis displacements per unit node displacement." Introduce a set of virtual displacements $\{\delta V_q\}$ at the nodes so that (omitting brackets)

$$\delta V_r = a_{rq} \delta V_q$$

Let S_r and S_q be the corresponding sets of forces, and equating the virtual work of either system,

$$\delta V_q^T S_q = \delta V_r^T S_r$$

Substituting from above

$$\delta V_q^T S_q = \delta V_q^T a_{rq}^T S_r$$

Since

$$S_r = K_r v_r = k_r a_{rq} V_q$$

Then

$$S_q = a_{rq}^T k_r a_{rq} v_q = k_q v_q$$

with the desired transformation expressed as

$$\underset{8X8}{k_q} = \underset{8X6}{a_{rq}^T} \underset{6X6}{k_r} \underset{6X8}{a_{rq}} \tag{3.16}$$

Using the displacement modes of Figure 3-5, the transformation $[a_{rq}]$ is constructed in the form

$$[a_{rq}]_{6\times 8} = \begin{bmatrix} \frac{1}{2} & 0 & 0 & 0 & 0 & 0 & \frac{1}{2} & 0 \\ 0 & \frac{1}{2} & 0 & 0 & 0 & 0 & 0 & \frac{1}{2} \\ 1/d & 0 & 0 & 0 & 0 & 0 & -1/d & 0 \\ 0 & 0 & \frac{1}{2} & 0 & \frac{1}{2} & 0 & 0 & 0 \\ 0 & 0 & 0 & \frac{1}{2} & 0 & \frac{1}{2} & 0 & 0 \\ 0 & 0 & 1/d & 0 & -1/d & 0 & 0 & 0 \end{bmatrix}$$

A key assumption in this transformation is that the transverse displacement of the median reference axis is the average of the transverse displacements of the two adjacent corner nodes. For this reason, referring to Figure 3-5, the coefficients a_{22}, a_{28}, a_{54}, and a_{56}, have the value $\frac{1}{2}$ and this device permits the corner node transverse displacements to occur independently as is usually implied by the 8 × 8 stiffness array [k]. However, since such independent movements also imply expansion or contraction of the beam segment across its depth, and since rigid body transverse displacement is required in fact, then the corresponding stiffness terms were made very large (multiplied by an arbitrary factor of 200). Consequently the corner nodes and the median axis exhibit equal transverse displacements in the desired fashion.

The direct results of the structural analysis are the node displacements {r}. These are separated into individual vectors {v} for each segment, the cross-section strains are recovered and stresses are computed for the extreme concrete fibers and for the reinforcement layers. These stresses are average values which are constant

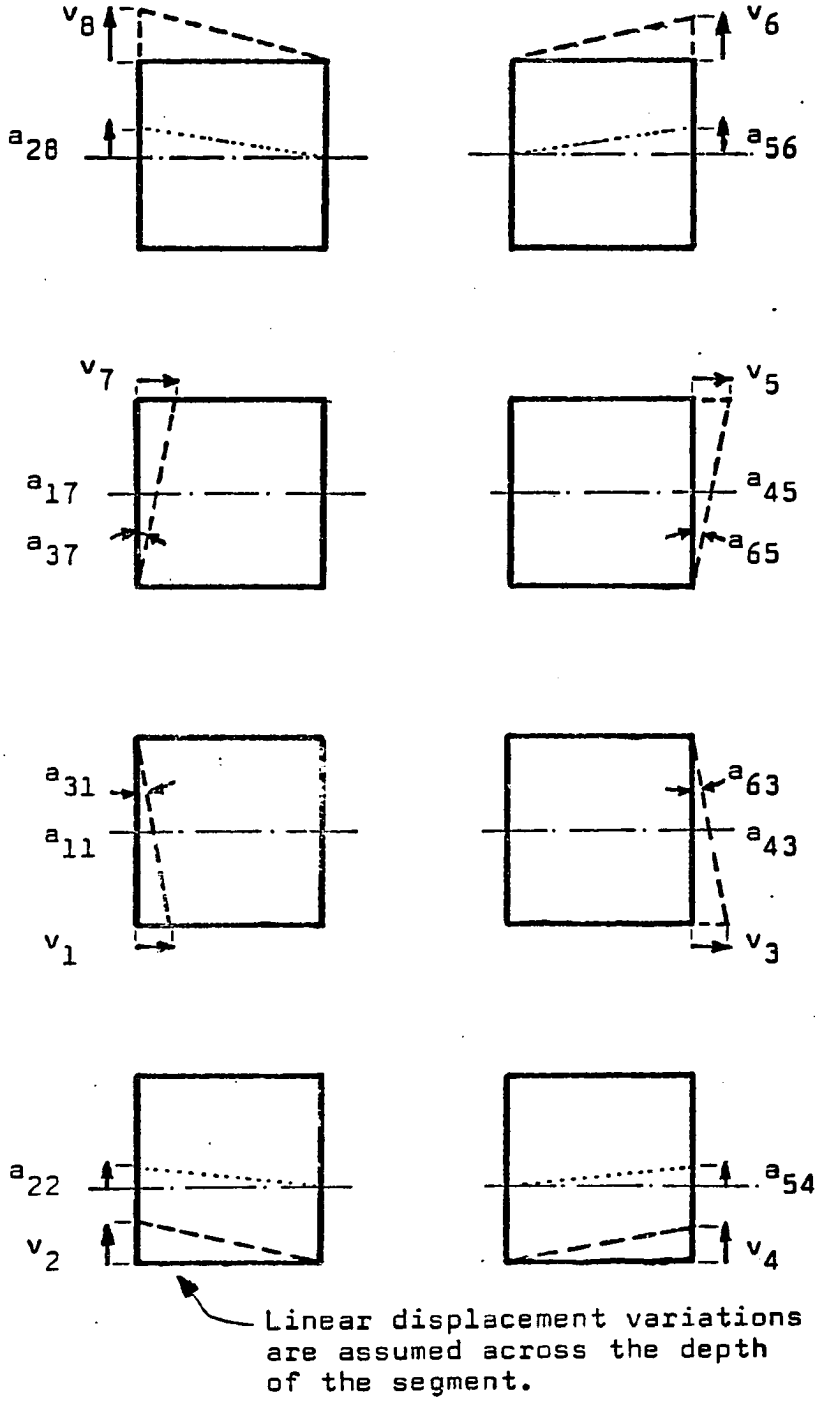

FIGURE 3.5 DISPLACEMENT TRANSFORMATION RELATIONSHIPS.

along the length of the element and which are properly related to the mid-length section of the element for plotting stress variations along the lengths of members. In addition, the axial and shear forces, and moments acting on the segment end faces, at the median axis, are computed and printed. Knowing the distribution of these forces, the load-carrying action of a reinforced concrete member can be examined.

The recovery of the segment end forces can be related to the earlier transformations. The dimensional relationships of the transformation (3.16) using also the basic Eq. (3.15), may be expressed as

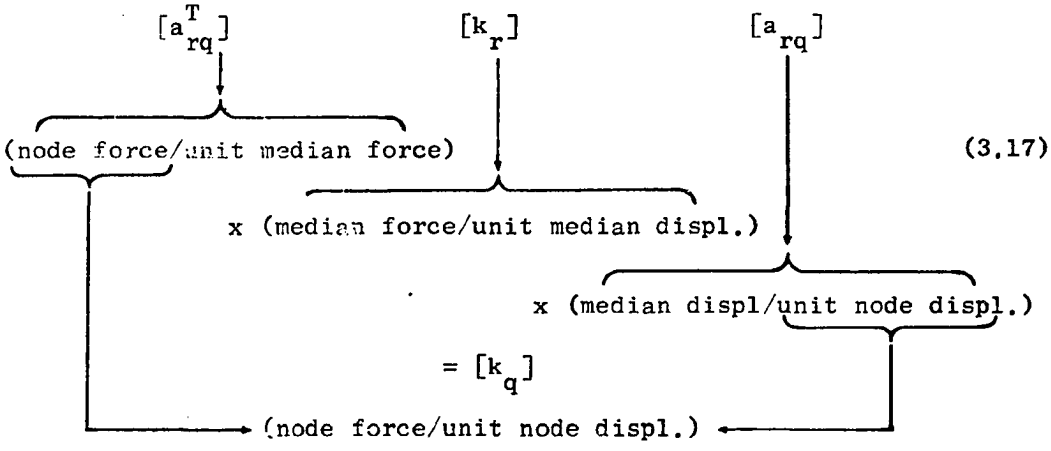

(3.17)

Similarly, if the converse to Eq. (3.15) is taken in the form

$$\underset{8X1}{\{V_q\}} = \underset{8X6}{[b_{qr}]}\ \underset{6X8}{\{V_r\}} \tag{3.18}$$

then the related stiffness transformation is

$$k_r = b^T_{qr}\, k_q\, b_{qr} \tag{3.19}$$

This can then be expressed dimensionally as

$[b_{qr}^T]$ $[k_q]$ $[b_{qr}]$

(median force/unit node force) x (node force/unit node displ.) x (node displ/unit median displ)

= (median force/unit median displ.) = $[k_r]$

Noting the dimensional transformation implied by $[b_{qr}]$ then the required six beam-type forces at the segment end faces are given by

$$\underset{6X1}{\{P\}} = \underset{6X8}{[b_{qr}]^T} \underset{8X1}{\{S\}} \qquad (3.20)$$

The forces $\{P\}$ give the force state existing in frame members. The transformation $[b_{qr}]$ is obtained directly from the unit median displacements by a process similar to Figure 3-5 and has the form

$$[b_{qr}] = \begin{bmatrix} 1 & 0 & \frac{d}{2} & 0 & 0 & 0 \\ 1 & 1 & 0 & 0 & 0 & 0 \\ 0 & 0 & 0 & 1 & 0 & \frac{d}{2} \\ 0 & 0 & 0 & 0 & 1 & 0 \\ 0 & 0 & 0 & 1 & 0 & \frac{-d}{2} \\ 0 & 0 & 0 & 0 & 1 & 0 \\ 1 & 0 & \frac{-d}{2} & 0 & 0 & 0 \\ 0 & 1 & 0 & 0 & 0 & 0 \end{bmatrix}$$

Having obtained $[b_{qr}]$ then the median forces are obtained by expanding Eq. (3.20) to give

$$\underset{6X1}{\{P\}} = \underset{6X8}{[b_{qr}]^T}\ \underset{8X8}{[k]}\ \underset{8X1}{\{V\}} \qquad (3.21)$$

3.3 One-Dimensional Rod Elements

Figure 3-6 shows representations of the one-dimensional rod element with degrees of freedom shown in both coordinate systems. This element can be used either to represent a reinforcement between selected nodes in a two-dimensional structure, or to model an individual pin-joined structural member as in a truss. The axis of the element may be at some orientation θ relative to the global system. In the element coordinate system, the force-displacement relations may be expressed as $\{F\} = [k_e]\ \{u\}$ which expands as

$$\begin{Bmatrix} F_1 \\ F_2 \end{Bmatrix} = \frac{AE}{L} \begin{bmatrix} 1 & -1 \\ -1 & 1 \end{bmatrix} \begin{Bmatrix} u_1 \\ u_2 \end{Bmatrix} \qquad (3.22)$$

Using the basic displacement transformation $\{u\} = [\lambda]\ \{V\}$ to relate the generalized coordinates of both systems, the desired stiffness transformation is obtained,

$$[k] = [\lambda^T]\ [k_e]\ [\lambda].$$

For this element, the transformation $[\lambda]$ is constructed as follows, using $C = \cos\theta$ and $S = \sin\theta$ for convenience,

$$\begin{Bmatrix} u_1 \\ u_2 \end{Bmatrix} = \begin{bmatrix} C & S & 0 & 0 \\ 0 & 0 & C & S \end{bmatrix} \begin{Bmatrix} v_1 \\ v_2 \\ v_3 \\ v_4 \end{Bmatrix}$$

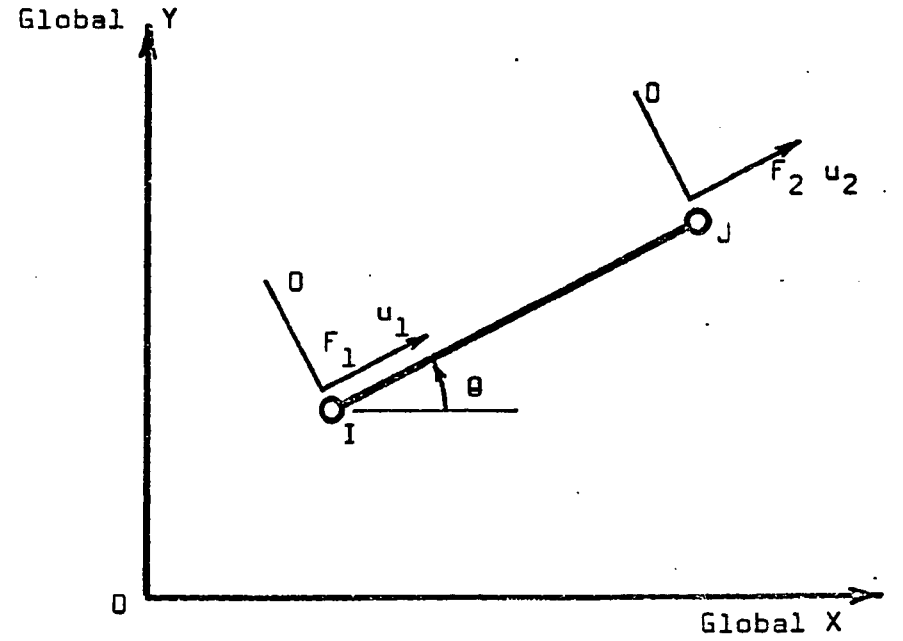

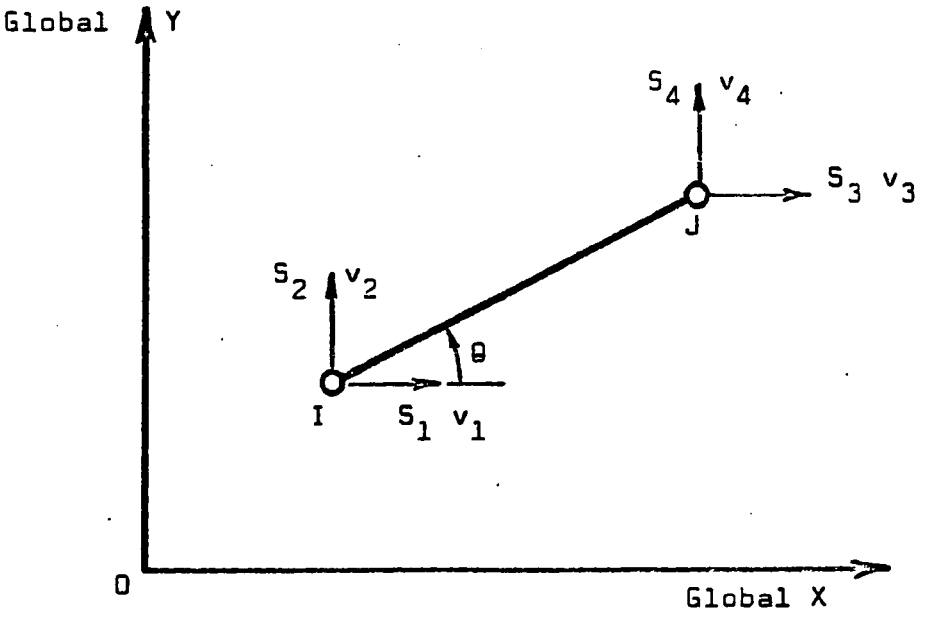

FIGURE 3.6 ROD ELEMENT GENERALIZED COORDINATES.

From this the stiffness in a global system is

$$[k] = \frac{AE}{L}\begin{bmatrix} C & 0 \\ S & 0 \\ 0 & C \\ 0 & S \end{bmatrix}\begin{bmatrix} 1 & -1 \\ -1 & 1 \end{bmatrix}\begin{bmatrix} C & S & 0 & 0 \\ 0 & 0 & C & S \end{bmatrix}$$

Finally,

$$[k] = \frac{AE}{L}\begin{bmatrix} C^2 & CS & -C^2 & -CS \\ CS & S^2 & -CS & -S^2 \\ -C^2 & -CS & C^2 & CS \\ -CS & -S^2 & CS & S^2 \end{bmatrix} \qquad (3.23)$$

4X4 4X4

The material properties are included by means of the value selected for modulus E at any stage of the analysis. The final stress state of the element is recovered by first determining element $\{u\}$ from the node displacements $\{v\}$, then computing the rod axial strain $e = \frac{1}{L}(u_2 - u_1)$, and finally converting to stress from the element stress-strain relationship.

3.4 Tie Link Elements

Figure 3-7 shows the arrangement of the artificial node connections called tie links. Such a linkage was developed (8,9) to allow for a slip relationship between two originally coincident nodes. This was done by establishing two orthogonal "springs" to connect the node-pair. This special linkage may be oriented at some angle θ relative to the global system according to the specification of the analyst, just as in the case of previous discrete elements. The necessary global stiffness [k] may be developed as follows. Construct

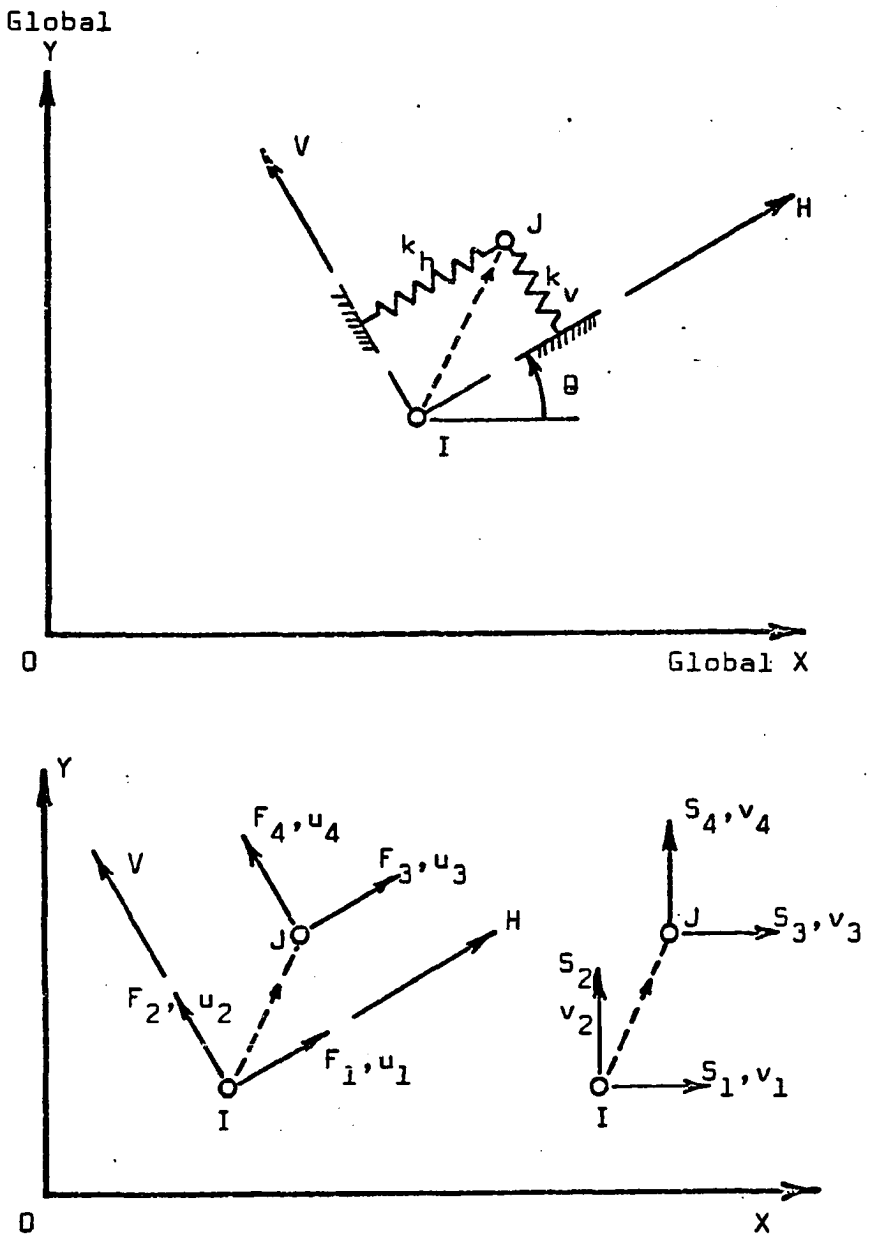

FIGURE 3.7 GENERALIZED COORDINATES FOR TIELINKS.

the force-displacement equations in the element coordinate system, $\{F\} = [k_e]\{u\}$, which then appear as

$$\begin{Bmatrix} F_1 \\ F_2 \\ F_3 \\ F_4 \end{Bmatrix} = \begin{bmatrix} k_h & 0 & -k_h & 0 \\ 0 & k_v & 0 & -k_v \\ -k_h & 0 & k_h & 0 \\ 0 & -k_v & 0 & k_v \end{bmatrix} \begin{Bmatrix} u_1 \\ u_2 \\ u_3 \\ u_4 \end{Bmatrix} \tag{3.24}$$

Next derive the displacement transformation in the form $\{u\} = [\lambda]\{v\}$, using $C = \cos\theta$ and $S = \sin\theta$,

$$\begin{Bmatrix} u_1 \\ u_2 \\ u_3 \\ u_4 \end{Bmatrix} = \begin{bmatrix} C & S & 0 & 0 \\ -S & C & 0 & 0 \\ 0 & 0 & C & S \\ 0 & 0 & -S & C \end{bmatrix} \begin{Bmatrix} v_1 \\ v_2 \\ v_3 \\ v_4 \end{Bmatrix} \tag{3.25}$$

This relationship is then used for the stiffness transformation $[k] = [\lambda^T][k_e][\lambda]$, thus

$$[k] = \begin{bmatrix} C & -S & 0 & 0 \\ S & C & 0 & 0 \\ 0 & 0 & C & -S \\ 0 & 0 & S & C \end{bmatrix} \begin{bmatrix} k_h & 0 & -k_h & 0 \\ 0 & k_v & 0 & -k_v \\ -k_h & 0 & k_h & 0 \\ 0 & -k_v & 0 & k_v \end{bmatrix} \begin{bmatrix} C & S & 0 & 0 \\ -S & C & 0 & 0 \\ 0 & 0 & C & S \\ 0 & 0 & -S & C \end{bmatrix}$$

By using some further symbols for the terms,

$$k_h C^2 + k_v S^2 = A$$

$$(k_h - k_v)\, CS = B$$

$$k_h S^2 + k_v C^2 = D$$

then

$$[k] = \begin{bmatrix} A & B & -A & -B \\ B & D & -B & -D \\ -A & -B & A & B \\ -B & -D & B & D \end{bmatrix} \tag{3.26}$$

The forces in the element coordinates that act to connect a node-pair may be recovered by applying a modification of Eq. (3.24) in the form:

$$\begin{Bmatrix} F_1 \\ F_2 \end{Bmatrix} = \begin{bmatrix} k_h & 0 \\ 0 & k_v \end{bmatrix} \begin{Bmatrix} u_1 - u_3 \\ u_2 - u_4 \end{Bmatrix}$$

2X1 2X2 2X1

This is developed further by using Eq. (3.25) in the new form

$$\begin{Bmatrix} u_1 - u_3 \\ u_2 - u_4 \end{Bmatrix} = \begin{bmatrix} C & S \\ -S & C \end{bmatrix} \begin{Bmatrix} v_1 - v_3 \\ v_2 - v_4 \end{Bmatrix}$$

which finally gives,

$$\begin{Bmatrix} F_1 \\ F_2 \end{Bmatrix} = \begin{bmatrix} k_h & 0 \\ 0 & k_v \end{bmatrix} \begin{bmatrix} C & S \\ -S & C \end{bmatrix} \begin{Bmatrix} v_1 - v_3 \\ v_2 - v_4 \end{Bmatrix}$$

To study the static equilibrium of a selected free-body portion of a structure it is often desirable to have the linkage forces related to the global system. This is done by using a condensed version of Eq. (3.26) to give

$$\begin{Bmatrix} S_1 \\ S_2 \end{Bmatrix} = \begin{bmatrix} A & B \\ B & D \end{bmatrix} \begin{Bmatrix} v_1 - v_3 \\ v_2 - v_4 \end{Bmatrix}$$

These equations have been developed for arbitrary spring stiffnesses. In order to specialize the linkage to act as a tie link and rigidly lock a node-pair together, the values k_h and k_v are set very large. Conversely, the links are released by setting these to zero. In this manner, shear panels may be disconnected from adjacent frame members when necessary.

4. NONLINEAR STRUCTURAL ANALYSIS

4.1 Sources of Nonlinear Behavior

Several factors that contribute to nonlinear structural behavior may be readily identified and will be briefly discussed in the following categories:

(a) nonlinear materials,

(b) geometric effects of the structure, and

(c) variable boundary conditions.

After discussing these items then the basic analytical procedures used in this research investigation will be developed and explained.

4.1.1 Nonlinear Materials

A major source of nonlinearity in many problems is simply the existence of a nonlinear material constitutive law. Many engineering materials in widespread use today have nonlinear stress-strain laws when loaded to failure. Some common examples of this are concrete (nonlinear inelastic), rubber (nonlinear elastic), and mild steel (elasto-plastic with strain hardening). In addition, the material laws may be influenced by shrinkage or viscoelastic behavior. These factors might suggest that nonlinear behavior is the rule rather than the exception, but in fact most materials are adequately described by Hookean relationships at the lower, working stress levels selected for design. Sometimes total structural behavior needs to be analyzed for situations involving loads and deformations that cause the structure to operate at stress levels well above the linear design stress values. Such a demand is typical of research situations and may also be created by the need to validate significant design

features. Under these circumstances, the complete nonlinear stress-strain laws are fundamental to an accurate analysis.

The internal stress field of an element is sometimes amplified into the nonlinear range of behavior by the presence of holes or notches. This may cause nonlinear response of the structural member even though the external loads are not greatly extended above design magnitudes. Again, the complete nonlinear stress-strain law becomes a very desirable feature of an analysis.

Since it was the intent of this research to consider structures loaded to near failure, then it was clearly necessary to try to represent the complete stress-strain law of each material.

4.1.2 Geometry Changes

Another source of nonlinear behavior found in some structures may be classified as geometric effects. Essentially this means that when deflections of the structure are sufficiently large then the linear equilibrium equations are no longer valid and need to be adjusted. This effect usually occurs in analytical procedures in either of two places--in the force-displacement equations, when additional internal forces are generated because of the deflected geometry (beam-columns and flexible arches), and in the strain-displacement equations, when certain, otherwise negligible, strain terms have to now be included because of the relatively large deformations (general plate and shell theory). It has already been noted that this research is concerned with structures that may be loaded to near failure. This suggests that large deformations may occur in the structural system. Such deflections are easily generated in laboratory models and have

been observed in actual buildings after the occurrence of severe earthquakes. The large deflections can cause force amplifications to occur in some frame members, but in this research no special methods were included to account for this kind of nonlinearity.

4.1.3 Variable Boundary Conditions

Changes in the external boundary conditions can be another source of nonlinear behavior, as demonstrated by the classic problem of a loaded beam sitting on an elastic, no-tension foundation. The size and location of the beam-to-foundation contact zones depend on the nature of the applied loading. This causes the nonlinear response.

In general, the external boundary conditions describe the nature of the element-to-foundation connectivity and likewise the internal element-to-element connectivity may be regarded as the internal boundary conditions. Both sets of conditions can influence the magnitude and assembly of the system stiffness array. Connectivity changes that are caused by the external loading will give a nonlinear system response even if all the structural elements remain linear.

When a reinforced concrete structure is loaded to failure it is reasonable to expect that complete elements may be destroyed and should be removed from the system, or that cracking may cause separation, disconnection, of adjacent elements, or that cracking can directly separate the structure from the rigid base of reference in some places. This meant that this kind of behavior had to be recognized in the analytical procedure in a suitable manner.

4.2 The Nature of Topological Changes

The structural topology in a problem is described by that set of parameters that define the force-displacement relationships of the structure. Changes in the topology are caused by (a) changes in the element stiffnesses, or the magnitudes of the terms that go into the global $[K_{xy}]$, (b) changes in the internal connectivity between elements, hence the way in which element stiffnesses are superimposed in the global array, and (c) changes in the external boundary conditions which will affect the way in which the global $[K_{xy}]$ is modified before solution.

During the course of monotonic loading of the structure, without failures beginning, the system stiffness topology may be thought of as a slowly changing n-dimensional surface. The changes may be due either to reductions of element stiffnesses as higher strains correspond to reduced material moduli, or to the propagation of existing cracks in flexural type members. Superimposed on this picture of a gradually changing surface some localized discontinuities occur, produced by the initiation of cracks or fractures and releases occurring between elements when, for instance, linkages fail. Another cause of sudden changes in the stiffness topology is the presence of abrupt changes in the material constitutive law, such as happens at the yield point of mild steel when a specimen is first loaded.

When the stiffness topology is gradually changing with load then the process of applying the external loads in a sequence of increments and solving a set of linear structures is the best analytical approach. Since failures cause sudden changes in the topology then

it is essential to make some attempt to allow these changes to occur in proper succession. This is to help the system to adjust in the correct manner. The incremental approach is very important from the point of view of providing some isolation for successive failures. In order to establish the equilibrium of the system within each load increment and satisfy the stress-strain laws, then the solution should be repeated when required. These iterations are performed while the external load increment is kept constant. The entire process is called incremental iteration and will now be developed in more detail.

4.3 The Incremental Iteration Method

General methods of nonlinear analysis have been developed and demonstrated in several papers (1,11,14,15,17) for problems that involve nonlinear effects due to stress-strain laws, thermal changes, viscoelasticity, large deformations, and the development of unstable equilibrium states.

In general a complete procedure recognizes that total strains $\{e\}$ may be due to several causes, thus

$$\{e\} = \{e\}_E + \{e\}_p + \{e\}_t$$

where the subscripts represent the cases

E for the compliance strains,

p for the plastic and viscoelastic strains,

and t for the thermal strains.

The usual transformations are applied to $\{e\}_E$ to develop the force-displacement coefficients [k], and then equivalent nodal forces are derived from the remaining strain terms, assuming that the nodes are fixed. This gives the equations

$$\{R\}_L = [K]\{r\} + \{R\}_p + \{R\}_t$$

Subscript L is used for the external applied loads. It may also be shown (5,16,17) that where an incremental solution is proposed when stresses are present at the beginning of the increment, then the system stiffness [K] should properly be regarded as having the form $[K] = [K]_M + [K]_G$. The array $[K]_M$ is the stiffness derived from the material properties and using the linear strain-displacement equations, while $[K]_G$ is a correction stiffness array related to the non-linear strain-displacement terms only and independent of the material properties. This last array is called either the geometric stiffness, or incremental stiffness, or initial stress stiffness. This modification gives the general equations in the form

$$\{R\}_L = [K_M + K_G]\{r\} + \{R\}_p + \{R\}_t$$

In this work the element stiffnesses are derived on the basis of infinitesimal strain theory and so $[K]_G$ is assumed to be identically zero. Omitting the remaining subscript on [K] the basic form to be used is

$$\{R\}_L = [K]\{r\} + \{R\}_p + \{R\}_t$$

Usually the incremental method is favored for solution of these equations since it allows better definition of the pseudo-load vectors $\{R\}_p$ and $\{R\}_t$. In this research these particular forms are not included since no thermal effects or plasticity theory are utilized. However, a rather similar term occurs because of the changes that occur in the system due to fractures and failures. This is discussed in Section 4.3.3 later.

4.3.1 The Incrementing Process

During this basic part of the analysis a solution of the equations $R_L = K\ r$ (now omitting the brackets for convenience) is obtained in the form of a series of linear subsystems. Thus,

$$R_1 = K_1\ r_1$$

$$R_2 = K_2\ r_2$$

$$\vdots$$

$$R_n = K_n\ r_n$$

so that finally the increments are summed to give total system displacements.

$$\sum_{i=1}^{n} R_i = R_L \quad \text{and} \quad \sum_{i=1}^{n} r_i = r$$

The process is shown in Figure 4-1 where it should be noted that secant values of stiffness are used rather than tangent values. The stiffness is improved within each increment by iteration, but it is not practical to apply unlimited iterations to achieve near-perfect values for K_i. The truncation of the iteration within a particular increment requires that the deviation of the system from true equilibrium be accounted for in some suitable manner. If the increment has been solved using an incremental stiffness K_i over the last iteration cycle, and if re-evaluation now gives K_i^* as the true value, then for nodes fixed against motion,

$$R_i = K_i\ r_i = K_i^*\ r_i + R_i^*$$

The vector of unbalanced nodal forces R_i^* is a measure of the accuracy

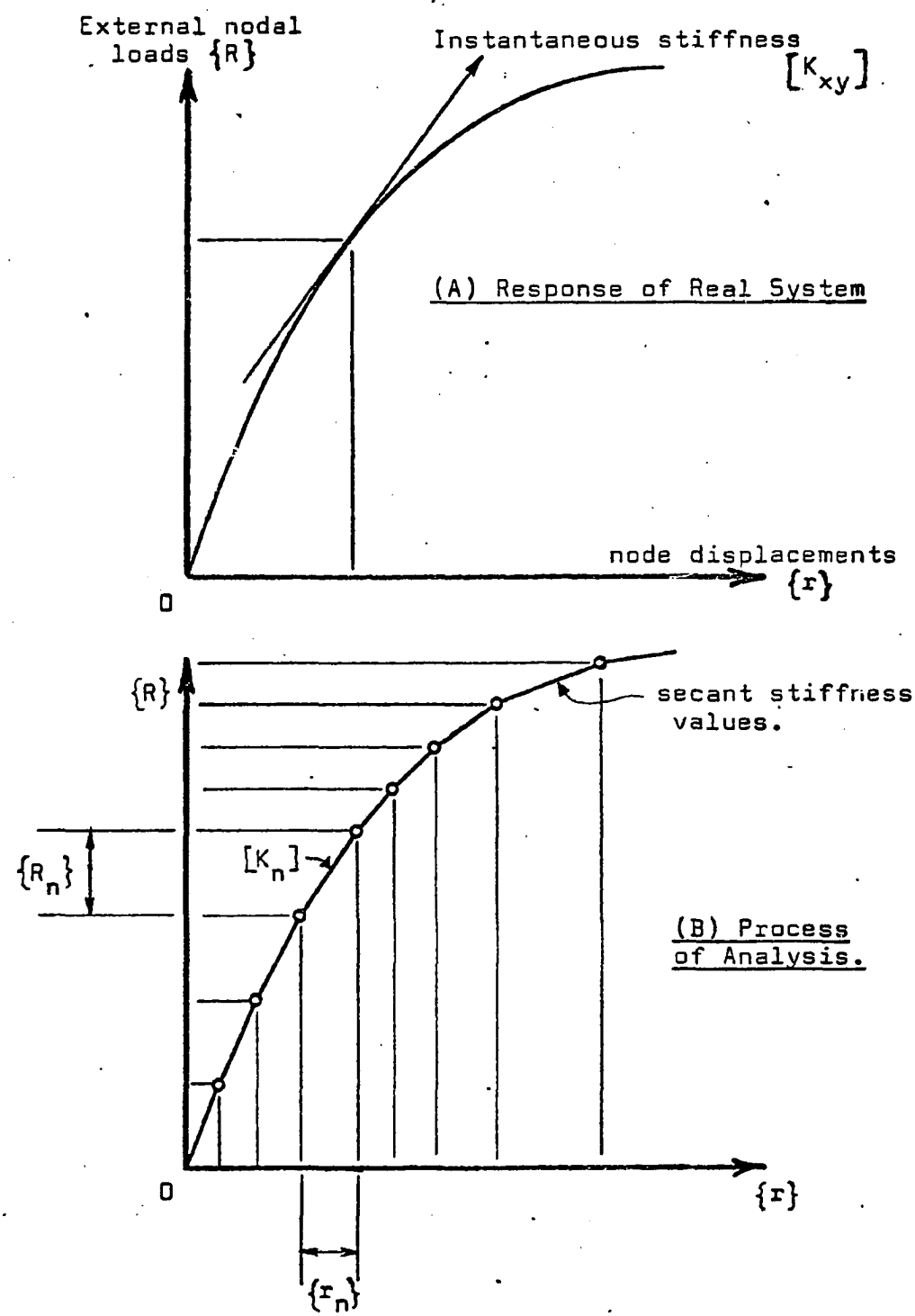

FIGURE 4.1 THE INCREMENTAL SOLUTION METHOD.

of the solution at any stage and is given by

$$R_i^* = (K_i - K_i^*)\, r_i$$

The bracket term may be regarded as a residual stiffness change. Clearly, R_i^* occurs only because of these small residual changes, and is routinely calculated during the analysis. This gives a visual measure of the accuracy of the solution at any stage and the vector is incorporated into the calculating process in order to reduce accrual of truncation errors and to ensure the satisfaction of equilibrium at all times. The incrementing process thus takes the following form:

$$\begin{aligned}
R_1 &= K_1 r_1 = K_1^* r_1 + R_1^* \\
R_2 + R_1^* &= K_2 r_2 = K_2^* r_2 + R_2^* \\
R_3 + R_2^* &= K_3 r_3 = K_3^* r_3 + R_3^* \\
&\vdots \\
R_n + R_{n-1}^* &= K_n r_n = K_n^* r_n + R_n^*
\end{aligned}$$

This finally gives summations of the form

$$\sum_1^n R_i + \sum_1^{n-1} R_i^* = Q \sum_1^n r_i + \sum_1^n R_i^*$$

or $R_L = Q\, r + R_n^*$ where Q is a symbolic stiffness transformation since the K_i cannot be summed. Equilibrium is identically satisfied in this array and the deviation from the specified loading R_L is given by the unbalanced forces R_n^* of the final increment alone. However, in systems that are very path-dependent, the accuracy of

the final set of nodal displacements depends on having each R_i^* as small as possible. Figure 4.2 illustrates the incrementing process including the vectors R_i^* being used for system corrections.

4.3.2 The Iteration Process

The correct secant stiffness for an increment i may not be evaluated until the increment deflection r_i is known. To start the solution of the first increment the initial K_1 is taken from input data values. To begin each subsequent increment, K_1 is taken as the final stiffness K_{i-1} from the previous increment. The first set of displacements r_1 gives the interval limits over which an improved secant stiffness K_2 is computed, and the solution may be iterated until initial and final K arrays vary within some preset tolerance. The change of stiffness for any element is determined from the material modulus E over the corresponding strain increment. The relationships between global stiffness K, element stiffness k, and material stiffness E are shown by the diagrams of Figure 4.3 for iterations within a given increment.

Iteration control is actually based on a % tolerance for successive material E values. Typically, when these values vary less than 3% then the derived material secant modulus is regarded as a 'converged' value. Thus even when the analysis signals convergence for all the material properties, there can still be some truncation with regard to precise convergence (satisfying an equivalent 0% tolerance). The inclusion of the out-of-balance force vector R^* is still important to account for slight residual changes in the 'converged' system.

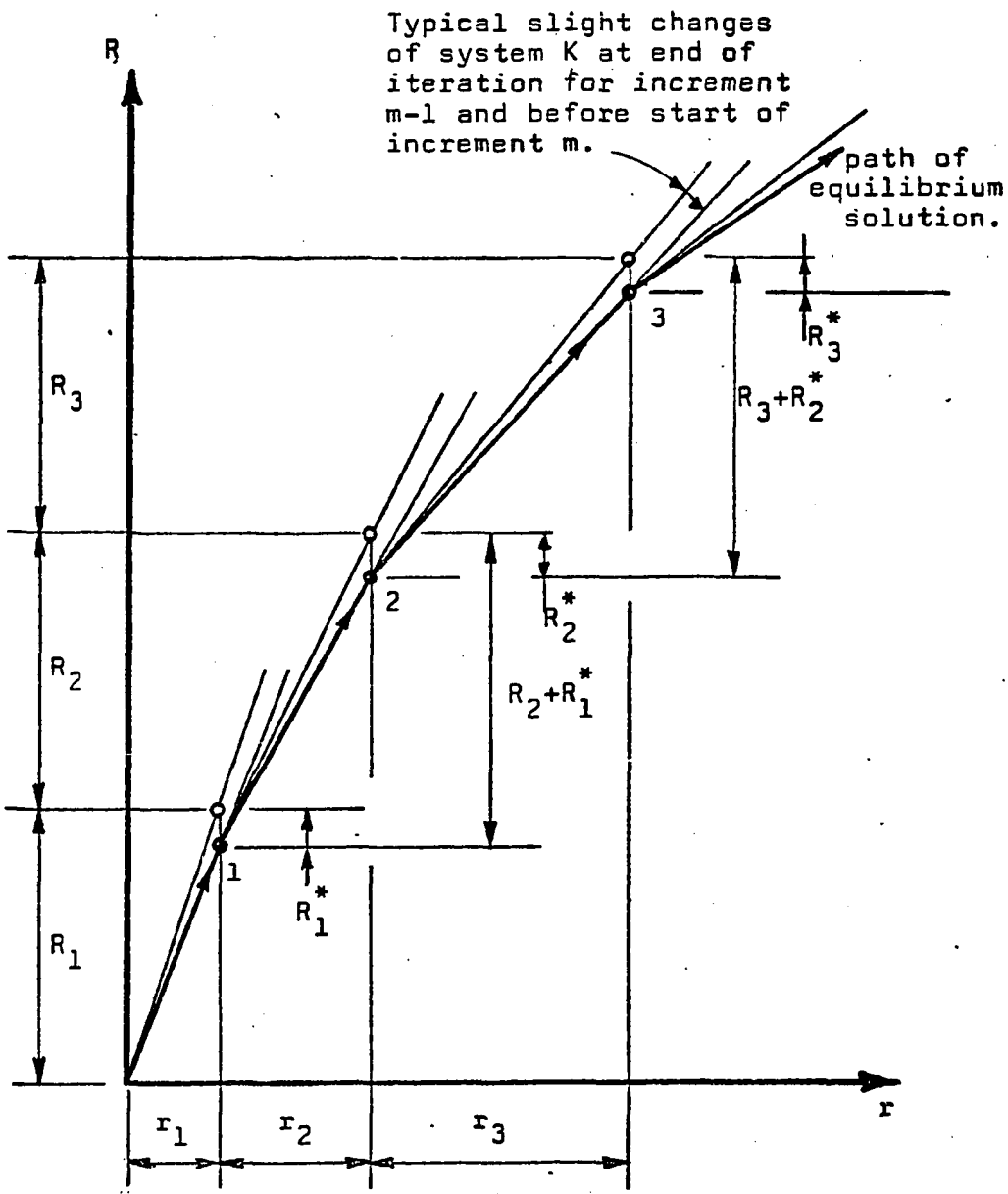

FIGURE 4.2 ADJUSTMENTS FOR EQUILIBRIUM.

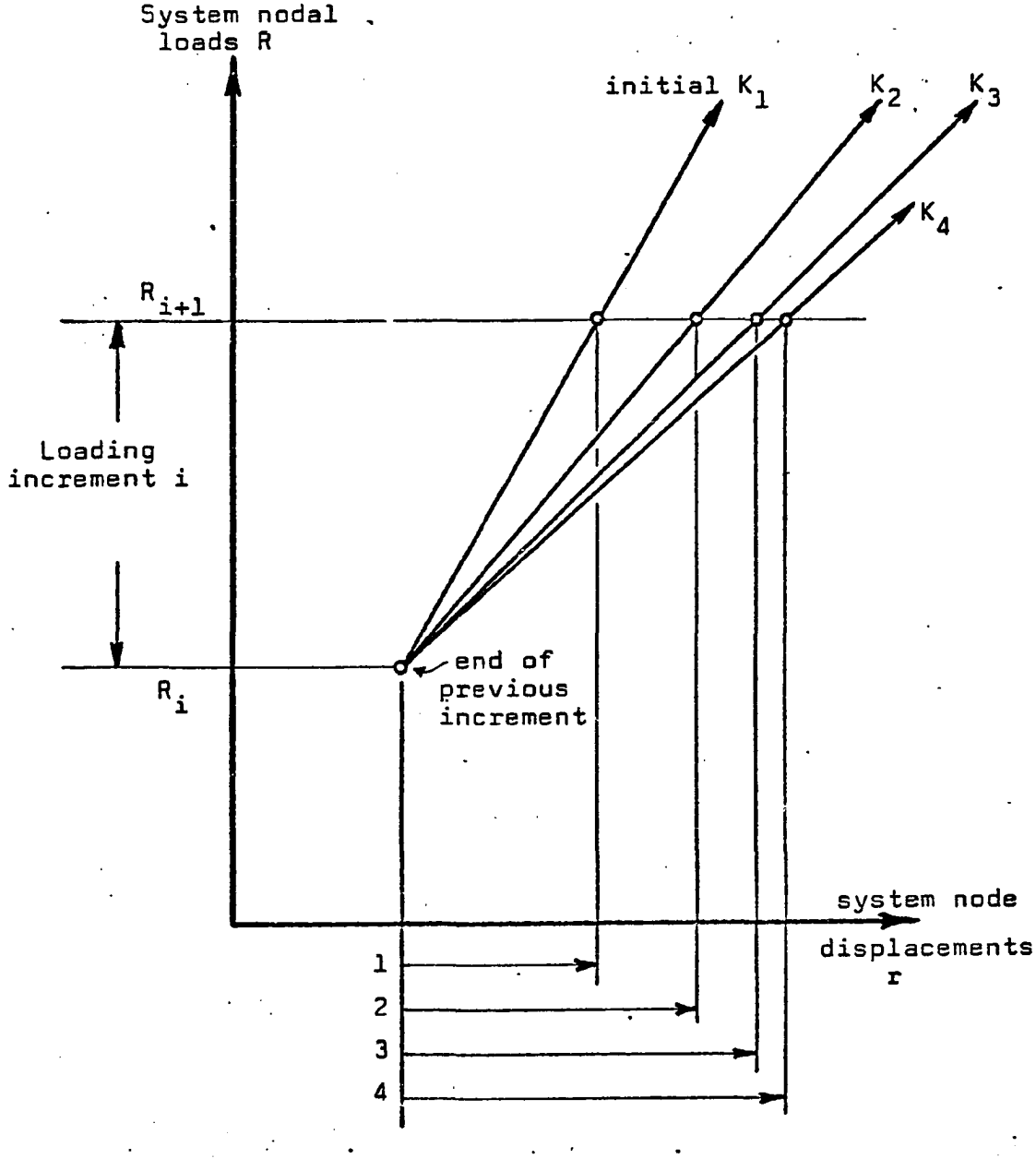

FIGURE 4.3 (A) SYSTEM CHANGES WHILE ITERATING.

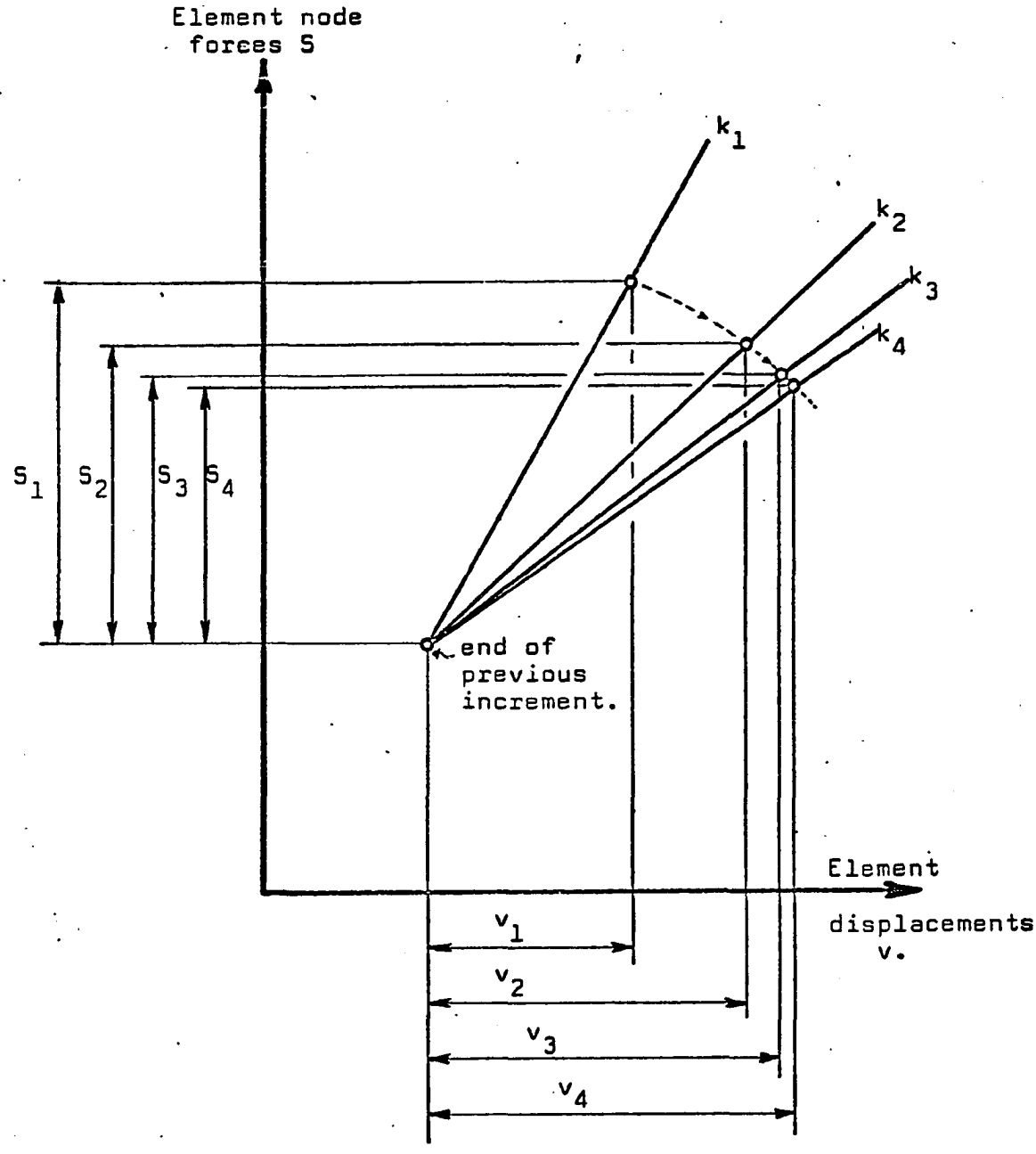

FIGURE 4.3 (B) ELEMENT CHANGES DURING ITERATION.

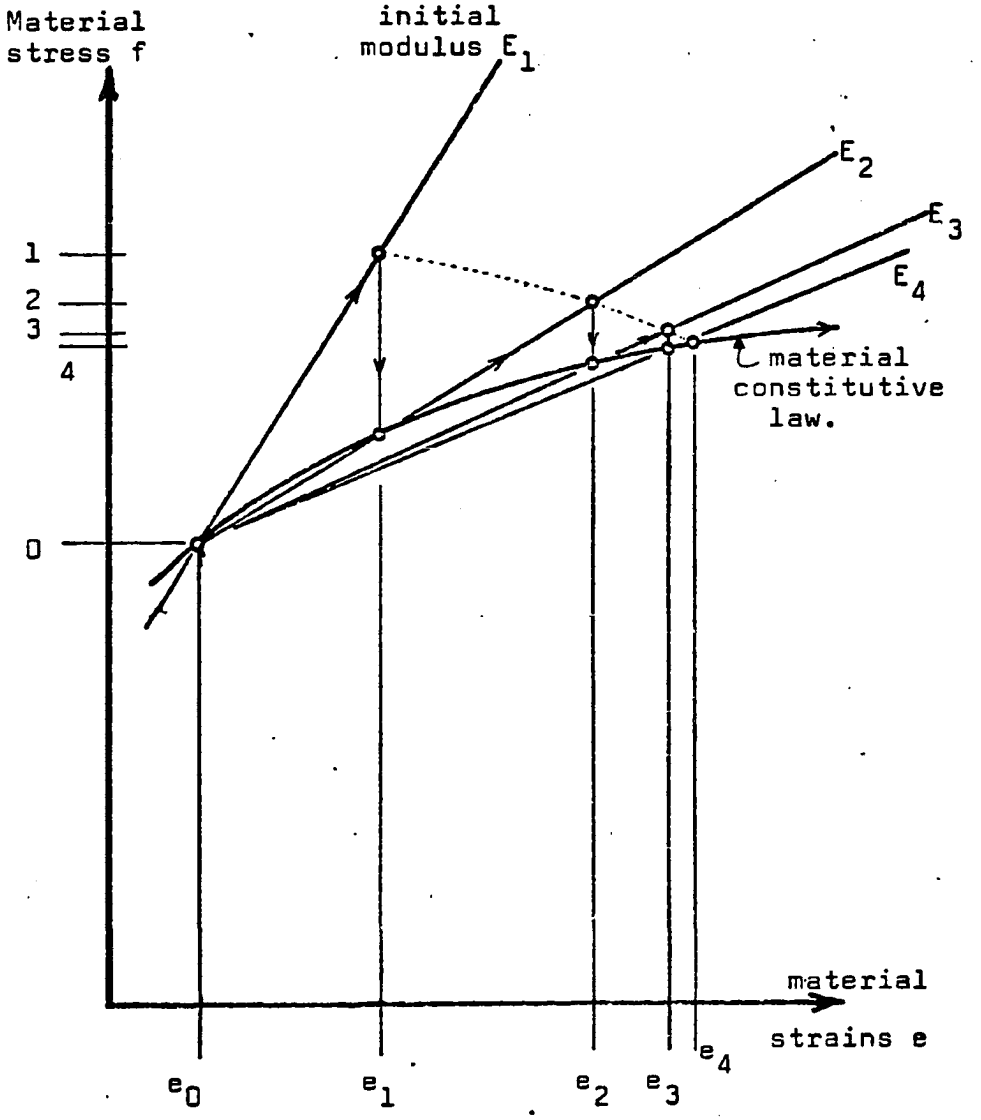

FIGURE 4.3 (C) CHANGE OF MODULUS DURING ITERATION.

Another possibility for iteration control is to use some function of the nodal deflections, but this was not thought to be as meaningful as a control based on changes in material properties. However, to provide another check of the system convergence, the increment deflections r_i at the end of cycle i are compared with the earlier values,

$$r_i - r_{i-1} = dr_i \text{ , where } \lim_{i \to \infty} (dr_i) = 0.$$

A measure of the changes that have occurred is then given by the Euclidean norm of dr_i,

$$\text{Norm} = (dr_i^T \, dr_i)^{\frac{1}{2}}$$

and this number is printed out in the computer program for information purposes.

4.3.3 The Influence of Fracturing

The fracture of an element produces two effects of importance to the analysis. These are (a) the sudden occurrence of partial or total loss of element stiffness and (b) an inability to carry some or all of the presently imposed loads.

The purpose of iteration within each increment is to adjust the system response to changes of stiffness and so this aspect of fracture is simply an event that disturbs the convergence rate of the iteration process. This then needs no further special treatment. When rod or linkage elements fracture to give open cracks, then the element k becomes zero, but fracture of a quadrilateral element, or of a few slices of a frame element, or linkage fracture that gives a closed crack, then such actions will give a partial loss of stiff-

ness.

The key aspect of fracture is the process of unloading an element and redistributing some or all of the strain energy into the surrounding system. Consider that fracture occurs for an element during the iteration of increment m. After the previous m-1 increments consider that the total nodal forces and total nodal deflections of this element are given by S_1 and v_1, achieved along some nonlinear path as seen in Figure 4.4. Fracture now causes a new element stiffness k_2 and, for fixed nodes, a new set of nodal forces S_2 correspond to equilibrium of this element,

$$S_2 = k_2 v_1 \neq S_1$$

The self-equilibrating release forces at the nodes are given by the unbalance forces,

$$S_F = S_1 - k_2 v_1$$

and if k_2 is zero then the equation represents the necessary total release of strain energy. For k_2 not zero, then partial release occurs. These element fracture forces S_F are combined to give the self-equilibrating set R_F which appears as an extra external loading. The basic equations for the solution of this increment now take the form

$$(R_L + R_F)_m = (K_F r)_m$$

and the iterations continue until convergence occurs.

The solution of the system when several successive fractures occur is shown in Figure 4.5, assuming an otherwise linear

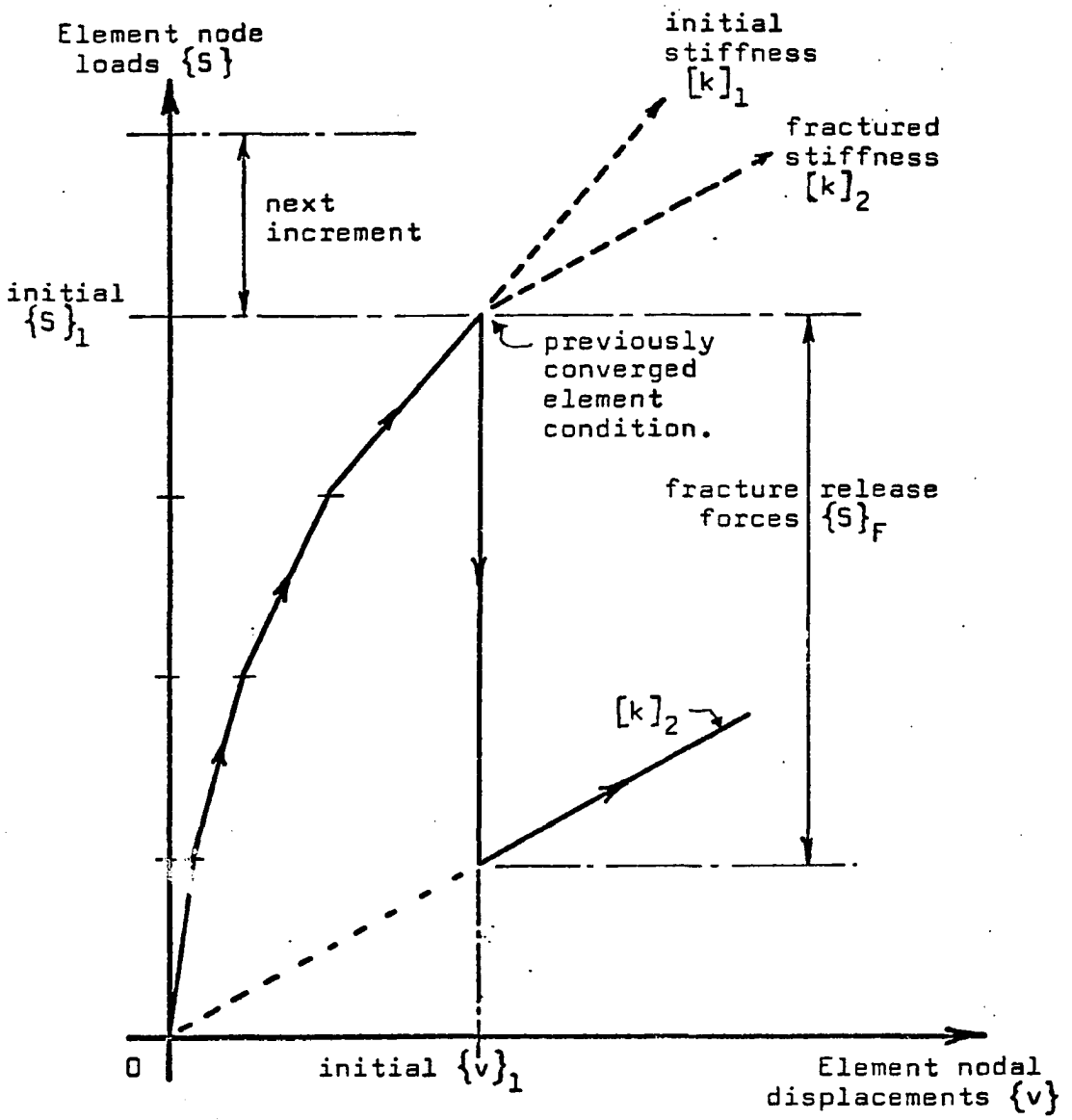

FIGURE 4.4 FRACTURE ADJUSTMENT OF ELEMENT FORCES.

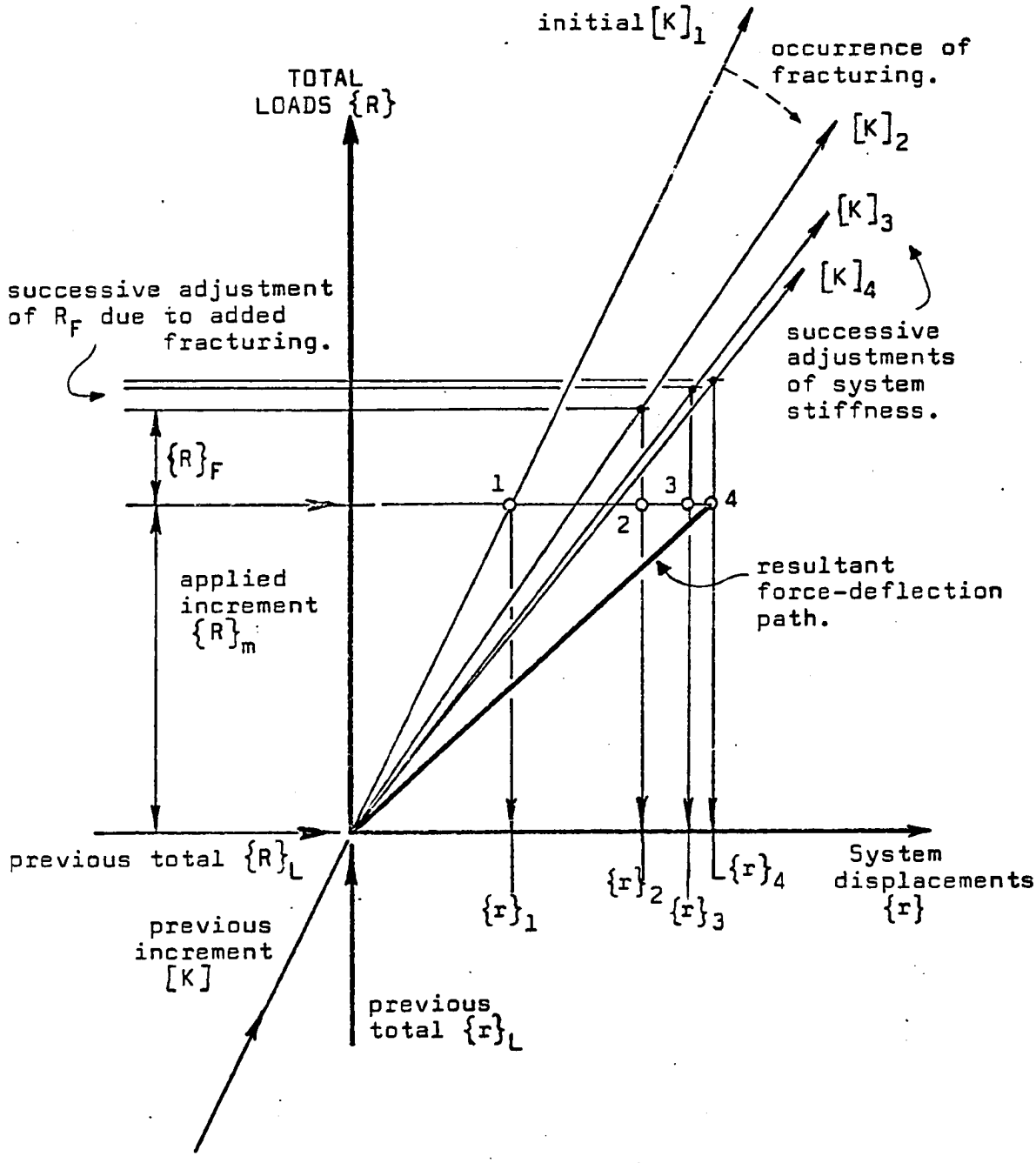

FIGURE 4.5 ITERATING THE FRACTURING SYSTEM.

behavior for clarity. Each fracture gives a typical reduction of system stiffness K and simultaneously provides an addition to the total set of fracture loads R_F. Iteration is essential for attaining a stable equilibrium position, however, small increments of external load will isolate potential fractures (and their locally abrupt stiffness changes) in a way more closely modelling the true behavior of the system. This enhances the stability of the iterations. Conversely, a single large load increment may encompass so many element fractures (which normally would not occur together, but which appear to do so in the computations) that the analysis can exhibit iterative instability, and oscillations or divergence can occur. This is easily identified by the analyst and changes can be made to the input data.

Fracture loads are not carried over to later increments. Each fracture vector R_F is uniquely related to the solution of the equilibrium of the fracturing system for a given increment. At the beginning of each increment the fracture loads are zero and the incrementing process with fracture has the following typical sequence,

$$R_1 + 0 = K_1 r_1 \quad \text{(no fracture)}$$
$$R_2 + 0 = K_2 r_2 \quad \text{(no fracture)}$$
$$R_3 + R_{F3} = K_3 r_3 \quad \text{(fractures begin)}$$
$$\vdots \quad \vdots \quad \vdots \quad \vdots$$
$$R_n + R_{Fn} = K_n r_n$$

This sequence shows that fractures do not occur during the first two load increments. When load increment R_3 is applied then fracturing

occurs which produces a set of release forces R_{F3} at some of the nodes. Iterations for this load increment may produce changes in R_{F3} which stabilize for convergence. The set of increment deflections r_3 correspond to the external load increment R_3 and are added to the earlier deflections to give the total deflections. In the next load increment a new fracture load vector R_{F4} will be included with the increment loading R_4 only if element fractures occur. All load increments are treated in this manner until the solution is completed.

5. MATERIAL PROPERTIES AND FAILURE

In this work, the direct result of any analysis of a structure is a vector of nodal point displacements which may be converted directly into strains in the elements that connect the nodes. The simplest of these conversions is for an axial force rod element. The relative axial displacement between the two end nodes gives the change in length of the element and the axial strain is obtained by knowing the distance between those nodes. The most complex conversion is for the quadrilateral plane stress elements which utilizes a strain-displacement transformation array to operate on the 8 nodal displacements of a selected element to give the 3 strain components at the center node location of that element. The general procedure is thus to enter the stress-strain law of the material with knowledge of the strains in order to derive both a value of stress and a value of the secant modulus or stiffness.

The complete stress-strain description of each material is used in this work. A question that occurred early in the development phase was whether to use functional descriptions of stress-strain laws or to use multilinear descriptions. A curve-fit relationship for the data from tests of some steels may be feasible but is impractical for mild steels which have a yield region followed by a period of strain-hardening. A curve-fit relationship has been suggested by Saenz (26) that is suitable for describing concrete under compressive stress, while the tensile stress-strain behavior is generally ignored for concrete. The functional description for the materials was not considered further and the

multilinear stress-strain curve was used as the basic material description. Thus specific data that was available for any material could be used and any discontinuities in the behavior would be included. Examples of the multilinear descriptions are given in Figures 5.1 and 5.2. Each curve is given by a set of 9 pairs of values, one stress and one strain per point, while the Poisson Ratio is assumed to be constant for each material over the complete range of material behavior (equal to the value that is initially input for that material).

The structural behavior of concrete is not easily given in simple terms. Concrete is made from a group of materials of widely differing properties, each of which imparts some influence on the mixture. Temperature, age of the mix, duration of loading, and speed of load application all have an effect on the stress-strain curves and indeed this suggests that the constitutive law is likely to be a constantly changing relationship during the life of a concrete structure (27). In this work the effects of temperature and creep under sustained loads are omitted. Also the loading rate, which in fact is at seismic speeds, is not regarded as altering the stress-strain behavior. The effect of age of the concrete may be included by using the data from tests of suitably aged specimens, however, such specimens are not likely to have precisely the same history of exposure, temperature, and loading as the real structure. Even then, specimens of the same mix and curing history can give sufficiently different stress-strain curves that, for this work, it was assumed that a median curve selected from the

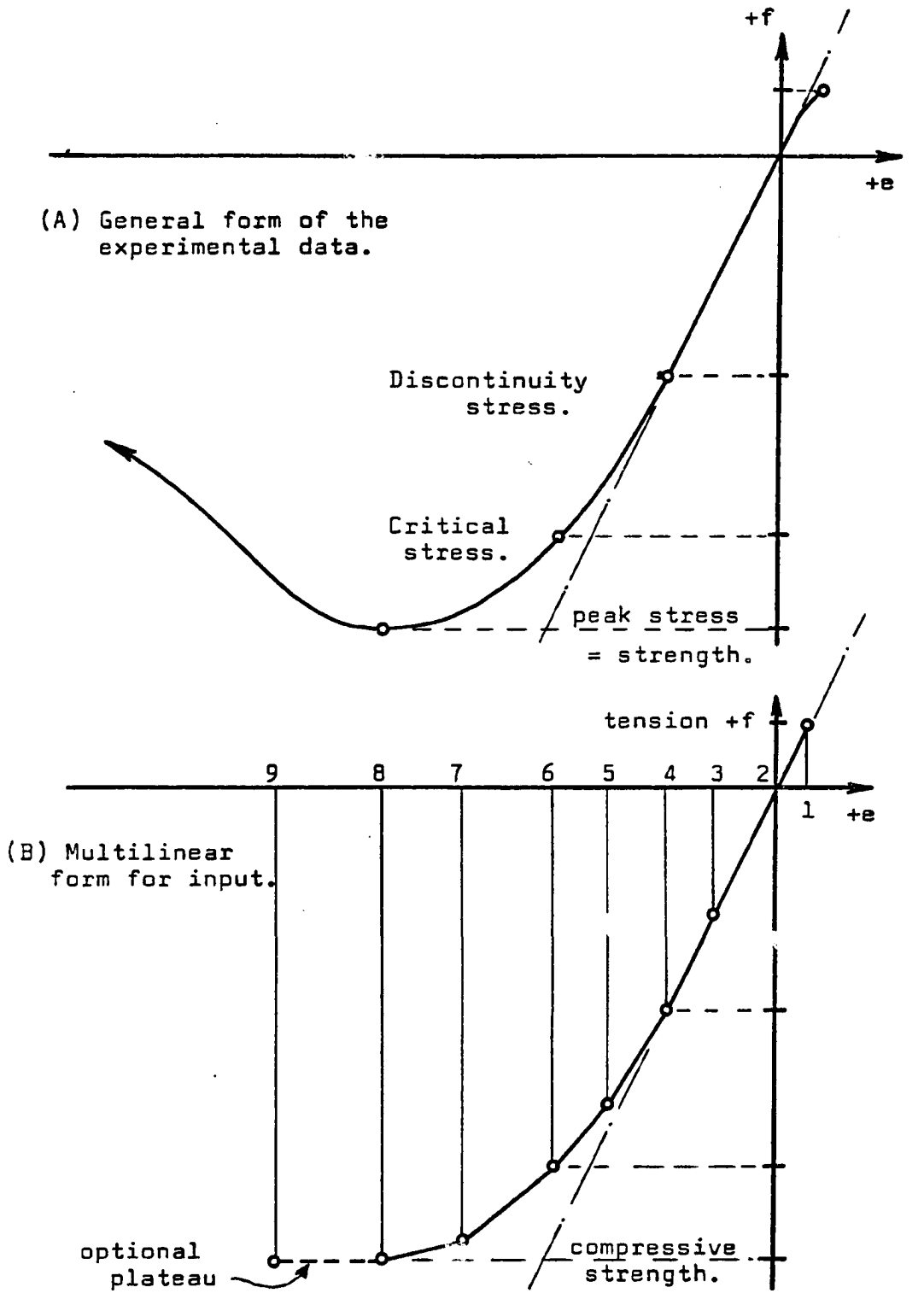

FIGURE 5.1 MULTILINEAR CONCRETE STRESS-STRAIN CURVES.

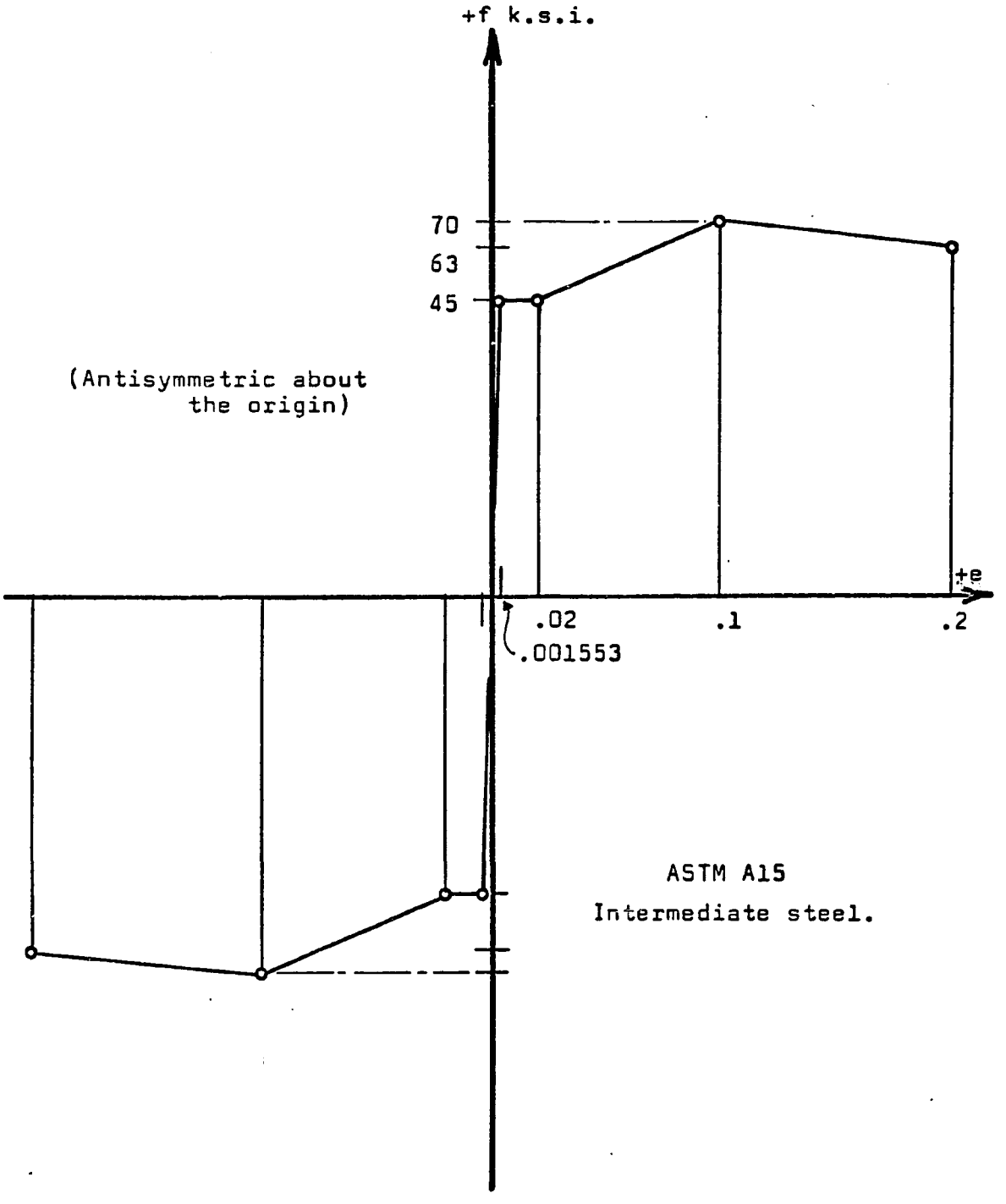

FIGURE 5.2

A STRESS-STRAIN CURVE FOR REINFORCEMENT.

results of a set of uniaxial compression tests was the best approach available.

If the results of uniaxial tests could provide an acceptable stress-strain description for each material then other considerations occur when a biaxial stress field exists in an element. This will be discussed in Section 5.3 with regard to the material properties of the quadrilateral plane stress elements.

The strength of a concrete is defined as the peak stress value reached during a test. A very stiff testing machine may permit the behavior to be recorded for strains beyond the peak stress occurrence, whereas less-stiff machines can cause explosive failure of specimens near the peak stress loading. The existence of the stress-strain curve beyond the peak stress is important. It corresponds to the realistic situation in a structural member where a local redistribution of stresses occurs after the strength is locally exceeded, rather than experiencing a local failure of the material. In this work a stress plateau was often used in case the concrete peak stress was achieved so that redistribution could occur. This approach is also useful to prevent the occurrence of negative values of modulus E_i for the slices of the frame elements during the transformation process used there.

5.1 Basic Procedures

The rod element will be used to discuss the basic methods for handling material properties in this work since the other elements use suitable variations of the same processes. For a given load increment the initial total strain e_1 in the element is known

and stored. An iteration cycle will directly produce a set of displacement increments, which are used to give the final total displacements of the nodes. The new total strain e_2 in the element is obtained from these values and so the initial and final strain values are available. Interpolation of the tabulated stress-strain curve is now used to obtain (a) the secant modulus over the given strain increment and (b) the value of stress that corresponds to the latest final strain value. This process is shown in Figure 5.3 for two situations. The first case presumes that $e_2 \neq e_1$ so that the usual gradient computation gives the secant modulus E. However, the process does not identify an increase or decrease of strain from e_1 so that unloading of an element is not identified. The implication of this is that hysteresis loops of structural deflections due to cyclic loading cannot be obtained by this program. The second case presumes that $e_2 = e_1$ and that they also coincide with a tabulated value of strain. The procedure is then to get a value of secant modulus corresponding to the total strain range given by the adjacent intervals and thus provides an approximate mean value for E. The final stress f_2 relating to e_2 is produced during the interpolation process. As successive iterations occur during a load increment then new values of modulus E_i are provided for the subsequent stiffness computations while new values of stress f_i are output to describe the latest state of the changing system. This process has already been shown in Figure 4.3(C).

Before interpolation begins, it is necessary to determine whether the latest e_2 lies within the region of definition of the constitutive law. If e_2 exceeds the ultimate tensile strain

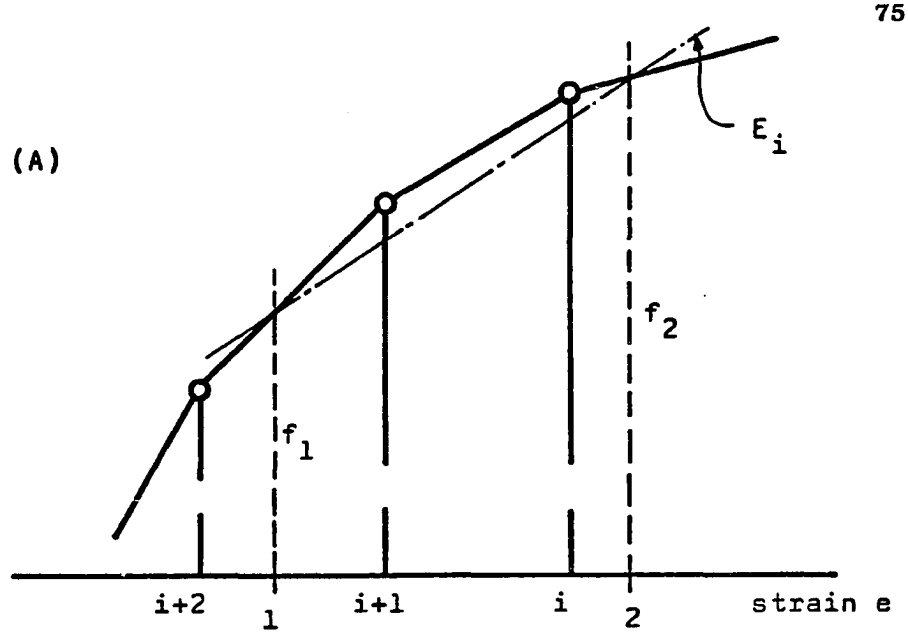

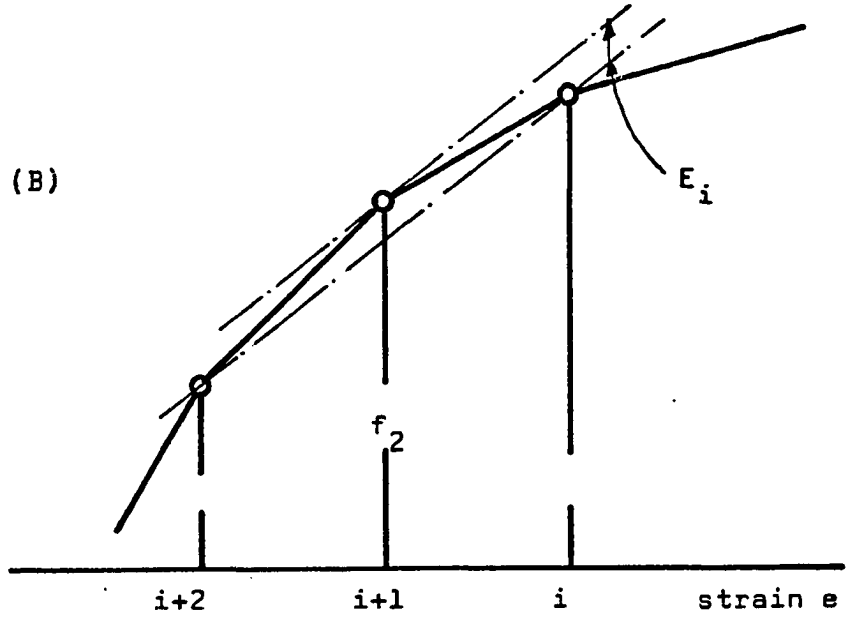

$e_2 = e_1$
$= e_{i+1}$

FIGURE 5.3 THE INTERPOLATION PROCESS.

then a simple fracture is signalled, but if e_2 exceeds the ultimate compressive strain then destruction of the element is assumed. For a rod element both of these cases mean total loss of stiffness and unloading of the element. But in the case of fracture, the crack is assumed to be capable of closing again at some future time so that the element can carry compression, whereas destruction means that the element is permanently removed from the structural system.

A basic flow diagram of logic for determining the failure status, and to interpolate the latest modulus and stress values is given in Figure 5.4. The process shown there is elaborated for later elements that have different fracture and interpolation procedures.

5.2 The Frame Element Materials

Transformation of a flexural member cross-section is a useful method for simplifying the analysis of a section composed of several different materials. The modular ratios $n_i = E_i/E_r$ are used to convert materials of different rigidities E_i into equivalent section widths of reference rigidity E_r. The modular ratio at working stress levels in reinforced concrete design is familiar to all designers and analysts. This approach has always been in conflict with the efforts to establish valid factors of safety in structures by considering the ultimate strength of the reinforced concrete members (20). The modular ratio n_i of two materials presumes two values of material moduli that are unchanging during the loading and is furthermore a number which can be characteristic of the entire cross-section in usual design practice. At ultimate loads

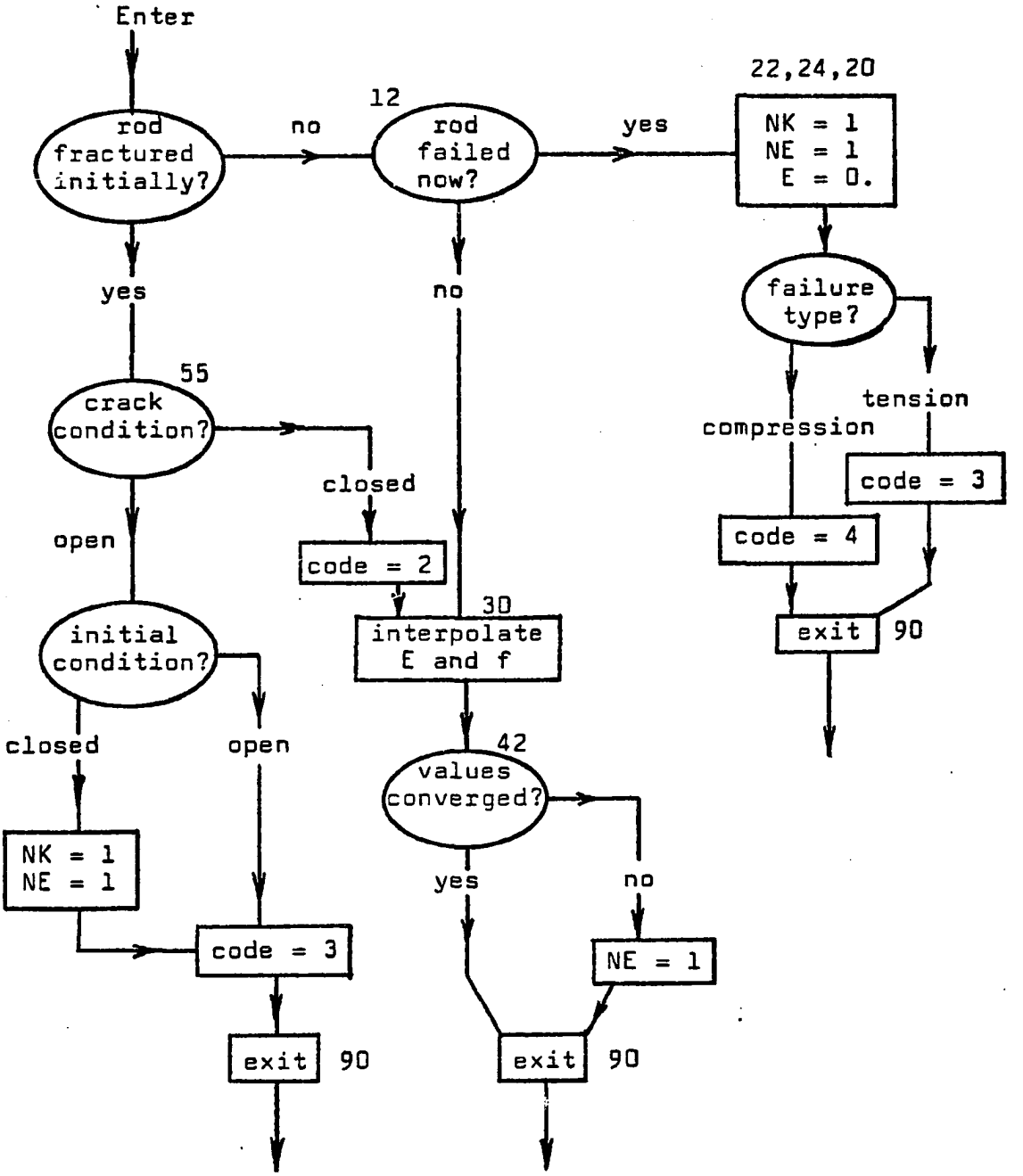

FIGURE 5.4

FAILURE AND INTERPOLATION LOGIC, ROD ELEMENTS.

the nonlinear concrete stresses over the compression zone and the yielding of reinforcement produce considerable uncertainties in the value of n_i, the transformation of the section becomes quite impractical, and in fact modern methods of ultimate strength design abandon this idea completely.

The segment cross-section is assumed to be cut into layers or slices which are regarded as different (and changing) materials. The difference in each case is expressed by the modulus of the material of the slice, which depends upon the amount of total strain developed at any stage of the loading, and hence accounts for the gradual changes which may occur in the material rigidity. In this way the concept of transforming the section is recovered but many different modular ratios are in operation during the analysis. The derivation of the appropriate material modulus at each level of the cross-section is discussed next, but first it is necessary to consider the relationship between stress-strain curves derived from flexural tests and those that come from direct compression tests of 6" X 12" cylinders.

Plain concrete prismatic sections have been suitably tested with eccentric loading in order to investigate the compression zone of a concrete beam (18). The assumptions made were (a) that a linear distribution of strains existed over the depth of the cross-section (which has been well verified by numerous tests), and that (b) all concrete 'fibers' follow one and the same stress-strain curve, so that the concrete stress is only a function of the strain at any level. These assumptions allowed the flexural stress-strain curves

to be reconstructed after loading the sections to failure. In addition the flexural stress-strain curves have been investigated by means of embedded pressure cells in an attempt to read stress patterns directly (19). These tests have verified that the flexural stress-strain curve of the concrete during loading to failure is essentially the same as that derived from direct compresssion tests of 6" X 12" cylinders. This is called herein the uniaxial curve for the concrete.

Perhaps the significant difference between these families of stress-strain curves was the behavior beyond the peak stress and before failure. Direct compression tests usually terminate quickly after the maximum load in a manner which is a function of the stiffness of the testing machine. The flexural tests show a greater continuity beyond the maximum load, probably due to a process of stress transfer occurring between adjacent 'fibers.' This latter effect requires a negative modulus for the extreme section 'fibers' near ultimate loads and implies some negative areas and moment-areas for the transformation process. In order to avoid this effect the input stress-strain curves were arranged so that the maximum stress is assumed to be the failure stress and no region of negative modulus is included beyond this peak. In this work it was assumed that the flexural members have either balanced or under-reinforced sections so that the desirable tension failure modes are going to predominate. This also assumes that terminating the concrete stress-strain curves at maximum stress will provide a reasonable description of the behavior of a concrete 'fiber' throughout its loading in compression.

In order to include progressive cracking in the analytical model the tensile failure of segment slices is considered. Values of ultimate tensile strains are needed for the concrete. However, the cracking stress f_{cr} for a reinforced concrete member is a complex function of the tensile strength f'_t, the amount and distribution of the reinforcement, and the nature of the bond between steel and concrete. The concrete between cracks carries some tension so the steel stress varies accordingly. This condition causes the tensile strength f'_t to generally differ from the computed value f_{cr}. The modulus of rupture f'_r is the apparent tensile strength obtained from flexural tests of unreinforced concrete specimens, and often is a value considerably higher than f'_t. In view of the complexity of this situation then the procedure used in this work was to assume that

(a) the cracked slice is a zero-strength continuum so that the crack spacing is not considered,

(b) consequently there is zero bond to adjacent reinforcement, the stresses are constant along the segment steel, and

(c) the tensile failure of the slice is determined by an ultimate strain value. However, the fact that tensile fracture of concrete is usually discussed in terms of two kinds of stress values and rarely in terms of strain values may force the analyst to estimate these strains. Figure 5.5 is given to illustrate this problem.

(i) The modulus of rupture f'_r and the initial modulus E can be used to give a minimum value of fracture strain e_r. If necessary, f'_r can be estimated from the compressive strength f'_c by using a suitable formula (21). An example of this is

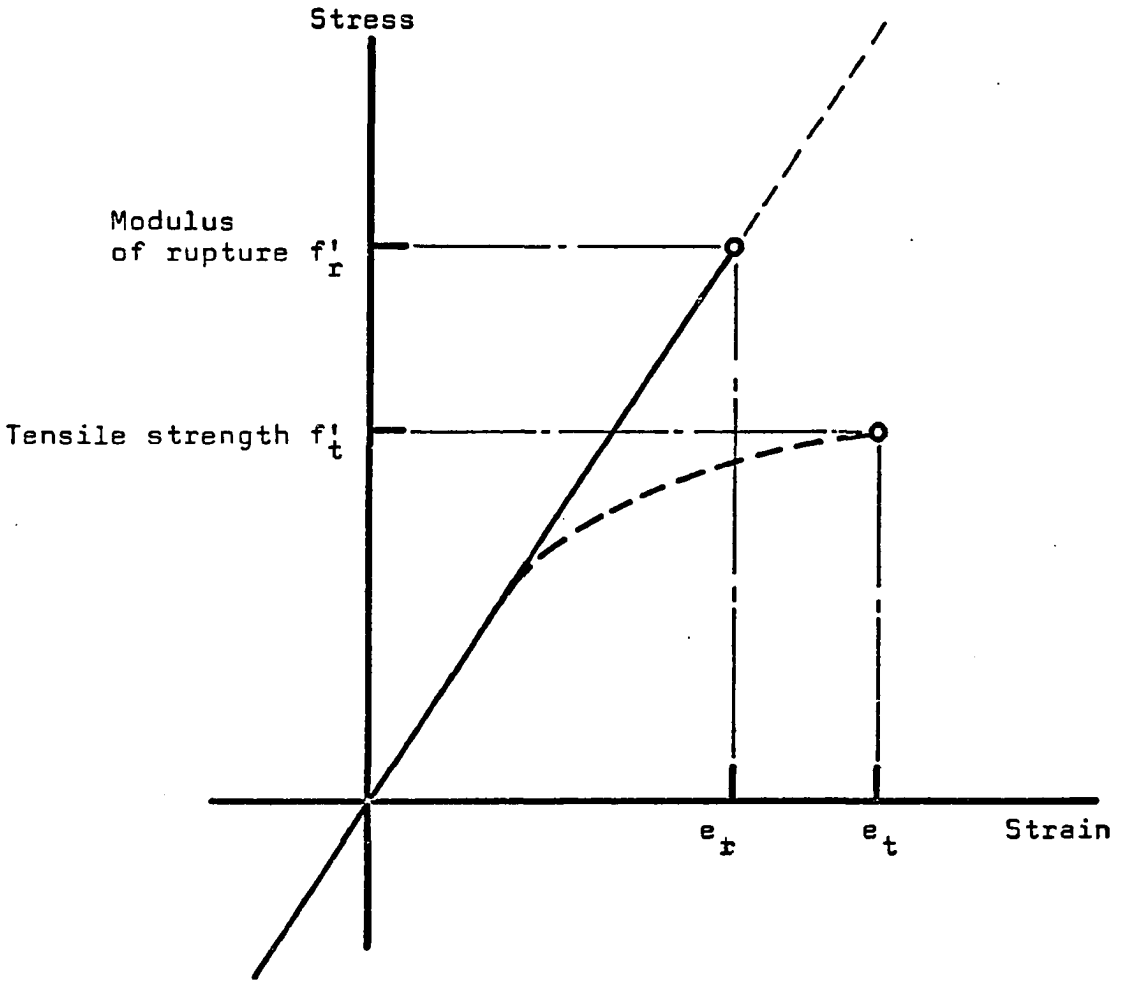

FIGURE 5.5

TENSILE STRENGTH PARAMETERS FOR CONCRETE.

$$f'_r = 0.08\ f'_c + 280 \text{ psi}$$

(ii) If the average direct tensile strength f'_t is known (say from splitting tests) then comparison with f'_r will indicate whether the tensile curve is reasonably linear.

(iii) A test computation to compare the analytical cracking load with an observed cracking load may also be used to secure a reasonable value for e_t.

In this work it was typical to use a line with constant slope E_t terminating at either the modulus of rupture f'_r or at the estimated tensile strength f'_t while exploring the strain values e_t.

A stress-strain curve is required for each of the two materials of a frame element. The curve for concrete is interpolated for each slice according to the strain increment at that level while the single curve for the reinforcement is interpolated for each nonzero layer. Thus 10 to 14 interpolations generally occur for each frame element.

Stresses in the top and bottom extreme fibers are also interpolated as part of the output description of the element condition.

Failure of a slice simply zeros the transformed area of that slice and the section properties are influenced accordingly.

If a section is largely subjected to tension then it is possible to have only the reinforcement contributing to the section stiffness, and if yielding occurs then the stiffness can become small or negligible. If crushing of the concrete occurs then again the stiffness depends largely on the contribution of the reinforcement. It was considered in this work that a very small value of

stiffness would generally imply considerable disintegration of the element anyway and so an arbitrary limit was set to denote destruction of the element; when the total transformed area reduced to less than 0.01% of the original stress-free transformed section area. Beyond this limit the frame element is disregarded for the system stiffness. The basic process used for evaluating the frame element failure status and to interpolate material moduli and stresses is given in Figure 5.6.

5.3 The Biaxial Stress Quadrilateral Elements

The derivation of the stiffness [K] for a quadrilateral element requires definition of the material stiffness in the form of a modular matrix [C] which relates stresses and strains,

$$\{\sigma\} = [C]\{e\}$$

where

$$[C] = \frac{1}{1 - \nu_1 \nu_2} \begin{bmatrix} E_1 & E_1 \nu_2 & 0 \\ E_2 \nu_1 & E_2 & 0 \\ 0 & 0 & G_{12}(1 - \nu_1 \nu_2) \end{bmatrix}$$

In this array the values E_i are the material stiffnesses in orthogonal directions i, and each Poisson ratio ν_i is measured by a uniaxial test in direction i such that the lateral strain e_L is given by

$$-e_L = \nu_i e_i$$

The determination of the true values E_i is dependent on the existence and nature of the biaxial stress field. Evidence shows that

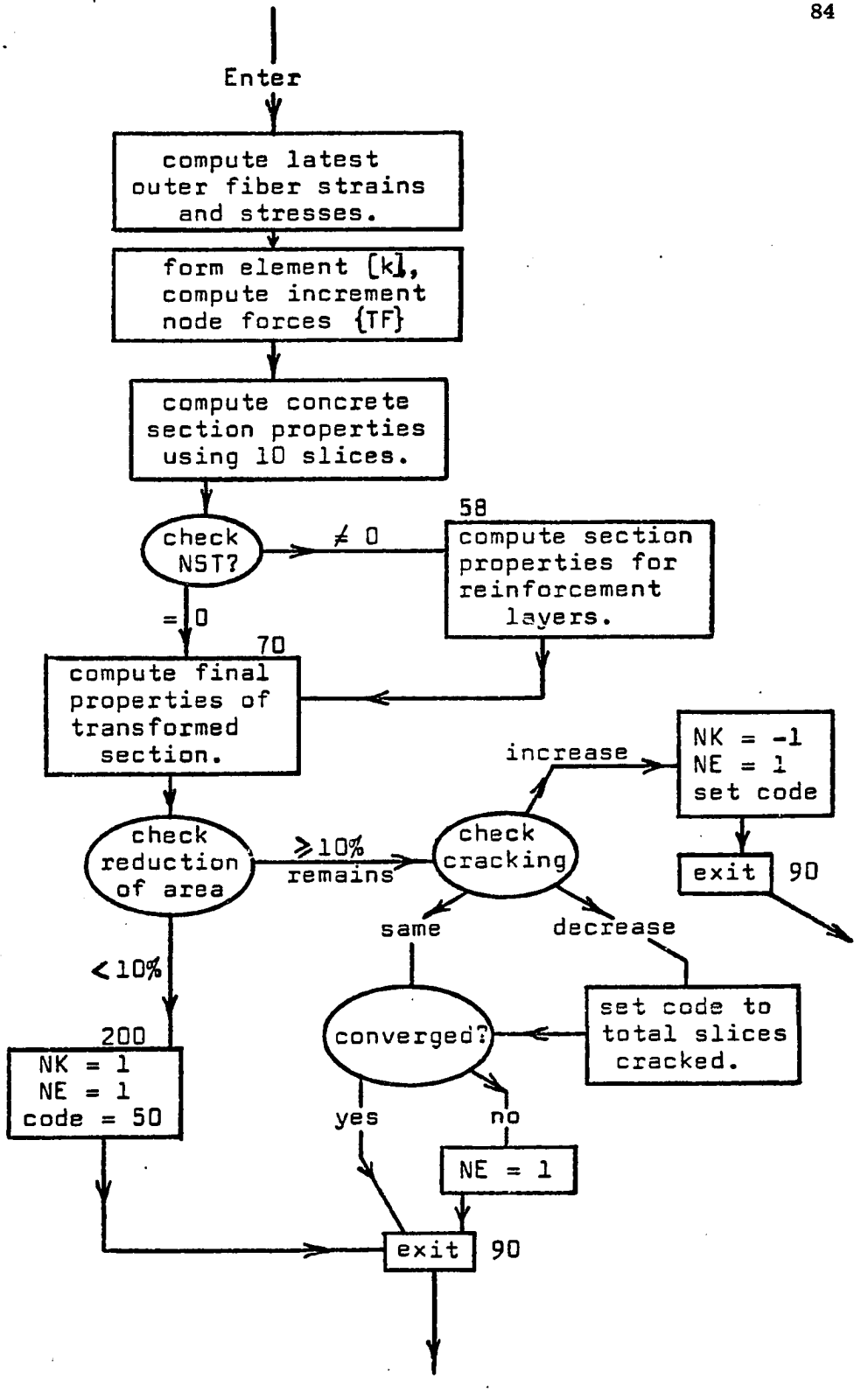

FIGURE 5.6

FRAME ELEMENT INTERPOLATION AND FAILURE.

the material stiffness E_1, in direction 1, can be affected by the presence of a lateral stress f_2. However, test results concerning the behavior of a material subjected to biaxial stress fields are very limited, and no biaxial stress-strain laws have been developed. Multi-axial testing nearly always concerns triaxial compression and, in particular, the failure or yield behavior of the material is the objective rather than the stiffness characteristics during loading. Only in recent times has interest begun to develop in the changing condition of the material in a biaxially stressed, two-dimensional structural element during loading to failure (53, 54).

Element node displacements $\{v\}$ give the element center node strains $\{e_c\}$ according to the application of the strain-displacement transformation for that element (see Eq. (3.5)). The principal total strains e_1 and e_2, and the rotation θ_p to the principal strain axes, are first derived from the total strains $\{e_c\}$. Total strain consists of an effective strain e_i^* due to the parallel direct stress field and a coupled strain due to the transverse effective strain and the Poisson effect.

$$e_1 = e_1^* - \nu_2 e_2^*$$

$$e_2 = e_2^* - \nu_1 e_1^*$$

This set is solved for the effective strain values since these correspond to stresses in the interpolation process. Solution gives

$$e_1^* = (e_1 + \nu_2 e_2) / (1 - \nu_1 \nu_2)$$

and

$$e_2^* = (e_2 + \nu_1 e_1) / (1 - \nu_1 \nu_2)$$

The initial and final effective strains e_i^* are derived for each iteration cycle and are used in the standard interpolation procedure to produce two secant stiffness values E_i and two final stresses f_i for the principal directions. Interpolation is performed using the unaltered uniaxial stress-strain curve of the element material as a first approximation to the true, but unknown, constitutive law of the biaxially stressed element.

Determination of failure is a two-stage process. The first stage identifies failure when the final effective strains e_i^* exceed the ultimate strain limits of the material. This is part of the normal interpolation process and is shown in Figure 5.7. If the element has not failed by this criterion then the second stage uses the newly derived biaxial stresses and checks for failure in terms of a biaxial stress failure criterion.

A suitable phenomenological failure criterion was produced from work by B. Bresler and K. Pister (28) which used octahedral stresses as the basic parameters. Their criterion showed good agreement with published triaxial and biaxial strength data from various sources. When expressed in terms of the principal normal stresses then the corresponding biaxial strength envelope is given in Figure 5.8(A). This was modified in the present work to the form given in Figure 5.8(B). The assumptions are made that (a) the compressive and tensile strengths are not changed for a biaxial stress state and (b) failure in the compression-tension stress region is determined by a linear form of the Bresler-Pister envelope. If this failure criterion is exceeded in an element then the computer program prints

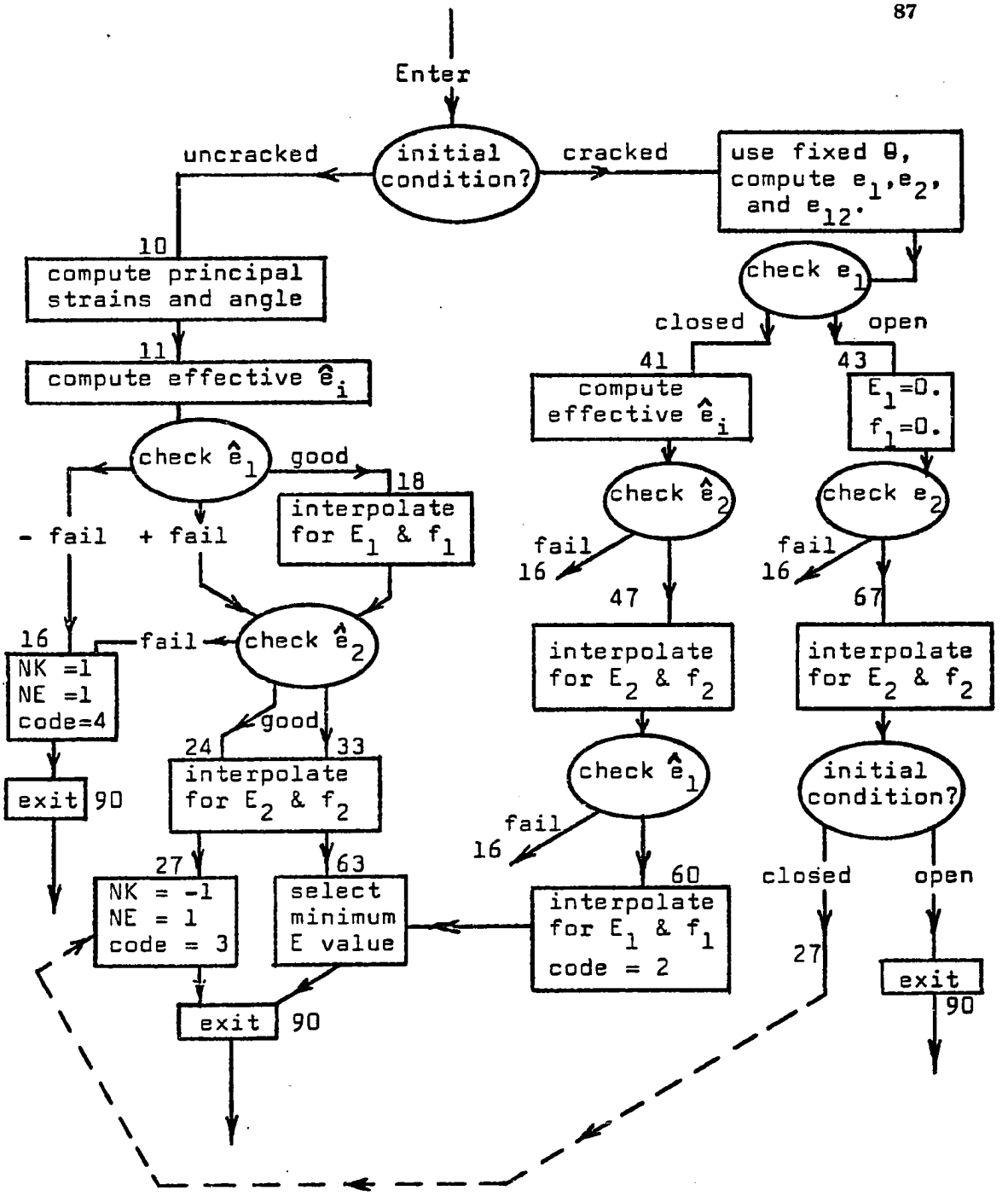

FIGURE 5.7

QUADRILATERAL ELEMENT INTERPOLATION AND FAILURE.

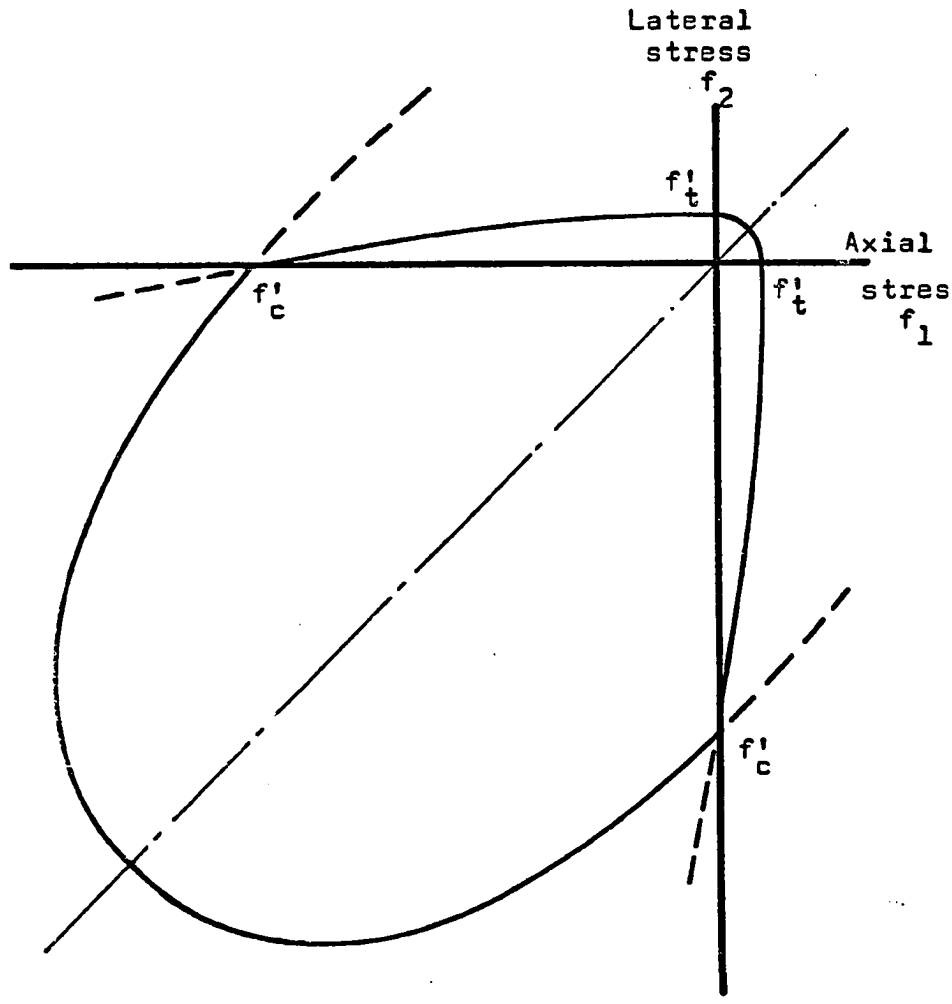

FIGURE 5.8(A)

BRESLER-PISTER BIAXIAL FAILURE ENVELOPE.

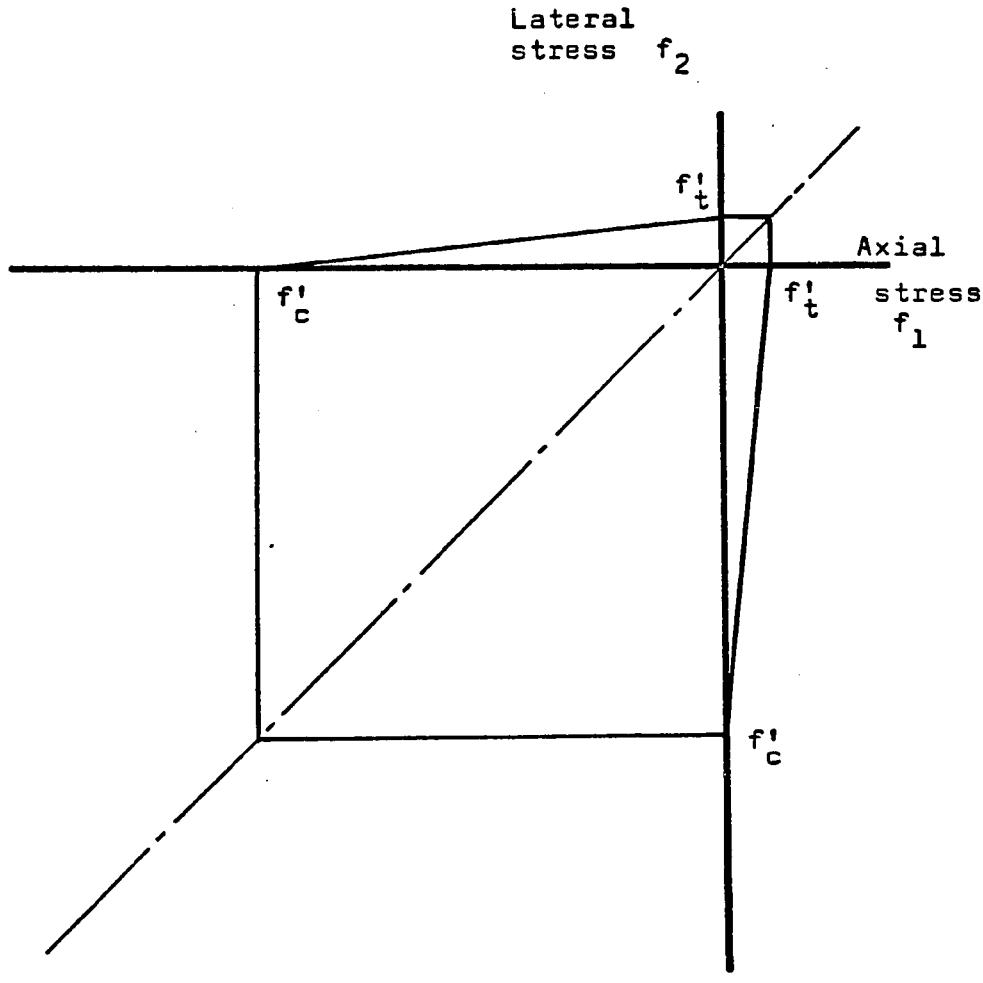

FIGURE 5.8(B)

MODIFIED BIAXIAL FAILURE ENVELOPE.

the message "D - T Failure" to identify the event from the maximum strain criterion failures.

Little is known about the dependency between the biaxial stiffnesses E_1 and E_2 or about the changes that occur in the Poisson ratios ν_1 and ν_2 during loading to failure. Symmetry of the array [C] gives a dependency relationship,

$$\nu_2 E_1 = \nu_1 E_2$$

If E_1 and E_2 should differ considerably from separate interpolations this would require ν_1 and ν_2 to differ accordingly. Should ν_1 be assumed to remain constant then ν_2 must obviously vary according to the ratio E_2/E_1. This difficulty made it desirable to assume that ν_1 and ν_2 are equal and constant during loading. Conversely, this now requires that E_1 and E_2 be equal and an isotropic state is defined. This was adopted and set a control on the possibility of deriving widely differing E values for an uncracked element. The reasoning behind this was as follows. If a biaxially stressed concrete element has large axial stress with small transverse stress, then reduction of axial stiffness is related to increasing damage in the material. But this damage makes it possible that the interpolated, higher transverse stiffness cannot exist and in fact may be a value much closer in magnitude to the reduced axial stiffness. This idea of damage was used to justify adopting the minimum interpolated E value as that single value used to describe the isotropic stiffness of the materials rather than taking a mean value.

Since the modular array [C] has become isotropic for the analytic process, the computation of the shear modulus G for the uncracked

element is resolved by using the usual relationship

$$G = E/2\ (1 + \nu)$$

However, for the case where an element is fractured then extreme anisotropy is in effect and the evaluation of G cannot be directly defined. The approach used here was to consider the general anisotropic material with unequal stiffnesses E_1 and E_2. A rotation of [C] through 45° will produce an apparent state of isotropy with equal moduli along the new axes. If the shear modulus G is now taken to be the corresponding term of this rotated [C] array then the following relationship is found,

$$G = \frac{E_1\ (1 - \nu_2) + E_2\ (1 - \nu_1)}{4\ (1 - \nu_1\ \nu_2)}$$

It may be noted that if $E_1 = E_2$ then this reduces to the usual expression for the isotropic G. When this equation is used for a cracked element then E_1 becomes zero and it follows that ν_1 is zero, so that finally an estimate for the shear modulus is given by

$$G = E/4$$

This is the value used in the formation of [C] when the stiffness of a cracked element is derived.

5.4 Tielink Element Properties

A stress-strain concept is not involved in the properties of the tielinks since they are artificial devices which lock pairs of nodes together. As a result, the two orthogonal stiffnesses k_h and k_v are simply set to very large values to represent infinite

magnitudes and to minimize the relative deflections of the "locked" nodes.

A failure condition may be specified by either a tensile or shear fracture across the interface between connected elements. These fractures are determined by comparing the interface shear or tensile forces with the corresponding strengths. No special failure theory was utilized to predict failure on the interface plane under critical combinations of shear and normal stresses. The linkage strengths are determined as follows. Let S_i be the length of interface tributary to link i and select b_i as the least member thickness at the interface, so that the tributary contact area $A_i = S_i \times b_i$. The linkage failure forces are given by

$$F_t = A_i \times f_t' \quad \text{in tension,}$$

and

$$F_s = A_i \times f_s' \quad \text{in shear,}$$

using the appropriate tensile and shear strengths of the material. The typical interface dimensions are shown in Figure 5.9.

Failure implies that a crack forms along the interface between elements along the length tributary to the failing link. The assignment of stiffnesses to the failed linkage depends on the crack condition, whether it be open or closed. An open crack has both stiffness values set to zero, but the closed crack retains the normal stiffness k_v at a large, rigid value and, at first cracking, the tangential k_h is set to a reduced value to represent friction. The maximum tangential force that can be transmitted by friction is arbitrarily

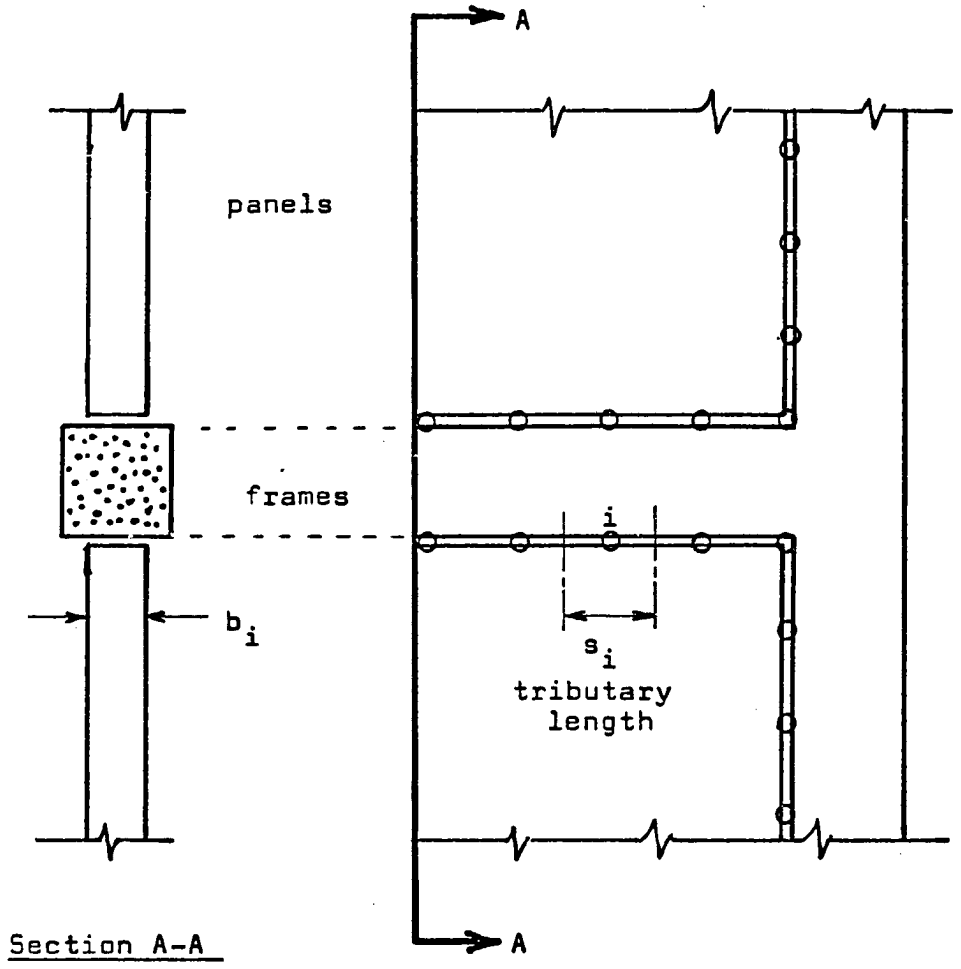

FIGURE 5.9 TIELINK CONTACT DIMENSIONS.

chosen to be one half of the linkage shear strength. If this is exceeded over a closed crack then slipping is assumed to occur by setting k_h to zero. After the initial fracture the assignment of linkage stiffnesses is controlled by the opening or closing of interface cracks. This is demonstrated in the flow diagram of Figure 5.10.

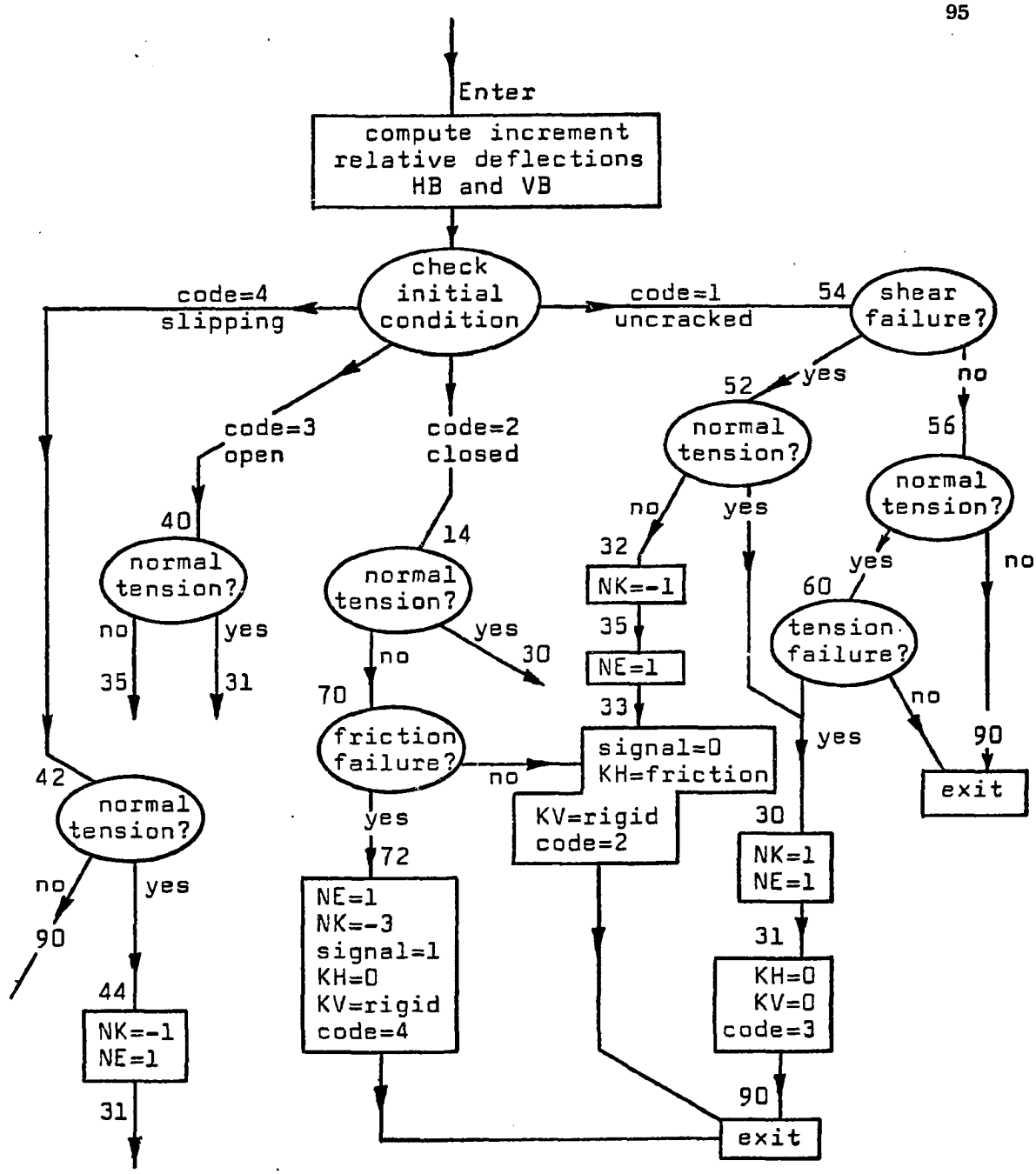

FIGURE 5.10 TIELINK FAILURE PROCESSES.

6. EXAMPLES OF NONLINEAR ANALYSIS

The descriptions of several test problems are now presented but the details of the data decks required for each problem are omitted. This information is given in general form for the computer program in Appendix A.

6.1 The Yielding 3-Bar Truss

This example is used to demonstrate the incremental iteration method for nonlinear material properties. This truss was one of several that were loaded experimentally in order to check an analytical method developed by Steinbacher et al. (22). The arrangement shown in Figure 6.1 includes two tension and one compression member. The stress-strain curves for the aluminum alloy 24S-T4 are plotted in Figure 6.2. The actual material stress-strain relation was used for the tension members, but an average, equivalent stress-strain law was derived from compression tests of an identical compression member. The causes of the difference between tension and compression states was not explained by these researchers, but the effect of buckling is a possible reason. The selected loading increments and the required iterations are listed in Table 6.1, while the comparisons between the member forces occurring in the test and those deduced by this analysis are listed in Table 6.2. These member force variations are related to the external loading in Figure 6.3. The experimental measurements of node deflections are not available from the reference but the results given by this analysis are plotted in Figure 6.4. The total time taken for the analysis

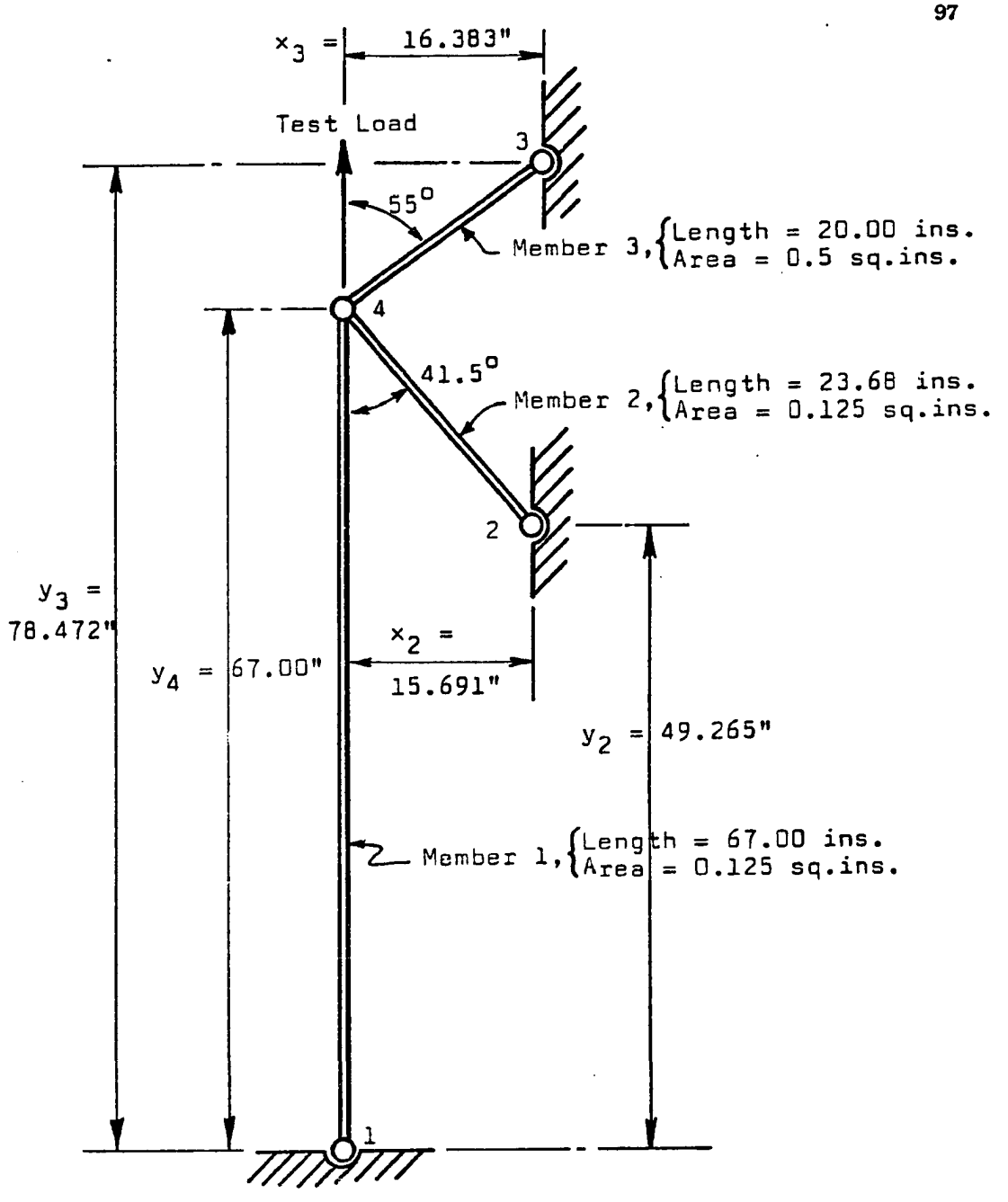

FIGURE 6.1 GEOMETRY OF YIELDING TRUSS.

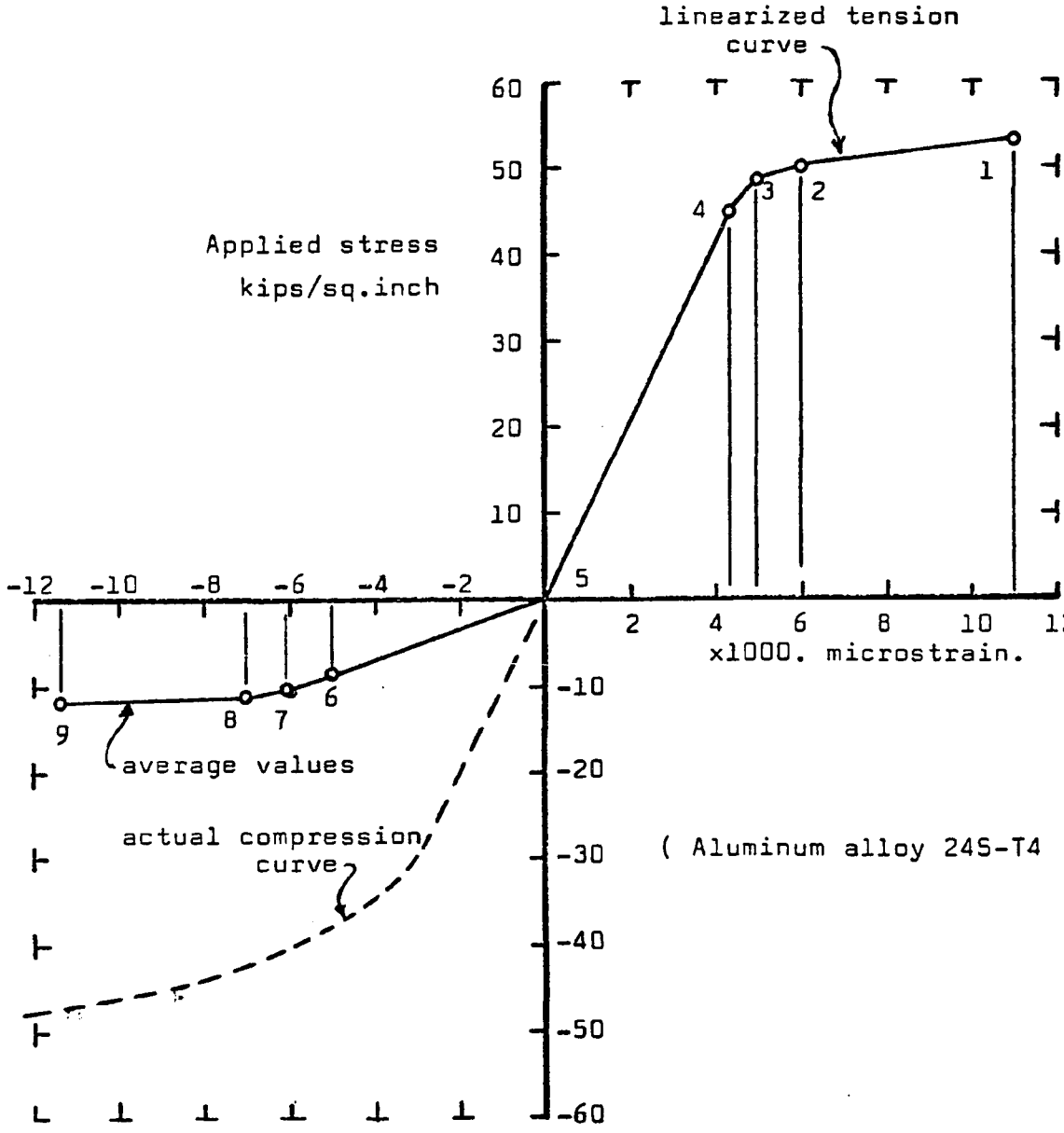

FIGURE 6.2 EQUIVALENT STRESS-STRAIN RELATIONS.

Load Increment		No. of Solution Cycles	Total Load
No.	Size (kips)		(kips)
1	8.	1	8.
2	2.	3	10.
3	1.	4	11.
4	1.	4	12.
5	0.5	2	12.5
6	0.5	1	13.
7	0.5	2	13.5
8	0.5	3*	14.

* Total fracture occurred during this load increment, and required 3 cycles to determine the complete degeneration of the truss.

TABLE 6.1

INCREMENTS AND ITERATIONS FOR THE YIELDING TRUSS.

External Load (kips)	Member 1		Member 2		Member 3	
	Actual Expt	Calc.	Actual Expt	Calc.	Actual Expt	Calc.
8.	2.390	2.383	4.675	4.631	-3.730	-3.746
9.	2.690		5.220		-4.200	
10.	3.030	3.005	5.710	5.754	-4.670	-4.665
11.	3.510	3.525	6.120	6.147	-5.080	-4.987
12.	4.210	4.327	6.350	6.324	-5.290	-5.125
12.5		4.759		6.382		-5.162
13.	5.030	5.192	6.490	6.437	-5.390	-5.207
13.5		5.625		6.492		-5.251
14.	5.950	fr.	6.575	fr.	-5.450	fr.

TABLE 6.2

COMPARISON OF TRUSS MEMBER FORCES.

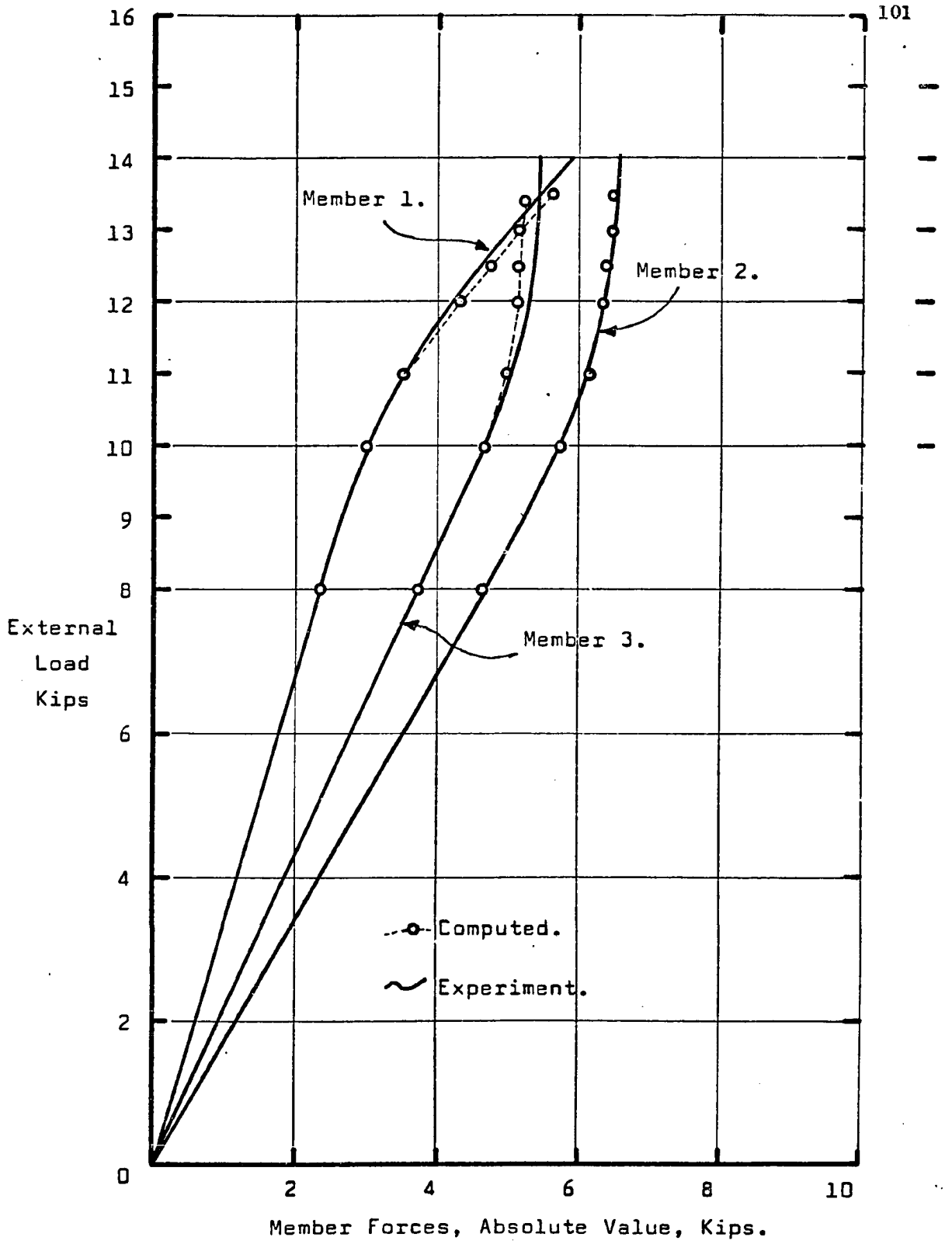

FIGURE 6.3 VARIATION OF MEMBER FORCES.

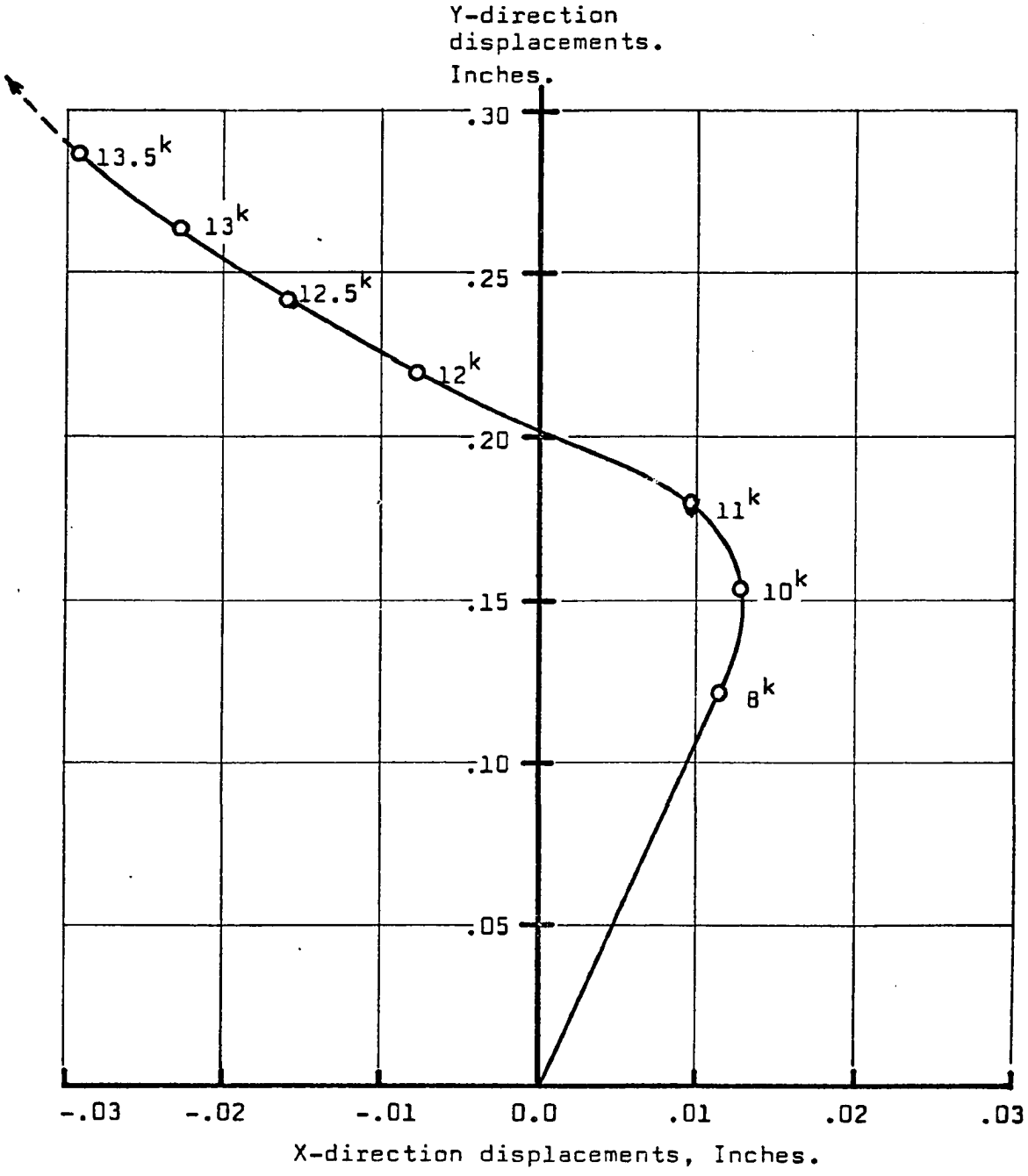

FIGURE 6.4 DEFLECTION PATH OF JOINT 4.

was 62.34 seconds on the CDC-6400 computer.

Using the tables and diagrams, the agreement between the computed and observed member forces is within 3 1/2% at the worst cases. Forces in members 2 and 3, Figure 6.3, approach a constant value as their stiffness decreases due to yielding at the higher stress levels. This causes member 1 to approach a 45° asymptote in its response as it becomes forced to provide the only support for additional loads. However, fracture of member 2 creates an overloaded, yielding 2-bar truss, which in turn fails when member 1 fractures. The computation is forced to end at this point. Smaller load increments towards the end regions would give better estimates of the precise fracture points if this were of interest.

6.2 The Fracturing Linear Truss

This example is used to demonstrate the form of the analysis when fracturing occurs during loading. Tensile fracture of axially loaded members results in zero stiffness and so total discharge of load is required for the element. The truss shown in Figure 6.5 is a modification of an example used in a textbook (23) and has two redundant members that have been set to fracture sequentially. A stable primary system results under full load and shows how the system adjusts itself during loading. Fracture is arranged for the selected members simply by giving them suitably low tensile strengths. This is shown in Figure 6.6. Since the member forces are always in the linear range of stress, then adjustments after fracture were rapid. This is shown in Table 6.3 where the iteration cycles are listed for each load increment. Table 6.4 shows

Top chord and end diagonals = 1.50 sq. ins.
all others = 1.0 sq. ins.

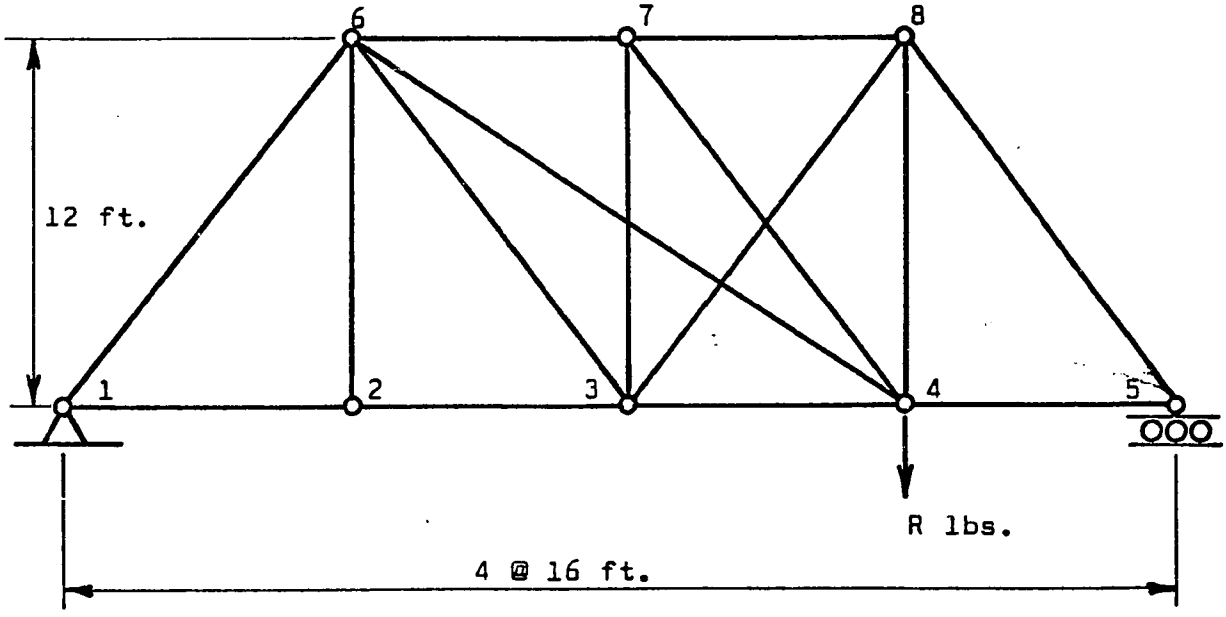

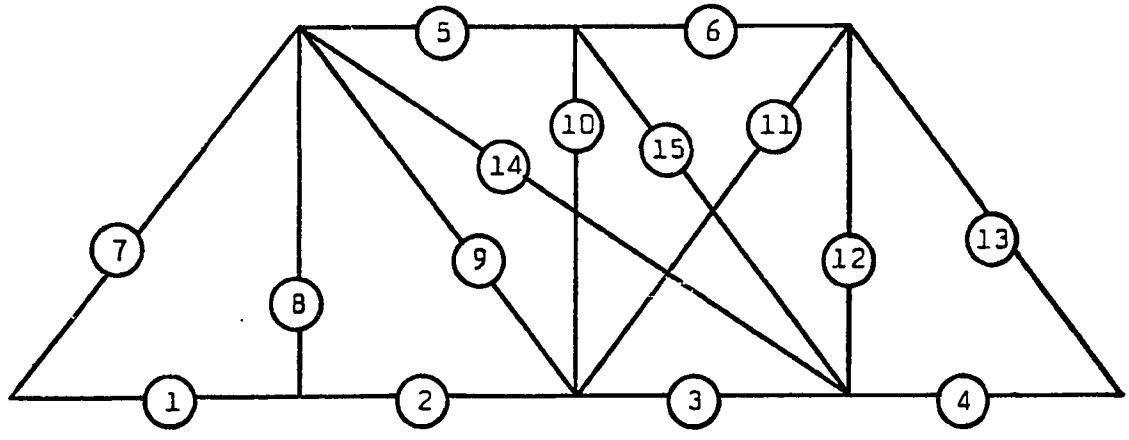

FIGURE 6.5 LAYOUT OF FRACTURING TRUSS.

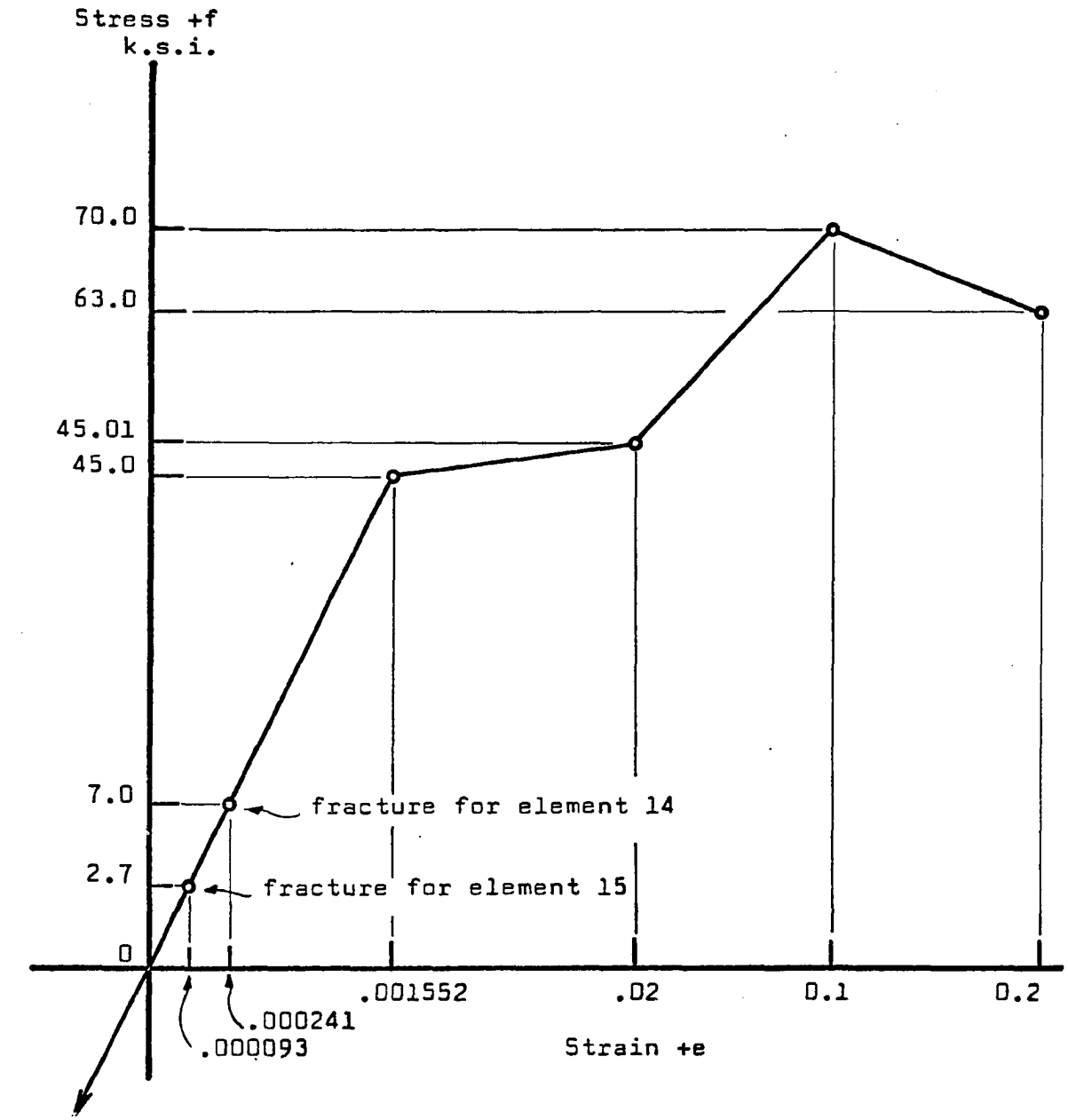

FIGURE 6.6 MATERIAL STRESS-STRAIN CURVES.

Load Increment		Total Load	No. of Cycles
No.	Size	Kips	
1	11.	11.	1
2	1.	12.	2
3	9.	21.	1
4	1.	22.	2
5	2.	24.	1

TABLE 6.3
ITERATIONS REQUIRED BY FRACTURING TRUSS.

Rod No.	Loading Stages.						
	11^k	12^k	12^k	21^k	22^k	22^k	24^k
1	3.67	4.00	4.00	7.00	7.33	7.33	8.00
2	3.67	4.00	4.00	7.00	7.33	7.33	8.00
3	6.60	7.20	8.32	14.56	15.25	22.00	24.00
4	11.00	12.00	12.00	21.00	22.00	22.00	24.00
5	-8.46	-9.23	-9.84	-17.22	-18.04	-14.67	-16.00
6	-10.61	-11.57	-9.84	-17.22	-18.04	-14.67	-16.00
7	-4.58	-5.00	-5.00	-8.75	-9.17	-9.17	-10.00
8	0.	0.	0.	0.	0.	0.	0.
9	3.17	3.46	2.70	4.73	4.95	9.17	10.00
10	-1.61	-1.76	0.	0.	0.	0.	0.
11	-.49	-.53	-2.70	-4.73	-4.95	-9.17	-10.00
12	8.54	9.32	10.62	18.59	19.47	22.00	24.00
13	-13.75	-15.00	-15.00	-26.25	-27.50	-27.50	-30.00
14	2.41	2.63	3.93	6.88	fr.	-	-
15	2.68	fr.	-	-	-	-	-

TABLE 6.4

MEMBER FORCES DURING LOADING AND FRACTURING.

the changes in member forces during loading and when fractures occur in the system, while Figure 6.7 gives the load-deflection relationship at the loaded joint. The total time taken for this analysis was 44.20 seconds on the CDC-6400 computer.

The load-deflection behavior for this truss problem is related to three possible paths in Figure 6.7 that belong to each of the three possible truss configurations. Fractures are events that shift the behavior from path to path, ideally by a horizontal step i.e. finite deflection for fracture at constant load. However, the computing process identifies only the end conditions of the given increment and whether a fracture has occurred in this interval. As a result, the behavior over the small, specially selected fracture increments is plotted with the corresponding slopes.

If fractures can be isolated by extremely small load increments, then these transfers become more nearly horizontal, in accordance with the ideal case. On the other hand, if the load in this example had been increased directly to 24^k from 11^k then both fractures would have been recognized but the end result would apparently be a single line between 11^k and 24^k in Figure 6.7. The steps would seem to have been removed from the solution.

6.3 The Nonlinear Reinforced Concrete Beam

This example was taken from a graduate student research report (24) in order to demonstrate the application of the frame elements to analyze a reinforced concrete beam that has nonlinear behavior due to cracking. The materials were given the usual multilinear stress-strain descriptions as shown in Figures 6.6 and 6.10, but

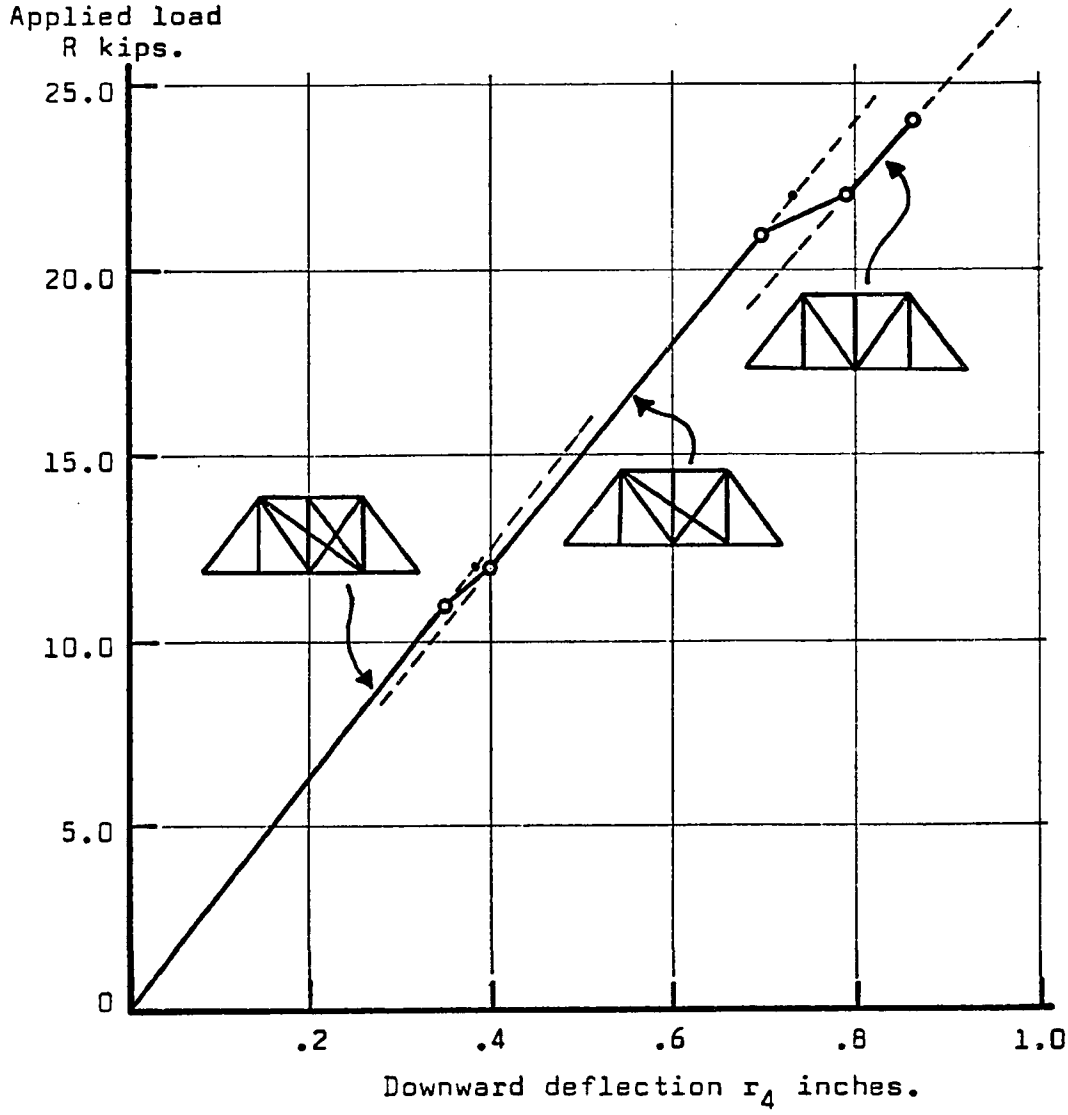

FIGURE 6.7 LOAD-DEFLECTION BEHAVIOR.

this source of nonlinear behavior was not significantly activated by the test loads. The beam layout is shown in Figure 6.8 and represents half of a symmetrical, 2-span continuous beam. The cross-section details in Figure 6.9 show how the reinforcement % and geometry varies along the span. The original report (24) used the approach of constructing the nonlinear M-φ curves at each cross-section in order to determine the new section stiffnesses. These constructions recognized whether or not the section was cracked and so the example was useful for testing the frame elements. The load-deflection results are plotted in Figure 6.11 for both methods and the agreement of these two analyses confirmed the correct operation of the frame element model with its slice fracture and unloading processes. The iteration effort required for this problem is shown in Table 6.5 while taking a total time of 332.58 seconds on the CDC-6400 computer.

An interesting aspect of this test example is the cracking sequence that occurs as the solution proceeds. Cracking is initiated in element 1 at the centerline. This 'hinge' development (or weakening of the local M-φ relation) changes the load sharing pattern of the beam; adjacent elements are temporarily protected from cracking while at the other high-moment location under the load, cracking becomes imminent. The two crack zones then continue to develop in a dependent manner until the analysis ended. This process is shown by the data of Table 6.6 where slice-by-slice cracking is listed, and the amount of cracking at the end of the problem is shown by Figure 6.12.

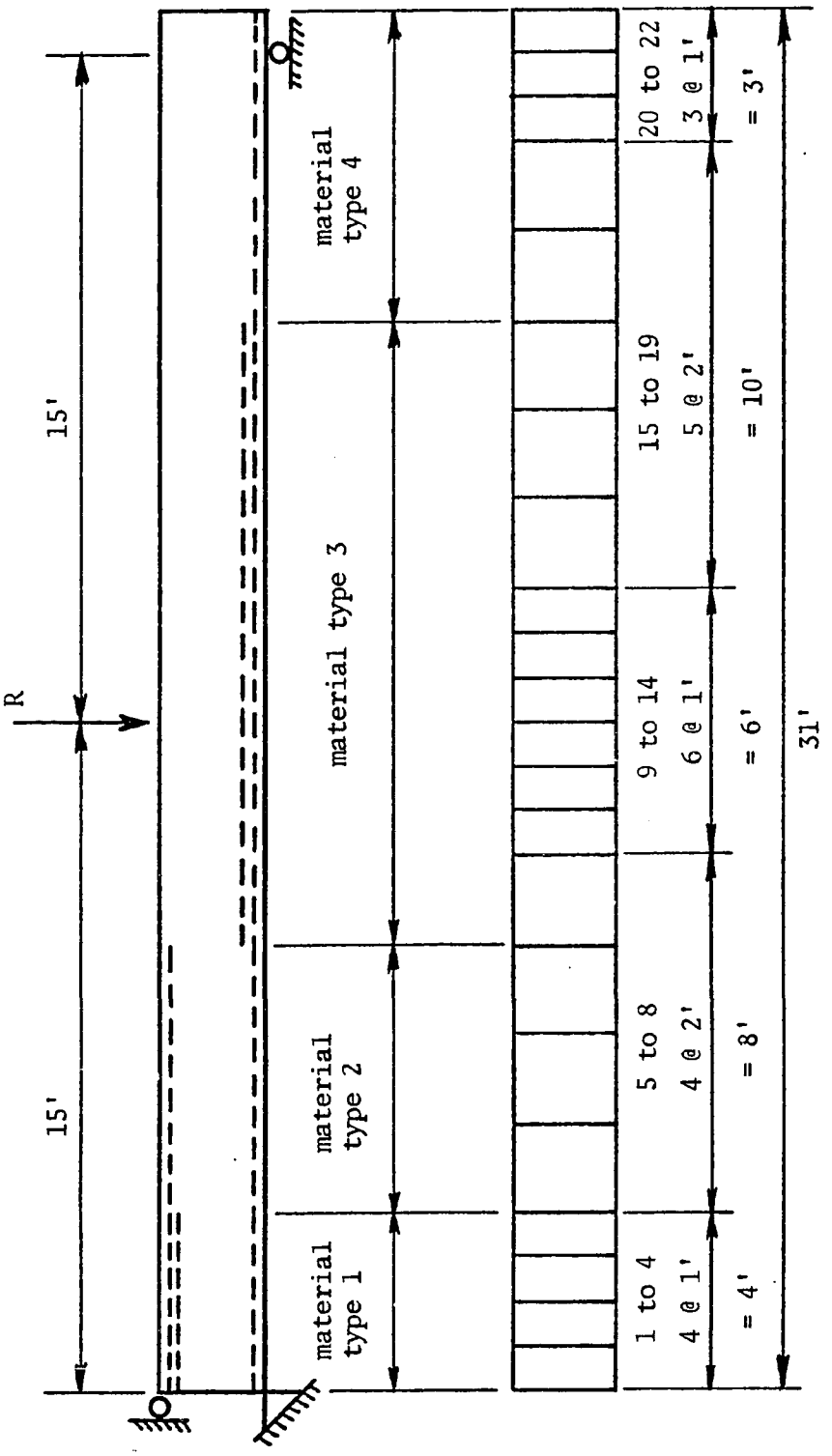

FIGURE 6.8 BEAM LAYOUT AND DISCRETIZATION.

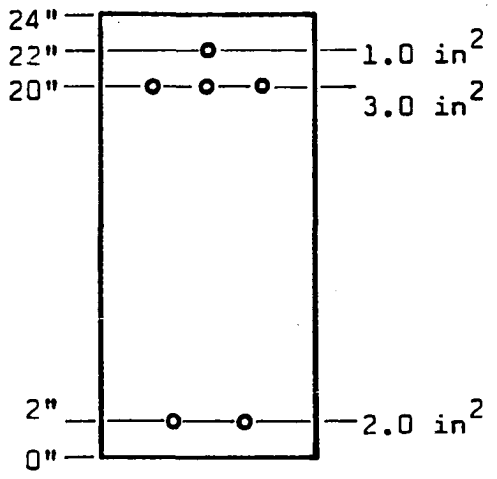

Material Type 1.

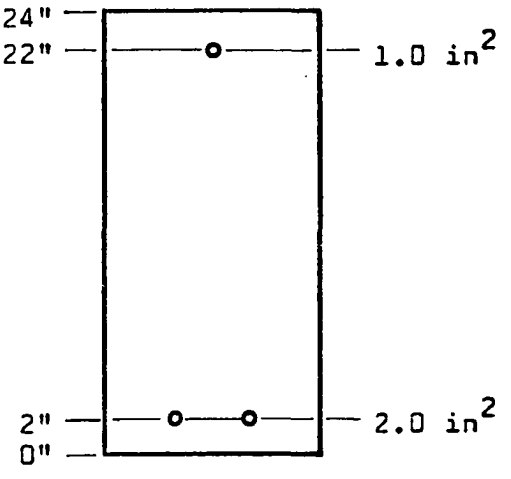

Material Type 2.

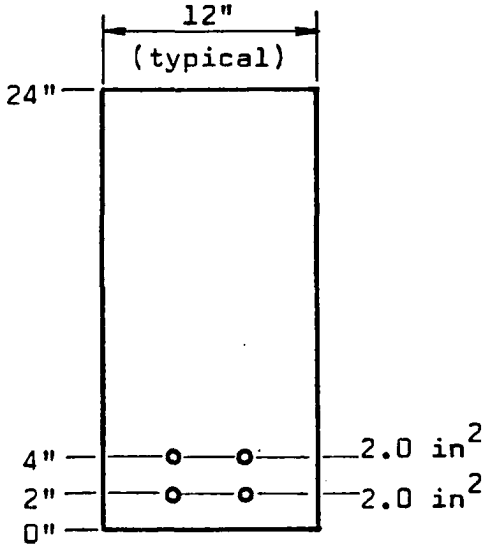

Material Type 3.

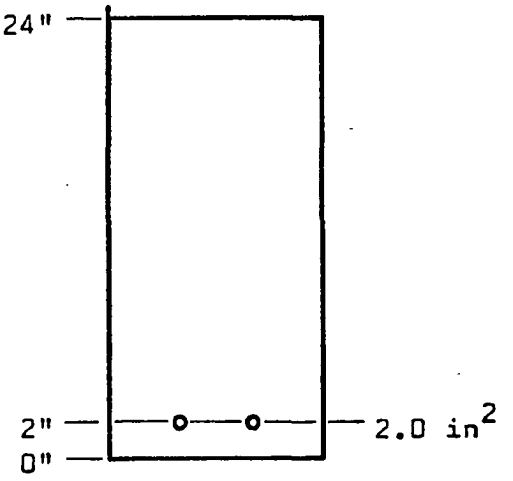

Material Type 4.

Note: Reinforcement areas are shown as individual rods only for illustration purposes.

FIGURE 6.9 REINFORCEMENT FOR CRACKING BEAM

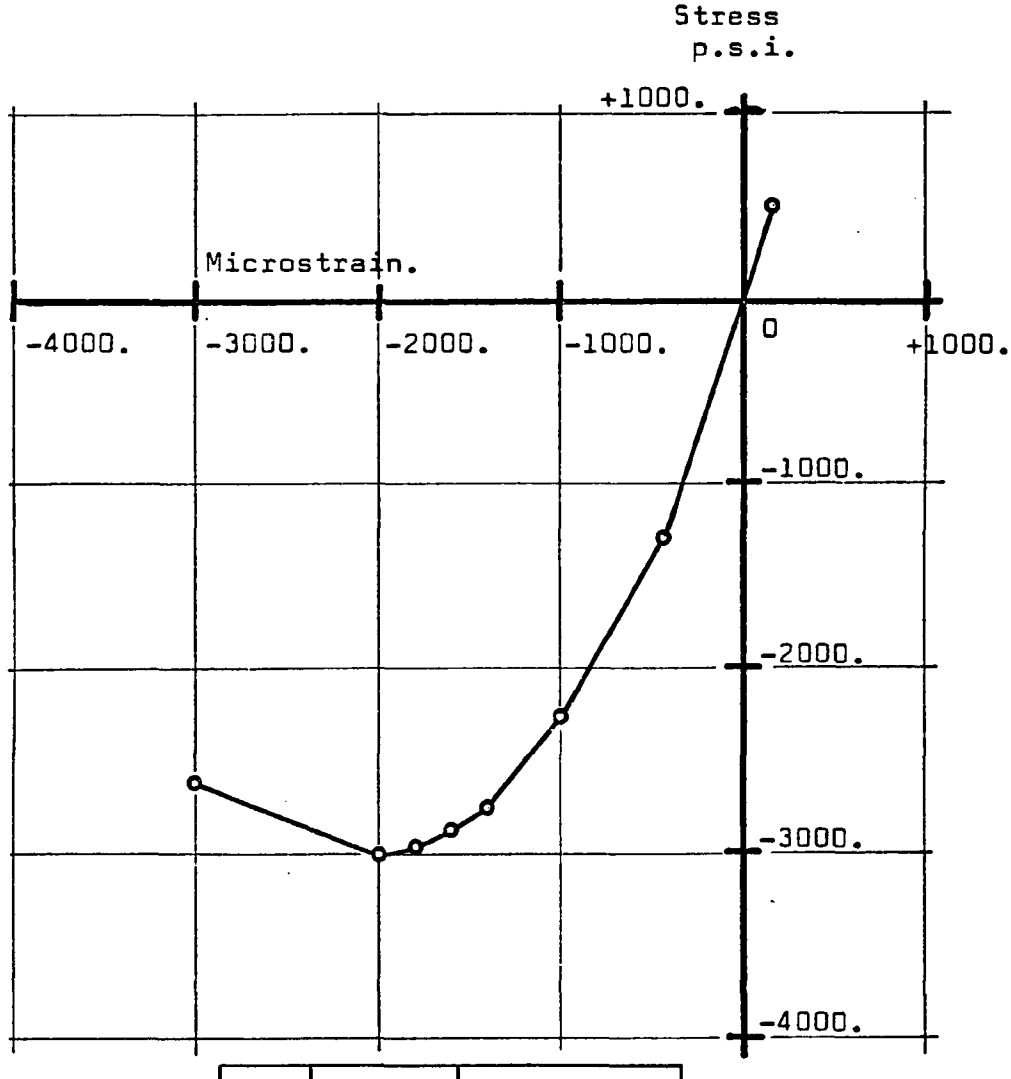

Ord	Stress	Microstrain
1	500.	167
2	0.	0
3	-1300.	-434
4	-2250.	-1000.
5	-2750.	-1400
6	-2870.	-1600
7	-2970.	-1800
8	-3000.	-2000
9	-2600.	-3000

FIGURE 6.10 SELECTED CONCRETE STRESS-STRAIN CURVE.

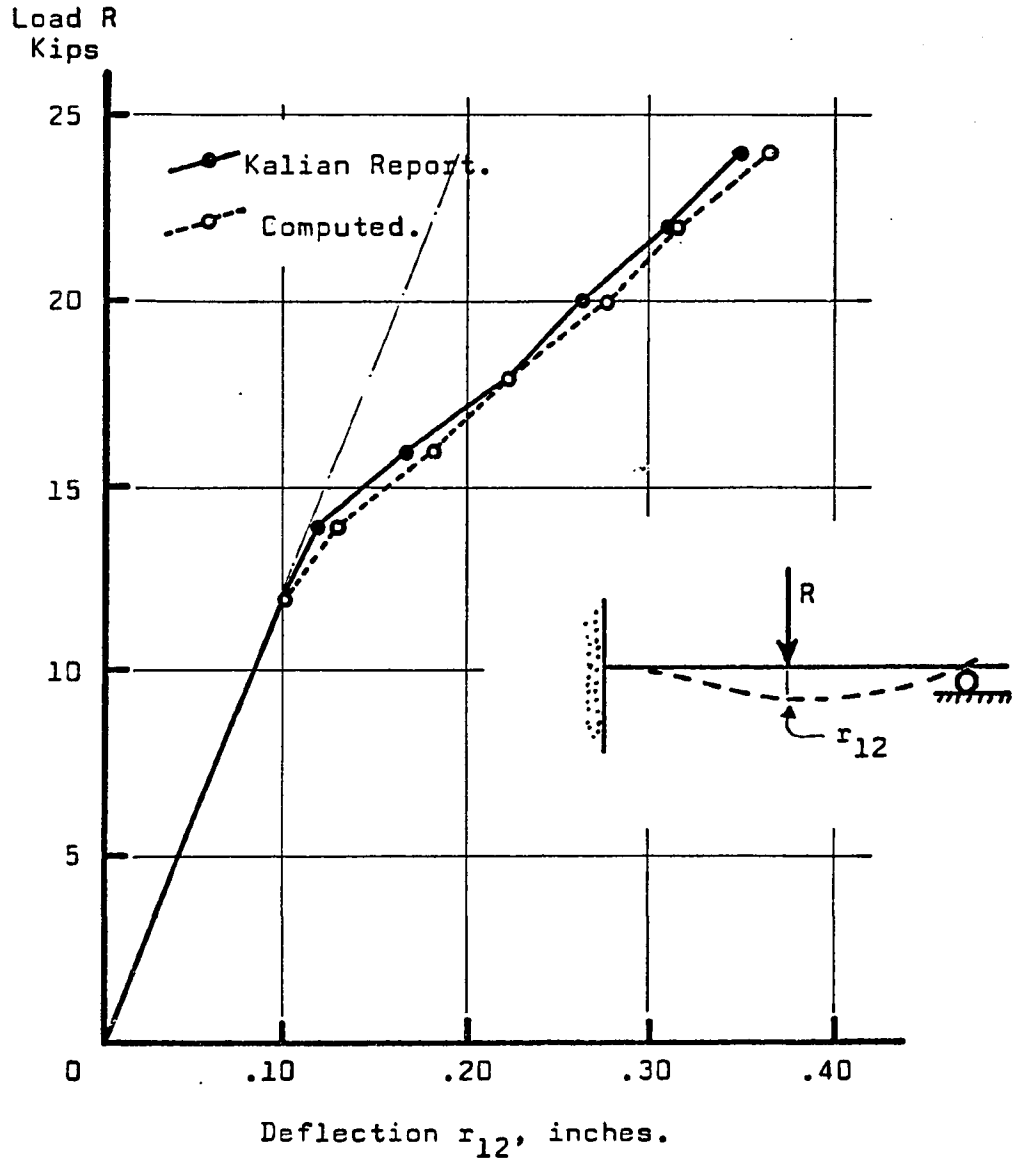

FIGURE 6.11 LOAD-DEFLECTION RESULTS.

Load Increment		Total Load	Total Deflection	No. of
No.	Size	Kips	r_{12} inches	Cycles
1	12.	12.	-.101076	1
2	2.	14.	-.131405	5
3	2.	16.	-.187518	7
4	2.	18.	-.225266	4
5	2.	20.	-.285489	5
6	2.	22.	-.322657	3
7	2.	24.	-.367172	5
		Total cycles =		30

TABLE 6.5

ITERATIONS REQUIRED FOR BEAM SOLUTION.

N	Total Cycles	Total Newly Failed Slices	Total Fractured Slices Per Element.										
			1	2	3	4	9	10	11	12	13	14	15
1	1	0	0	0	0	0	0	0	0	0	0	0	0
2	5	4	4	0	0	0	0	0	0	0	0	0	0
3	7	14	4	4	0	0	0	0	3	4	3	0	0
4	4	6	5	4	0	0	0	0	4	4	4	3	0
5	5	13	5	5	4	0	0	4	4	4	4	4	3
6	3	4	5	5	5	0	0	4	5	5	4	4	4
7	5	8	5	5	5	4	3	4	5	5	5	4	4

TABLE 6.6

DEVELOPMENT OF BEAM CRACKING.

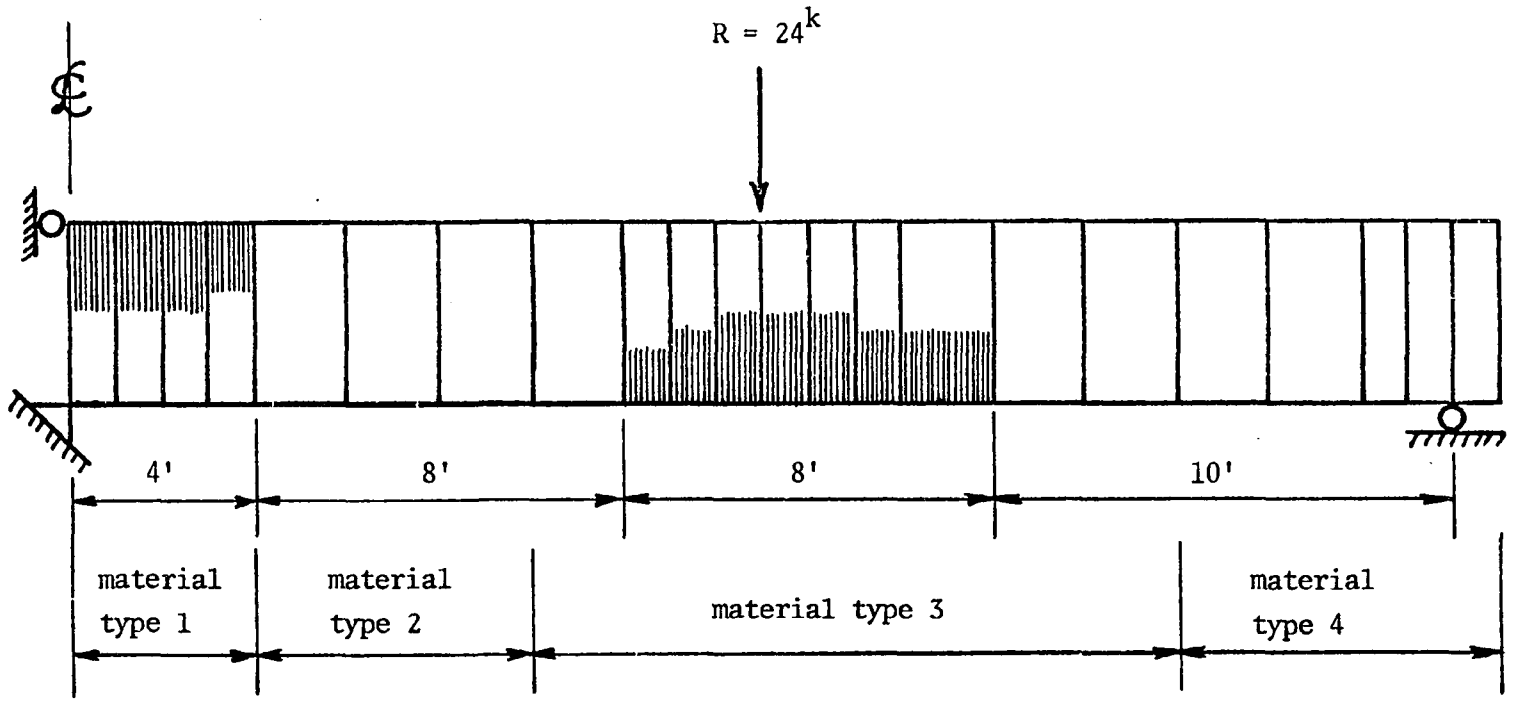

FIGURE 6.12 CRACKED CONDITION AT MAXIMUM LOAD.

6.4 Analysis of Experimental Beams

A fundamental way of assessing the value and characteristics of any analytical method is to compare the results obtained for a given structural system by analysis and by experiment. Accordingly the present formulations for a nonlinear, fracturing system were applied to a reinforced concrete beam that was selected from an extensive experimental testing program (25). This program of earlier years provided a large amount of data about testing to failure several groups of beams. In particular, there were load-deflection curves, cracking patterns and crack development data, and details of the geometry and material stress-strain laws. The selected beams (XOB-1 and OB-1) had no web reinforcement and were weaker, less complicated examples for a trial analysis. Their geometry and general layout is shown in Figure 6.13.

6.4.1 The Beam Discretization

The analysis was performed in duplicate with two kinds of finite elements so that the accuracy of both elements could be assessed. The first model used the quadrilateral finite elements for the beam concrete and also rod elements for the steel reinforcement layers. The layout of this discretization is given in Figure 6.14 and can be immediately compared with the second model, using frame elements, shown in Figure 6.15. Each frame element is chosen to correspond to a column of quadrilateral elements in the other model so that comparisons of stresses could be facilitated.

The numbering of the nodes in both models is arranged specifically to minimize the band width of the stiffness array and

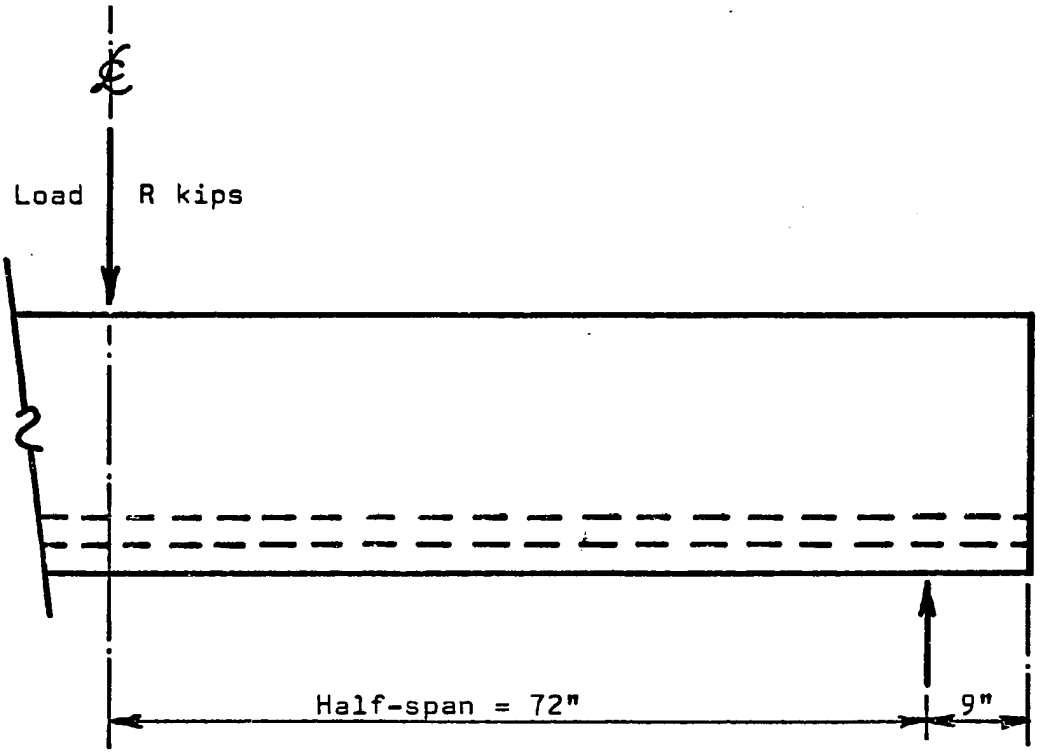

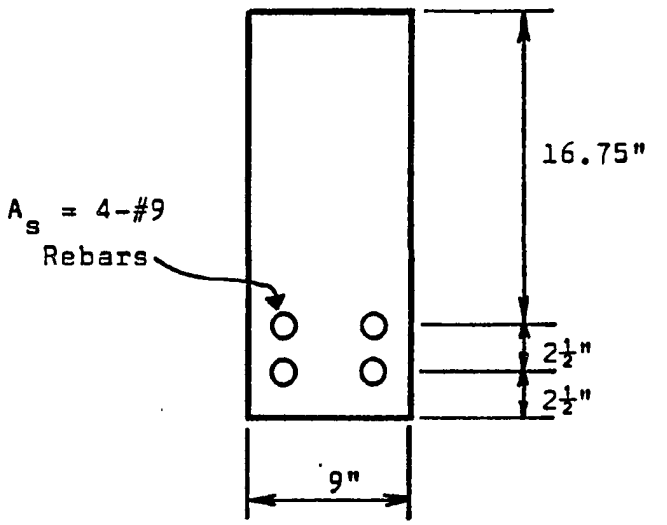

FIGURE 6.13 GEOMETRY OF BEAM SPECIMENS.

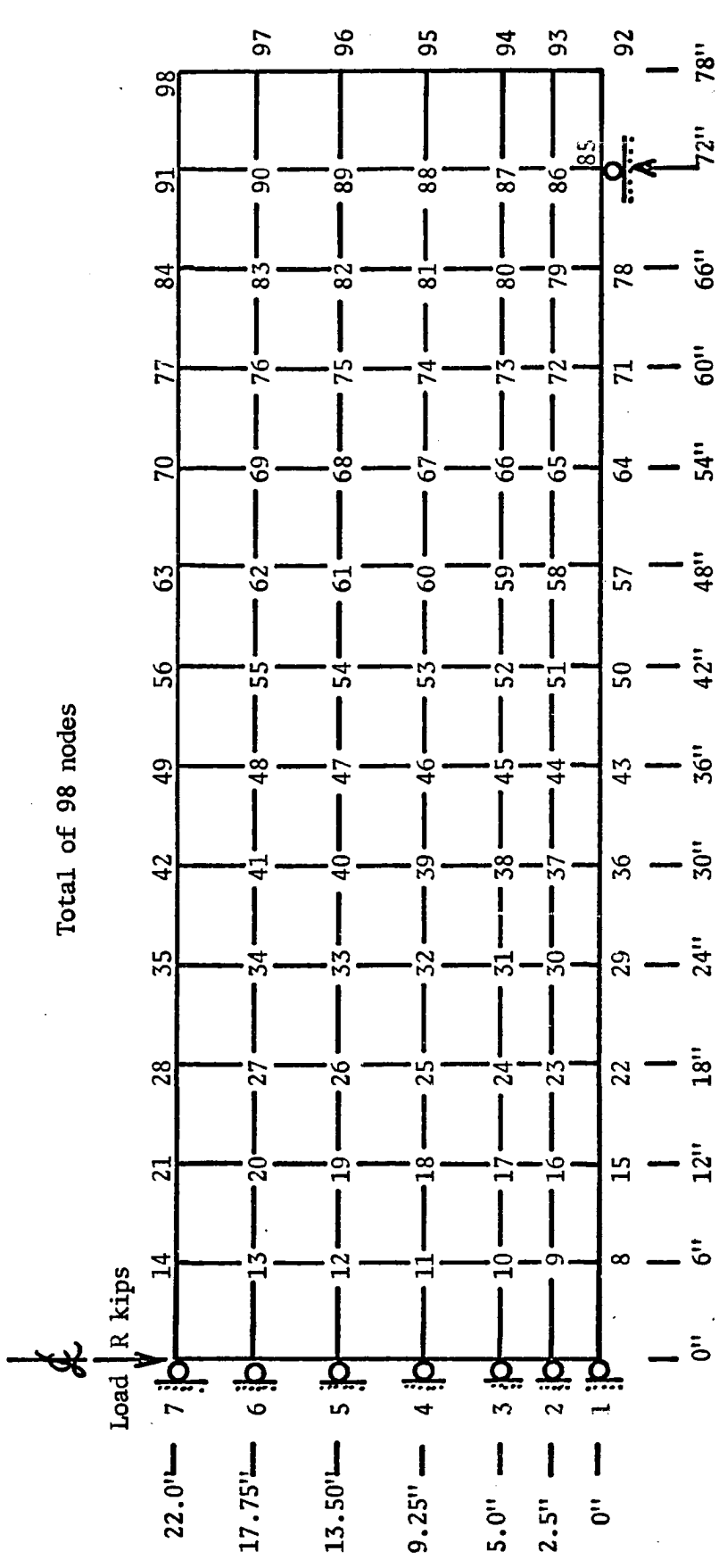

MODEL WITH QUADRILATERAL AND ROD ELEMENTS

FIGURE 6.14 (A) MESH GEOMETRY AND NODE NUMBERS.

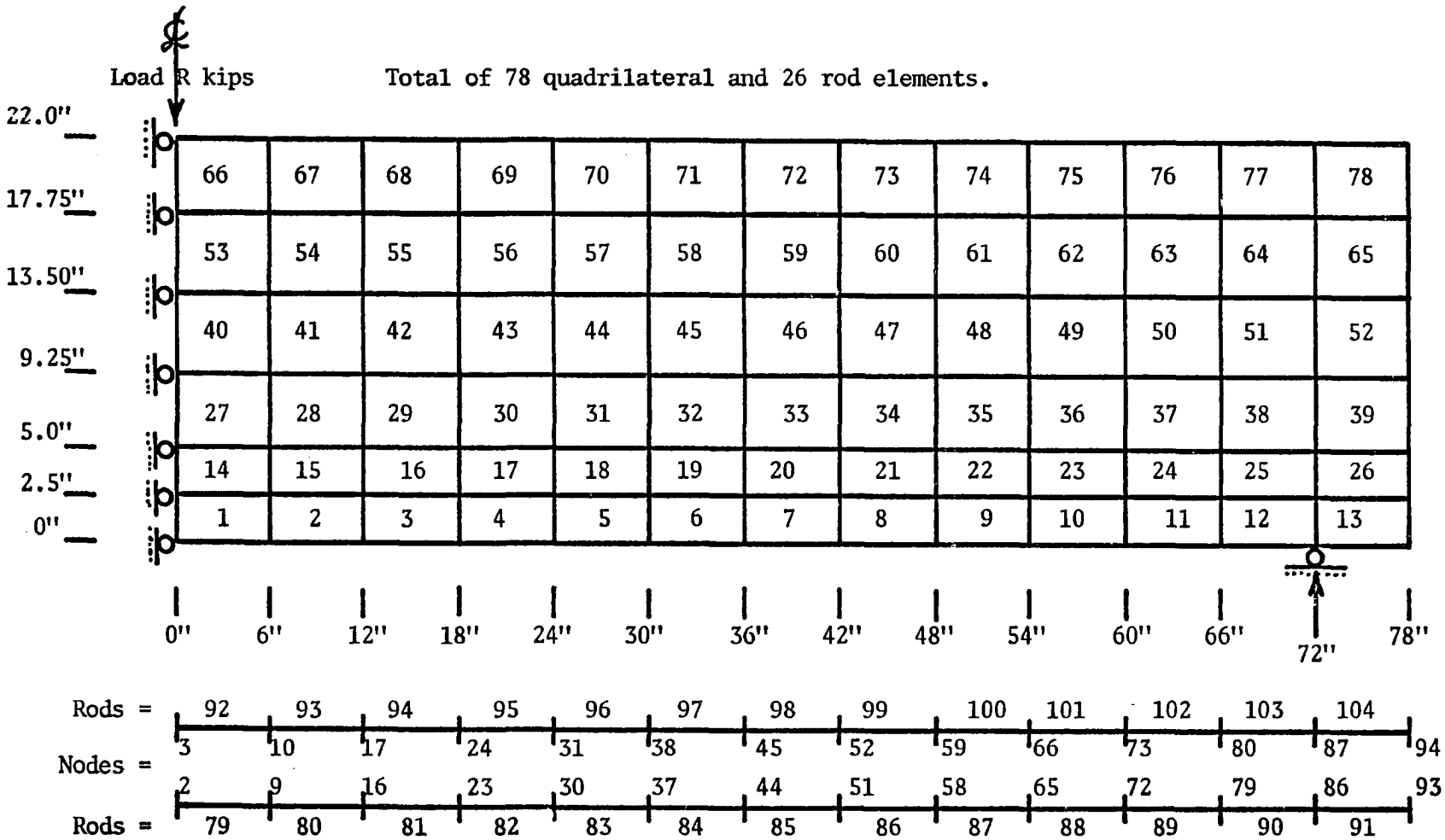

MODEL WITH QUADRILATERAL AND ROD ELEMENTS.

FIGURE 6.14(B) LAYOUT OF ELEMENTS.

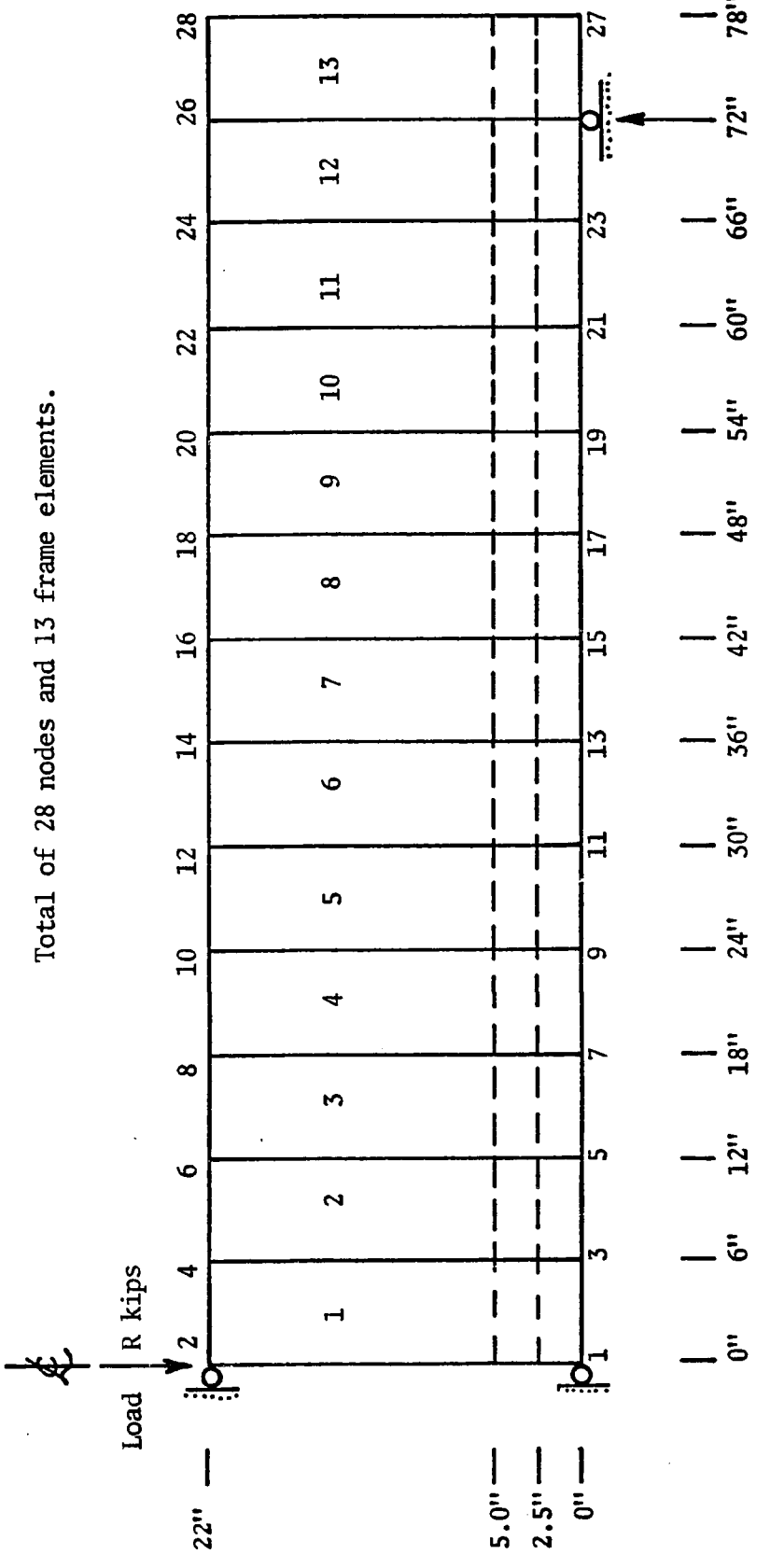

FIGURE 6.15 DISCRETIZATION WITH FRAME ELEMENTS.

maximize the efficiency of solutions. Numbering of the elements is arranged simply to reduce the number of cards required for the data input.

The average compressive strength of the actual concrete mixes for these beams was 3540 psi for an intended 3500 psi mix design. By using a plot of the measured range of stress-strain values for several mixes, the stress-strain curve for the analysis was constructed and is plotted in Figure 6.16. The direct tensile strength of this concrete was estimated at 300 psi by using approximately half of the average modulus of rupture given by tests. A complete stress-strain curve for the high-strength steel reinforcement was available and was modelled directly in the multilinear form needed for the analysis. This is plotted in Figure 6.17. These simple-span beams were recorded as failing at about 58 kips load so that the analytical load increments were chosen to go as high as 70 kips before terminating the problem.

6.4.2 Results Using Frame Elements

The analytical results that come from using these elements are discussed first and then their advantages or deficiencies will be brought out by comparison with the results given by the quadrilateral plane stress elements.

The analytical half-beam only required 28 nodes and 13 frame elements for its discretization (see Figure 6.15) and the analysis took 180.2 seconds on the CDC-6400 computer to increase the load up to 70 kips. Since each iteration is a complete solution of the system, then the listing of Table 6.7 shows that 40 solutions were

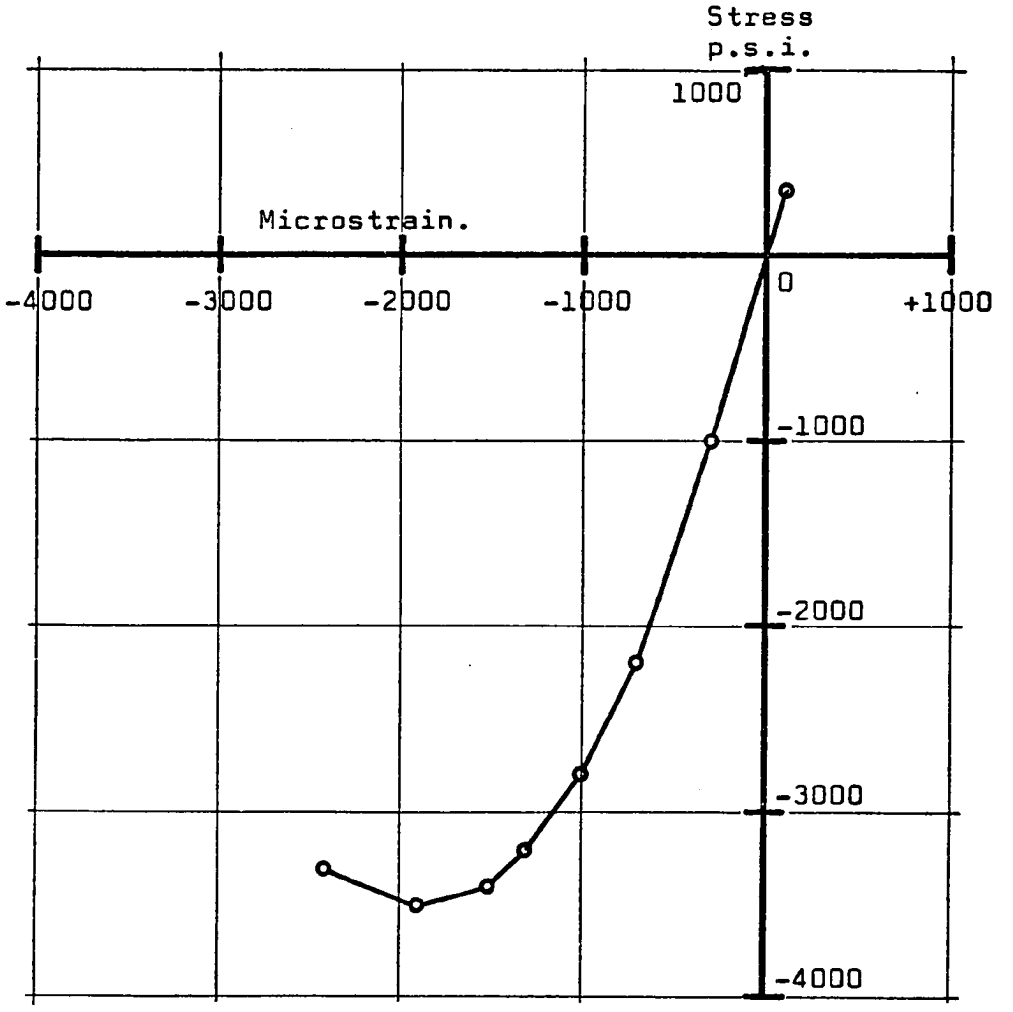

Ord	Stress	Microstrain
1	333.	100
2	0.	0
3	-1000.	-300
4	-2200.	-700
5	-2800.	-1000
6	-3200.	-1300
7	-3400.	-1500
8	-3500.	-1900
9	-3300.	-2400

FIGURE 6.16 EXPERIMENTAL CONCRETE STRESS-STRAIN CURVE.

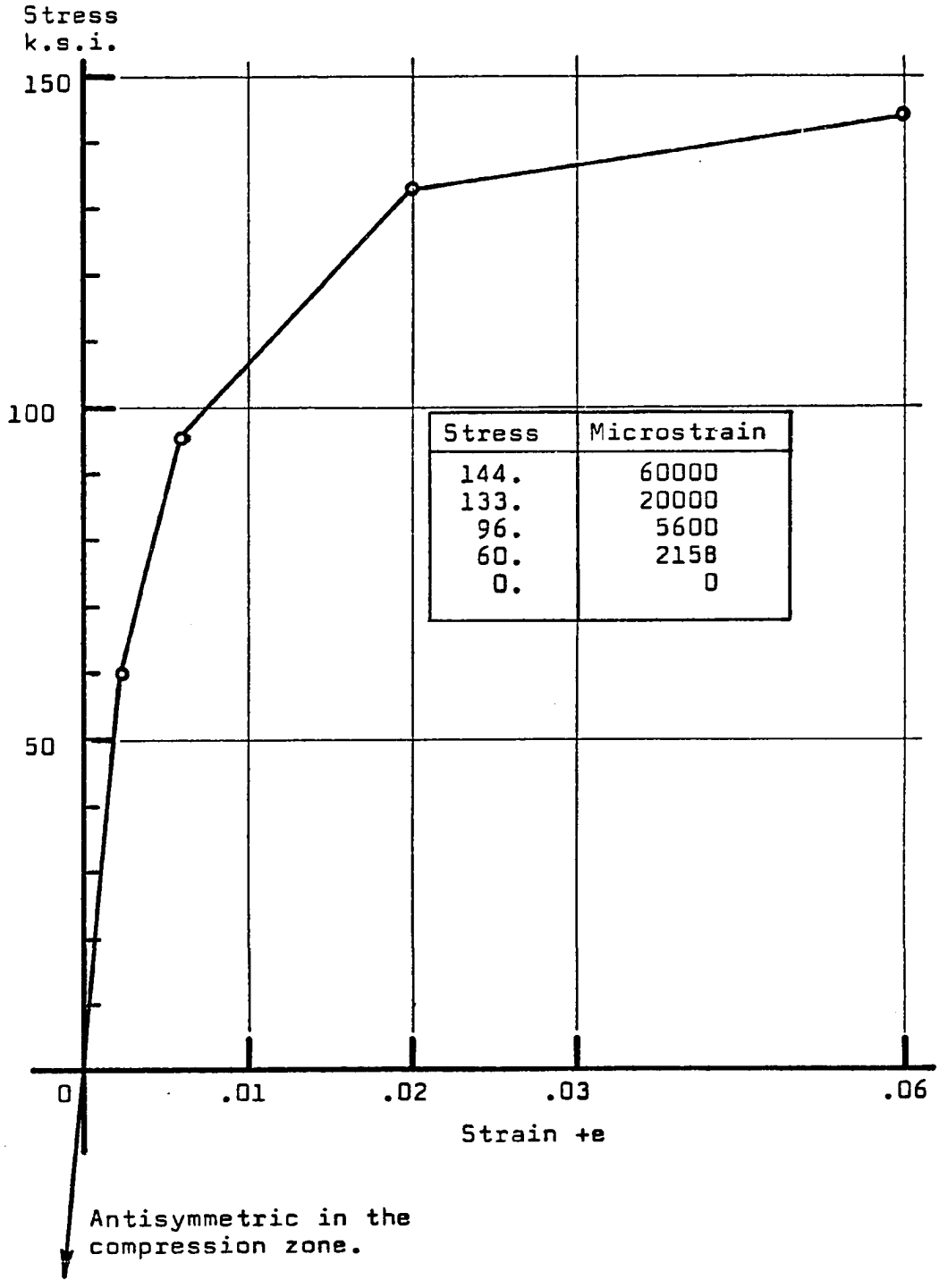

FIGURE 6.17 REINFORCEMENT STRESS-STRAIN CURVE.

Load Increment		Total Load	Total Deflection	No. of
No.	Size	Kips	Inches	Cycles
1	10.	10.	.019905	1
2	10.	20.	.073656	5
3	10.	30.	.117639	5
4	5.	35.	.140885	4
5	5.	40.	.162590	2
6	5.	45.	.183896	2
7	5.	50.	.206704	4
8	2.	52.	.215545	2
9	2.	54.	.224196	1
10	2.	56.	.233449	2
11	2.	58.	.242319	2
12	2.	60.	.251379	2
13	2.	62.	.260423	1
14	2.	64.	.269646	2
15	2.	66.	.279457	2
16	2.	68.	.288803	1
17	2.	70.	.298400	2
		Total cycles = 40		

TABLE 6.7

LOAD-DEFLECTION RESULTS WITH FRAME ELEMENTS.

required to produce the load-deflection curve given in Figure 6.18. The load-deflection curve (approximate) of the experimental beams OB-1 and XOB-1 (25) is also plotted there. These results show that the frame element model is much stronger and somewhat stiffer than the real beams. The material properties of the nonlinear concrete used for this analysis were averaged from the data given for these beams, and since the load-deflection behavior agrees very well before cracking occurs, then the definition of the materials may be discounted as a cause of the increased system stiffness. The other important source of nonlinear behavior is the cracking mechanism of the system, that is, the effects of the sequence of occurrence of cracks. The record of the occurrence of cracking during the analysis is given in Table 6.8. A definite transition to a cracked section condition occurs early in the loading and then slight cracking occurs occasionally thereafter up to the maximu applied load. The appearance of the analytical cracking at 56 kips loading is plotted in Figure 6.19 and is selected in order to correspond to the situation just prior to failure of the experimental beams. In order to express the actual cracking as realistically as possible, the crack patterns for a given experimental beam are taken from both sides of the beam and superimposed in the single view of that beam given in Figure 6.20. The depth of the analytic cracking agrees closely with the depth of the actual cracking at this high load level, and the increase in stiffness of the model causes the model to exhibit about the same deflection as the real beams just before their failure. However, the initiation of cracking in the model, after 10 kips loading, does not compare well with the real beams,

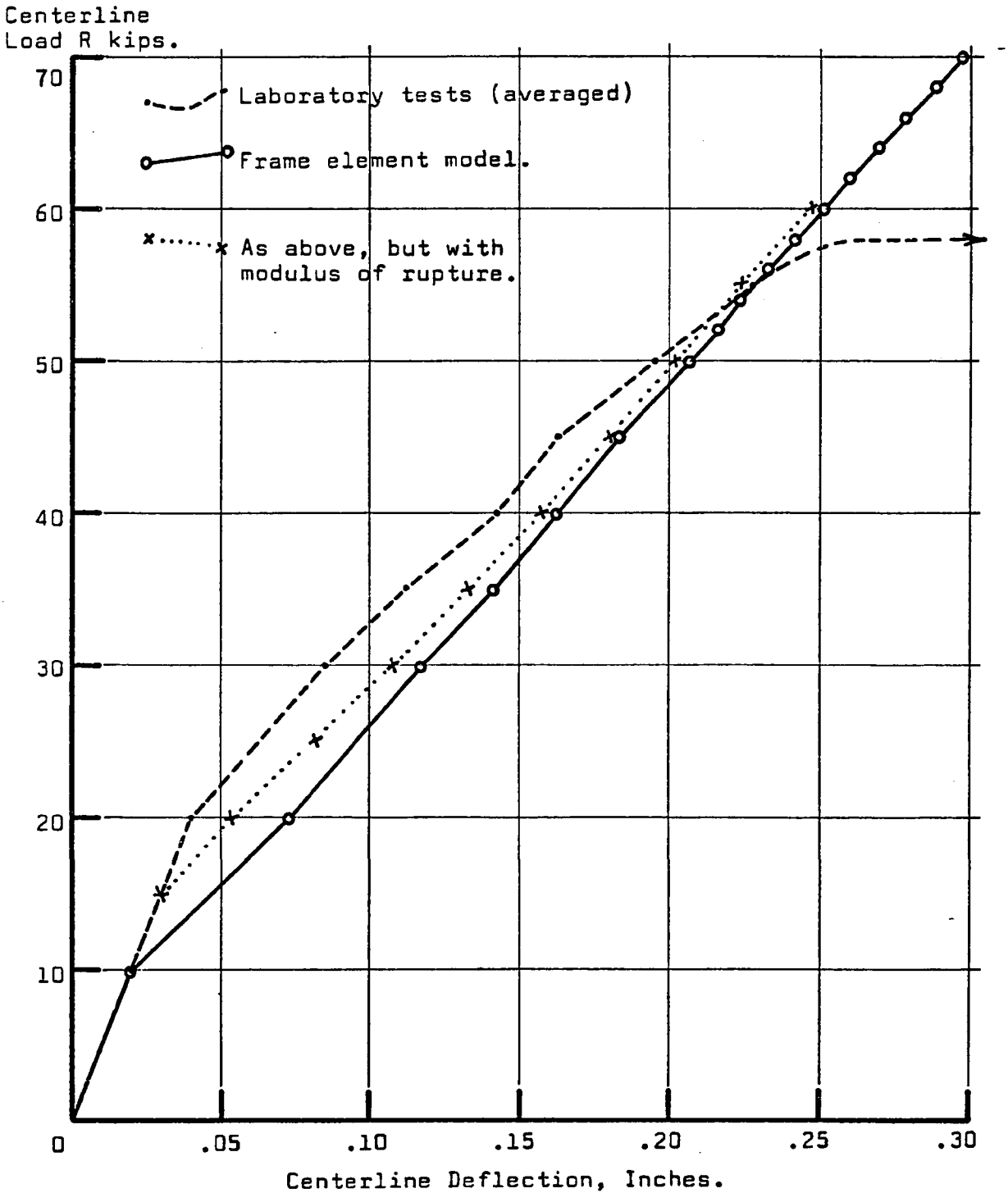

FIGURE 6.18 LOAD-DEFLECTION WITH FRAME ELEMENTS.

N	Total Cycles	Total Newly Failed Slices	Total Fractured Slices Per Element No.									
			1	2	3	4	5	6	7	8	9	10
1	1	0										
2	5	27	5	5	5	4	4	4				
3	5	11	5	5	5	5	5	5	4	4		
4	4	6	6	6	5	5	5	5	5	4	3	
5	2	3	6	6	6	5	5	5	5	5	4	
6	2	1	6	6	6	6	5	5	5	5	4	
7	4	1	6	6	6	6	6	5	5	5	5	3
8	2	1	6	6	6	6	6	5	5	5	5	4
9	1	0	6	6	6	6	6	5	5	5	5	4
10	2	1	6	6	6	6	6	6	5	5	5	4
11	2	0	6	6	6	6	6	6	5	5	5	4
12	2	0	6	6	6	6	6	6	5	5	5	4
13	1	0	6	6	6	6	6	6	5	5	5	4
14	2	0	6	6	6	6	6	6	5	5	5	4
15	2	1	6	6	6	6	6	6	6	5	5	4
16	1	0	6	6	6	6	6	6	6	5	5	4
17	2	1	6	6	6	6	6	6	6	5	5	5

TABLE 6.8

DEVELOPMENT OF BEAM CRACKING WITH FRAME ELEMENTS.

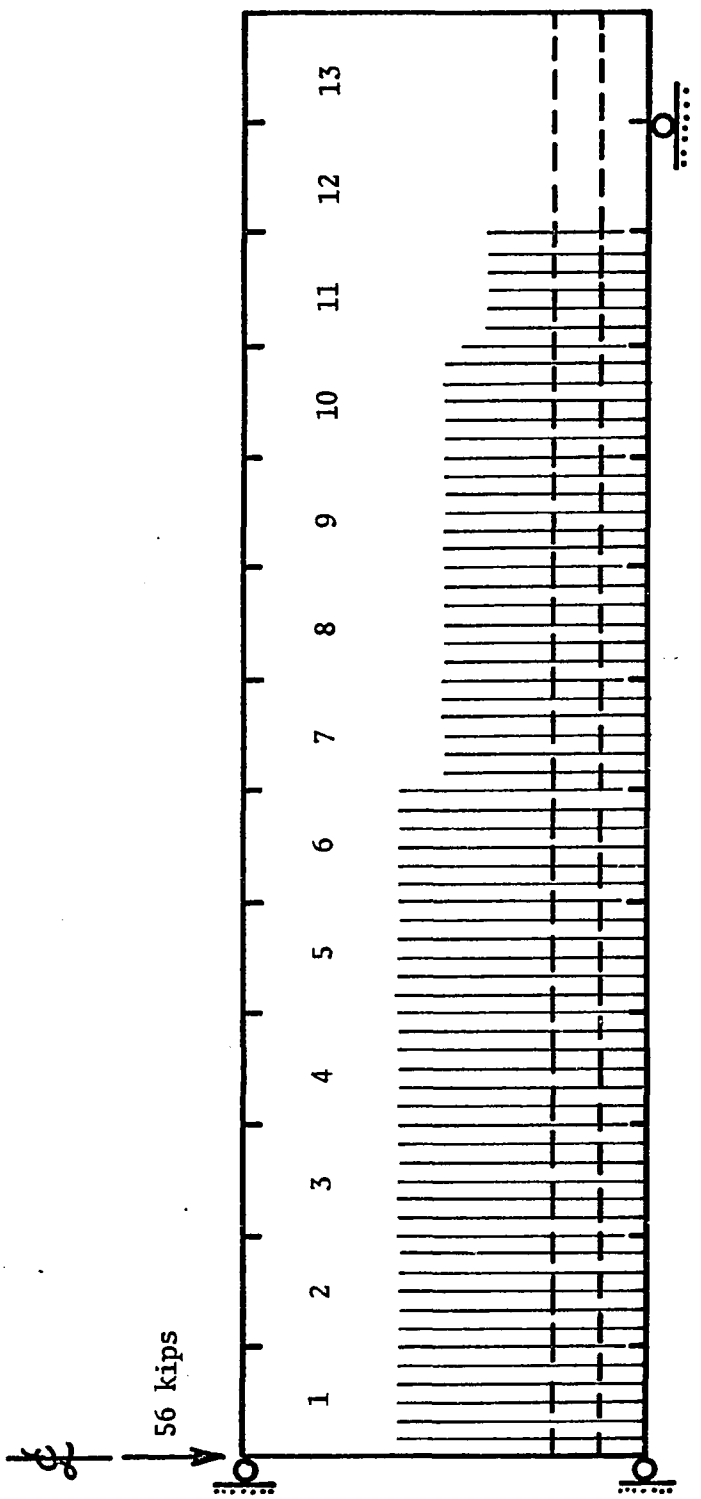

FIGURE 6.19 CRACKING OF FRAME ELEMENT MODEL

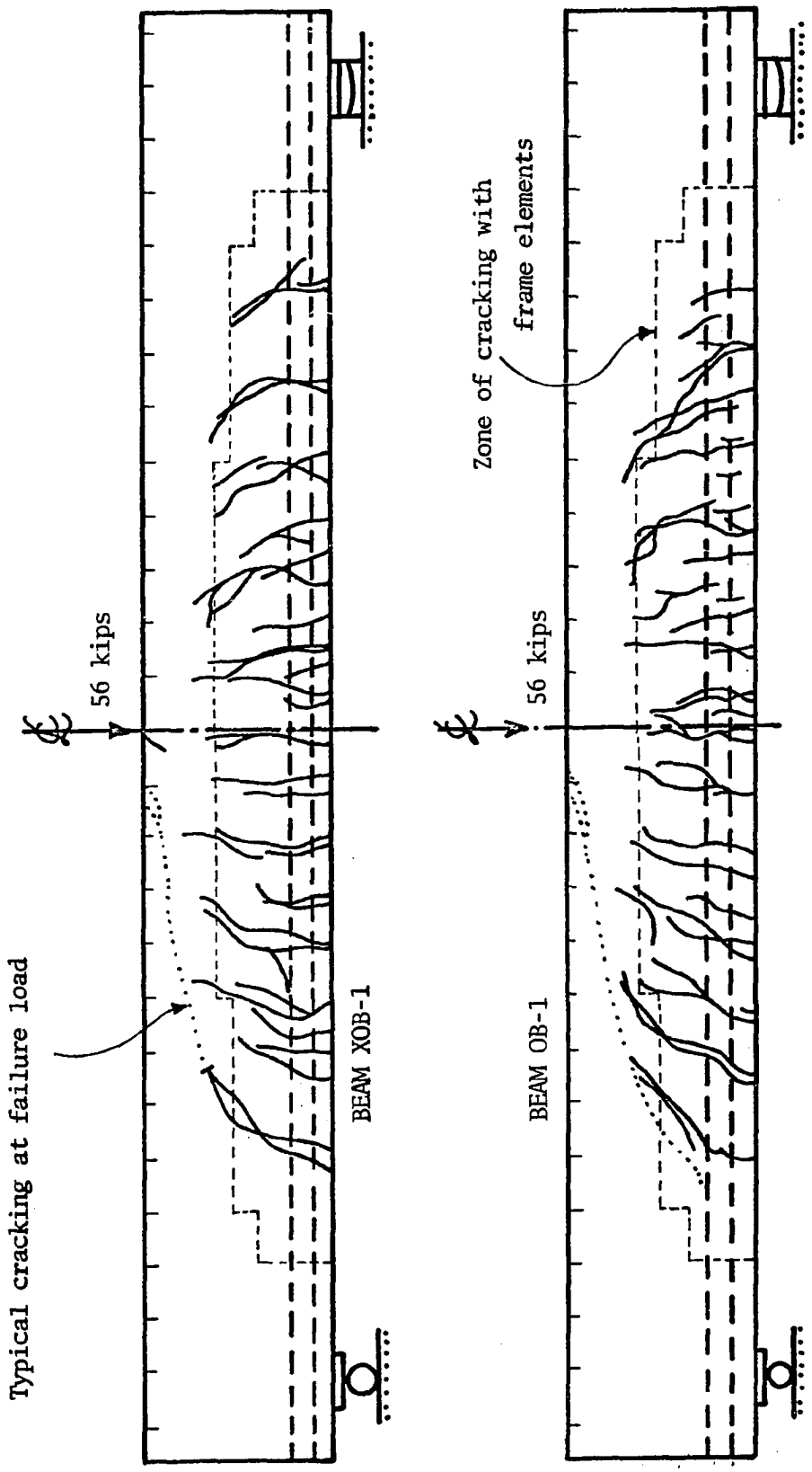

FIGURE 6.20 CRACKING OF EXPERIMENTAL BEAMS.

which started at about 20 kips loading. To seek some improvement, the analysis was repeated using the higher modulus of rupture (565 psi) of the concrete rather than the estimated tensile strength (333 psi). This increased the load capacity before cracking started but again failed to match the behavior of the real beams in this detail.

The error in this procedure derives from the fact that the failure criterion is really a strain criterion. Increasing the ultimate stress value did indeed increase the ultimate strain and so conveniently improved the analysis for cracking load. However, a better procedure would have been to increase the ultimate tensile strain limit to compare with the observed cracking load.

As loading increases, strain energy is stored in a very small area of tensile concrete and in an increasing area of compression concrete. As the ratio of the tensile area decreases relative to the total uncracked cross-section area so the significance of the tensile concrete decreases. Consequently, as the load goes beyond 2 or 3 times the cracking load, the significance of modulus of rupture versus tensile strength decreases, and the plots of Figure 6.18 verify that both models begin to show about the same behavior.

The redistribution of forces within the cracked beam is reflected by the changes in steel stress that occur from section to section as the load increases. No comparable data is available from the tests of the experimental beams but some of the analytical results are plotted in Figure 6.21.

The purpose of testing the frame elements was to determine whether they would be adequate for the modelling of a cracked

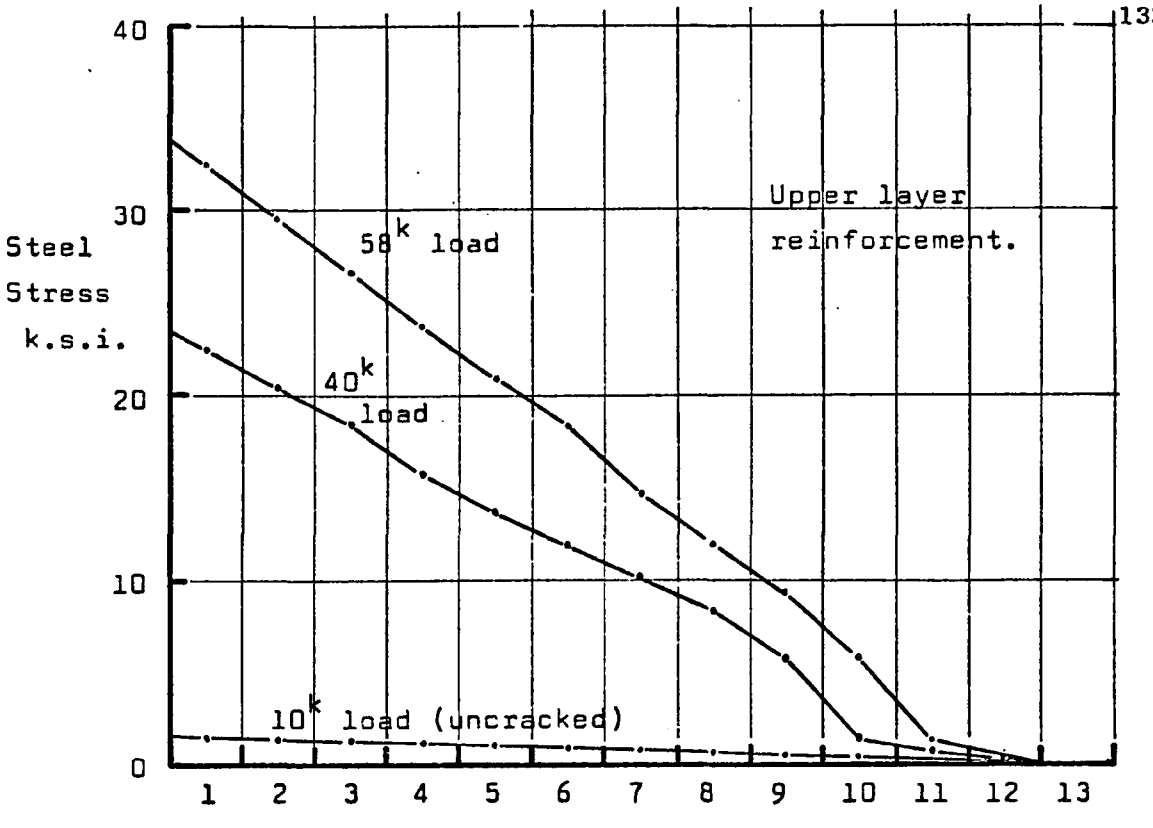

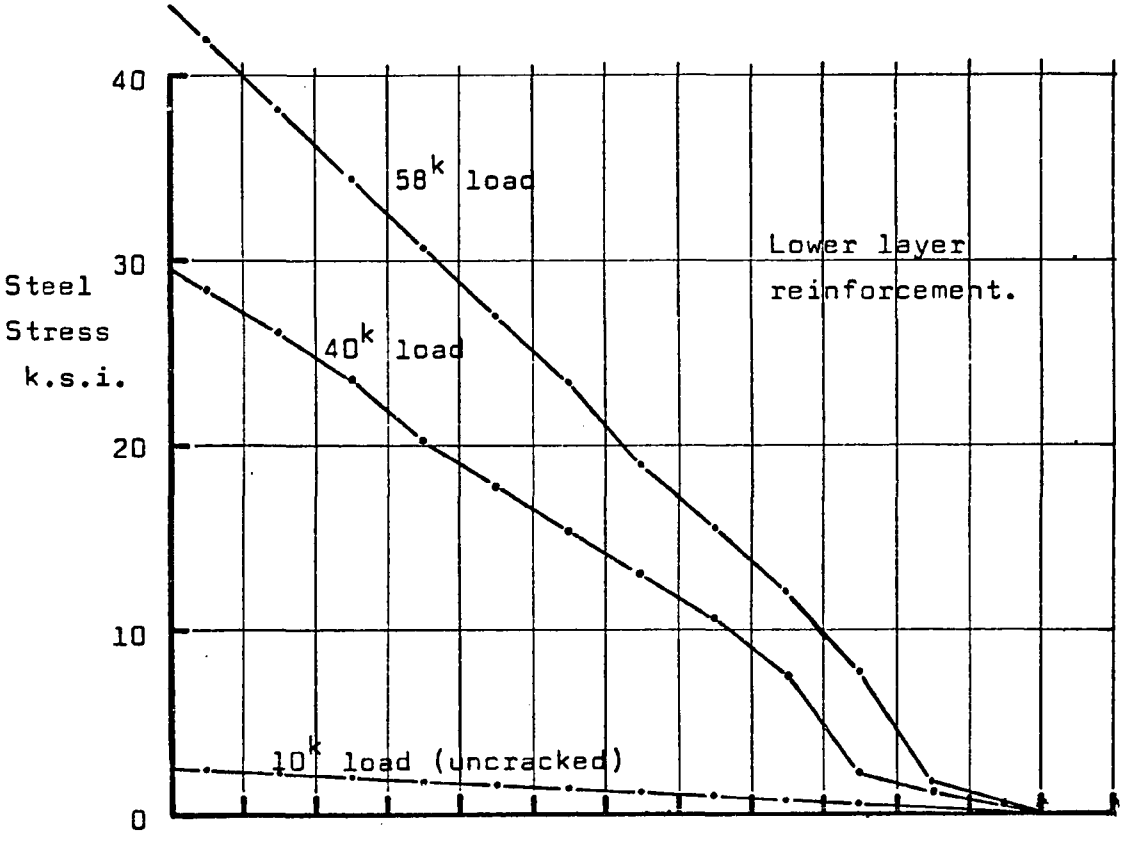

FIGURE 6.21 STEEL STRESSES, FRAME ELEMENT MODEL

concrete frame and to get some idea of their limitations. The results obtained so far show the following interesting features: (a) the determination of the cracking load is sensitive to the value used for the ultimate tensile strain of the concrete, (b) the model of the cracked beam is slightly stiffer and rather more linear than the real, cracked beams, and (c) the model maintains this linearity well past the failure of the real beams which show first some decrease in stiffness before a distinctively rapid diagonal tension failure. Thus the frame element model is inadequate for ultimate strength conditions which involve failure due to critical combinations of flexural and shear stresses rather than simple flexural failure modes.

6.4.3 Results Using Quadrilateral Elements

Testing the quadrilateral plane stress elements was done by modelling the same experimental beams as shown in Figures 6.14 and using rod elements for the two layers of reinforcement. The purpose of this testing was, of course, basically to verify that the formulations for their nonlinear and failure behavior would be adequate for modelling the plane stress panels. The beam example was used for this testing because (a) adequacy in modelling the complex internal state of a reinforced concrete beam would be satisfactory to confirm the adequacy of these elements for a plane stress shear panel, and (b) the results of these analyses could be used for further comparisons with the frame element model. Thus the same material properties were used for the concrete (Figure 6.16) and for the reinforcing steel (Figure 6.17). This meant also that the analytical steel was regarded as two concentrated areas at the

levels of the two actual steel layers, and so two lines of rod elements appear in this model. Since this model does not use the transformed area concept which occurs in the frame elements, then it is necessary to suitably reduce the section area of the rod elements before the analysis in order to make some compensation for the displaced concrete.

Let the actual reinforcement area be A_s and the reduced area be A_s^*. If the desired transformed area for equivalent force capacity is A_t, then using $n = E_s/E_c$ as usual,

$$A_t = (n-1)\ A_s = n\ A_s^*$$

This gives

$$A_s^* = (n-1)\ A_s/n$$

For the materials of these tests, the initial values of moduli give $n = 27.80/3.33 = 8.35$, so that for a real area $A_s = 2.00$ sq. inches then the equivalent reduced area is

$$A_s^* = 7.35\ (2.00)/8.35 = 0.88 \times 2.00$$
$$= 1.76 \text{ sq. inches.}$$

All of the quadrilateral element models except the first included the reduced area A_s^* and so some results are given that show the effect on the beam stiffness.

The analytical half-beam now required 98 nodes, 78 quadrilaterals, and 26 rod elements (a total of 104 elements) for the discretization (Figure 6.14) and the analysis took 432.3 seconds on the CDC-6400 computer up to a maximum load of 70 kips. This load was reached in 14 increments with the iteration history shown in Table 6.9.

Load Increment		Total Load	Total Deflection	No. of
No.	Size	Kips	Inches	Cycles
1	10.	10.	.021002	1
2	10.	20.	.066486	4
3	10.	30.	.104609	4
4	5.	35.	.124681	2
5	5.	40.	.143651	2
6	5.	45.	.161712	1
7	5.	50.	.181415	3
8	4.	54.	.196050	1
9	4.	58.	.211101	2
10	4.	62.	.226095	2
11	2.	64.	.233780	2
12	2.	66.	.242531	3
13	2.	68.	.250012	1
14	2.	70.	.257528	1
		Total cycles = 29		

TABLE 6.9

LOAD-DEFLECTION RESULTS WITH QUADRILATERAL ELEMENTS.

The quadrilateral elements of this analysis used only the simple ultimate tensile strain theory for determining the cracking in the principal strain directions. Since this model gives a complete picture of the principal stress trajectories as a feature of the analysis, then the analytic cracking that occurs shows a realistic orientation compared with that obtained from using the frame elements. The analytic cracking at a load of about 56 kips is plotted in Figure 6.22(A) in terms of a 'continuum of cracking' in each element and then this is condensed by selecting a few typical continuous crack paths to give the picture of Figure 6.22(B). The analytic cracking compares favorably with the real situation in terms of three interesting features.

(1) If a set of tensile cracks were to be plotted using the original principal stress trajectories of the loaded beam, then the cracks would be perpendicular to the bottom face. In fact, the gradual occurrence of cracks causes successive disturbances of the principal stress field so that later cracks may be inclined in either direction to the bottom surface. This is to be seen in the real cracking of Figure 6.23 and in the analytic cracking of Figure 6.22.

(2) If a set of tensile cracks were plotted whose penetration was measured by the depth of the appropriate tensile zone in the uncracked state, then the crack penetrations would be maximum at the beam center-span and uniformly diminish to zero at some distance from the centerline. However, gradual cracking disturbs the tensile stress zones in a manner that gives a nonuniform crack penetration along the span. This behavior appears in the analytic cracking

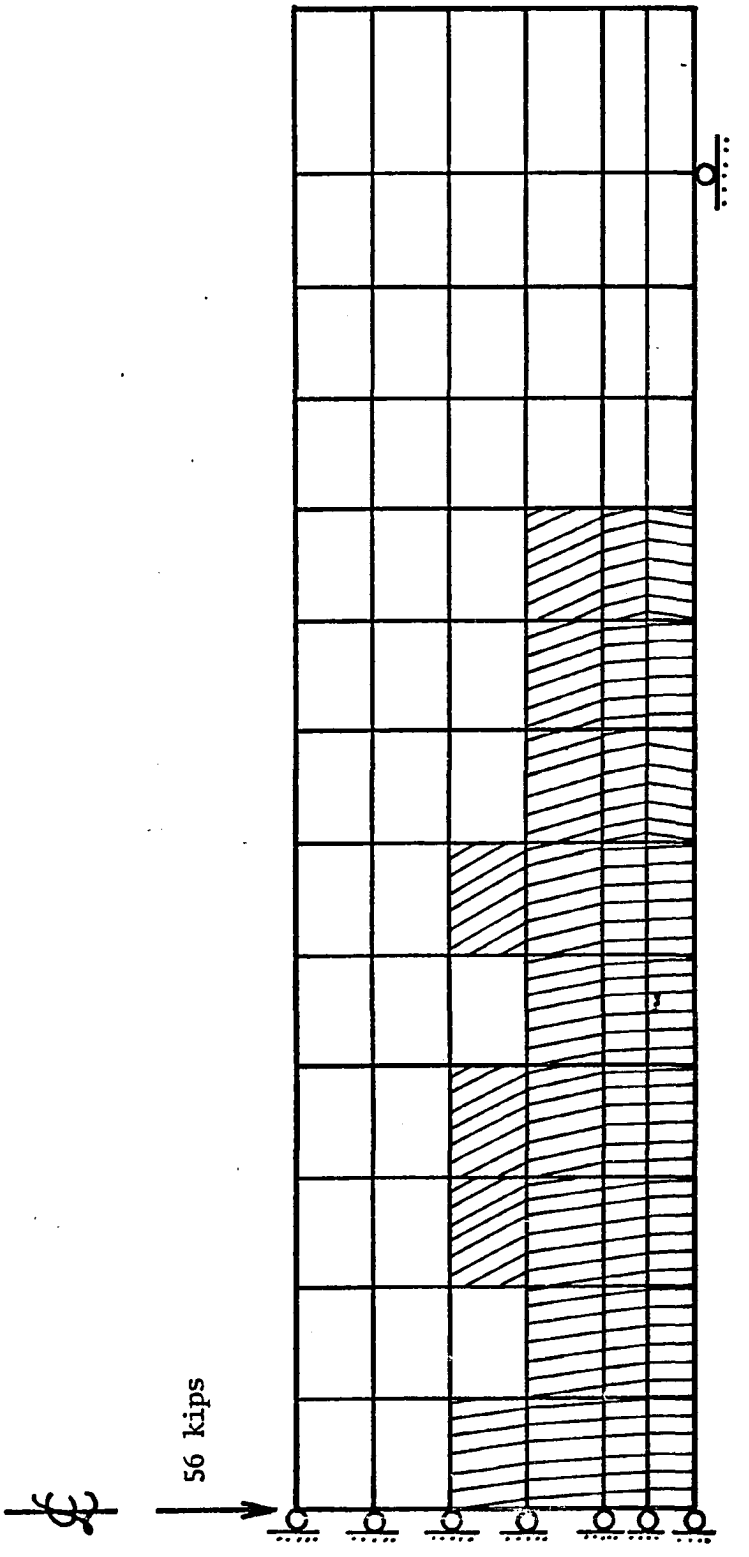

FIGURE 6.22(A) QUADRILATERAL ELEMENT CRACKING PATTERNS.

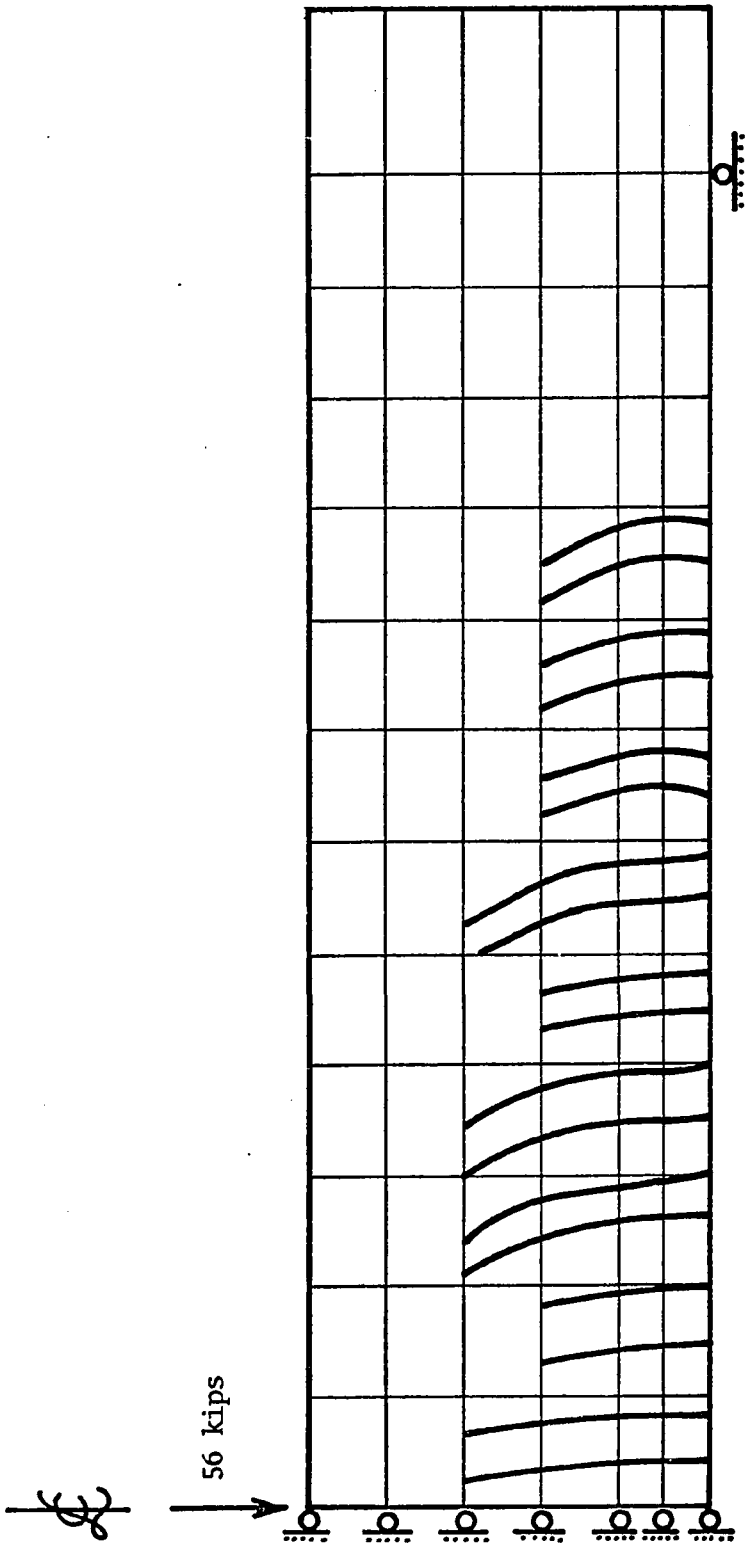

FIGURE 6.22(B) CONDENSATION OF THE ANALYTIC CRACKING.

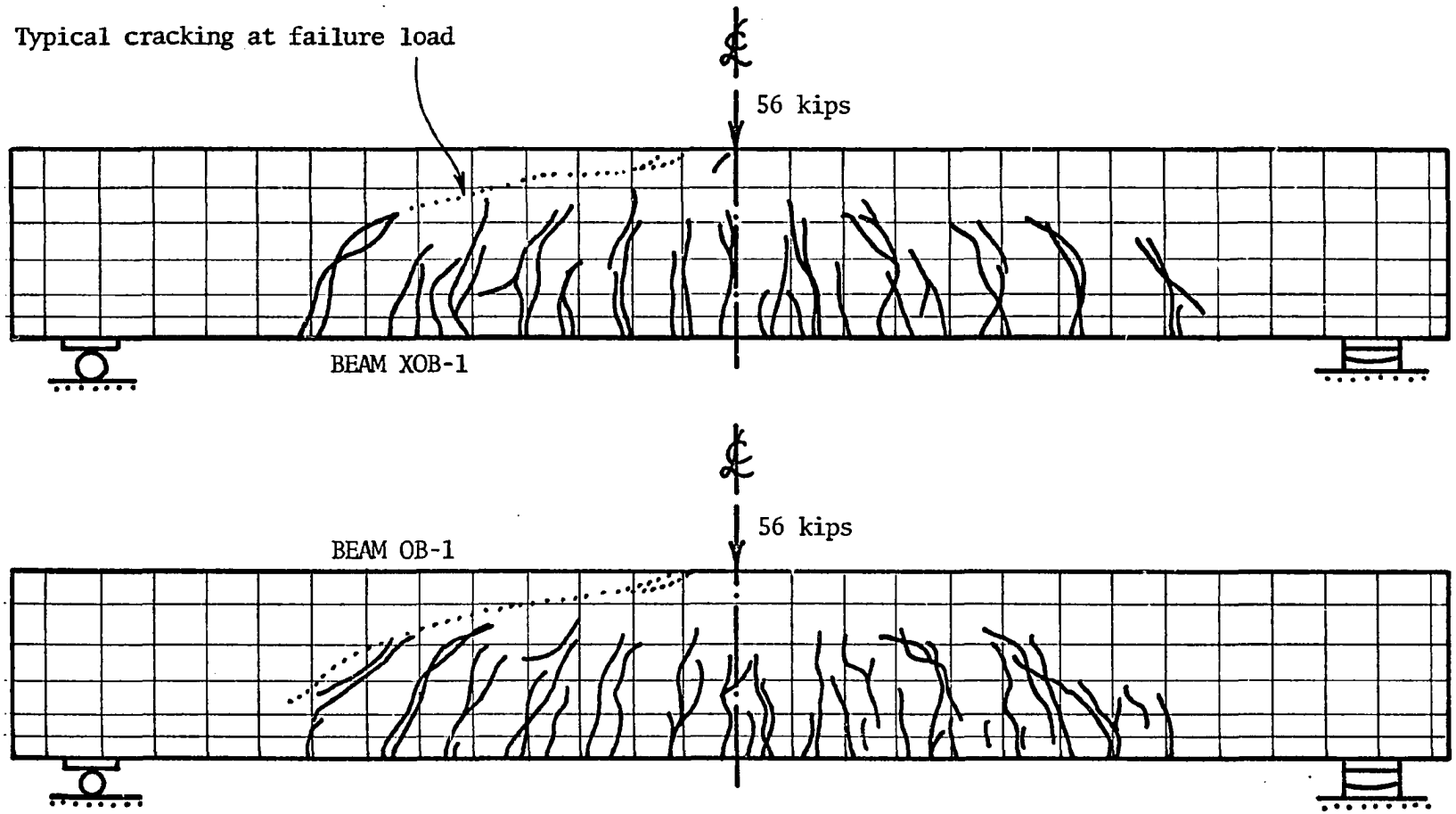

FIGURE 6.23 CRACKING OF EXPERIMENTAL BEAMS WITH QUAD ELEMENT MESH

(Figure 6.22) and may be seen by inspection of the real cracking (Figure 6.23).

(3) At this load magnitude, just before failure of the real beams, cracking in the quadrilateral model has extended over the same span distance as cracking in the real beams, whereas the frame element model showed cracking over a further 6" in each direction.

The load-deflection curve for this analysis (#111) is plotted in Figure 6.24 where it may be compared with the approximate curve obtained from the experimental beams. The additional stiffness of this model is partly due to using the full steel areas A_s rather than A_s^*. However, this seemed to be of little consequence compared to a major feature of the behavior, that the model was again much stronger than the real beams. The question now was to determine whether the system stiffness and strength increases were significantly related to the formulation of the quadrilateral elements (and so be relevant to determining their adequacy) or whether these factors were more dependent on other features of the construction of the model. This question was resolved by making two significant changes to the computer program for the next analyses.

Firstly, since the cracking behavior affects both the stiffness and strength of the system then an improvement in the cracking criterion should improve the overall results. This preliminary analysis used only the simple ultimate tensile strain to determine cracking, but some deficiency in the cracking of the quadrilateral elements is observed in the region where the diagonal

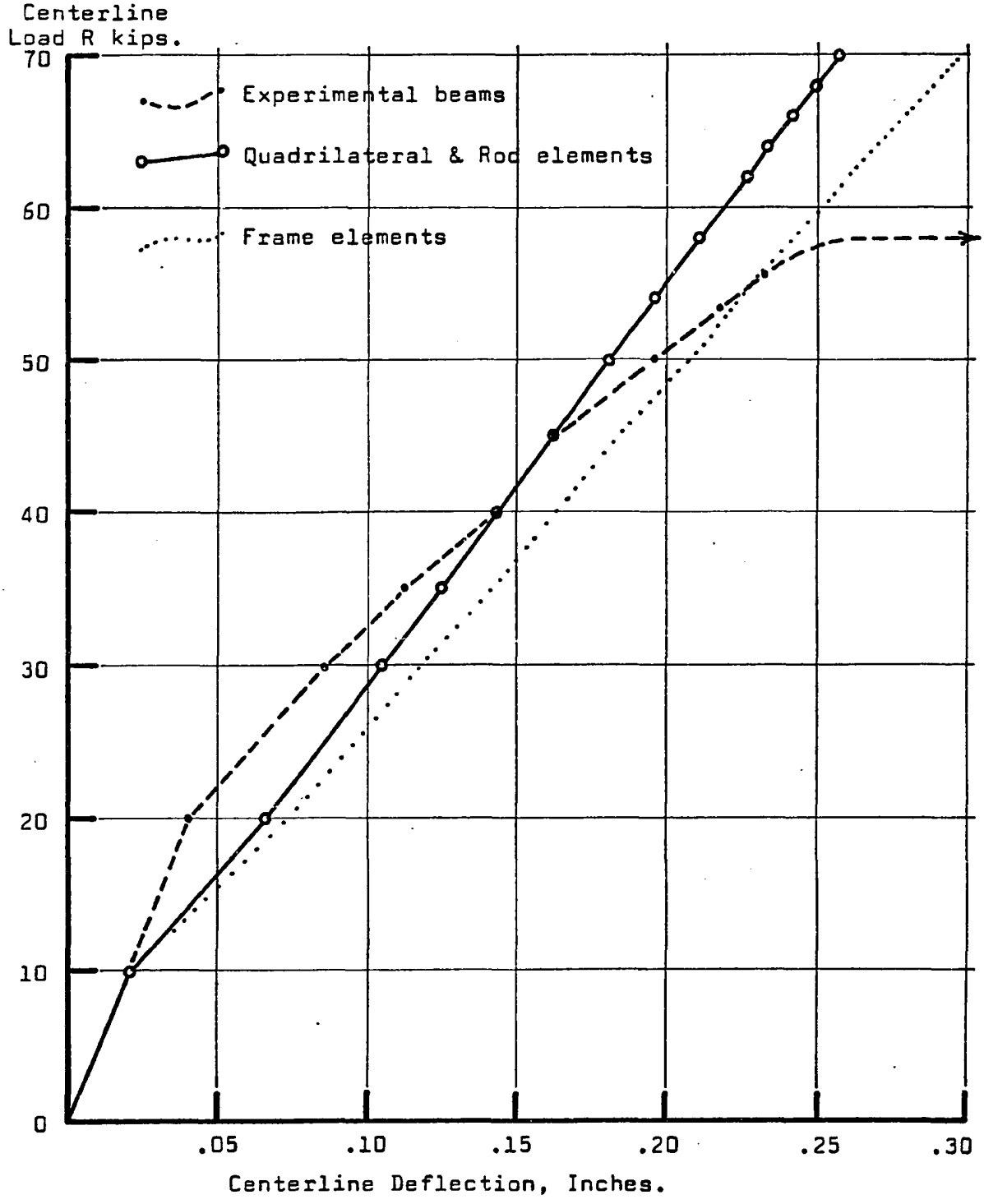

FIGURE 6.24 LOAD-DEFLECTION WITH QUAD ELEMENTS.

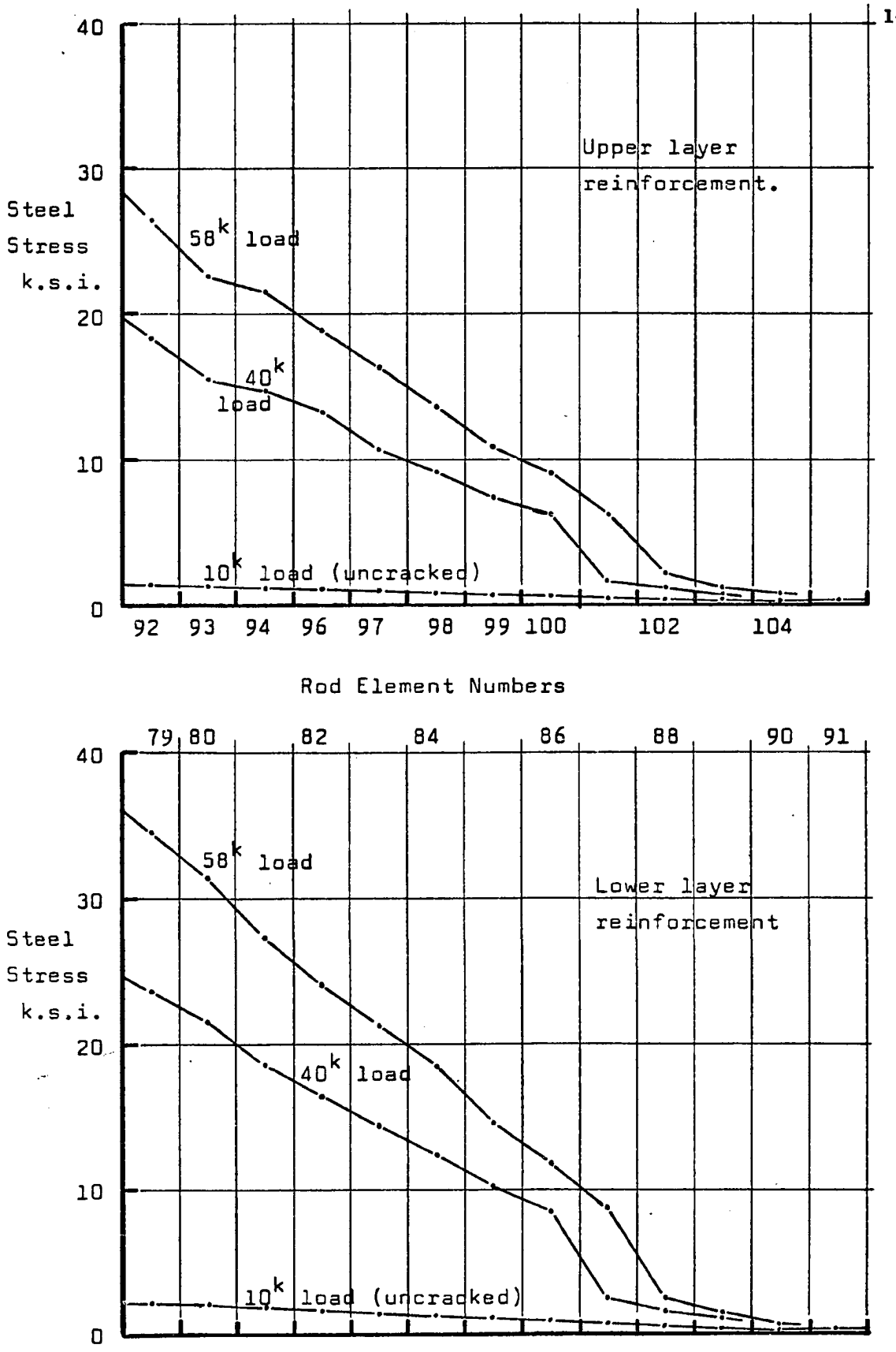

FIGURE 6.25 STEEL STRESSES, QUAD ELEMENT MODEL.

tension cracking is expected to propagate. Consequently, the following analyses included the linearized Bresler-Pister criterion in order to compare results with particular regard to the major diagonal tension crack formation.

Secondly, an important aspect of reinforced concrete beam behavior has been omitted from the method, namely the bondslip between steel and concrete. Concrete is a structurally useful material in non-prestressed beam-type members because of the inclusion of reinforcement to carry the internal tensile forces since plain concrete only has useful strength when in compression. If the reinforcement is perfectly bonded to the concrete then the theoretical, perfect load-sharing takes place and the reinforcement carries the maximum amount of tensile force. If zero bonding occurs, with complete slippage between reinforcement and the surrounding concrete, then the concrete carries the total external load alone and the reinforcement has zero stress. But since this implies large tensile stresses in the concrete, which the material cannot sustain, then failure takes place. These two situations may be condensed by saying that perfect bond gives perfect load sharing with least stressing of the concrete, and that zero bond gives maximum stressing of the concrete and failure so that varying degrees of bonding may contribute importantly to varying incidences of failure. Understanding too that cracking changes the principal stress patterns and the internal load-sharing then it may be expected that bond stress concentrations can be provoked, and possible local bond failures could provide the amplifications of stress in the concrete, which, in

conjunction with the improved cracking criterion, could now cause the model to fail in a realistic manner. Thus bondlinks (8) were added to the model for the next tests.

6.4.4 Comparison Model With Bondlinks

The computer program was temporarily changed by adding the bondlinks developed by Scordelis and Ngo (8) to attach the steel rod elements to the concrete plane stress elements. The necessary discretization layouts are given in Figures 6.26 using the same basic geometry as the previous cases. The new layout required 124 nodes and includes 78 quadrilateral elements, 26 rod elements, and 26 bondlinks for a total of 130 elements. Suitable failure logic was introduced that was appropriate for bond releases between embedded steel and concrete, and a linear stress-slip law was assumed after inspection of the results of pull-out tests analyzed by Nilson (9). This relationship is given in Figure 6.27 and provides a constant, average value of bond stiffness $du/ds = 2.33 \times 10^6$ psi/inch of slip, where u is the local intensity of bond stress and s is the local relative slip between the bonded surfaces. Bond stiffness must be charged to link stiffness k_h to satisfy the requirement that each link is to represent the bond over a 6" length of 2 X #9 bars. Thus, the tributary bond area per link is $A_L = 2 \times 6 \times 3.544 = 42.528$ sq. inches, and the link stiffness is given by $k_h = A_L \times du/ds$ = 99,232,000 lbs/inch slip. A bond strength value of 700 psi was chosen which results in a bond force limit for each link of 29,770 lbs. using the tributary area A_L. Finally, the steel reinforcement areas were adjusted to the proper value of 1.76 sq. inches.

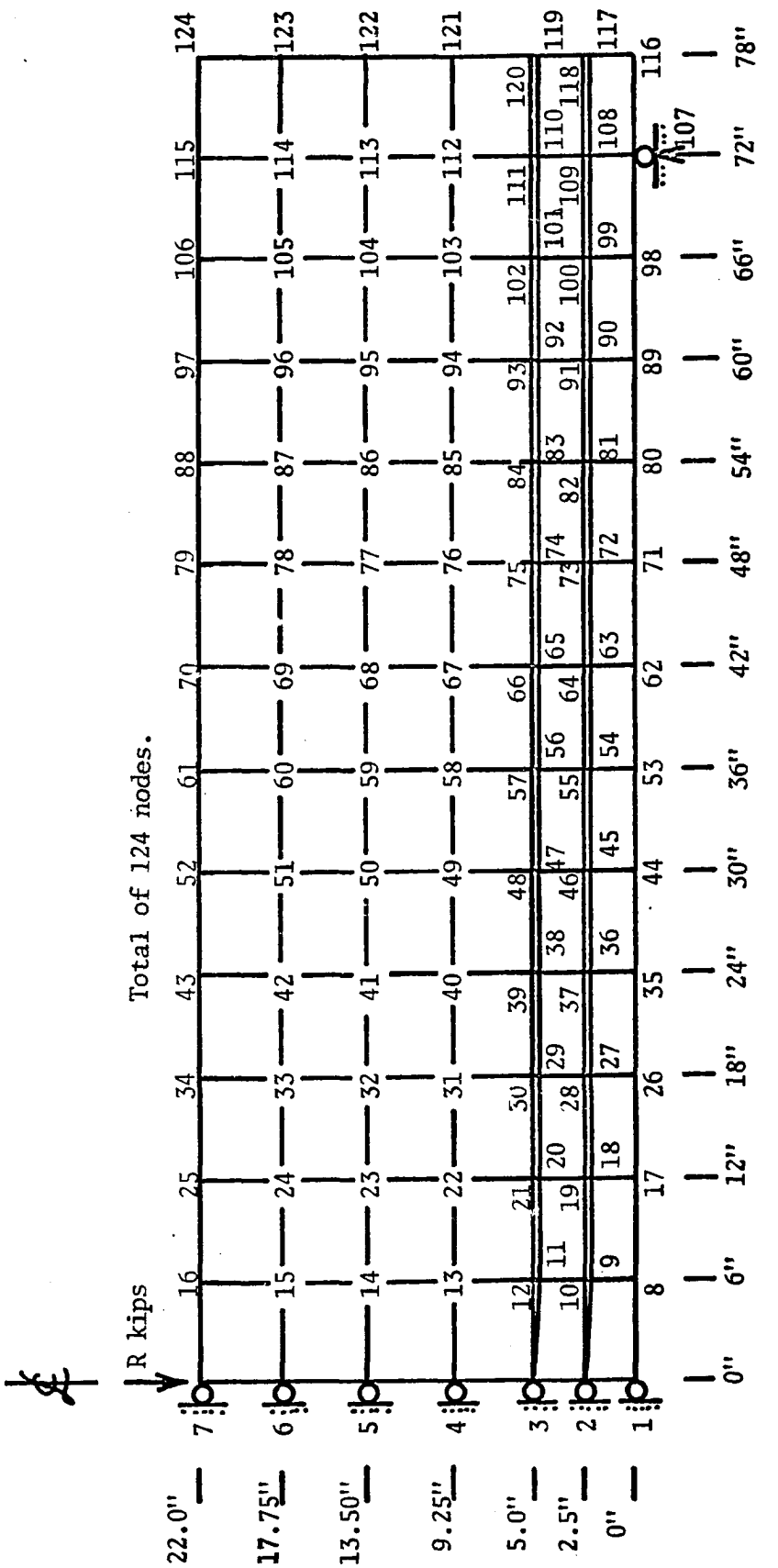

MODEL WITH QUADS, RODS, AND BONDLINKS.

FIGURE 6.26(A) MESH GEOMETRY AND NODE NUMBERS.

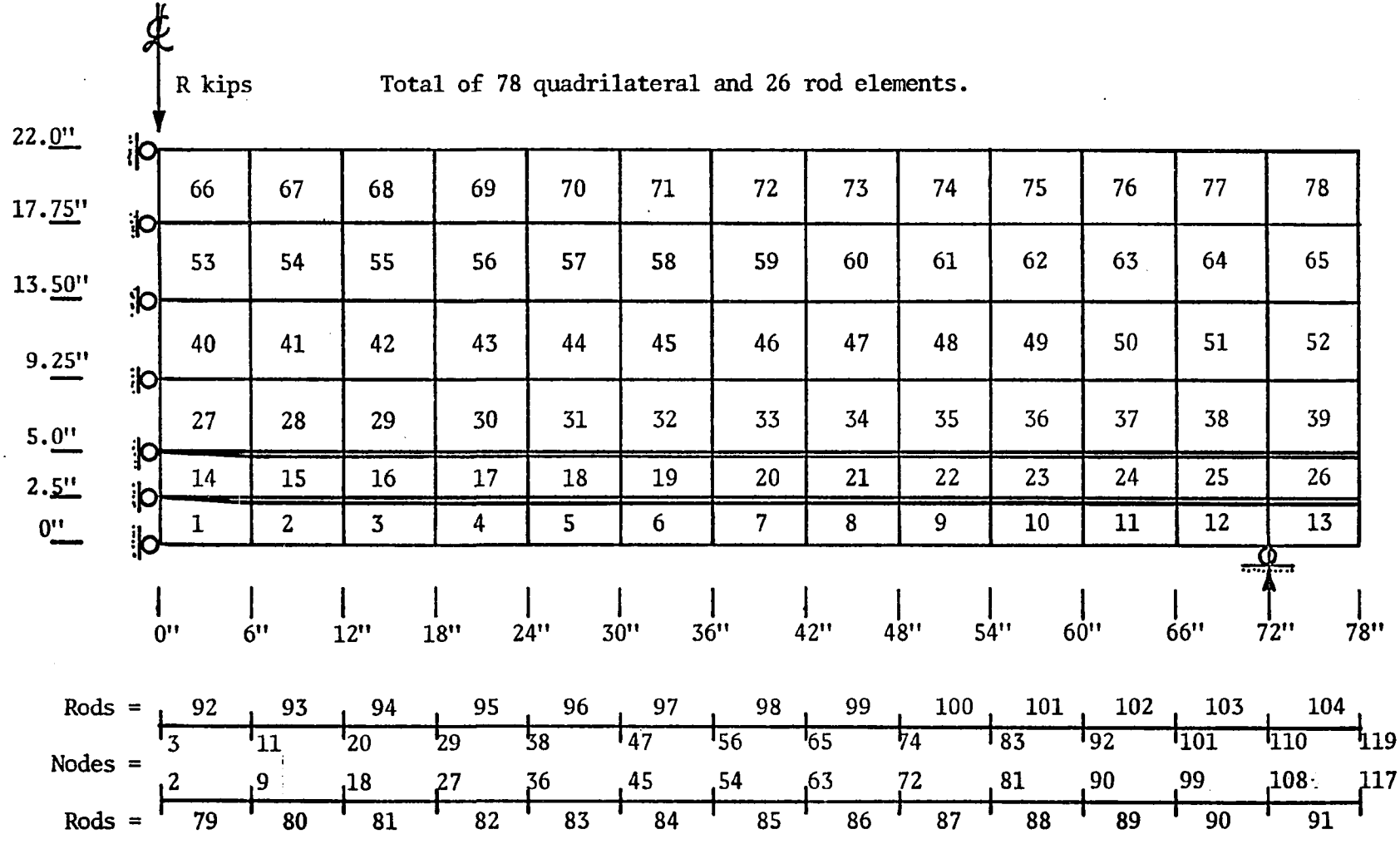

MODEL WITH QUADS, RODS, AND BONDLINKS.

FIGURE 6.26(B) LAYOUT OF QUAD AND ROD ELEMENTS.

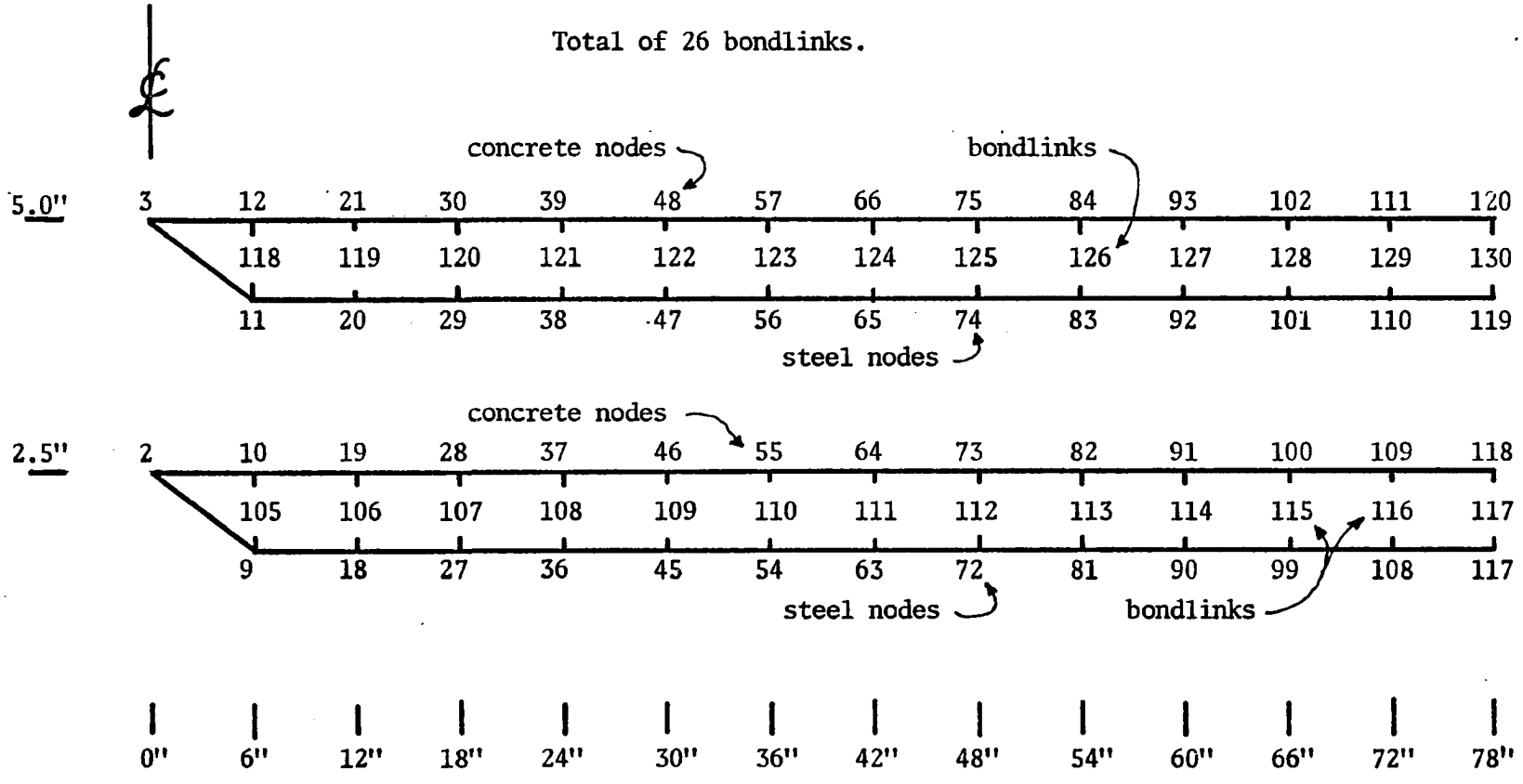

MODEL WITH QUADS, RODS, AND BONDLINKS.

FIGURE 6.26(C) LAYOUT OF BONDLINKS.

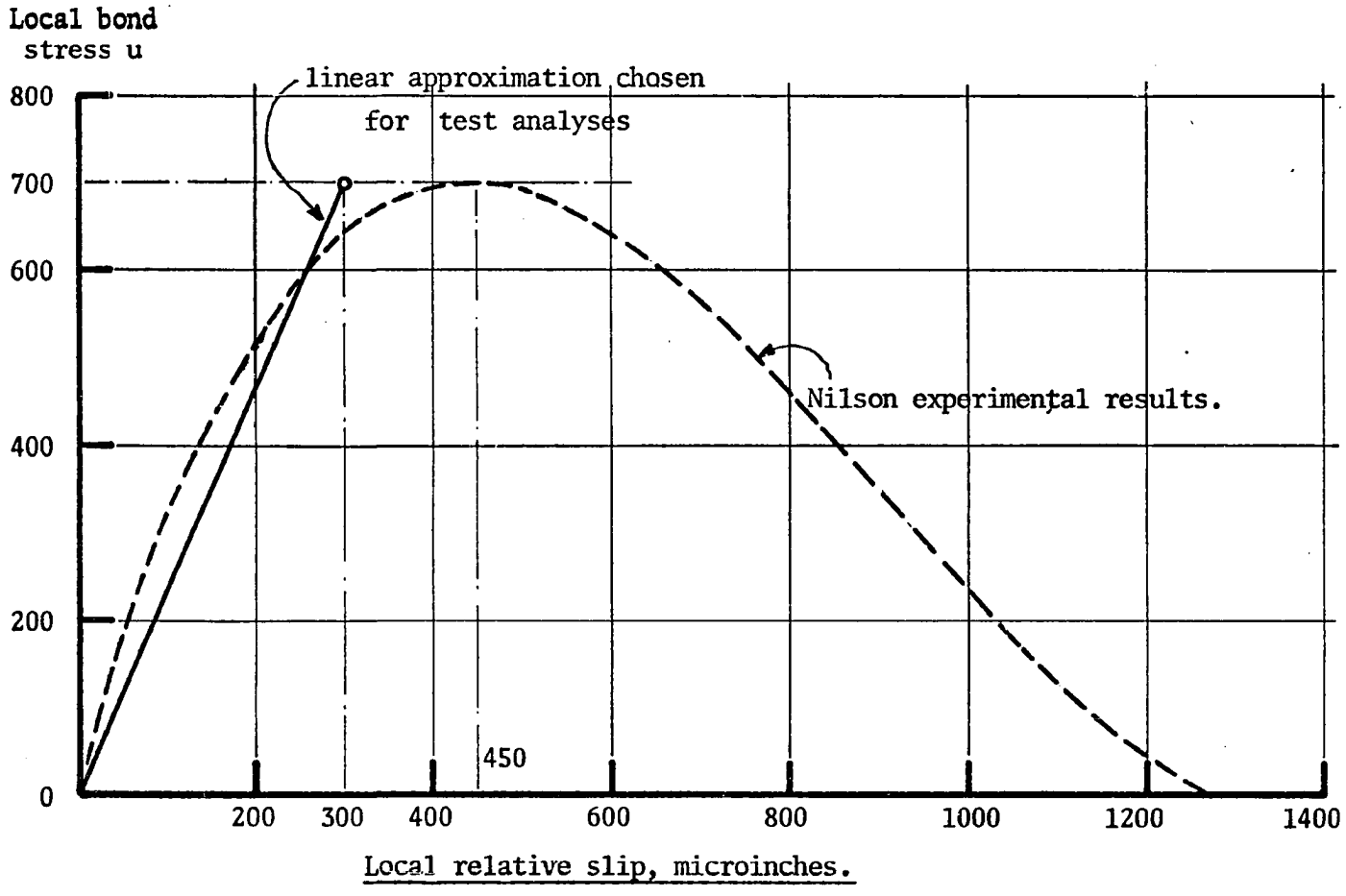

FIGURE 6.27 SELECTED BOND STRESS-SLIP RELATION.

The analysis (#123) took 605.65 seconds on the CDC-6400 computer to reach the maximum load of 70 kips. The details of the load increments and iteration cycles are given in Table 6.10, and the load-deflection response is plotted in Figure 6.28. As expected, the addition of bondlinks and reduction of steel area caused the deflections to increase (about 8%) for a given load, but this analytic system still remained stiffer than the frame element model. The improvement in the cracking criterion now had the effect of permitting an extra 7 elements to crack, of which only two (#44 and #47) failed before the load reached 58 kips (failure load of the real beams). The analytic cracking at 58 kips load is shown in Figure 6.29 and except for the additional cracked elements is very similar to that of the previous model without bondlinks. The steel stresses at this load are given in Figure 6.30 and show an increase over the corresponding data for the earlier model chiefly because of the reduction of steel area. A measure of the bond stresses is available from this analysis and gives some insight into this aspect of the internal force system. The bondlink forces are plotted in Figure 6.31 and are proportional to the average bond stress intensity over the tributary length of each link. During the analysis the bond stress intensity along the reinforcement showed a characteristic peak at the interface between the cracked and uncracked zones. This is seen in Figure 6.31 at links #113 and #126 for that particular loading. As the peaks move along the beam with the advance of cracking, so their magnitude increases and the local bond failure becomes more imminent. However, no link failures occurred in this analysis even

Load Increment		Total Load	Total Deflection	No. of
No.	Size	Kips	Inches	Cycles
1	10	10	.021342	2
2	10	20	.070437	3
3	10	30	.112828	3
4	5	35	.135039	2
5	5	40	.154411	1
6	5	45	.174449	2
7	5	50	.195336	3
8	2	52	.203541	2
9	2	54	.211572	2
10	2	56	.219668	2
11	2	58	.227626	1
12	2	60	.235591	1
13	2	62	.243570	1
14	2	64	.251796	2
15	2	66	.259862	2
16	2	68	.268303	2
17	2	70	.277847	2
		Total cycles =		33

TABLE 6.10

LOAD-DEFLECTION RESULTS INCLUDING BONDLINKS.

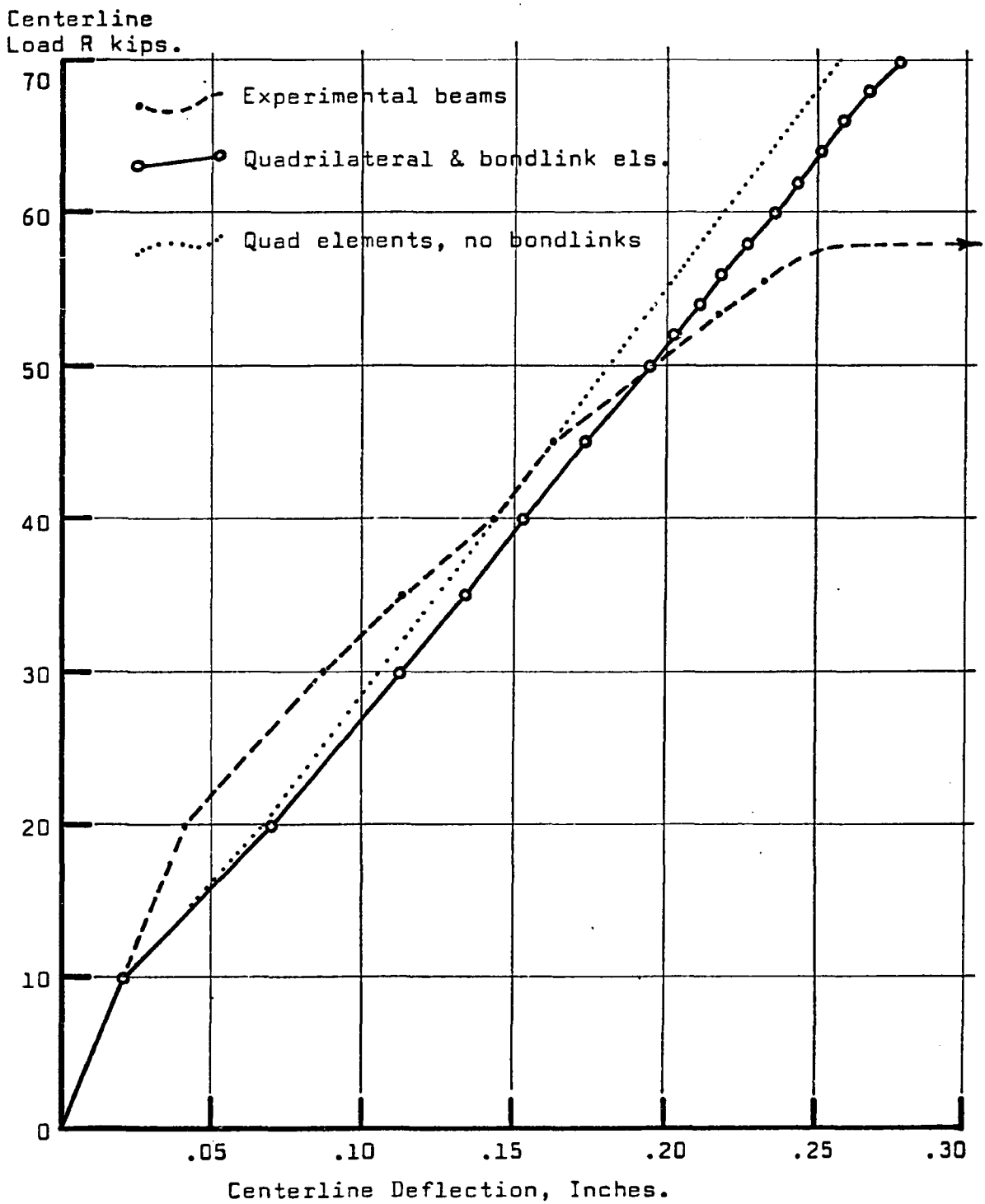

FIGURE 6.28 LOAD-DEFLECTION WITH BONDLINKS INCLUDED.

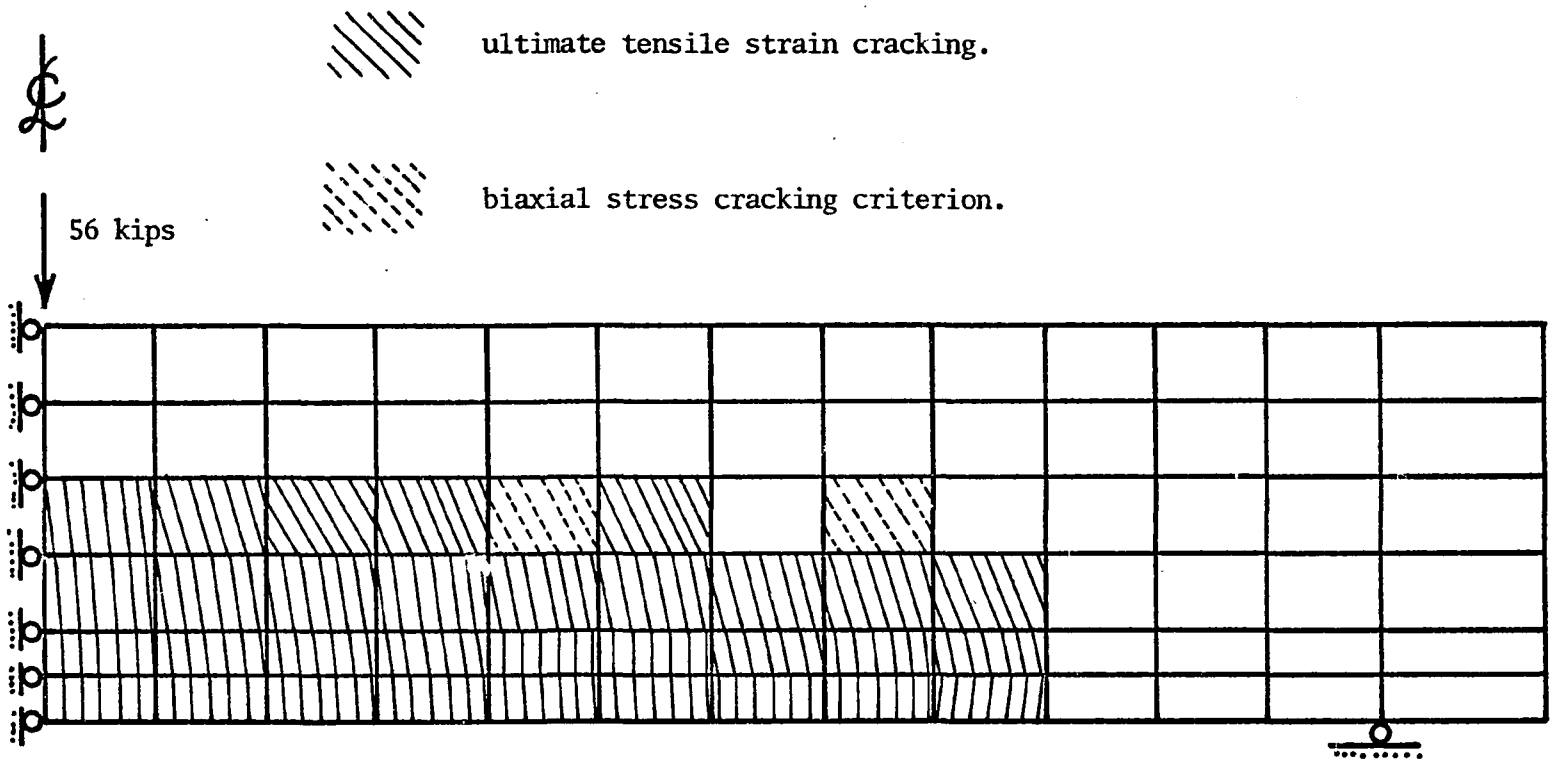

FIGURE 6.29 ANALYTIC CRACKING WITH BONDLINKS.

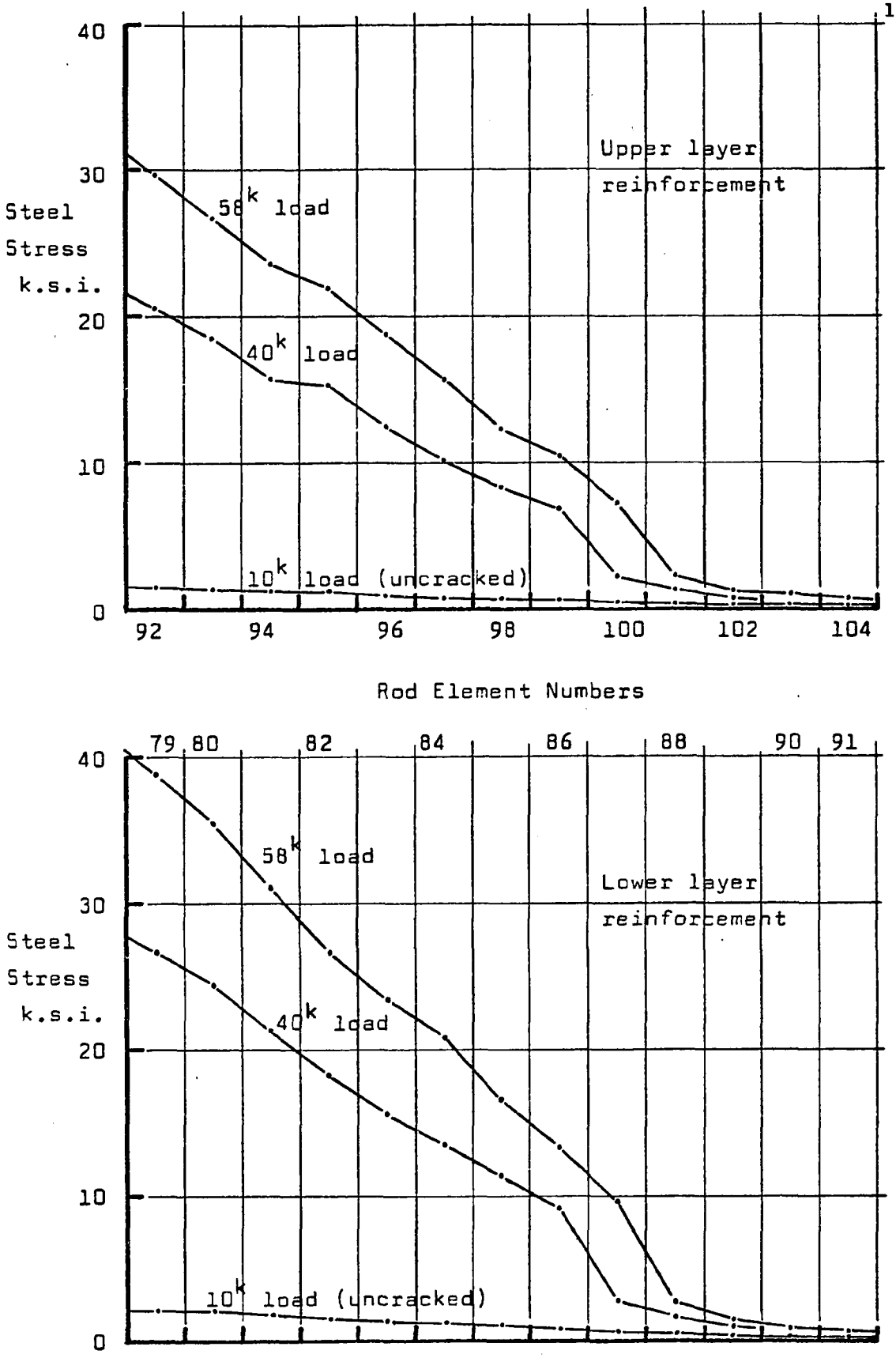

FIGURE 6.30

STEEL STRESSES, QUADRILATERAL ELEMENT MODEL WITH BONDLINKS.

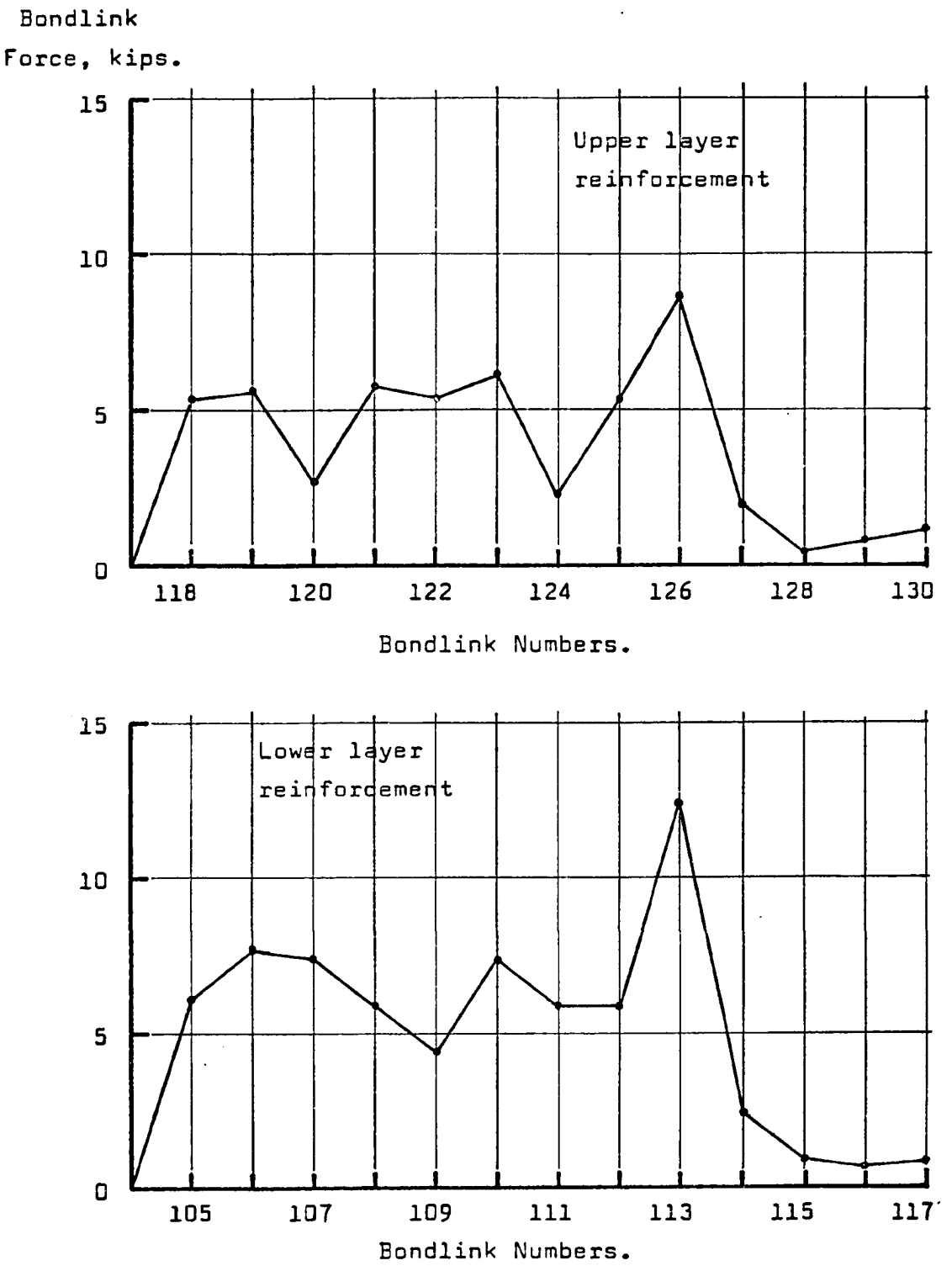

FIGURE 6.31 BONDLINK FORCES AT 58^{k} LOAD.

up to the maximum load so that the expectation that local bond failures are significant to the beam failure was not tested.

The quadrilateral element model with bondlinks was rerun (analysis #124) with the link bond strength value reduced from 29,770 lbs. to 12,000 lbs. This implied a bond strength stress value of only 282 psi but would induce failure in some of the bondlinks. The effect of this was to cause link #110 to fail at a load of 35 kips. This was followed by failure of link #112 at 40 kips but the system safely carried the next increase of load to 45 kips with no further local bond failures or element failures. Load increment #7 raised the external load to 50 kips and initiated a domino-like sequence of bondlink failures along both layers that left the reinforcement free from the concrete after links #109 and #122 and led to the inevitable collapse of the beam after about 7 iterations. The load-deflection data and iteration history are given in Table 6.11 while the deflection behavior is given in Figure 6.32.

The effect of local bond failure on the variation of stress in the reinforcement is given in Figure 6.33 at a load of 45 kips, just before termination of analysis #124. Bond stress, or link force, is directly related to the gradient of stress in the steel. If the rate of exchange of force between steel and concrete is large over a given distance, then the steel stress gradient is high and bondlinks show large forces (high bond stress), whereas bondlink failure (zero bond stress) allows no force transfer and the steel stress remains constant through such a region. Two such constant stress plateaus appear in Figure 6.33 for the lower layer of steel,

Load Increment		Total Load	Total Deflection	No. of
No.	Size	Kips	Inches	Cycles
1	10	10	.021342	2
2	10	20	.070437	3
3	10	30	.112828	3
4	5	35	.135303	2
5	5	40	.156442	2
6	5	45	.176114	1
7	5	50	collapse	7+
		Total cycles =		20

TABLE 6.11

LOAD-DEFLECTION RESULTS WITH FAILING BONDLINKS.

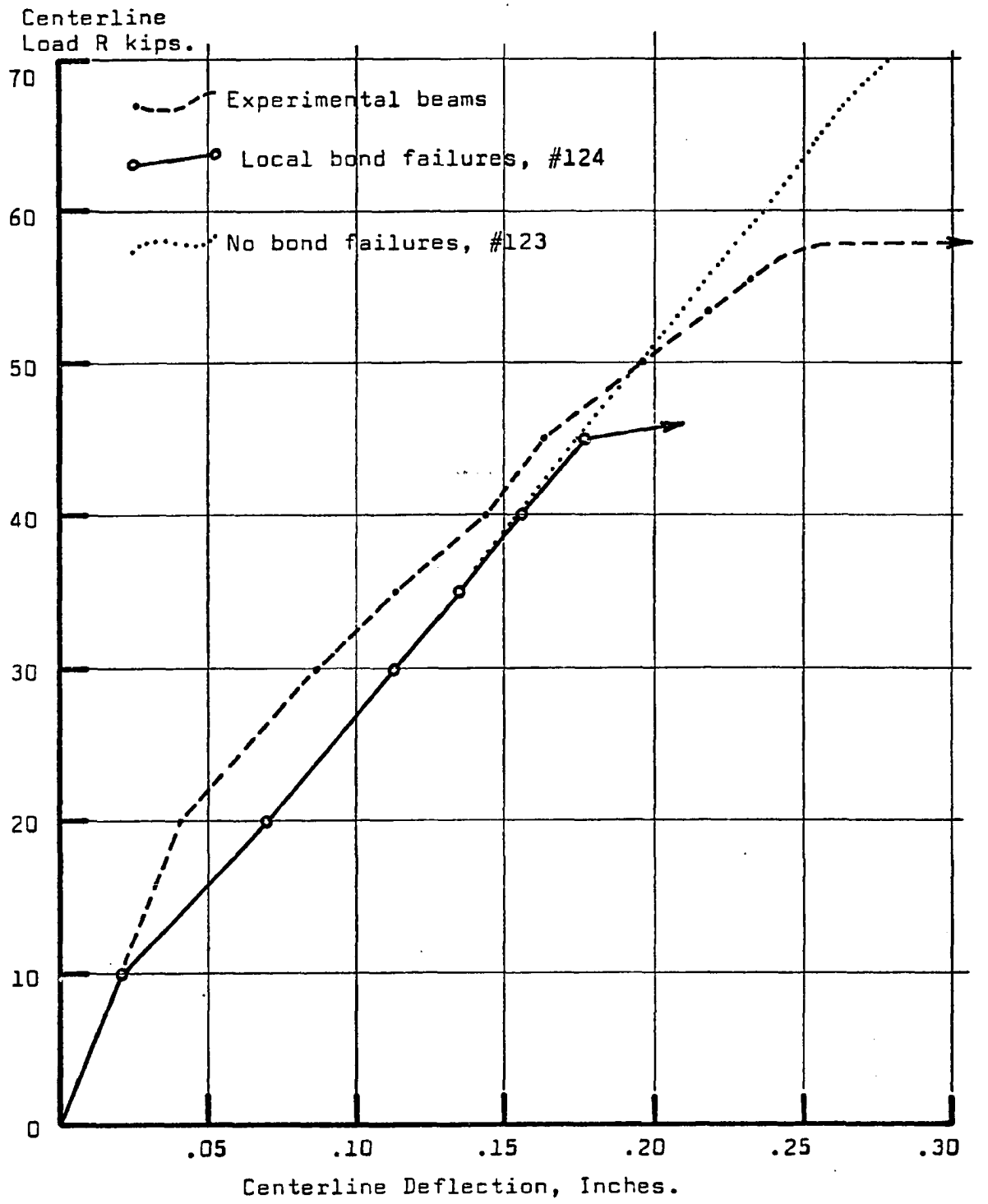

FIGURE 6.32 LOAD-DEFLECTION WITH BONDLINK FAILURES.

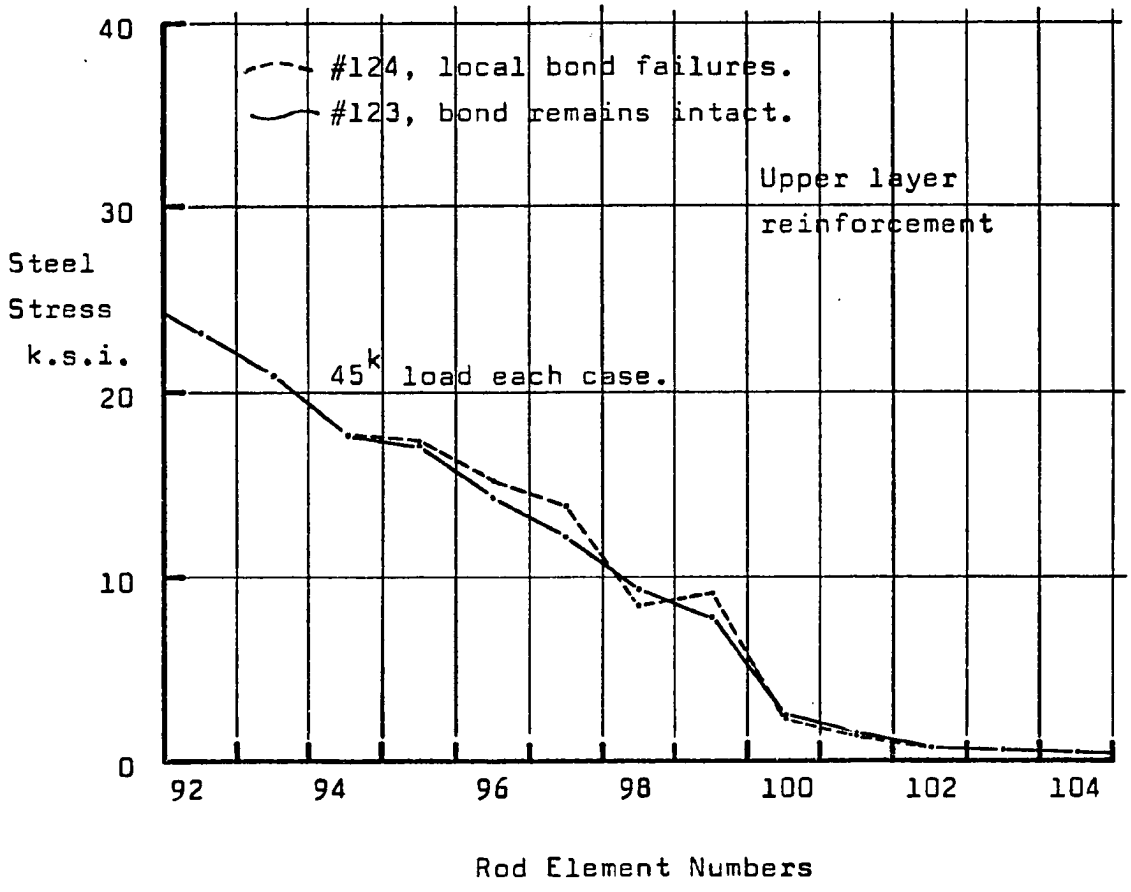

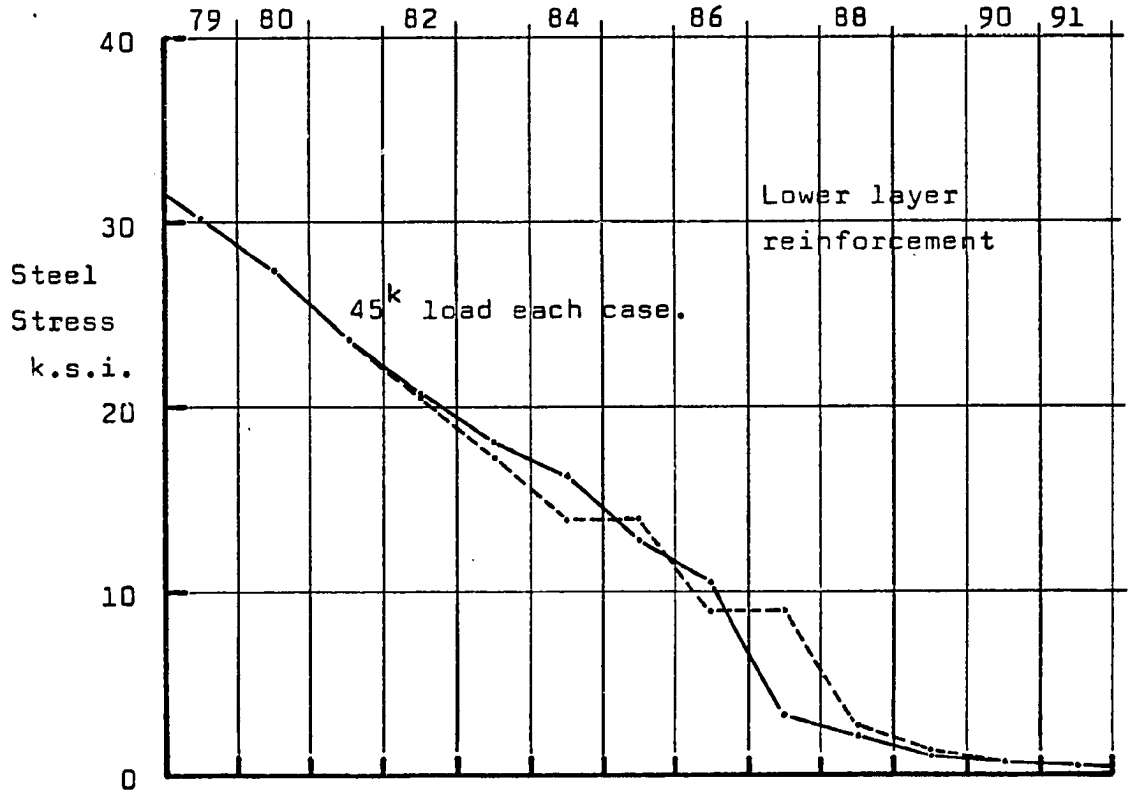

FIGURE 6.33

STEEL STRESS CHANGES WITH LOCAL BOND FAILURE.

corresponding to failure of links #110 and #112.

Evidently any further improvement of the analytic beam behavior would seem to require adjustments of the bond parameters, such as using a nonlinear bond stress law, including more sophisticated failure logic that included some dependency on the adjacent principal stress values, and perhaps variations of the tributary areas of the links. These kinds of improvements were beyond the scope of this test program and were not pursued further.

6.4.5 Summary Of The Evaluation Of The Elements

The frame elements have been shown to be about as stiff as the corresponding experimental beams and to yield crack penetrations that compare favorably with the real cracking. However, the frame element model is unable to give the real failure load of the reinforced concrete member. Consequently a frame modelled with these elements will appear to be much stronger than the real frame, but such a frame will be adequate for studies of the load transfers that occur as a frame-panel system deteriorates.

The plane stress quadrilateral elements provide a reliable description of the principal stress fields but give a stiffer model than the real structure. By using both the ultimate tensile strain criterion and the linearized Bresler-Pister criterion, these elements give a reasonable representation of crack development during increasing loads. The inability of this model to predict the failure of the test beams was decided to be mainly due to the construction of the model rather than being a defect in the quadrilateral element formulations, in particular, the bond phenomenon was seen to be

important for modelling the beams with regard to failure loads. The quadrilateral elements were thus considered to be adequate for describing the shear panels in a frame-panel system.

The combination of frame elements and quadrilateral elements could be expected to provide both a stiffer and stronger model than the real frame-panel structure.

7. REINFORCED CONCRETE FRAMES AND PANELS

The purpose in combining several kinds of analytical elements in this research was to model structural frames with or without shear panels attached. Building frames are not uniform in their design details and it is difficult to even determine categories for representative types of frames. Hence the use of a so-called 'typical' frame was abandoned. Actual building frames are not usually well reported in terms of the detailed description of the material properties used in their construction. Likely sources for descriptions of frames and structural members which have their corresponding material properties given in a fairly complete manner are of course to be found in structural testing laboratories.

The one and two-story frame and panel models used in this chapter were adapted from a series of five-story models that were experimentally tested to failure at the University of Illinois in 1967 (27). Whereas that experimental program used reinforced concrete frames with panels infilled with bricks and mortar, this analysis used the same structural sections, frame geometry, and material properties, but treated the panel infilling as a weak, unreinforced continuum. Strength properties of such panels were estimated from the strength data given for the experimental brick infilling.

Having selected a suitable structural model as a basis for this work then the discretization of the system could proceed. The analysis was restricted to the study of four analytical models subjected to lateral loading. These models are shown schematically in Figure 7.1, two are frames without panels, and then these are repeated

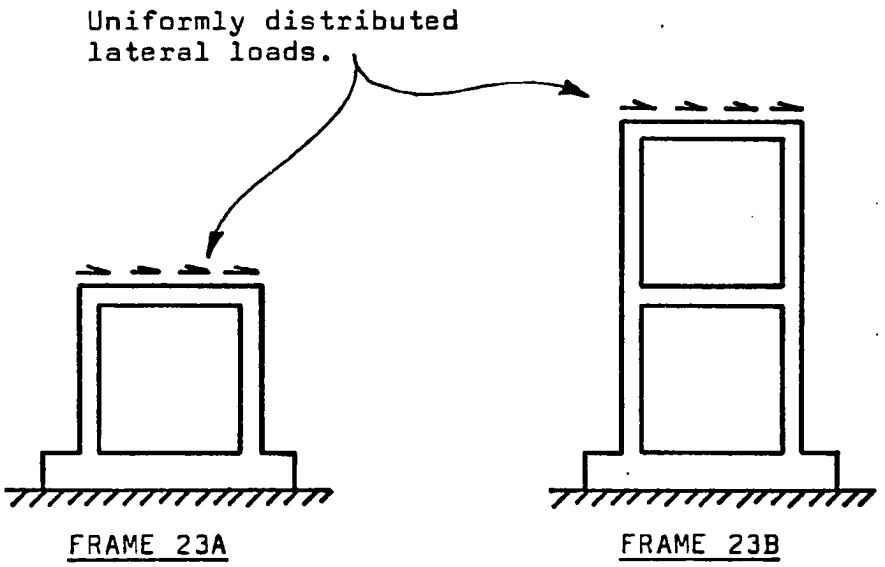

FRAMES ONLY.

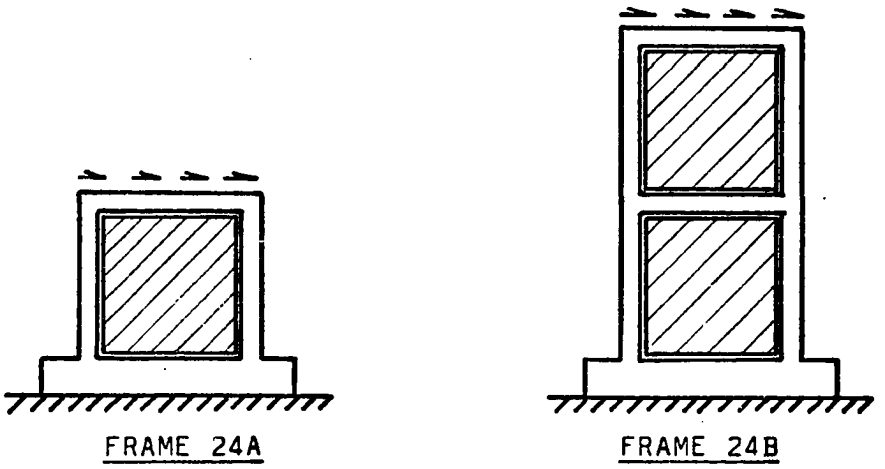

FRAMES WITH INFILLED PANELS.

FIGURE 7.1 SELECTED ANALYTIC FRAME MODELS.

with shear panels. A single lateral load was applied to the top beam of each model so that every story had equal shear acting, and the loading was increased incrementally until failure occurred. The details of these models are developed in the following sections.

7.1 The Analytical Models, Frames Only

The general layout of a typical frame is given in Figure 7.2 while the cross-section details of the members are shown in Figure 7.3. The actual sizes of the laboratory prototypes were maintained for the analytical models. An average stress-strain curve for the frame concrete was represented in the multilinear form of Figure 7.4, but the ultimate tensile strain had to be derived from the results of a separate analysis of cracking in a model which simulated the five-story experimental frames. The resulting value of tensile strength used for these analyses, 740 psi, lay between the average modulus of rupture (1260 psi) and the splitting strength (470 psi) of the laboratory material. The stress-strain curve of the drawn wire reinforcement is given in Figure 7.5.

The structure was discretized by using frame elements for columns and beams, and some quadrilateral elements for the base region and beam-column connections. The layouts of the nodes and elements are given in Figures 7.6 (A) and (B) for both frame models 23A and 23B. The lateral load was uniformly distributed along both edges of the top-story beams. This resulted in the patterns of nodal forces that are demonstrated in Table 7.1 for a suitable value of unit total load. Henceforth, the applied loads will be discussed only in terms of the total force applied at the top beam at any time rather than in terms

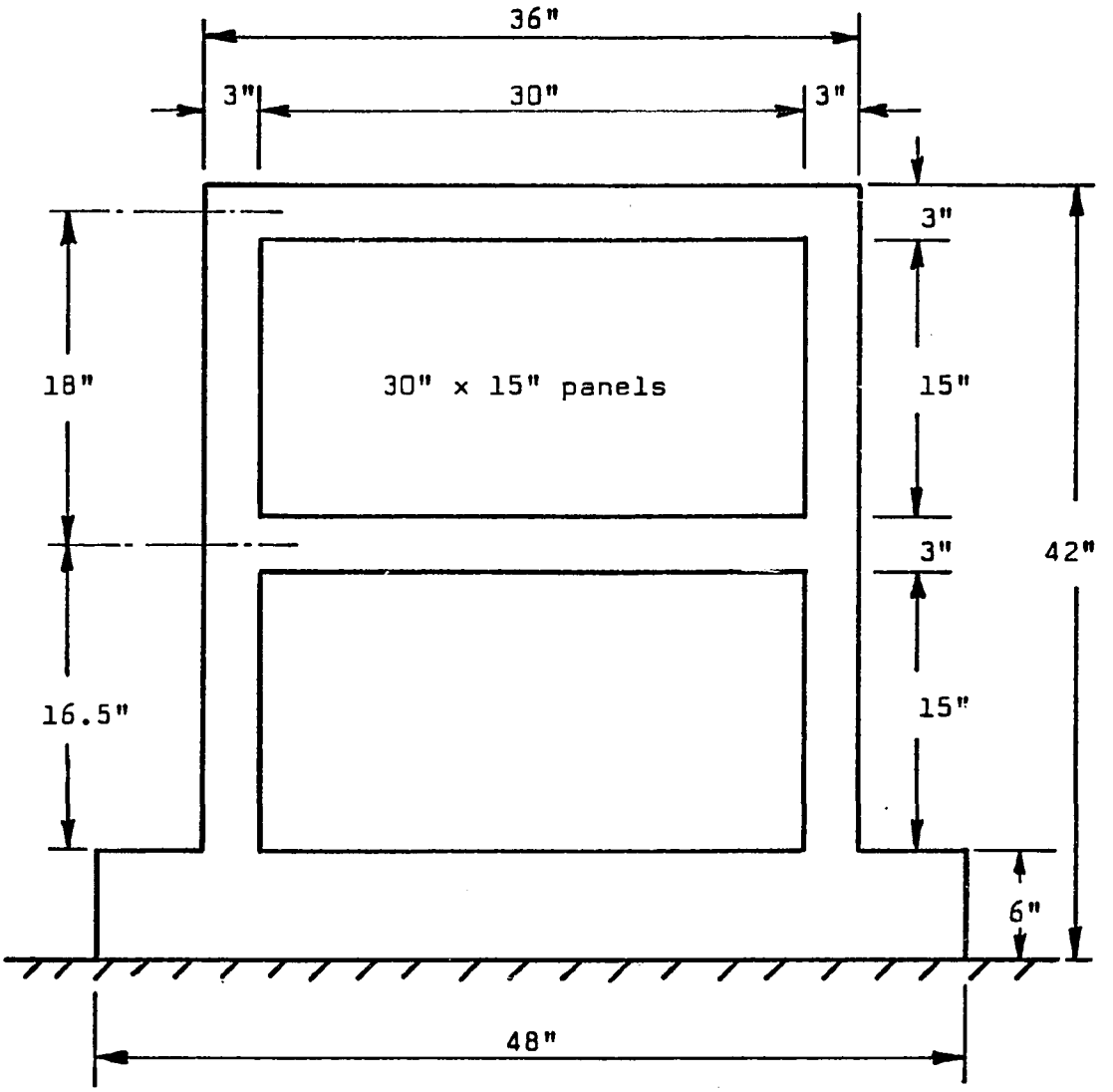

FIGURE 7.2 GENERAL LAYOUT OF FRAMES.

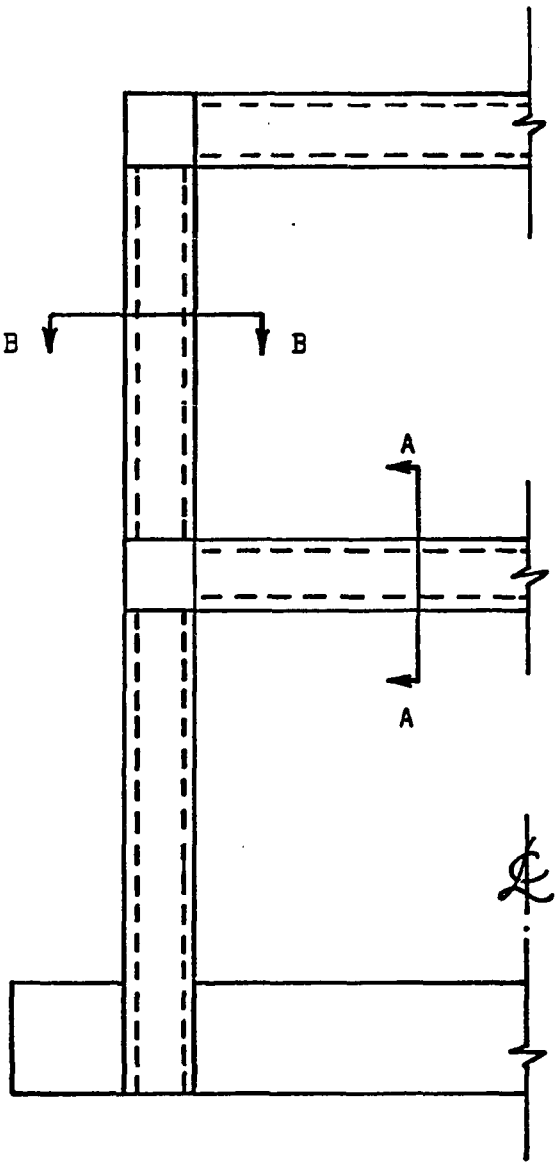

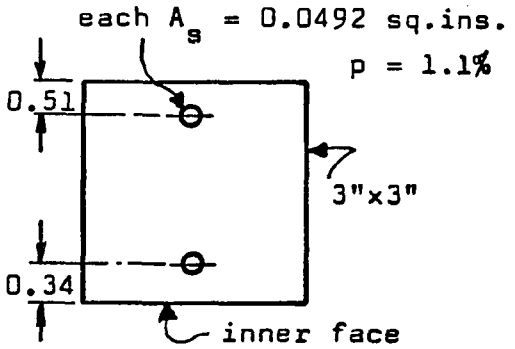

COLUMN SECTION B-B

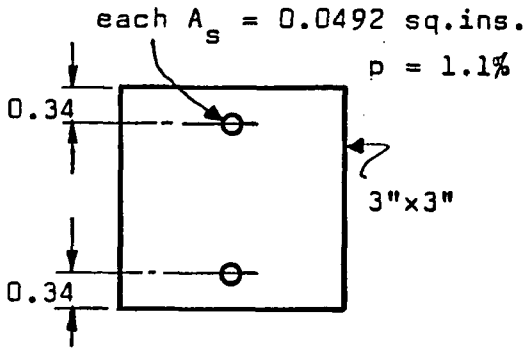

BEAM SECTION A-A

FIGURE 7.3 DETAILS OF FRAME REINFORCEMENT.

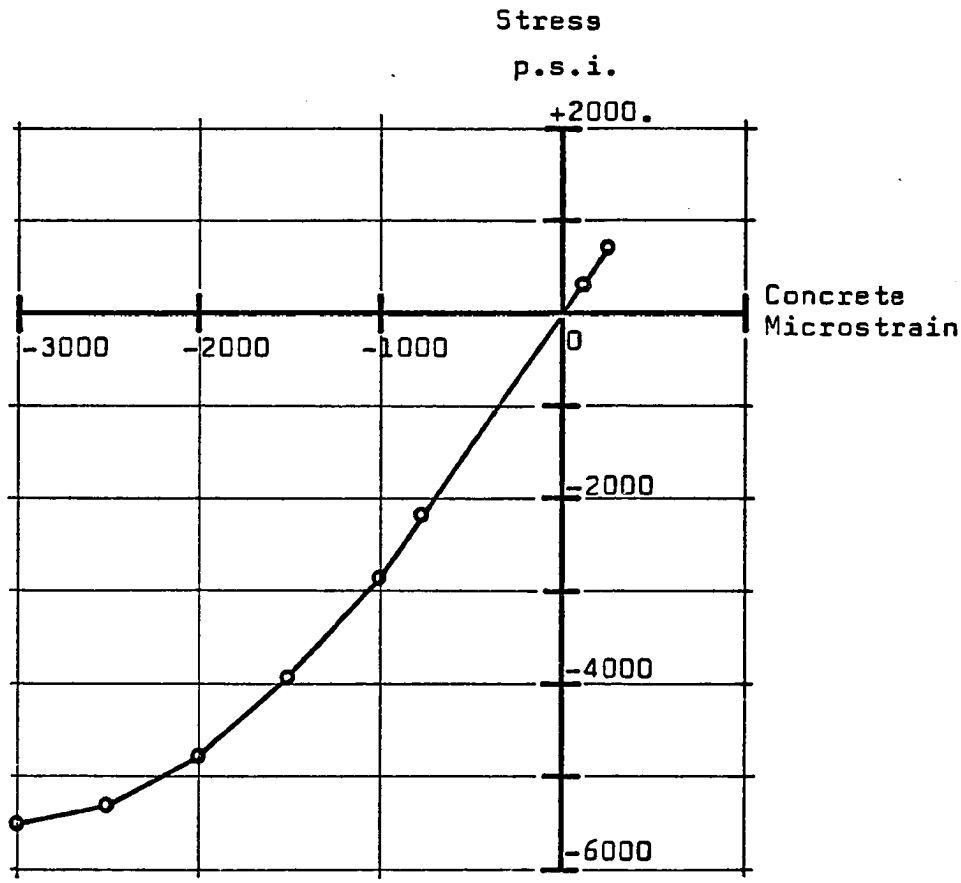

Ord	Stress	Microstrain
1	740.	257
2	370.	129
3	0.	0
4	-2190.	-760
5	-2850.	-1000
6	-3950.	-1500
7	-4790.	-2000
8	-5313.	-2500
9	-5500.	-3000

FIGURE 7.4 STRESS-STRAIN CURVE OF FRAME CONCRETE.

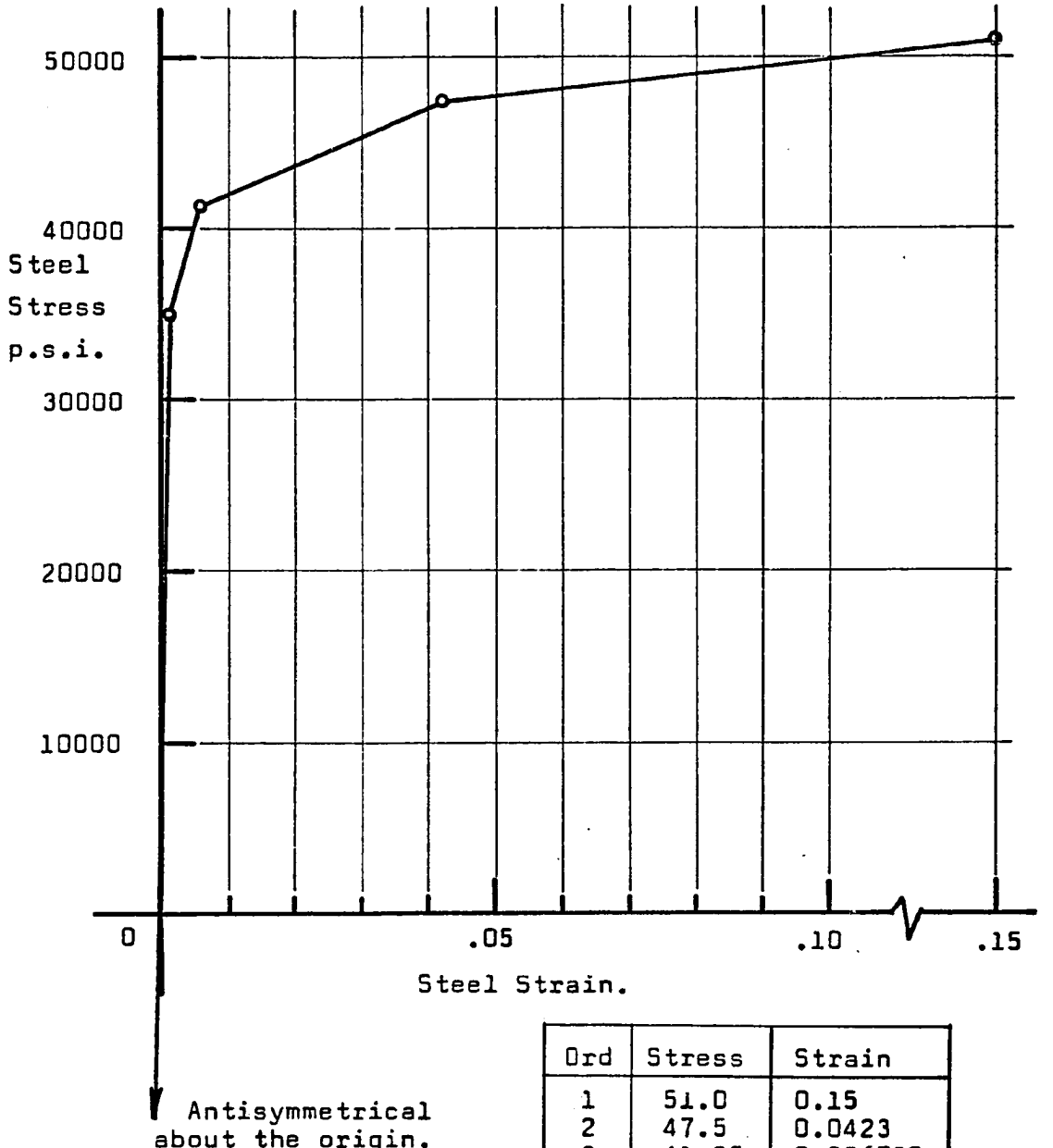

Ord	Stress	Strain
1	51.0	0.15
2	47.5	0.0423
3	41.25	0.006725
4	35.0	0.001208
5	0.0	0.0
6	-35.0	-.001208
7	-41.25	-.006725
8	-47.5	-.0423
9	-51.0	-.15

FIGURE 7.5 STRESS-STRAIN CURVE OF REINFORCEMENT

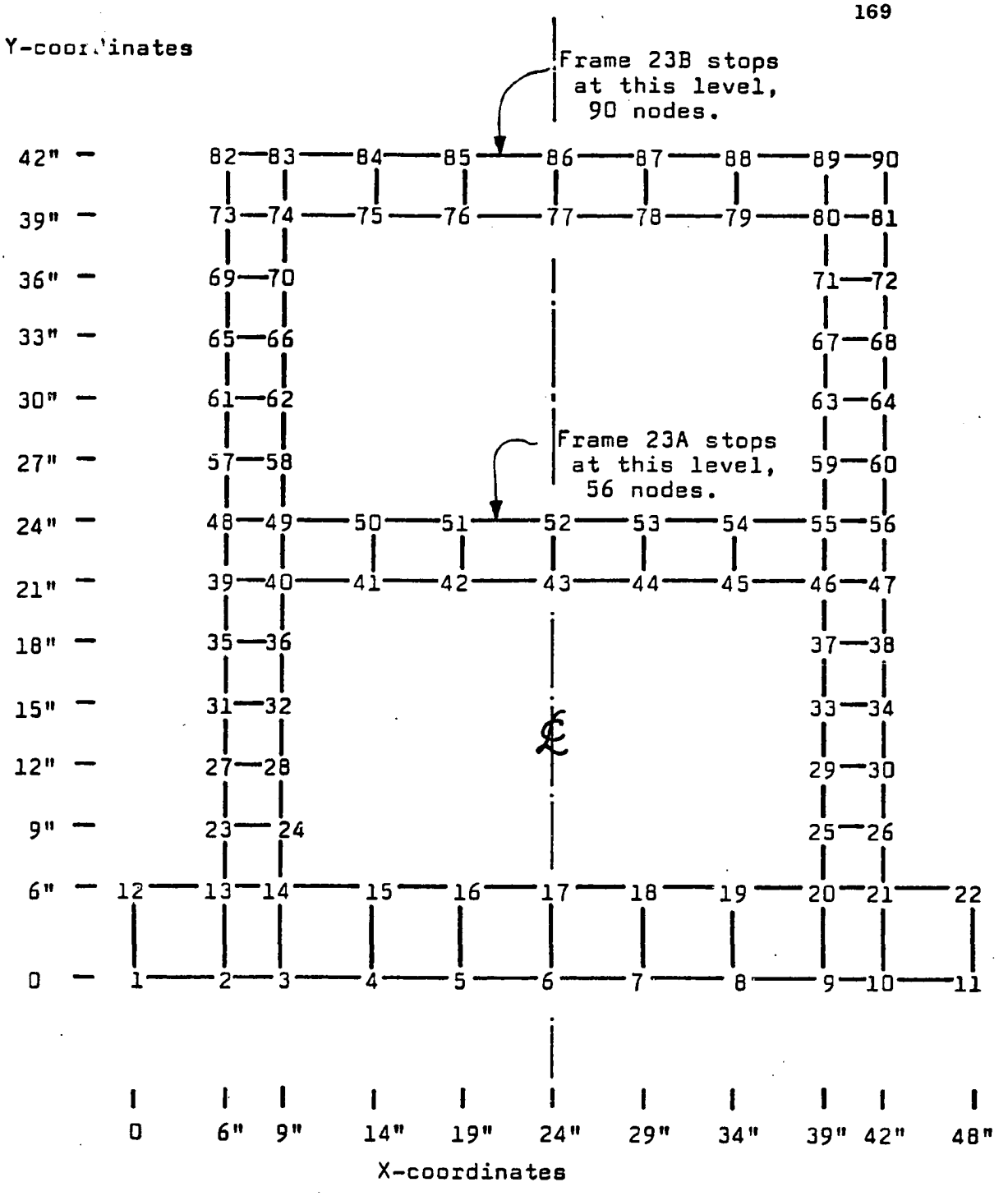

FIGURE 7.6(A) FRAME TYPE 23 NODE LAYOUT

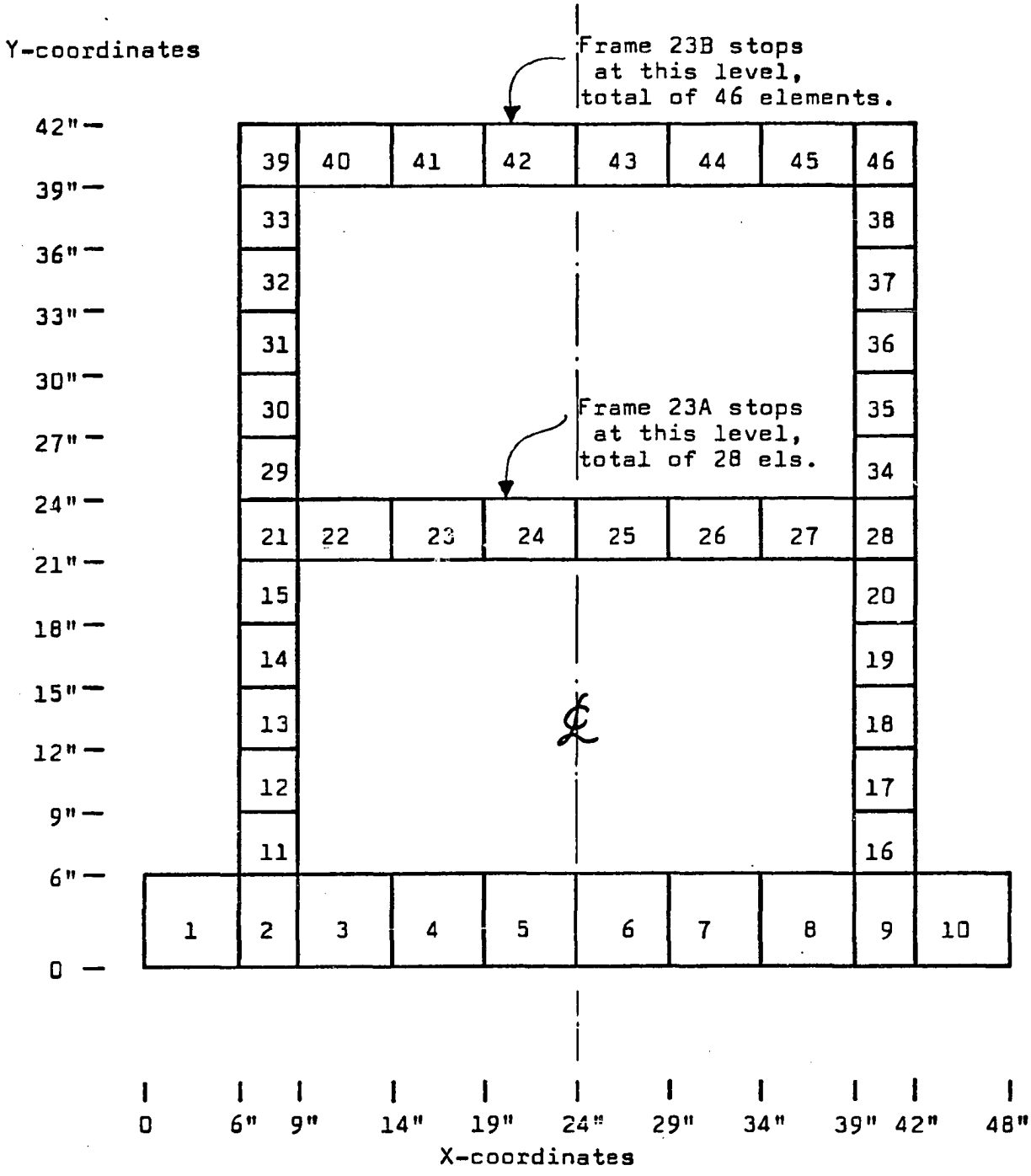

FIGURE 7.6(B) FRAME TYPE 23 ELEMENT LAYOUT

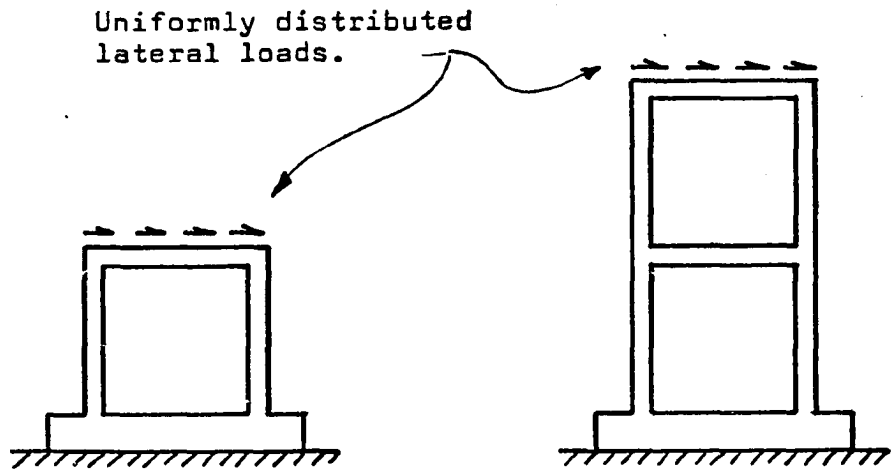

FRAME 23A FRAME 23B

Frame 23A node numbers	Applied forces in X-direction	Frame 23B node numbers
39	2.085 lbs	73
40	5.56	74
41	6.942	75
42	6.942	76
43	6.942	77
44	6.942	78
45	6.942	79
46	5.56	80
47	2.085	81
48	2.085	82
49	5.56	83
50	6.942	84
51	6.942	85
52	6.942	86
53	6.942	87
54	6.942	88
55	5.56	89
56	2.085	90
Total = 100.0 lbs.		

TABLE 7.1

DISTRIBUTION OF UNIT LATERAL LOADING

of individual nodal forces. The first increment of loading was selected as large as possible without initiating cracking or involving nonlinear effects so that the computational effort could be reduced. Much smaller increments were subsequently applied to solve the structure as cracking developed. The results of these analysis are discussed next.

7.1.1 Results From One-Story Frame 23A

This frame required 56 nodes and 28 elements for its discretization (Figures 7.6 (A) and (B)) and the analysis took 347.3 seconds on the CDC-6400 computer. The maximum lateral load of 1225 pounds was reached in 9 increments and needed 32 iterations as described in Table 7.2. This table also lists the lateral sway of the frame as computed at the upper right corner, node 56, as the reference position. If the load-deflection curve is plotted, as shown in Figure 7.7, then the frame shows a distinct change in stiffness after cracking begins in the high-moments regions, at elements #11 and #16. When the cracking load is reached (between 1050 pounds and 1075 pounds) then the column bases become severely cracked. Table 7.3 shows that 7 iterations are required to establish an equilibrium state with 50% cracking in the left column, 40% cracking in the right column. This type of adjustment occurred because of the small amount of reinforcement in the members; the tensile reinforcement ratios were 0.66% at the left and 0.62% at the right. Such low values require relatively large local curvature increases (accentuating the cracking) to develop the necessary steel stress for equilibrium. A larger steel percentage would develop the necessary internal tensile

Load Increment		Total Load	Total Deflection	No. of Cycles
No.	Size	lbs.	Inches	
1	1000	1000	.014543	1
2	50	1050	.015393	1
3	25	1075	.023139	7
4	25	1100	.024971	3
5	25	1125	.025538	1
6	25	1150	.038589	8
7	25	1175	.040046	2
8	25	1200	.043162	4
9	25	1225	failure	5
		Total cycles = 32		

Note: Lateral sway is measured at node 56, upper right corner of frame 23A.

TABLE 7.2

FRAME 23A LOADING AND ITERATIONS.

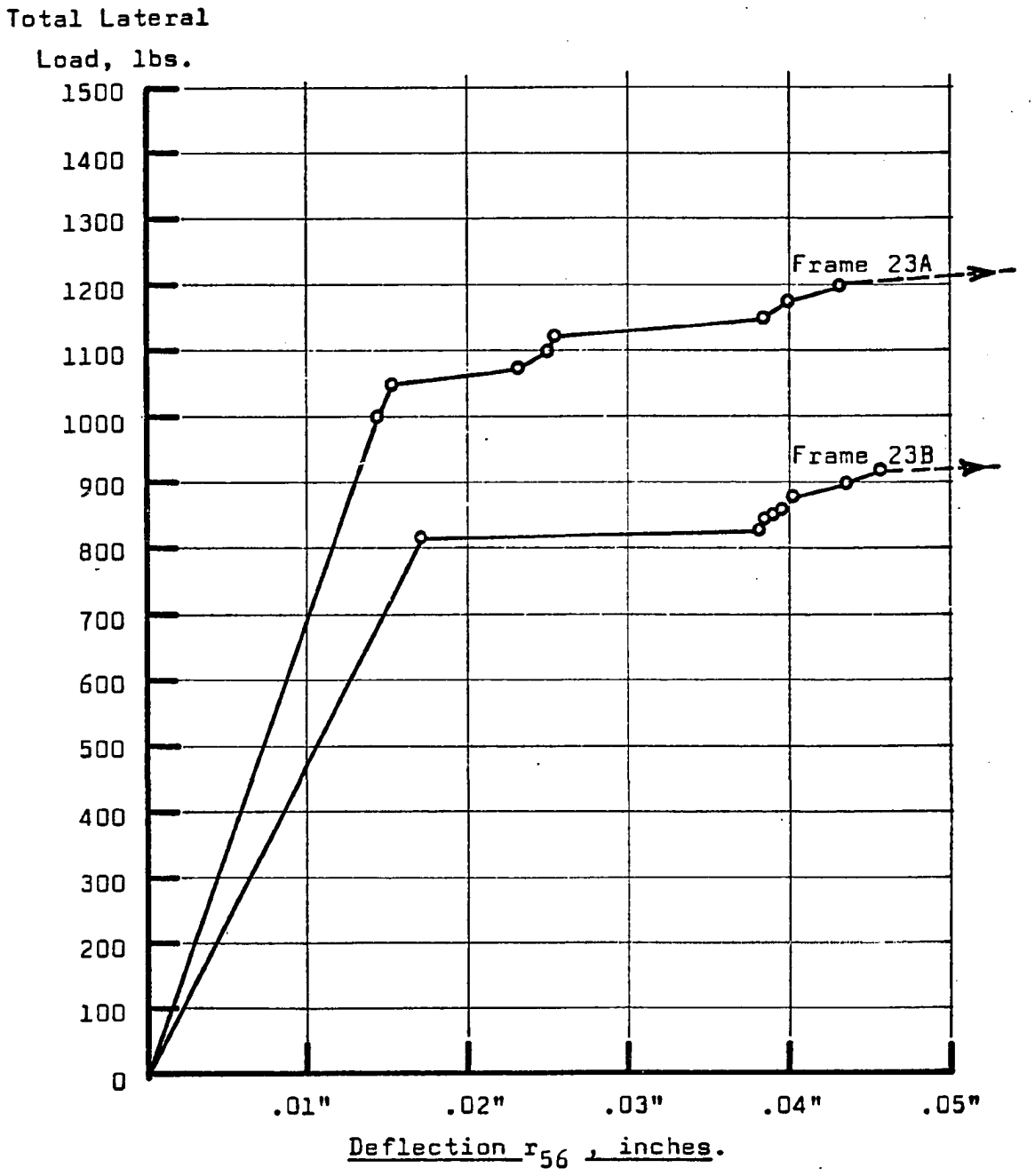

FIGURE 7.7 LATERAL DISPLACEMENT OF NODE 56.

Load Increment No.	Total Load lbs.	Slices cracked			
		Column Bases		Beam Ends	
		No.11	No.16	No.22	No.27
2	1050	-	-	-	-
3	1075	5	4	-	-
4	1100	6	5	-	-
5	1125	6	5	-	-
6	1150	6	6	5	4
7	1175	6	6	5	4
8	1200	6	6	6	4
9	fails with extensive cracking				

TABLE 7.3

CRACK PROPAGATION IN FRAME 23A

resultant with much smaller increases in local curvature (less cracking) and the loss of local stiffness would be curtailed. In general, tensile reinforcement ratios of 1 - 2% in beams are recommended for proper ductile behavior (28) whereas this frame showed an almost elasto-plastic response with little extra load capacity after cracking.

It is interesting to note that the loss of 6 'slices' of concrete (60% cracking) for each column base results in a reduction of the transformed section I values from 7.79 ins.^{4} for the uncracked case to 1.91 ins.^{4} for elements 11, and to 2.13 ins.^{4} for element 16. For the left column this means an amplification X 4.08 for the base M/EI diagram; similarly for the right column. These were effectively concentrated angle changes which had hinge-like effects and in fact represented the beginning of the formation of a classic 4-hinge failure mechanism for this structure.

Table 7.4 lists the moment changes that occurred in this system as cracking proceeded. Cracking of the column bases at A and D shifted the maximum moments up to the beam-column joints, B and C. This behavior corresponded to the partial conversion of the system to a 2-pinned frame. The next significant cracking occurred at the ends of the beam and again the effect was severe, stiffness was considerably reduced at those points because of the small amount of tensile reinforcement. At this stage, with little increase in load after first cracking, the frame had 4 locations with severely reduced stiffness corresponding to the final failure mechanism. Moments at these locations now converged to their ultimate values

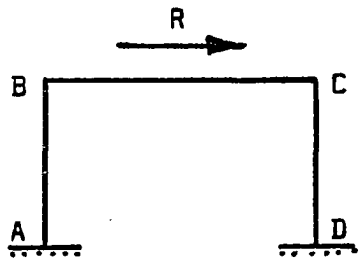

Inc. No.	Total Load	System Moments (inch lbs)			
		M_A	M_B	M_C	M_D
2	1050	-4797	3865	-3865	4796
3	1075	-3474	4906	-5000	4356
4	1100	-3402	5200	-5203	4260
5	1125	-3479	5319	-5409	4357
6	1150	-4160	4204	-5292	5320
7	1175	-4316	4353	-5440	5279
8	1200	-4382	4345	-5700	5372
		Normalized System Moments (max. values set = 100)			
2	1050	-100.	80.7	-80.7	100.
3	1075	-69.5	98.3	-100.	87.2
4	1100	-65.5	100.	-100.	82.0
5	1125	-64.4	98.2	-100.	80.6
6	1150	-78.2	79.0	-99.4	100.
7	1175	-79.3	80.0	-100.	97.0
8	1200	-76.9	76.2	-100.	94.2

TABLE 7.4

VARIATION OF MOMENTS IN FRAME 23A

appropriate for the axial forces present. The estimated M_{ult} for these sections (assumed balanced) is 5130 inch pounds (29). The lower moment values at A and B correspond to axial tension at those spots, whereas increased values at C and D correspond to axial compression forces.

Since the left side of the frame (tension forces) became less stiff than the right side (compression forces) then the shear distribution between columns was affected. Table 7.5 shows the small changes that occurred whence just before failure the left column carried 41% of the story shear, the right column carried 56%.

A further observation in this summary concerns the variation of tensile steel stresses. After the onset of cracking, at 1075 pounds load, these stresses were 22509 psi at A and 19504 psi at D. Just before failure, at 1200 pounds load, the tensile steel stresses at the hinge locations were as follows:

at A, 35096 psi (with + 305 pounds axial),

at B, 29944 psi (with + 345 pounds axial),

at C, 18341 psi (with -488 pounds axial),

at D, 35288 psi (with -304 pounds axial),

However, during the next load increment when failure occurred, the tension steel stresses at all these locations rose above 40000 psi in successive iterations. Thus, the concept of yielding of the steel in the hinge locations was indeed a feature of the final collapse.

The load-deflection curve (Figure 7.7) shows that the cracking load and yield load for this frame are nearly the same. Taking the

Total Shear lbs	Column Shears			
	Left lbs	Right lbs	Left %	Right %
1050	525	525	50.0	50.0
1075	508	567	47.2	52.8
1100	521	579	47.3	52.7
1125	533	592	47.4	52.6
1150	506	644	44.0	56.0
1175	524	651	44.6	55.4
1200	528	672	44.0	56.0

TABLE 7.5

VARIATION OF SHEARS IN FRAME 23A

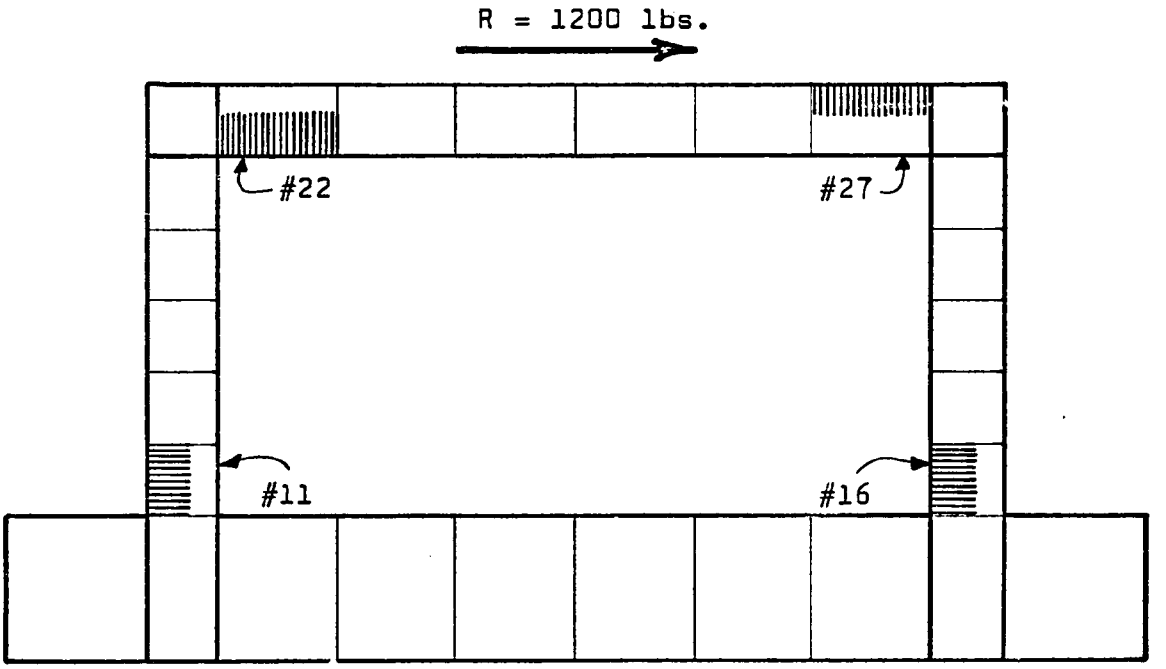

FIGURE 7.8 FRAME 23A CRACKING BEFORE FAILURE.

approximate area under the load-deflection curve as a measure of the energy absorption to failure of this frame,

$$W_{23A} = 0.5\ (1050.)\ (0.015393) + (1125.)\ (0.027769)$$
$$= 8.081 + 31.240$$
$$= 39.321 \text{ inch pounds}$$

This value will be used for comparisons with the next structures to be analyzed.

7.1.2 Results From Two-Story Frame 23B

Frame 23B was formed by adding an upper story to frame 23A, see Figures 7.6 (A) and (B), to give 90 nodes and 46 elements. The analysis to failure took 753.3 seconds on the CDC-6400 computer. The maximum lateral load of 854 pounds was reached in 14 increments and took 45 iterations as described in Table 7.6. This table also gives the lateral sway of the frame computed at node 90 as the reference position. The load-deflection curve is plotted in Figure 7.9 and shows that the response is of the same form as that of frame 23A. However, first cracking occurs at a lower load level (830 pounds) than for the single story frame and immediately involves 6 elements, rather than just the column bases. The development of cracking is listed in Table 7.7 and shows how the newly cracked system requires only a single small increment to involve a final hinge location at element 38. After reaching this loading (832 pounds) the system develops no new cracks with increasing load until immediate failure occurs beyond 852 pounds with extensive cracking. The cracking at elements 33 and 40 must be considered as a single stiff hinge

Load Increment		Total Load	Total Deflection	No. of Cycles
No.	Size	lbs	Inches	
1	828	828	.038751	1
2	2	830	.081742	12
3	2	832	.089994	6
4	2	834	.090213	1
5	2	836	.090431	1
6	2	838	.090650	1
7	2	840	.090875	3
8	2	842	.091172	4
9	2	844	.091495	2
10	2	846	.091888	4
11	2	848	.092322	2
12	2	850	.092755	1
13	2	852	.093187	1
14	2	854	failure	6
		Total cycles =		45

Note: Lateral sway is measured at node 90, upper right corner of frame 23B.

TABLE 7.6

FRAME 23B LOADING AND ITERATIONS.

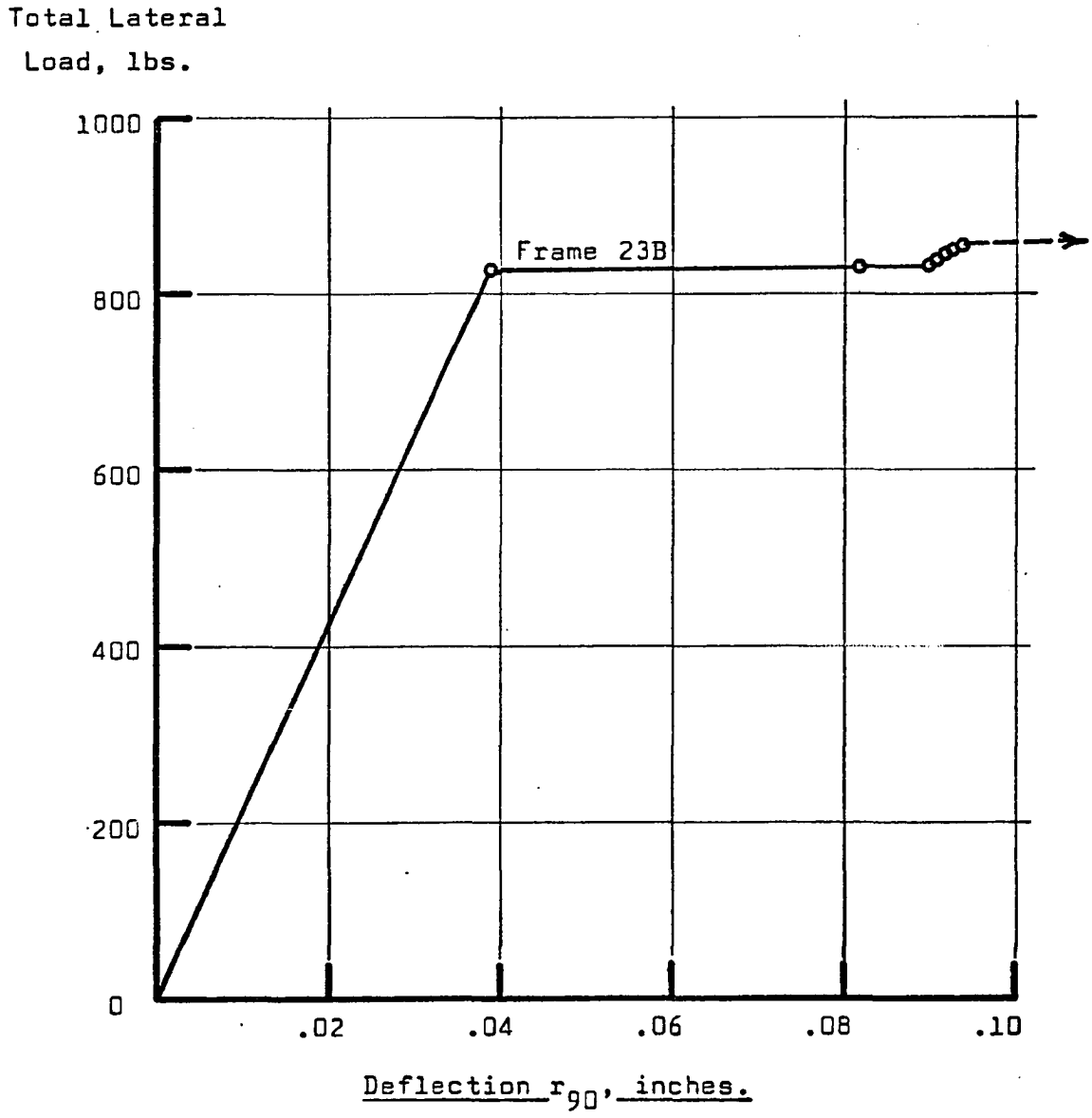

FIGURE 7.9 LATERAL DISPLACEMENT OF NODE 90.

Inc. No.	Total Load lbs	Slices Cracked In Elements						
		11	16	22	27	33	38	40
1	828	-	-	-	-	-	-	-
2	830	6	6	5	6	4	-	4
3	832	6	6	6	6	4	5	5
4	834	Cracking remains unchanged.						
⋮	⋮							
13	852							
14	854	Fails with extensive cracking.						

TABLE 7.7

CRACK PROPAGATION IN FRAME 23B

location at that corner. Since the other 5 cracked elements also behave as stiff hinges then the frame has reached a 6-hinge mechanism for potential failure almost immediately after first cracking. This again accounts for the elasto-plastic form of the load deformation response. The condition of the cracked frame failure is shown in Figure 7.10 and this may be related to the changes in frame moments recorded in Table 7.8 for the hinge locations. The hinge moment values converged asymptotically toward the appropriate values of plastic moments while the load increased. As expected, the compression hinges at D,F,B and C (see Table 7.8) converged towards higher values of plastic moments than the tension hinges at A and E.

The shear distribution between the columns of each story showed little change during the loading to failure once cracking had occurred. Before cracking the columns of each side carried 50% of the story shear. After cracking, the change in stiffness was greatest in the bottom story so that the left : right column shear distribution became about 38% : 62% as given in Table 7.9. However, the upper story columns showed less variation in their stiffnesses and reached about 51% : 49% sharing near failure.

The tensile steel stresses at the hinge locations are next listed for the situations just after cracking (830 pounds load) and just before failure (852 pounds load). Stresses are given as psi.

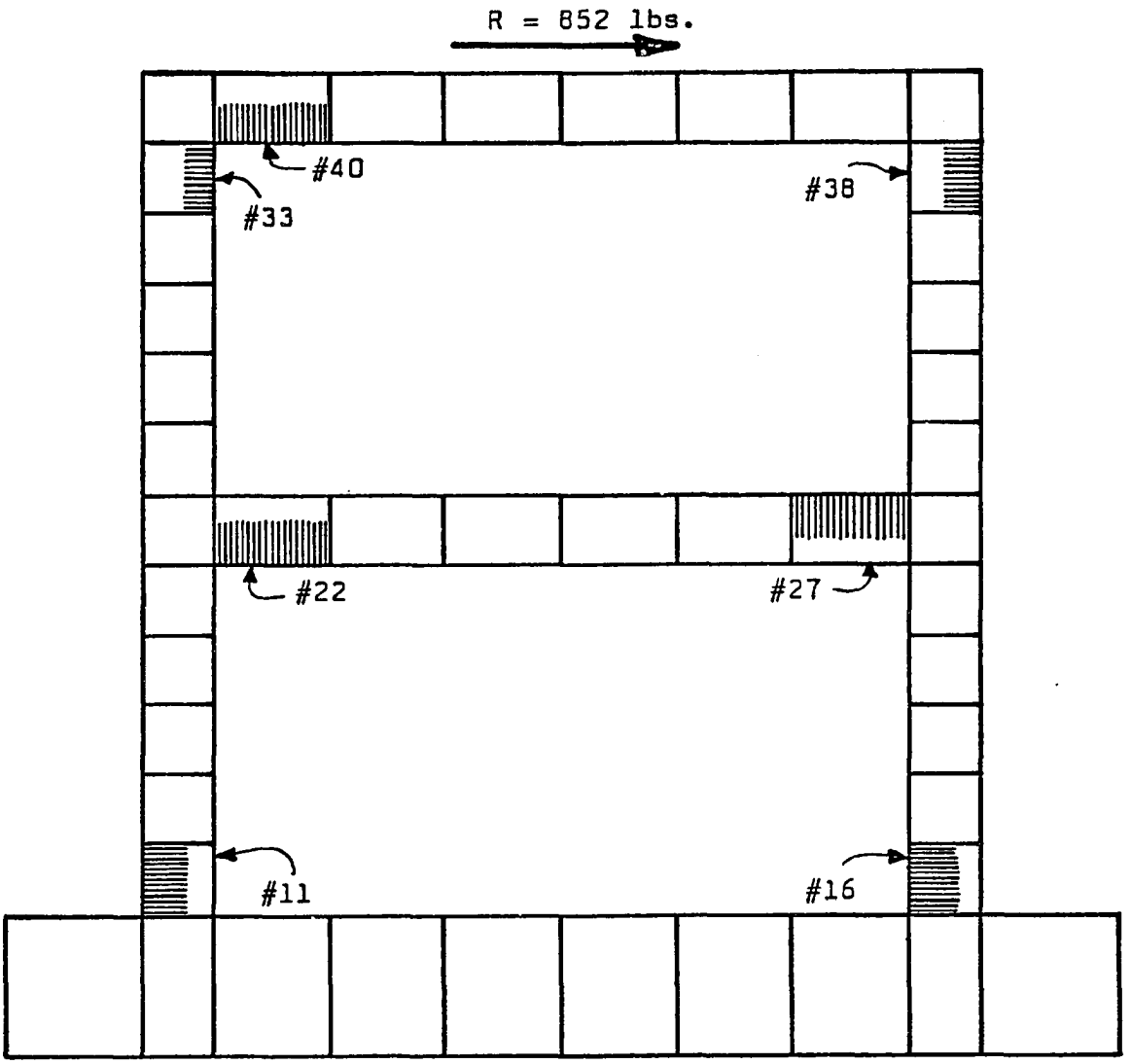

FIGURE 7.10 FRAME 23B CRACKING BEFORE FAILURE.

Inc. No.	Total Load	System Moments (inch-lbs.)					
		M_A	M_B	M_C	M_D	M_E	M_F
1	828	-4477	5677	-5677	4476	4130	-4130
2	830	-3525	5033	-4968	5496	3983	-5626
3	832	-3714	5171	-5379	5807	3868	-4804
7	840	-3748	5221	-5432	5861	3906	-4850
10	846	-3756	5268	-5454	5912	3944	-4893
13	852	-3768	5326	-5475	5934	3988	-4942

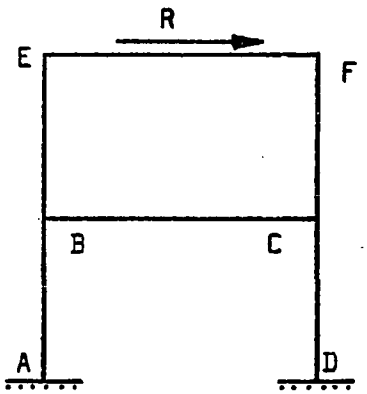

TABLE 7.8

VARIATION OF MOMENTS IN FRAME 23B

Load lbs.	Column Shears lbs.				Column Shears %			
	Bottom Story		Top Story		Bottom Story		Top Story	
	Left	Right	Left	Right	Left	Right	Left	Right
828	414	414	414	414	50.0	50.0	50.0	50.0
830	318	512	404	426	38.3	61.7	48.7	51.3
832	314	518	418	414	37.8	62.2	50.3	49.7
836	316	520	420	416	37.8	62.2	50.2	49.8
844	318	526	425	419	37.7	62.3	50.2	49.8
852	321	531	430	422	37.6	62.4	50.5	49.5

TABLE 7.9

VARIATION OF SHEARS IN FRAME 23B

Element	830 pounds	852 pounds
11	33047	35056
16	31869	35044
22	27707	33861
27	31815	35049
33	17857	17394
40	17679	23413
38	5386	25946

Again, during iterations to failure in the succeeding load increment, the tensile steel stresses rose well above 40000 psi at all hinge locations.

The cracking and yield loads were close again as a result of the minimum reinforcement percentage (828 lbs. and 854 lbs.). Taking the approximate area under the load-deflection curve as a measure of the energy absorption to failure for this frame then

$$W_{23B} = 0.5\ (828.)\ (0.038751) + (840.)\ (0.054436)$$
$$= 16.043 + 45.726$$
$$= 61.769 \text{ inch pounds}$$

The comparison with frame 23A shows that 23B only carried 71.0% of the maximum load achieved by 23A, but absorbed 1.57 times as much energy as 23A before failure.

The analyses of these frames showed the formation of failure mechanisms made of discrete stiff hinges with values of yield moments varying according to the axial forces present. These results were produced without assumptions concerning the moment-curvature

characteristics of the members and are an interesting feature of the analytical process.

Next these frames are analyzed with weak shear panels attached so that changes in their behavior could be demonstrated.

7.2 The Analytic Frames With Shear Panels

Two further analytic models, 24A and 24B, were prepared as shown in Figure 7.1, by adding weak, unreinforced panels to the frames 23A and 23B. The original panel material for laboratory testing (27) consisted of model bricks and mortar so that the experiment was concerned with frames with infilled panels rather than structural shear panels. In the present work no attempt was made to specifically represent a brick infilling but rather to consider the changes brought about by using panels of some defined, weak material. If necessary, panel reinforcement could be included (rod elements) but was omitted for this preliminary work.

The general layout and reinforcing of the frames remained unchanged from Figures 7.2 and 7.3. The discretization of the structures 24A and 24B was developed to suit the addition of panels and their attachment to adjacent frame members by tielinks. The necessary details are given in Figures 7.11 for the node geometry and element layouts.

The material properties for the frame concrete and reinforcement have already been given in Figures 7.4 and 7.5, but suitable properties for the panel material and tielinks had to be introduced. A linear, weak material (relative to the strength of the frame materials) was defined to have a tensile strength $f'_t = 100$ psi,

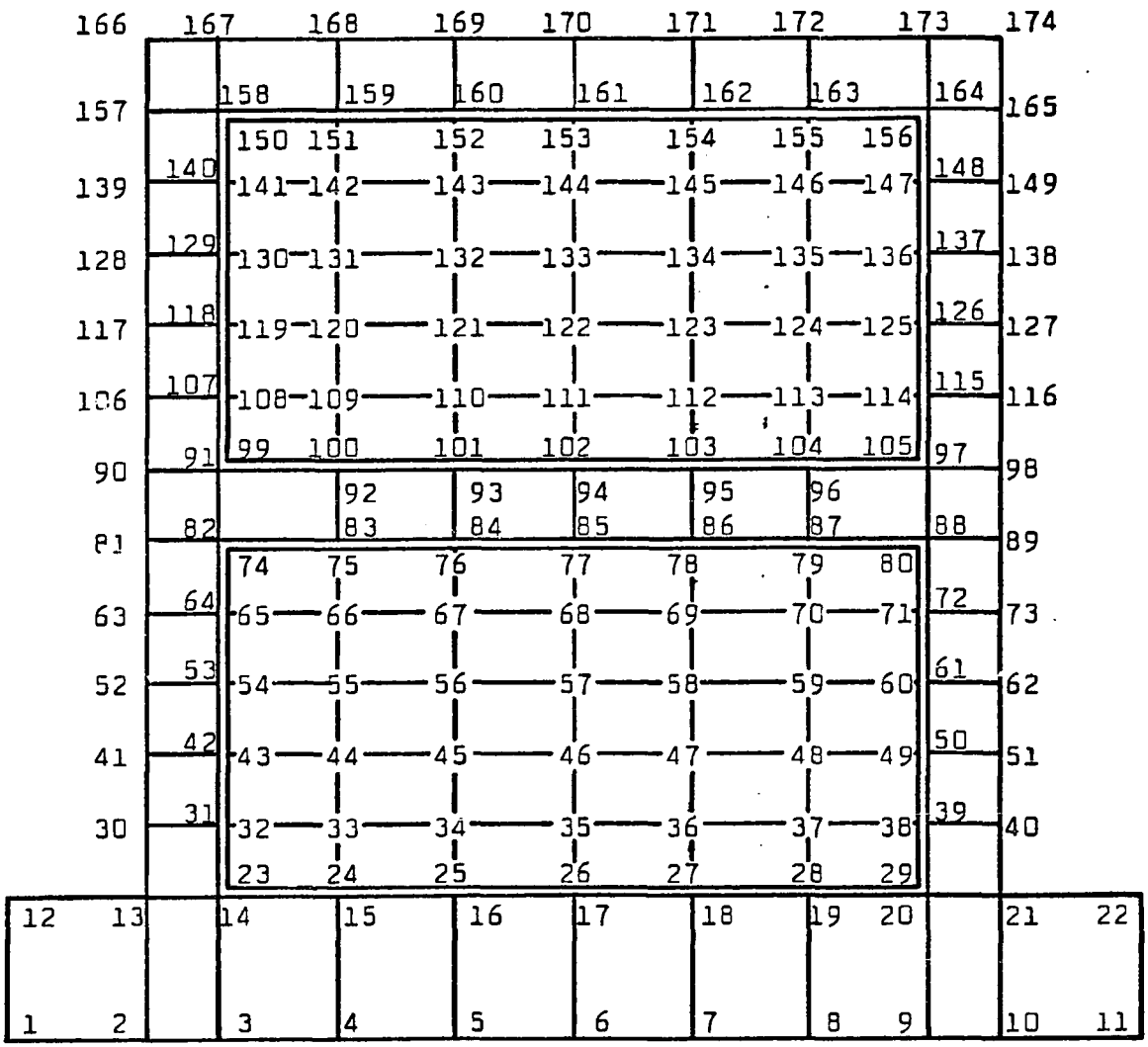

FIGURE 7.11(A) LAYOUT OF NODES INCLUDING PANELS.

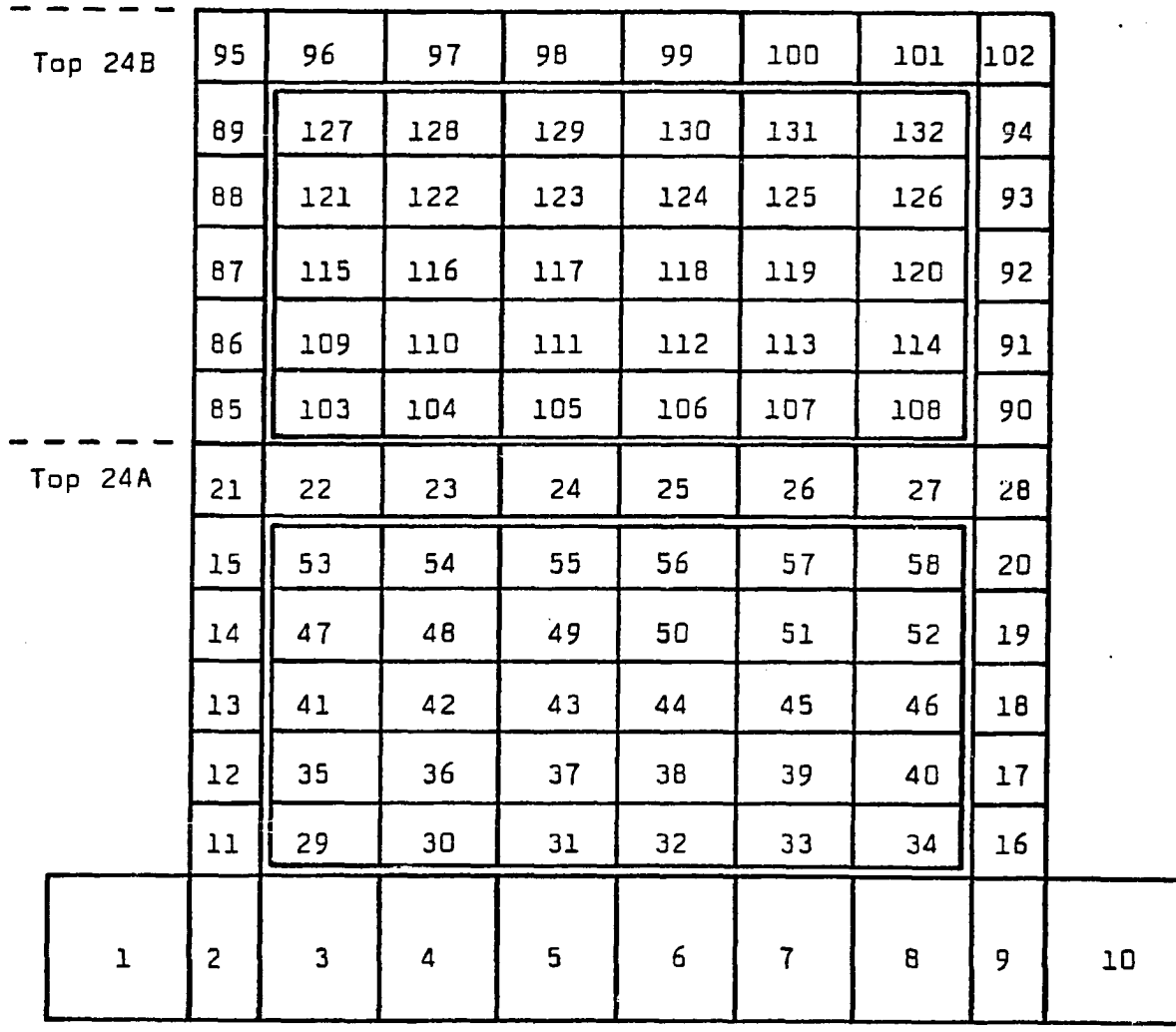

FIGURE 7.11(B) STRUCTURES 24A AND 24B.

LAYOUT OF QUADRILATERAL AND FRAME ELEMENTS.

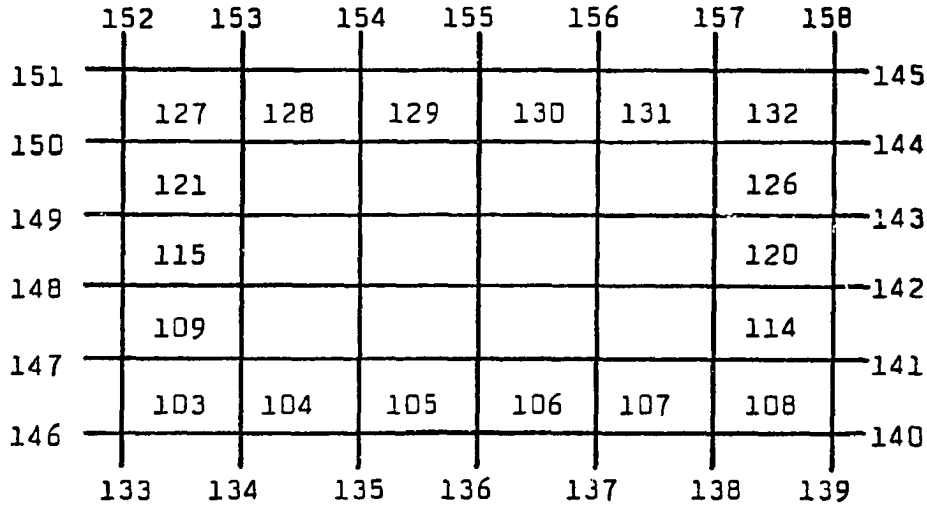

UPPER STORY TIELINKS 133 TO 158.

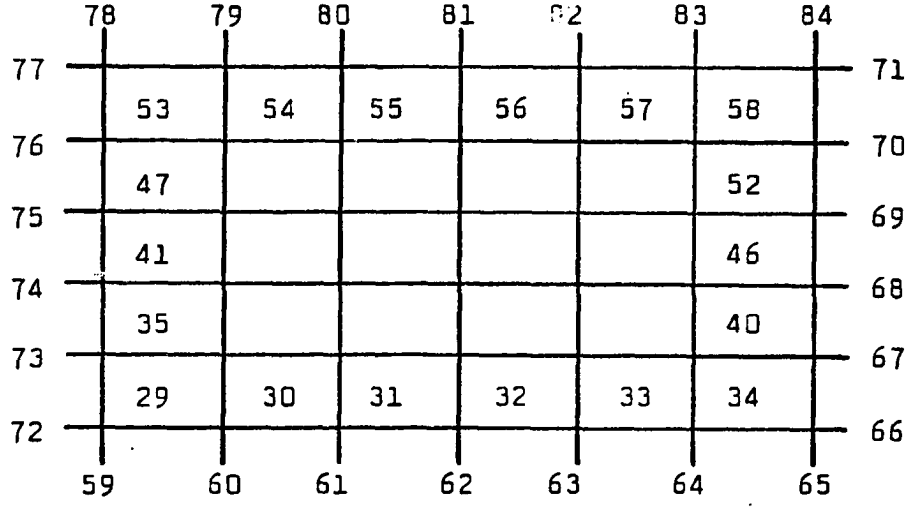

LOWER STORY TIELINKS 59 TO 84.

FIGURE 7.11(C) LAYOUT OF TIELINK CONNECTIONS.

a compressive strength f'_c = 500 psi, and a constant modulus of elasticity $E_c = 2.0 \times 10^6$ psi. The stress-strain curve for this material is given in Figure 7.12.

Four types of linkages are identified with this model arrangement according to the four magnitudes of tributary contact areas to be represented. Horizontal sides require each tielink to represent 5.0 X 0.875 = 4.375 sq. inches of contact area where the panel thickness of 0.875 inches provides the critical thickness dimension. Vertical sides require tielinks to each represent 2.625 sq. inches of contact while the corner links represent half of these values on any side. These areas were necessary for computing the tielinks strengths. The weakest material at the contact face is provided by the panel. This material has a tensile strength of 100 psi, but a shear strength of 100 psi was assigned to complete the list of properties required for the computations.

For example, the tensile strength assigned to tielinks on the horizontal sides was immediately given as 4.375 X 100. = 437.5 lbs. Likewise for the shear strengths and for the other tielinks. This yielded the following strength values:

Horizontal sides, non-corner,	437.5 lbs.
Horizontal sides, at corner,	218.75 lbs.
Vertical sides, non-corner,	262.50 lbs.
Vertical sides, at corner,	131.25 lbs.

Each tielink was assumed to be rigid in normal, uncracked operation and this was achieved by assigning a very large stiffness value, say 100×10^6 lbs/inch. However, each tielink also required

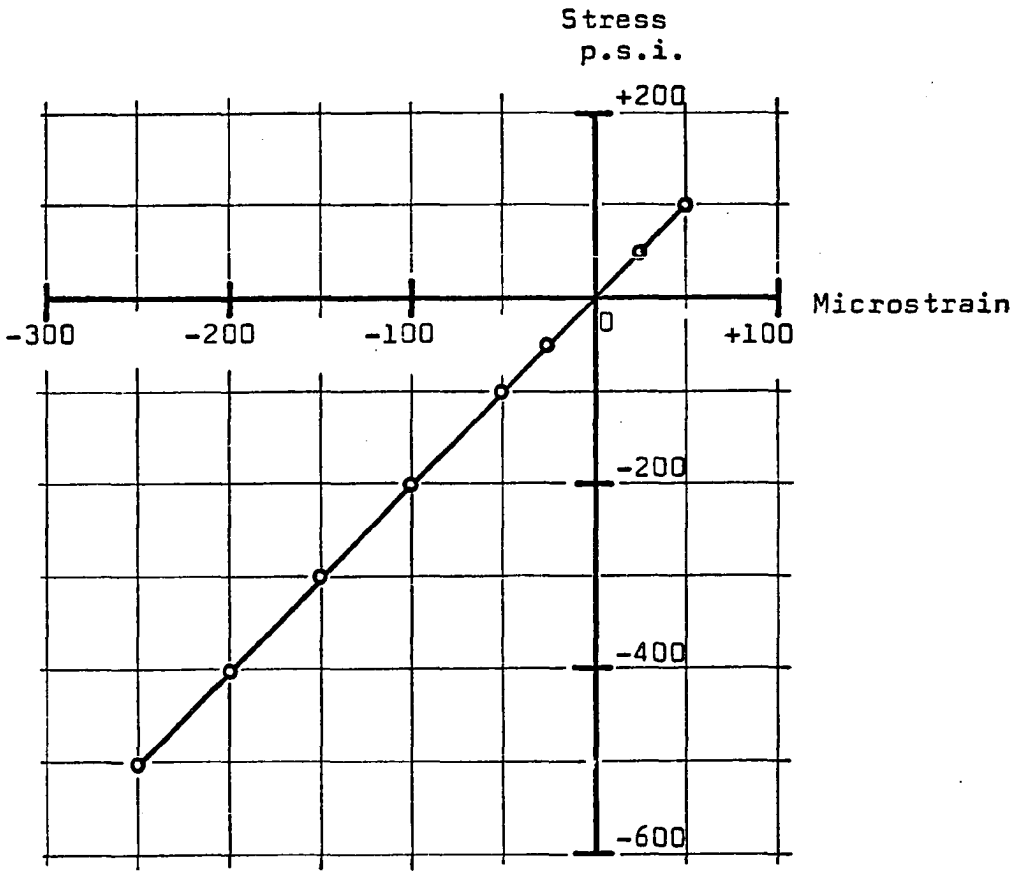

Ord	Stress	Microstrain
1	100.	50
2	50.	25
3	0.	0
4	-50.	-25
5	-100.	-50
6	-200.	-100
7	-300.	-150
8	-400.	-200
9	-500.	-250

FIGURE 7.12 STRESS-STRAIN CURVE FOR PANEL MATERIAL.

a stiffness value that could represent the frictional situation of a closed crack. This was done by arbitrarily taking one third of the bond stiffness that would be computed for the given contact areas and using an average value of bond stress per unit bond slip of 3.0 psi/microinch (9). For horizontal panel edges this gave a tie-link friction stiffness

$$K_f = (3 \times 4.375 \div 3) \times 10^6$$

$$= 4.375 \times 10^6 \text{ lbs/inch}$$

The other tielinks had proportional values computed for them.

The loading procedure for the panel structures was the same as that used for the previous frames; a lateral load was applied only along the top beam in each case (see Table 7.1 for a typical unit loading). The first load increment was made as large as possible without starting cracking or other nonlinear effects and then smaller increments were applied until failure occurred. The determination of these loads usually required several trial analyses beforehand. The results obtained for structures 24A and 24B will next be presented in separate sections.

7.2.1 Results For One-Story Structure 24A

The panel structure 24A required 98 nodes and 84 elements for its discretization (see Figures 7.11) and the analysis to failure took 573.4 seconds on the CDC-6400 computer. The maximum lateral load of 2500 lbs. was reached in 11 increments after a total of 25 iterations. This data is listed in Table 7.10 along with the load-deflection response at node 98 as the reference position (upper

Load Increment		Total Load	Total Deflection	No. of Cycles
No.	Size	lbs	Inches	
1	2000	2000	.001497	1
2	50	2050	.001535	1
3	50	2100	.001573	2
4	50	2150	.001612	2
5	50	2200	.001650	1
6	50	2250	.001688	2
7	50	2300	.001737	2
8	50	2350	.001803	2
9	50	2400	.001857	1
10	50	2450	.001912	3
11	50	2500	failure	8
		Total cycles = 25		

Note: Lateral sway is measured at node 98, upper right corner of structure 24A.

TABLE 7.10

STRUCTURE 24A LOADING AND ITERATIONS.

right corner). The load-deflection response was plotted in Figure 7.13 and showed a brittle behavior for this system with much increased strength and stiffness compared with the results for the frame alone (Figure 7.7). Assuming that the ultimate strength and deformation is represented by the calculation at 2450 lbs. applied load, then an estimate of the energy absorption of this structure is given by

$$W_{24A} = 0.5\ (2300)\ (0.001737) + 0.5\ (2300 + 2450)\ (0.000175)$$
$$= 1.997 + 0.416 = 2.413 \text{ inch lbs.}$$

Even the onset of cracking, which took place entirely in the panel itself, produced no significant deflection changes.

The sequence of cracking is listed in Table 7.11 and shows that progressive failure of the panel took place only after about 84% of the maximum load had been reached. No tielink fractures occurred for this model i.e. no separations between panel and frame; and no frame cracking occurred until the final disintegration of the system began under collapse loading.

All of the elements which cracked did so because of the biaxial failure criterion and the resulting cracks were oriented at practically 45° to the panel edges. The appearance of the cracking before failure is plotted in Figure 7.14. Some slightly curved crack paths may be discerned. During the final load increment to 2500 lbs. the entire panel became cracked, tielinks began to fracture, and eventually most of the panel elements became destroyed as compressive strengths were exceeded. This also represented the breakdown of diagonal strut action, and as large deflections became generated

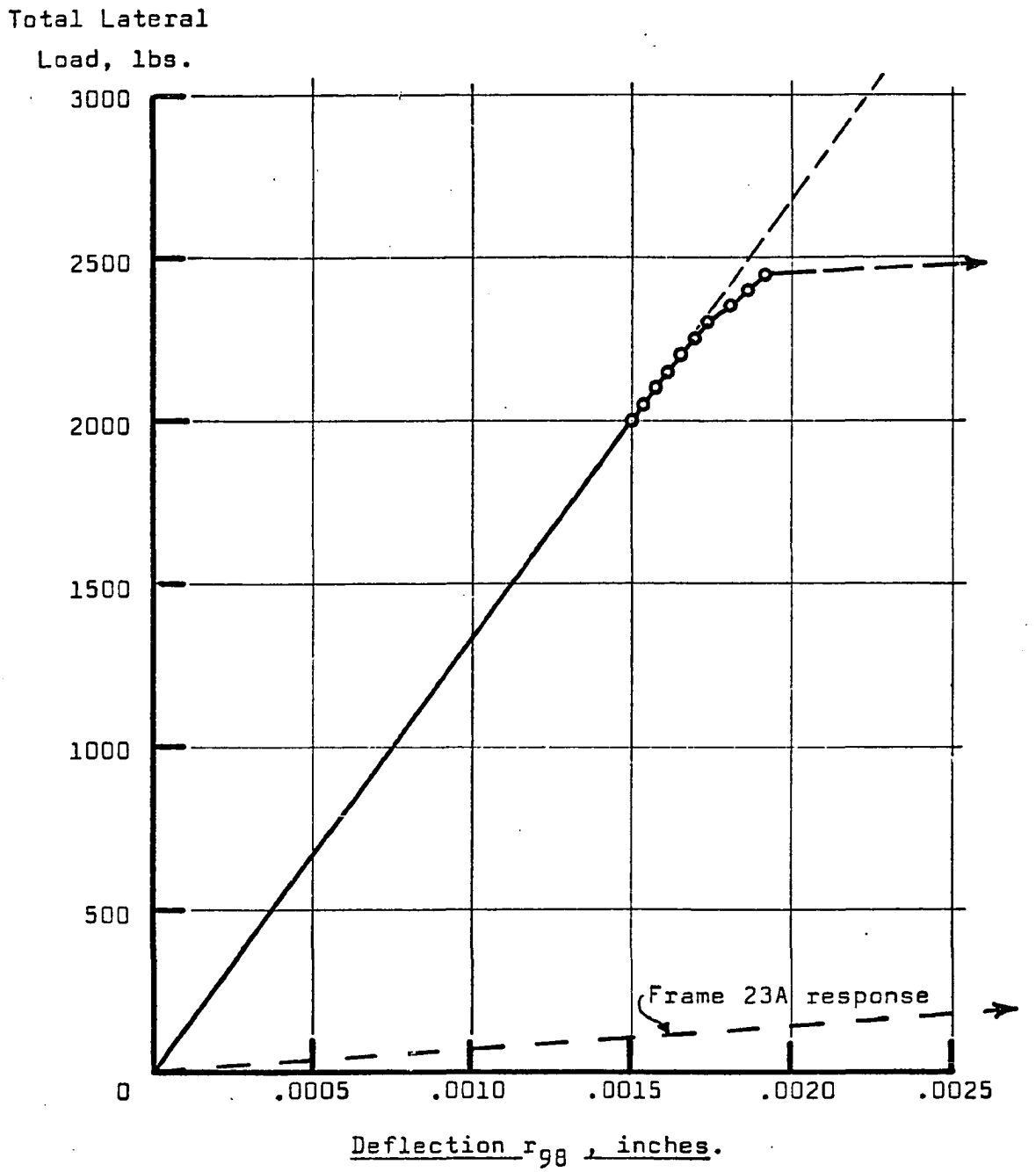

FIGURE 7.13

LOAD-DEFLECTION BEHAVIOR OF STRUCTURE 24A

Load lbs.	Cracks During Cycle No.	No. Of Each Element Which Becomes Cracked
2050	-	none
2100	1	35
2150	1	41
2200	-	none
2250	1	42 ; 49 ; 55 ; 56
2300	1	48 ; 50 ; 57
2350	1	43 ; 54
2400	-	none
2450	1	37 ; 44 ; 47
"	2	36
2500	General disintegration of panel quads and links.	

TABLE 7.11

CRACKING SEQUENCE OF STRUCTURE 24A

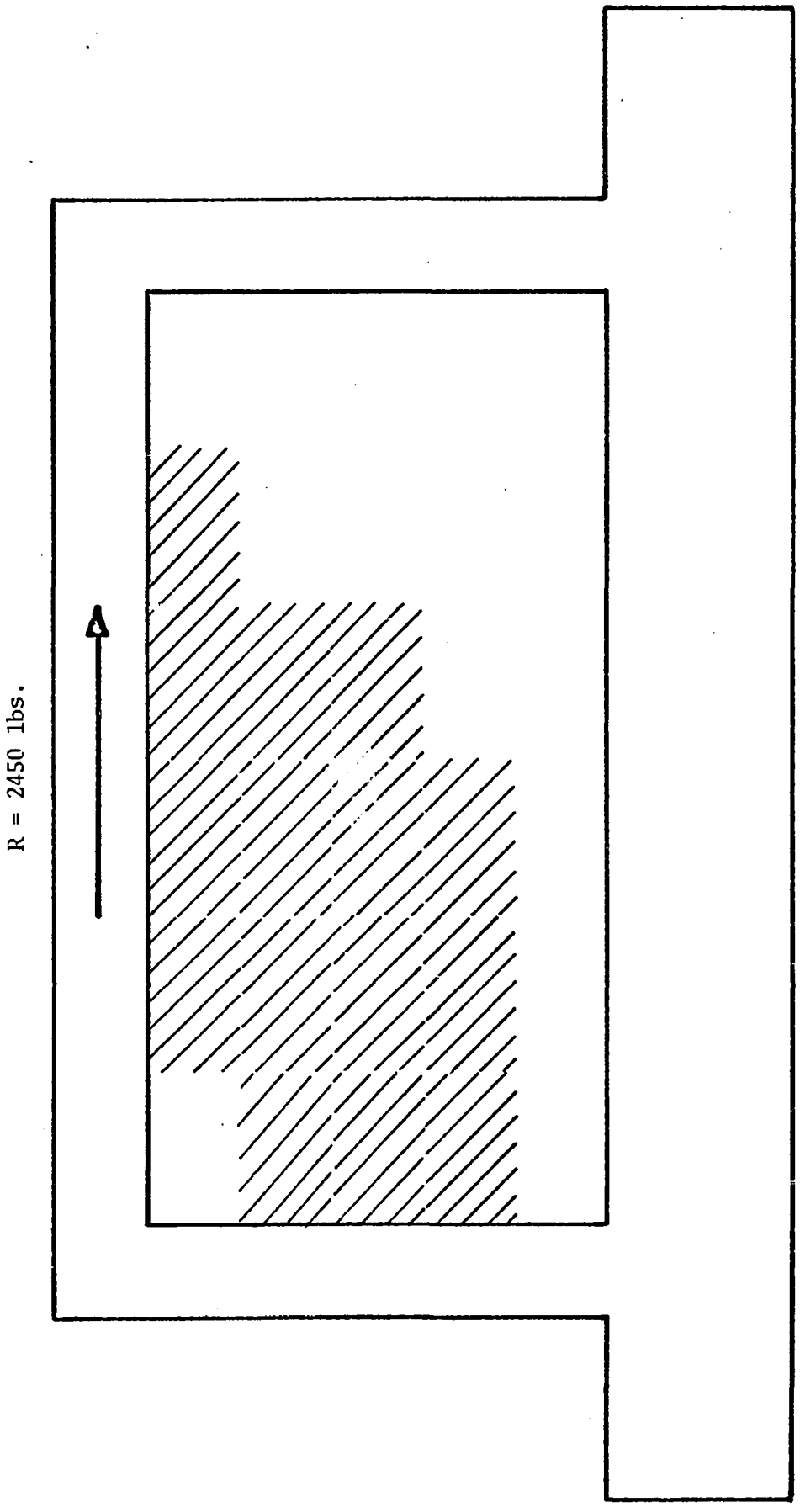

FIGURE 7.14 CRACKING BEFORE FAILURE, FRAME 24A.

so the computation was stopped.

Cracking is closely related to the magnitudes and orientations of the principal stresses within the panel. These values are plotted for each element in Figures 7.15 (A) and (B) for two load conditions; before cracking and before failure. Stress orientations remained practically unchanged during the development of cracking and the diagonal strut action is shown clearly by the principal compressive stress field in Figure 7.15 (B). The average 45° orientation of the principal stresses indicates that the panel was subjected predominantly to shear rather than flexure and this is consistent with the expected structural action. Further evidence of this comes from the shear stress values themselves. These values are shown in Figure 7.16 superimposed on the layouts of panel elements for the two reference load cases. Before cracking the shear stresses had the expected symmetry about the vertical centerline, with fairly uniform values across the panel width. Greatest deviations occurred at the edges where normal forces from the frame contact acted. On the other hand, a strong flexural action by the panel would have produced somewhat parabolic shear stress variations at any level. After cracking the shear stress values were lower over the cracked zone and higher over the uncracked elements according to the unbalance of stiffness in the panel system.

The distribution of the story shear force between columns and panel may be estimated from their relative stiffnesses. Subjecting the two columns to unit translations, bases fixed, then the column-resisted shear force P_c is given by

Applied Load = 2000 lbs.

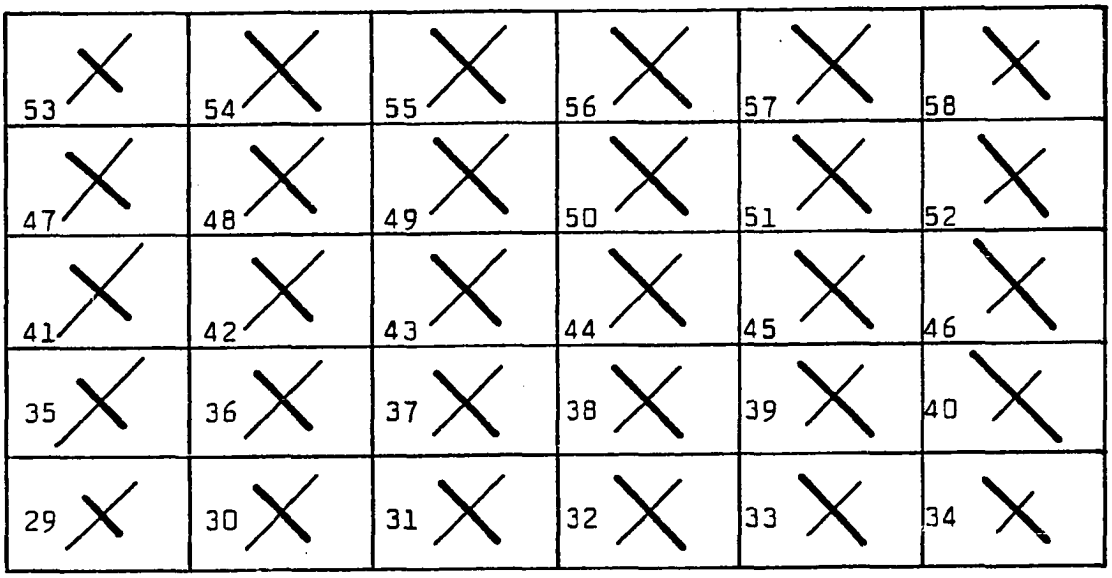

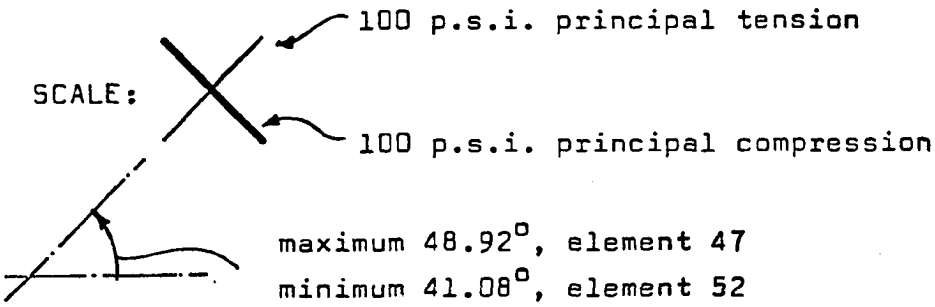

FIGURE 7.15(A)

PANEL STRESSES BEFORE CRACKING, STRUCTURE 24A

Applied Load = 2450 lbs.

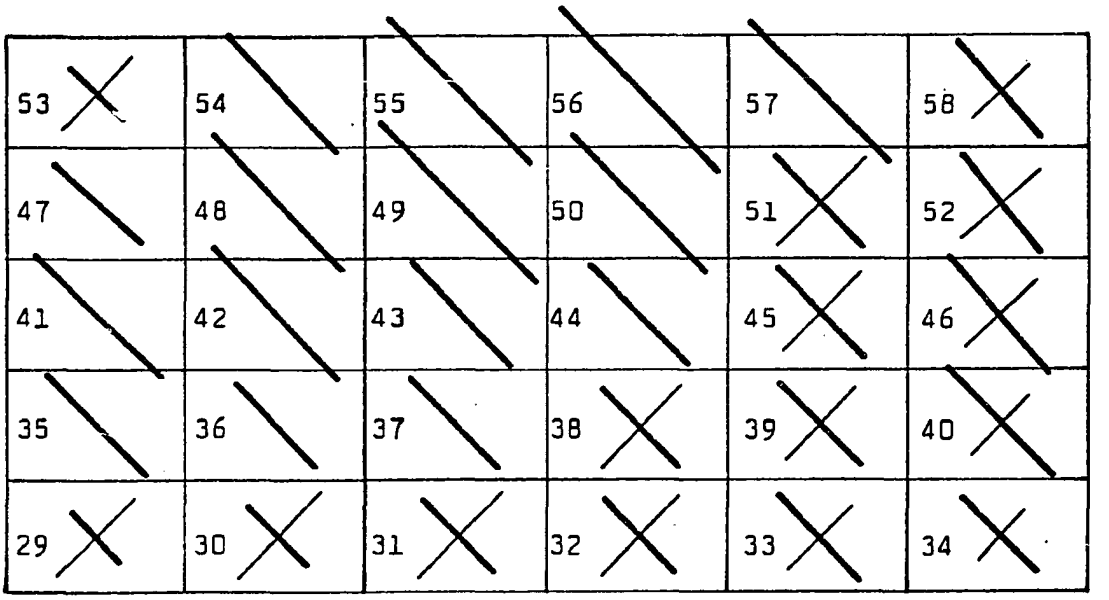

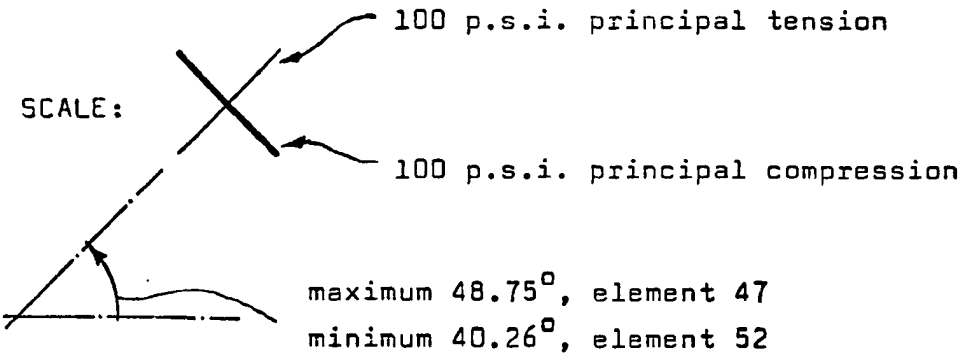

FIGURE 7.15(B)

PANEL STRESSES BEFORE FAILURE, STRUCTURE 24A

61.63	52.95	70.90	81.59	70.14	71.61
40.85	65.59	78.91	65.93	85.81	78.72
60.24	65.85	53.27	50.74	82.77	84.43
49.64	40.82	45.41	80.69	76.79	81.17
64.30	70.88	76.50	76.14	72.61	60.29

External Load 2450 lbs. Before Failure.

(Shear stress values shown in p.s.i.)

52.54	72.39	74.98	74.98	72.38	52.50
62.78	69.01	73.04	73.03	69.02	62.76
67.91	67.73	69.27	69.26	67.73	67.89
66.18	62.95	65.76	65.77	62.94	66.16
49.51	59.46	62.67	62.67	59.49	49.56

External Load 2000 lbs. Before Cracking.

FIGURE 7.16 PANEL SHEAR STRESS VARIATIONS.

$$P_c = 2 \times 12\ EI/L^3$$
$$= 24\ (2.88 \times 10^6)\ (7.79)/(15)^3$$
$$= 0.16 \times 10^6 \text{ lbs.}$$

Disregarding flexural action in the panel, then the wall-resisted shear force P_w is obtained from

$$P_w = AG/kL$$

where factor k = 1.20 is appropriate to compensate for the non-uniform shear stress distribution of a rectangular section, and where shear modulus $G = E/2(1+\nu)$. This gives

$$P_w = (30 \times 0.875)\ (2.0 \times 10^6)/(1.20 \times 15 \times 2.34)$$
$$= 1.25 \times 10^6 \text{ lbs.}$$

These may be combined to give the % distributions for this model as 88.6% to the panel and 11.4% of the story shear to both columns, or about 5.7% each. While this calculation serves to provide a single estimate of story shear distribution, it gives no indication of changes that may occur within the story height because of the actual frame-wall interaction. The % distributions of story shear obtained from the analysis are plotted in Figure 7.17 and it is evident that the above calculation is reasonably accurate in the upper two-thirds of the story, and that variations occur throughout the story height to increase the shear at the column bases to about 15-17%; about 3 times the estimate. However, shear distribution ratios between columns and panel, and variations of these ratios across the story height, show little change during panel cracking before failure.

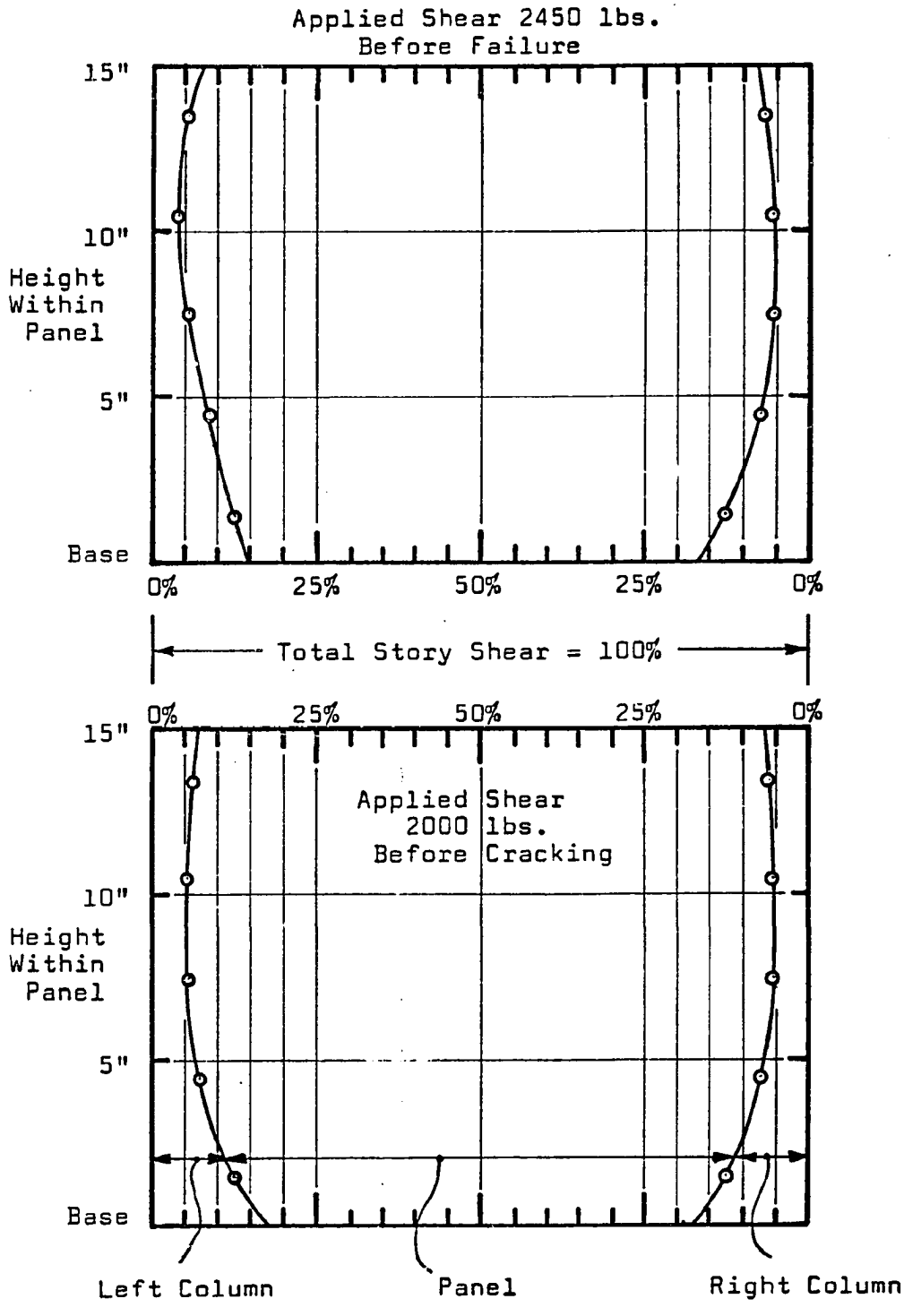

FIGURE 7.17 STORY SHEAR FORCE DISTRIBUTIONS.

Variations occurred in the column shears because of the interaction forces between columns and panel. In the analytic model these forces were represented by discrete forces at nodal connections and are shown in Figures 7.18(A) and (B) for two reference load cases. These forces show the predominant shear action of the panel as well as the influence of the frame-panel interaction. As a further illustration of the nature of the edge loading of the panel the vector resultants are plotted in Figure 7.19 along with the equilibrium polygon of forces for the panel.

The interaction forces between panel and frame have a significant effect on the moments in frame members. The moment diagrams for each reference loading are plotted in Figures 7.20(A) and (B) but are unrealistically discontinuous because of the discrete node connections to the panel. If edge connections were continuous, as in the real structures, then the moment diagrams would vary smoothly and this effect has also been noted on the diagrams. In general the panel forces cause an additional reduction of moments in the frame beyond the case where the frame alone would be carrying an equal amount of story shear without edge effects. This could be checked by comparing the moment diagrams of frame 23A (no panel) using a constant shear of 111 lbs., and those of the present structure 24A, which has an average upper region shear of 111 lbs. The paraxial edge forces produce most of the reduction moments. This becomes more evident when moment diagrams are separated into their contributing parts as is done in Figure 7.21 for the left column moments only.

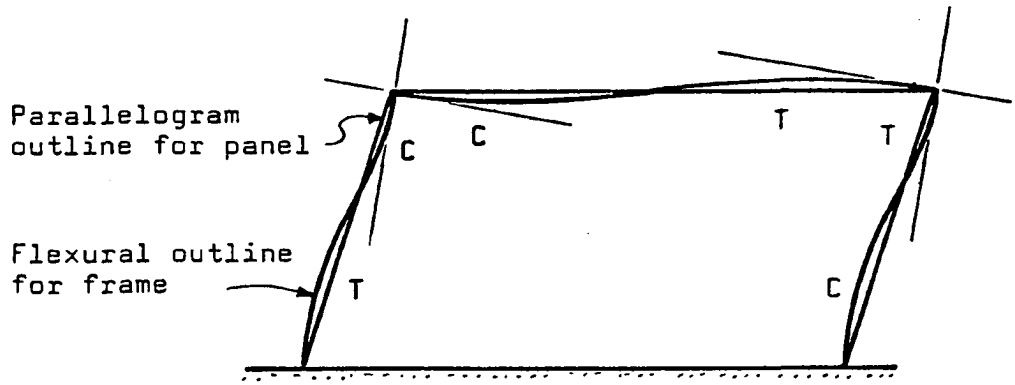

Interference Between Frame And Panel

Contact Forces Shown { C = Compression
T = Tension

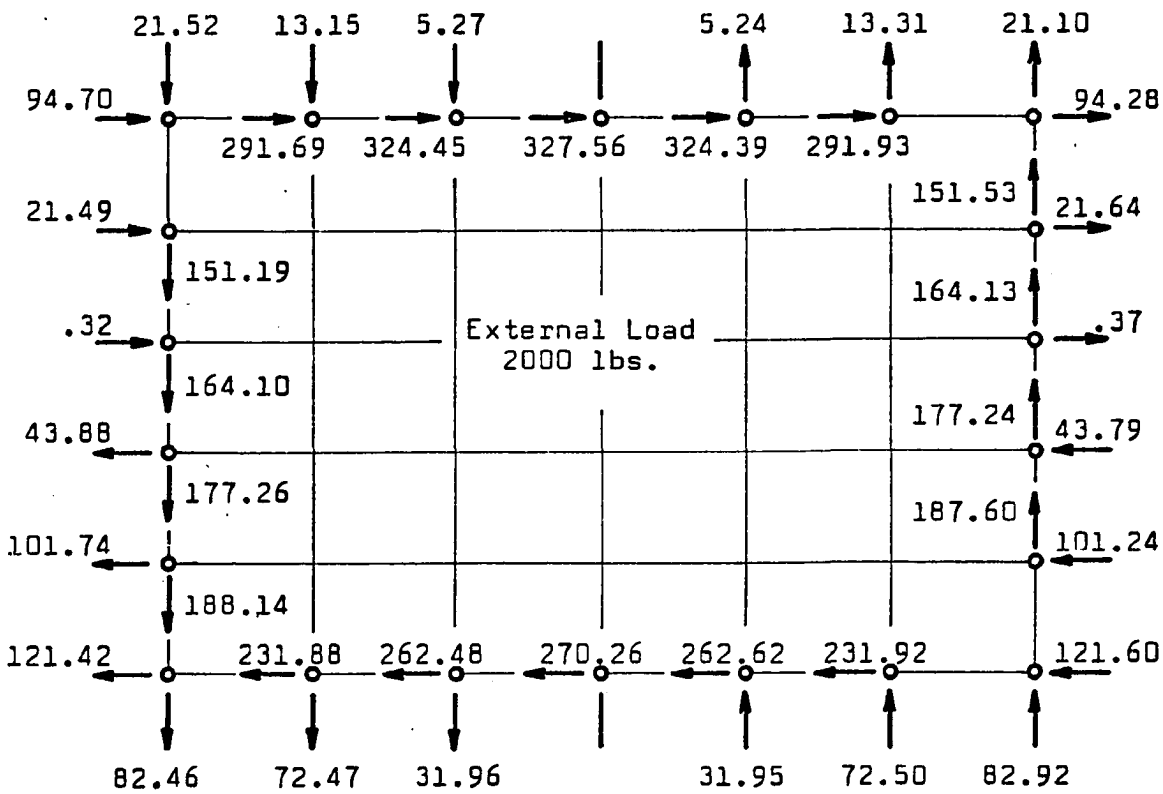

FIGURE 7.18(A) PANEL EDGE FORCES BEFORE CRACKING.

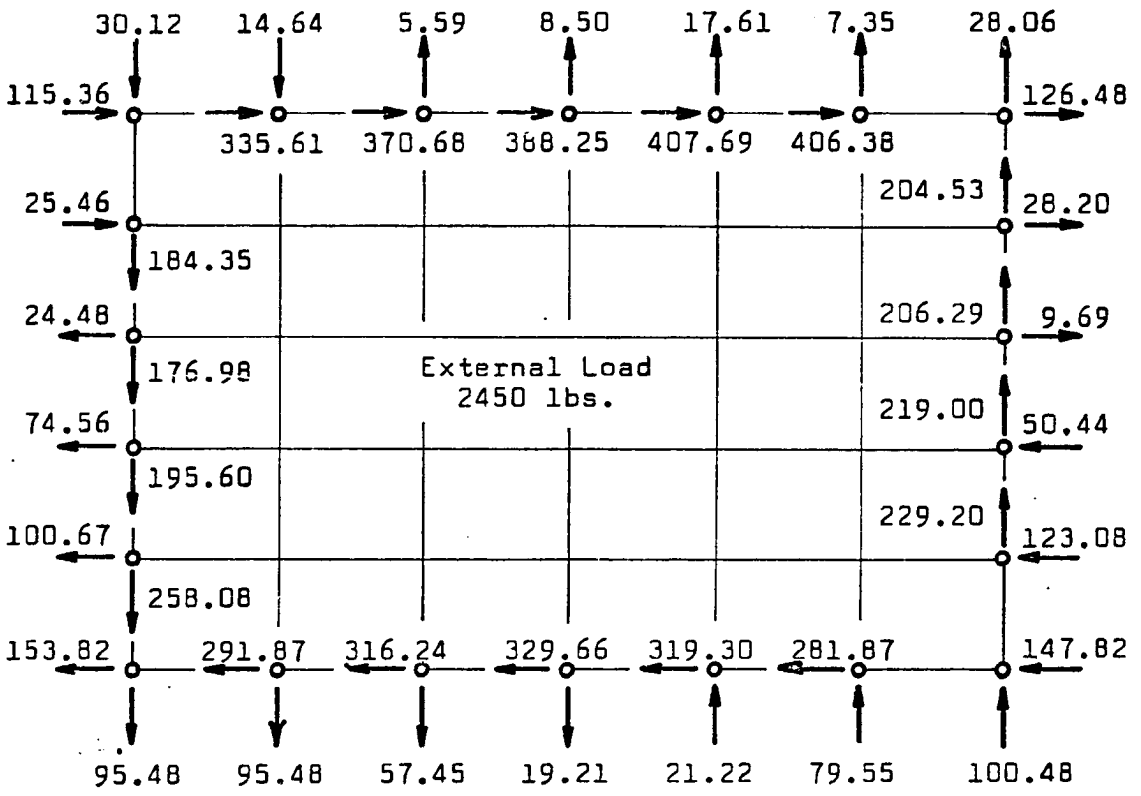

(Units are lbs. force.)

FIGURE 7.18(B) PANEL EDGE FORCES BEFORE FAILURE.

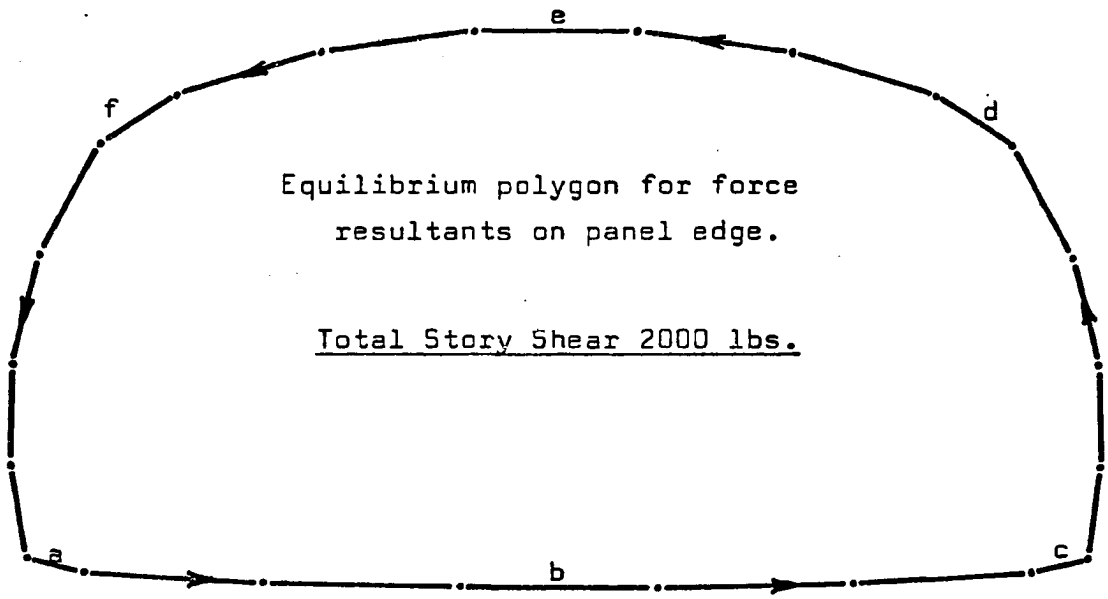

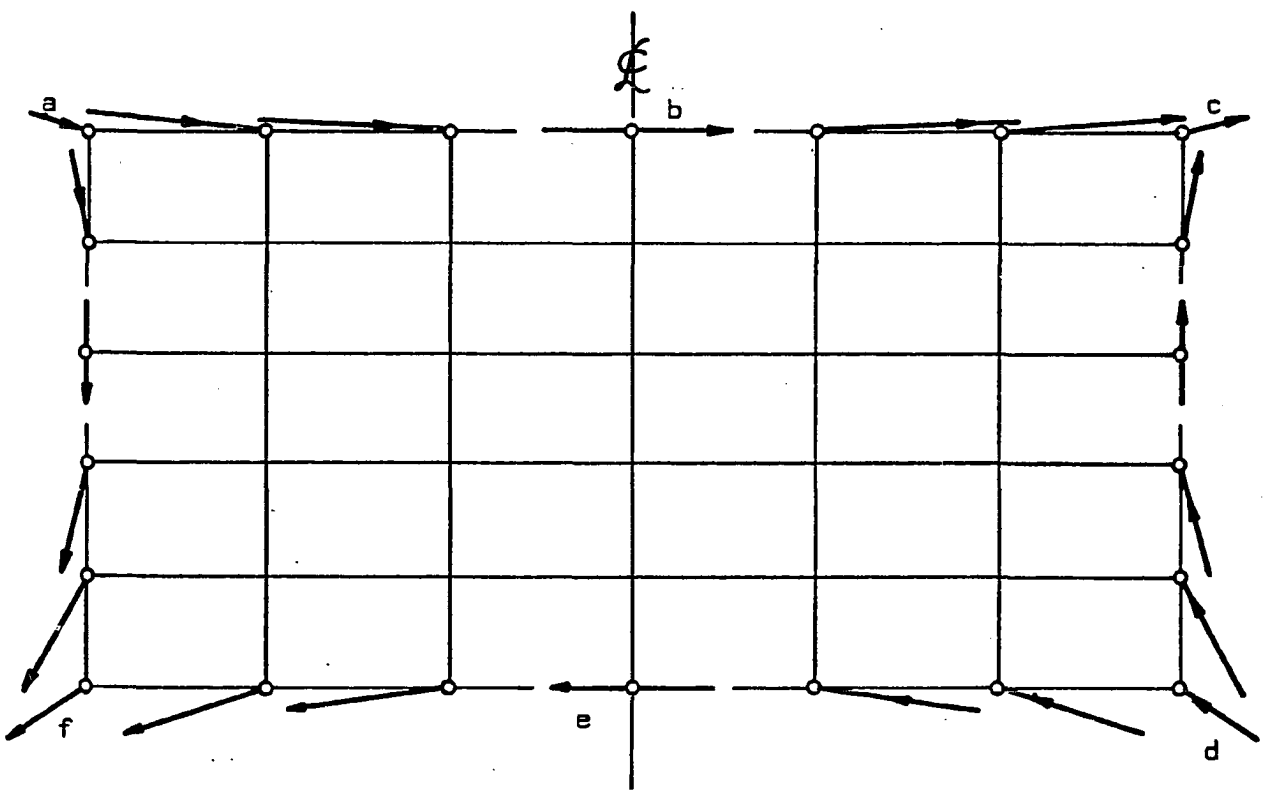

FIGURE 7.19

RESULTANT FORCES ON PANEL BEFORE CRACKING.

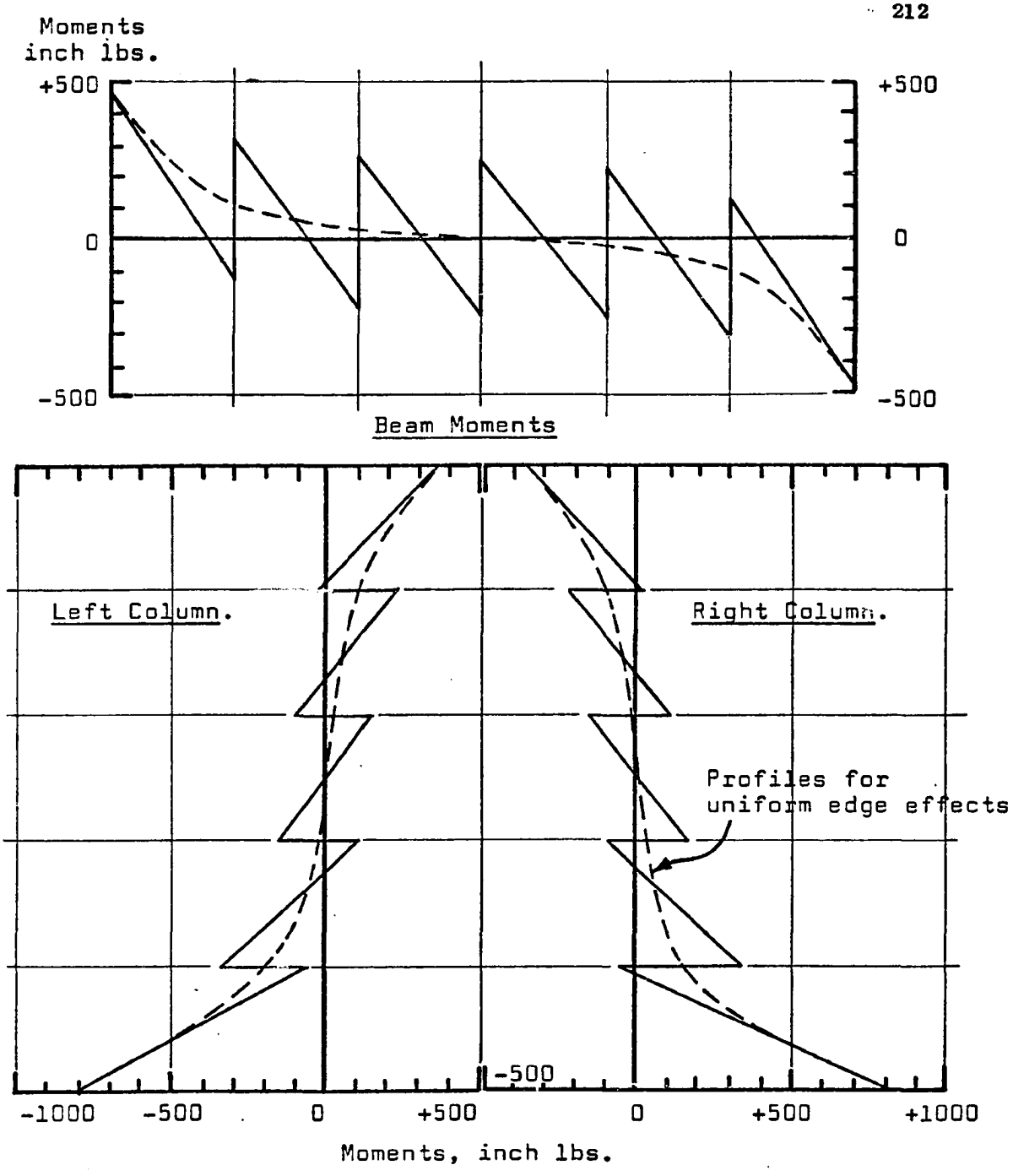

Total External Load = 2000 lbs.

FIGURE 7.20(A) FRAME MOMENTS BEFORE CRACKING.

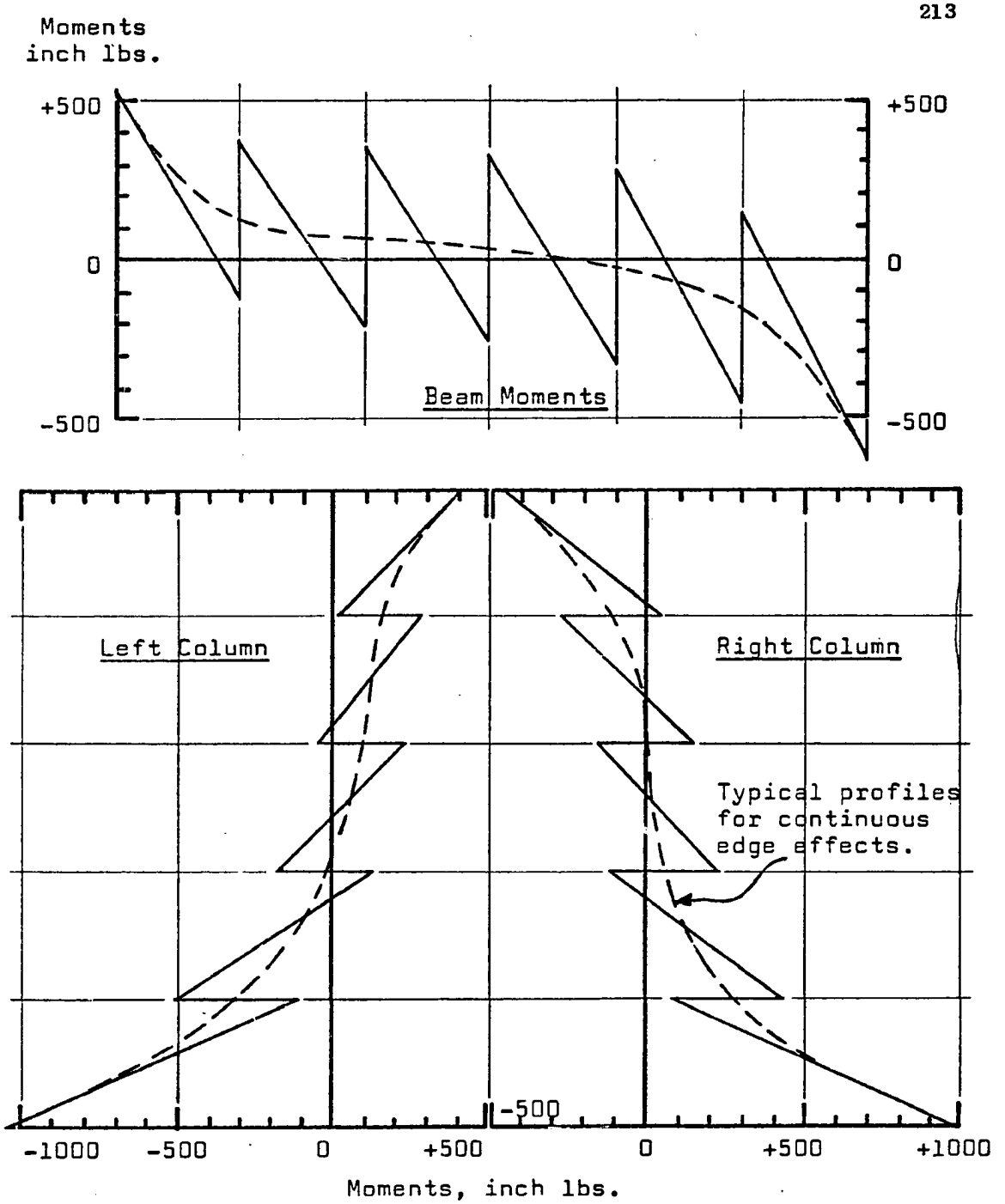

Total External Load = 2450 lbs.

FIGURE 7.20(B) FRAME MOMENTS BEFORE FAILURE.

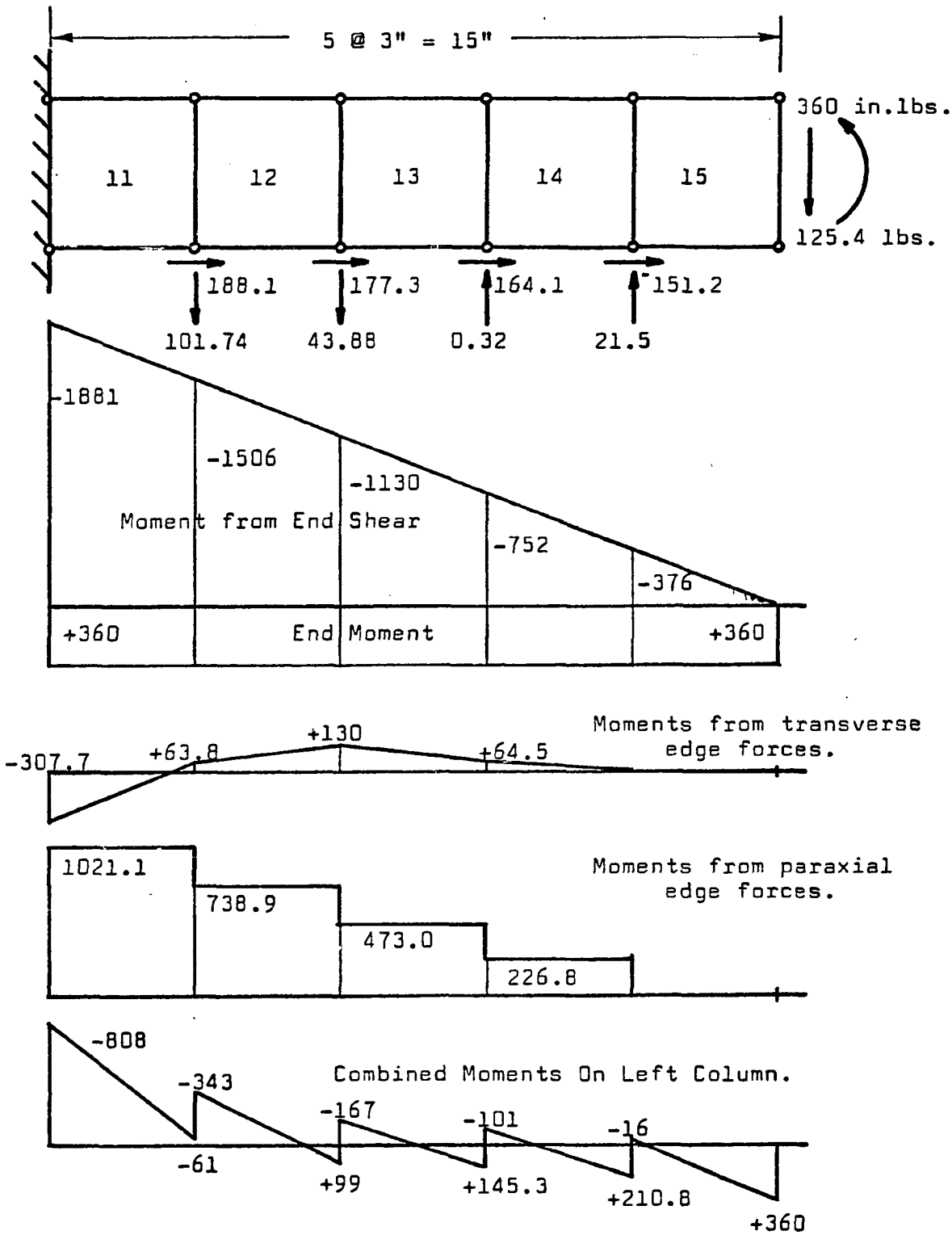

FIGURE 7.21 SEPARATION OF LEFT COLUMN MOMENTS.

7.2.2 Results For Two-Story Panel Structure 24B

This structure was discretized with 174 nodes and 158 elements (see Figures 7.11) and the analysis to failure took 1800 seconds on the CDC-6400 computer. The maximum lateral load of 2325 lbs. was reached in 19 increments after a total of 42 iterations. This data is listed in Table 7.12 and shows the load-deflection response at node 174 as the reference location (upper right corner of frame). This response is plotted in Figure 7.22 and shows the same generally brittle behavior previously observed for 24A. Assuming that the ultimate strength and deformation is given by the calculated results at 2300 lbs. load, then an estimate of energy absorption for this structure is given by

$$W_{24B} = 0.5\ (1900)\ (0.003964) + 0.5\ (1900 + 2300)\ (0.000977)$$
$$= 3.7658 + 2.0517 = 5.818 \text{ inch lbs.}$$

The sequence of cracking of panel elements is given in Table 7.13. Cracking was entirely contained within the weak panels, the frames were intact up to failure, and no panel-frame separations were induced before failure. Progressive failure of the panels took place after the initial cracking load of 1650 lbs. was reached (72% of ultimate load).

The appearance of the cracking is shown in Figure 7.23 for the applied load of 2300 lbs. just before failure. During the final load increment to 2325 lbs., extensive panel cracking occurred, tielinks began to fracture, frame cracking began and large deflections caused the computation to be stopped.

Load Increment		Total Load	Total Deflection	No. of Cycles
No.	Size	lbs	Inches	
1	1600	1600	.003303	1
2	50	1650	.003417	2
3	50	1700	.003528	2
4	50	1750	.003632	1
5	50	1800	.003735	1
6	50	1850	.003857	3
7	50	1900	.003964	2
8	50	1950	.004069	1
9	50	2000	.004175	2
10	50	2050	.004295	2
11	50	2100	.004415	3
12	50	2150	.004533	2
13	25	2175	.004603	3
14	25	2200	.004663	2
15	25	2225	.004736	3
16	25	2250	.004803	1
17	25	2275	.004869	2
18	25	2300	.004941	3
19	25	2325	failure	6
		Total cycles =		42

Note: Lateral sway is measured at node 174, upper right corner.

TABLE 7.12

FRAME 24B LOADING AND ITERATIONS.

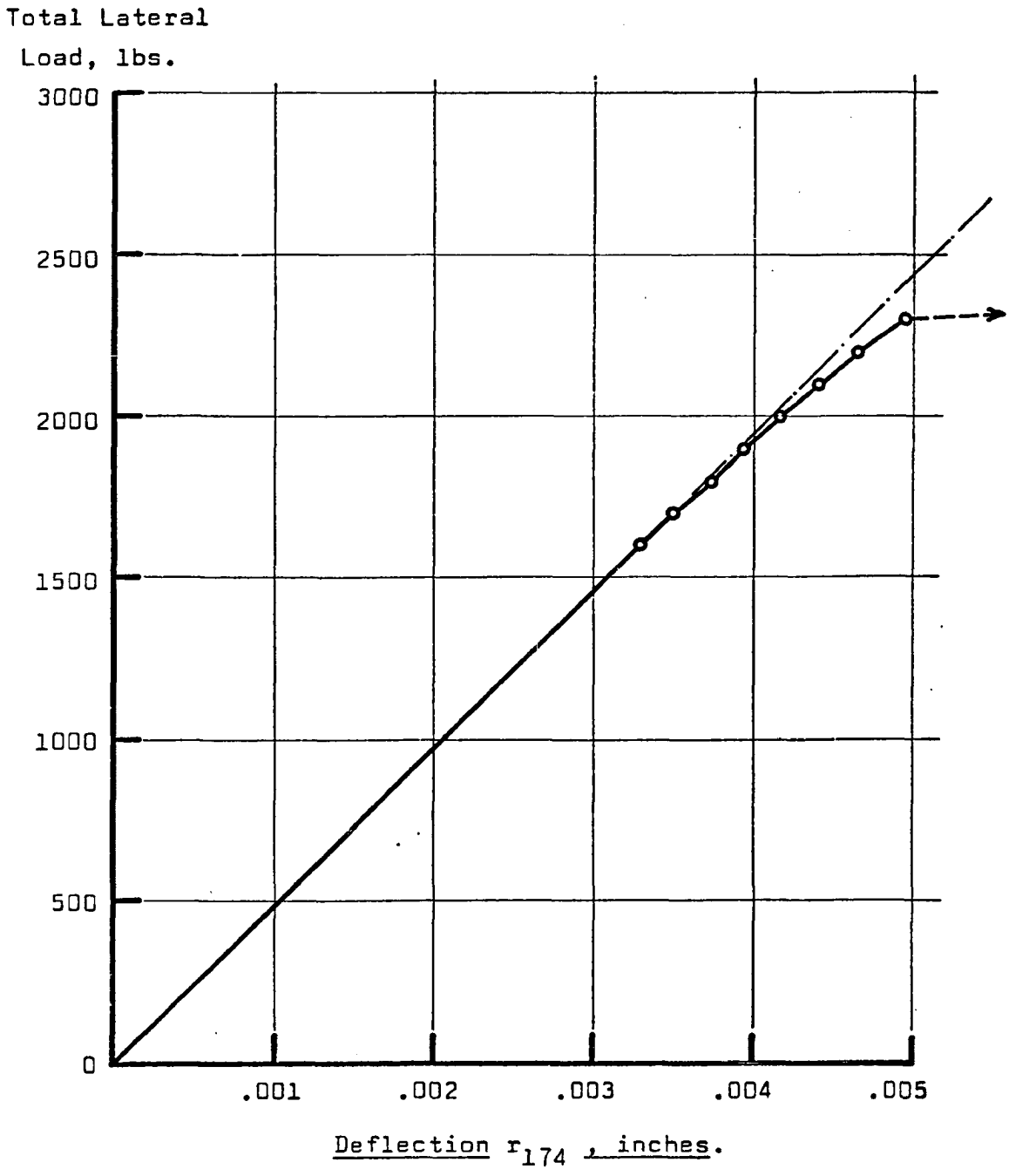

FIGURE 7.22

LOAD-DEFLECTION BEHAVIOR OF STRUCTURE 24B.

Load lbs.	No. of Cycles	No. of Each Element Which Becomes Cracked	
1600	1	none	
1650	2	41	
1700	2	35	
1750	1	none	
1800	1	none	
1850	3	47,48	
1900	2	42	
1950	1	none	
2000	2	49,55	
2050	2	36,54	
2100	3	53,56,43,	104
2150	2		105
2175	3	29,30	
2200	2		111,117,123, 129,130
2225	3	50,37	106,112,118 124
2250	1	none	
2275	2		116
2300	3		109,110,131
2325	6	General disintegration.	

TABLE 7.13

CRACKING SEQUENCE OF STRUCTURE 24B

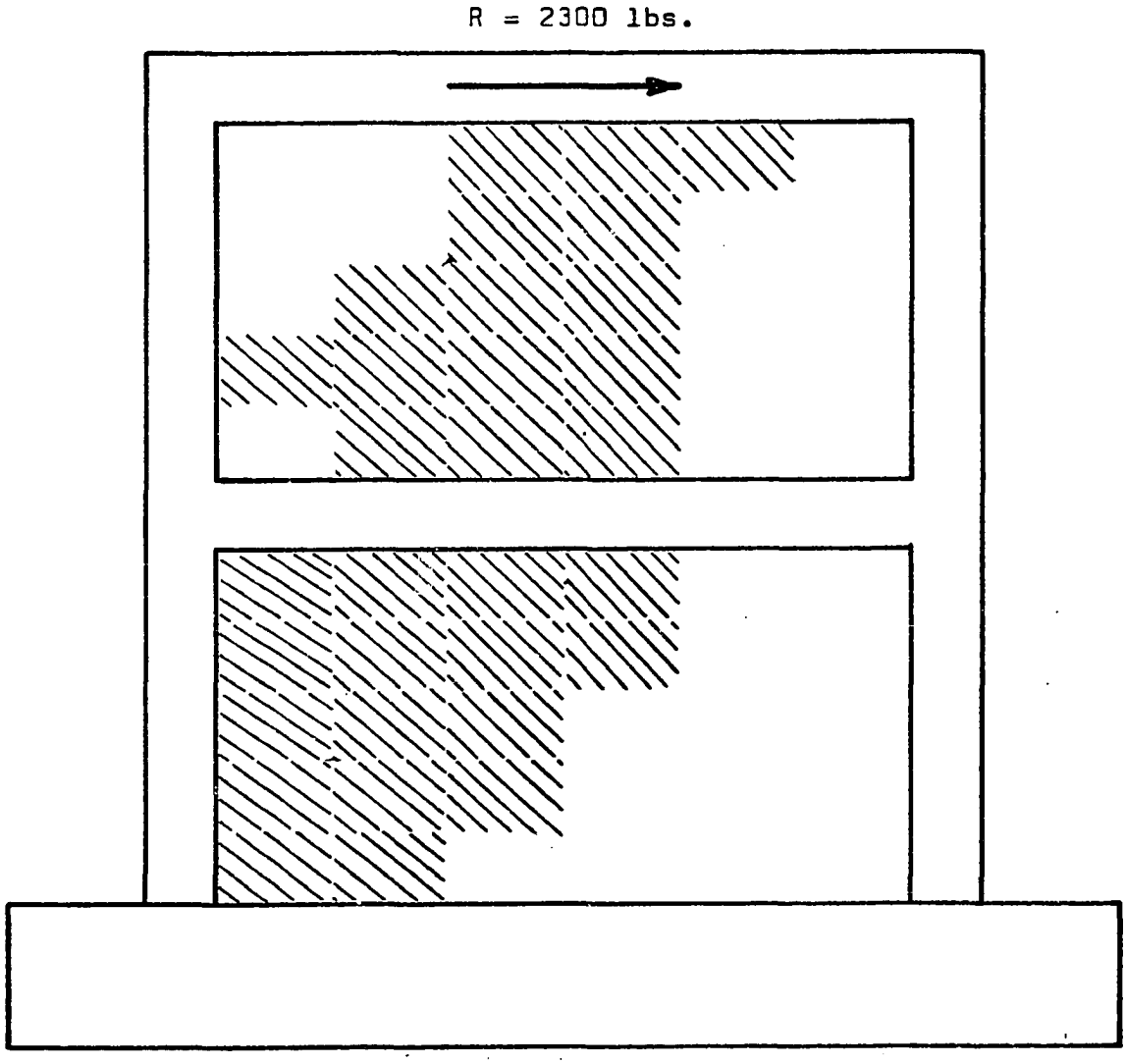

FIGURE 7.23

CRACKING BEFORE FAILURE, FRAME 24B.

The principal stresses existing in the panels before failure are shown in Figure 7.24. The stress orientations remained almost unchanged during the entire loading process. Once again the average 45° orientation of principal stresses over each entire panel indicated that the predominant structural action was one of shear rather than flexure. Shear stress values for both panels before cracking and before failure are given on panel layouts in Figures 7.25(A) and (B).

The distribution of story shear between frame and panels is given in Figures 7.26 for two loading conditions. The greatest deviation from the estimated distribution occurred in the lower panel where column base shears reached about 3 times the story estimate; about 20% in each column instead of about 6% of the story shear. However, in the upper panel, and in the upper part of the lower panel, the columns each carried an average 5% of story shear. These results can be compared to those for frame 24A shown in Figure 7.17.

Interaction forces between panels and frame were given by the data from tielinks at the connected nodes. These discrete force resultants are shown in Figure 7.27 for both panels before cracking begins, and represent the continuous interaction forces that are expected along panel edges. Such discrete forces cause the analytical moment diagrams to also be discontinuous (as was the case for structure 24A) and these results are plotted in Figure 7.28 for the reference loadings. The moment profiles shown dotted in that diagram are estimates of the actual moments expected to correspond to continuous, real panel-frame connections. The panels reduced

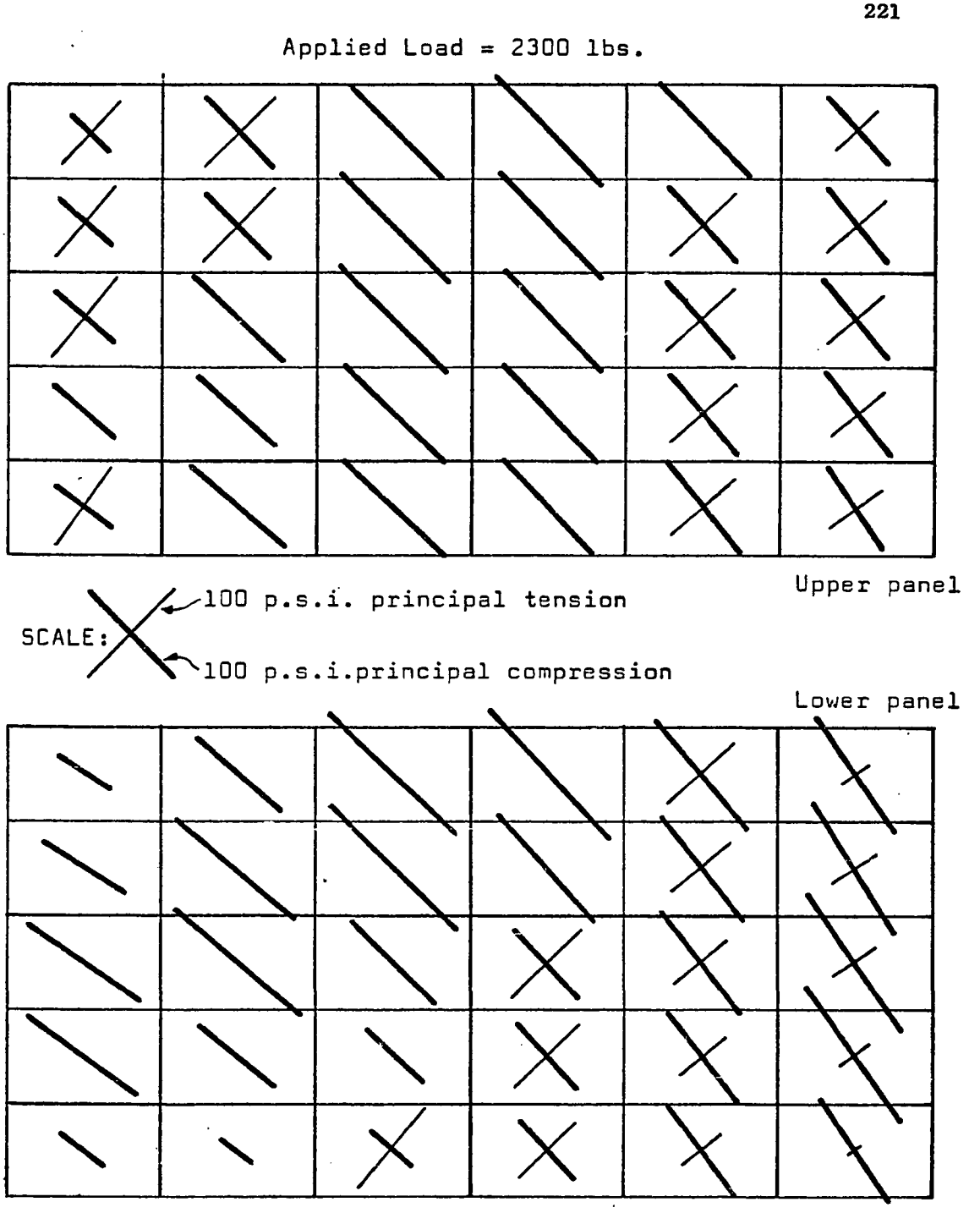

FIGURE 7.24

PANEL STRESSES BEFORE FAILURE, STRUCTURE 24B.

40.82	57.71	61.51	61.51	57.71	40.79
47.52	55.44	61.47	61.46	55.45	47.52
49.62	55.95	61.12	61.12	55.95	49.63
48.01	56.10	61.52	61.53	56.09	48.02
43.11	58.47	61.69	61.69	58.47	43.14

Upper Panel

Story Shear Before Cracking = 1600 lbs.

Lower Panel

43.32	60.03	62.62	62.61	60.02	43.28
49.75	56.22	59.67	59.66	56.22	49.72
54.00	54.27	55.75	55.75	54.27	53.96
52.47	49.62	52.12	52.13	49.61	52.44
36.29	46.19	48.47	48.48	46.24	36.35

(Shear stress values shown in p.s.i.)

FIGURE 7.25(A)

PANEL SHEAR STRESSES BEFORE CRACKING, FRAME 24B.

58.46	80.99	55.40	61.69	53.55	60.46
68.16	79.15	62.18	60.40	80.70	69.71
73.61	51.38	62.51	55.34	80.83	71.92
33.44	42.94	55.65	54.42	80.74	69.18
65.04	51.05	58.30	52.72	83.94	62.42

Upper Panel

Story Shear Before Failure = 2300 lbs.

Lower Panel

23.61	46.47	72.35	73.14	94.53	66.84
35.07	60.59	74.35	56.17	83.98	76.63
52.71	65.93	48.96	79.75	78.65	80.72
52.78	37.89	31.90	72.80	70.35	76.51
20.07	14.87	64.00	65.60	64.44	51.83

(Shear stress values shown in p.s.i.)

FIGURE 7.25(B)

PANEL SHEAR STRESSES BEFORE FAILURE, FRAME 24B.

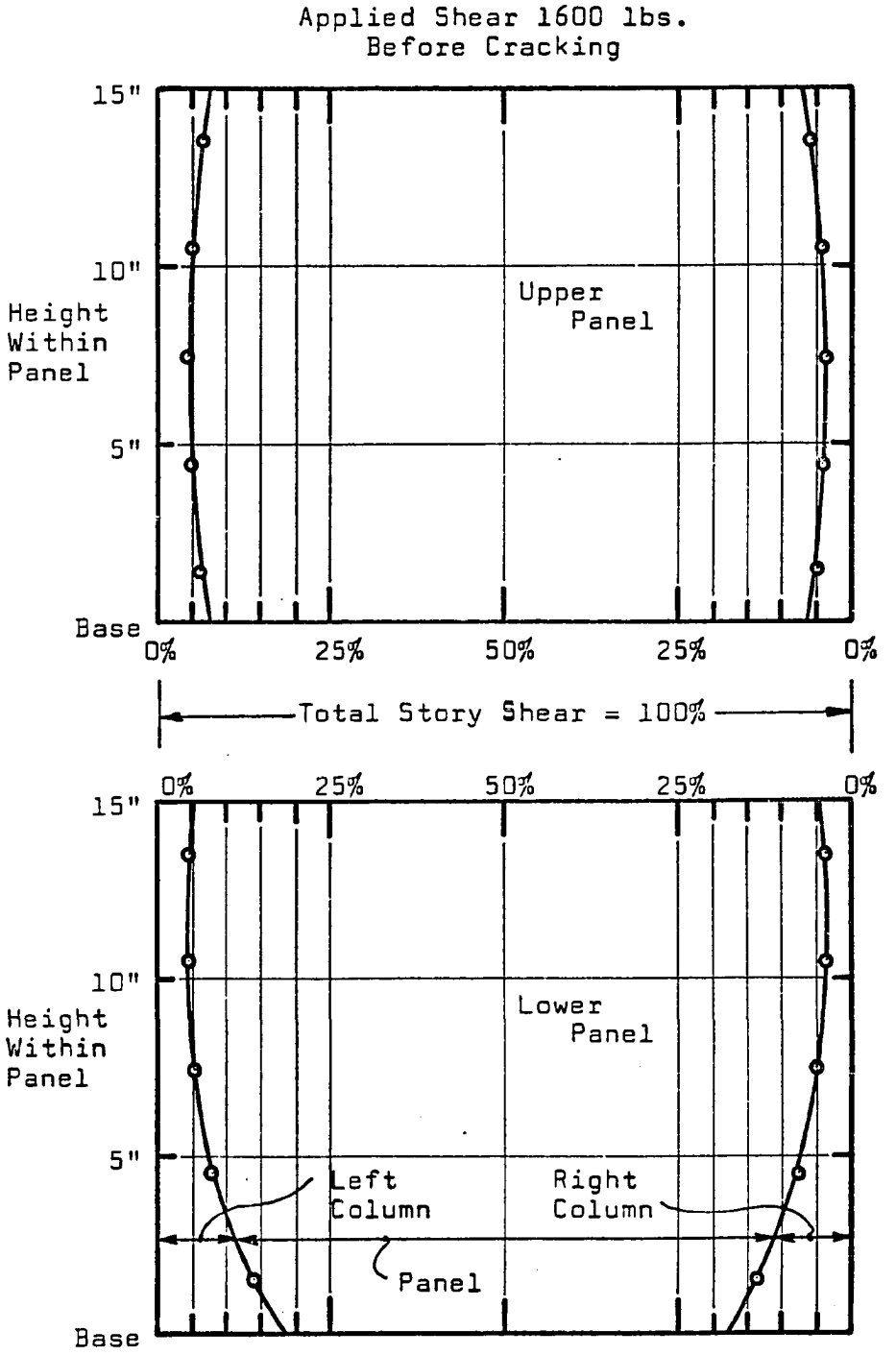

FIGURE 7.26(A)

STORY SHEAR DISTRIBUTION BEFORE CRACKING, FRAME 24B.

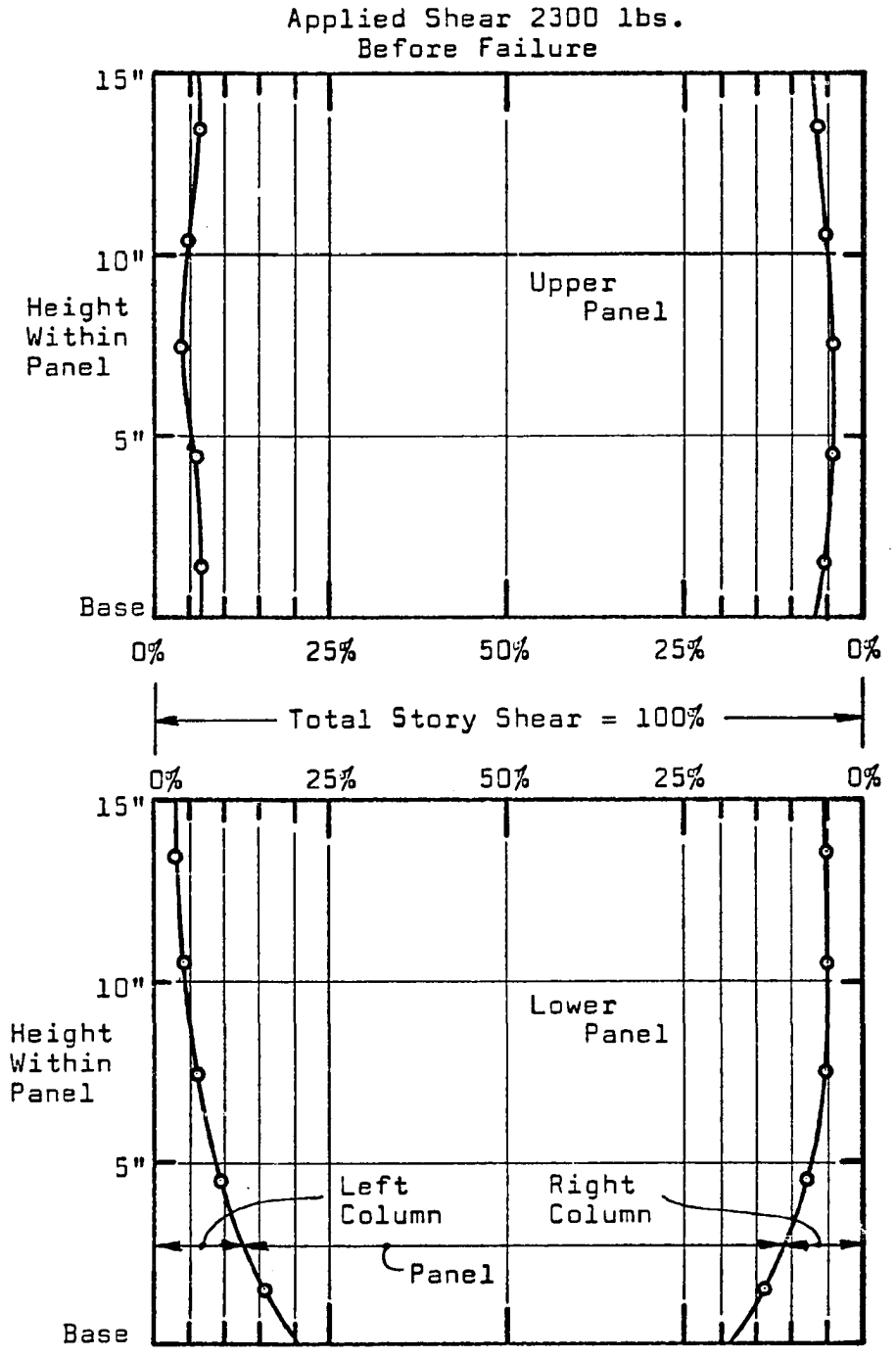

FIGURE 7.26(B)

STORY SHEAR DISTRIBUTION BEFORE FAILURE, FRAME 24B.

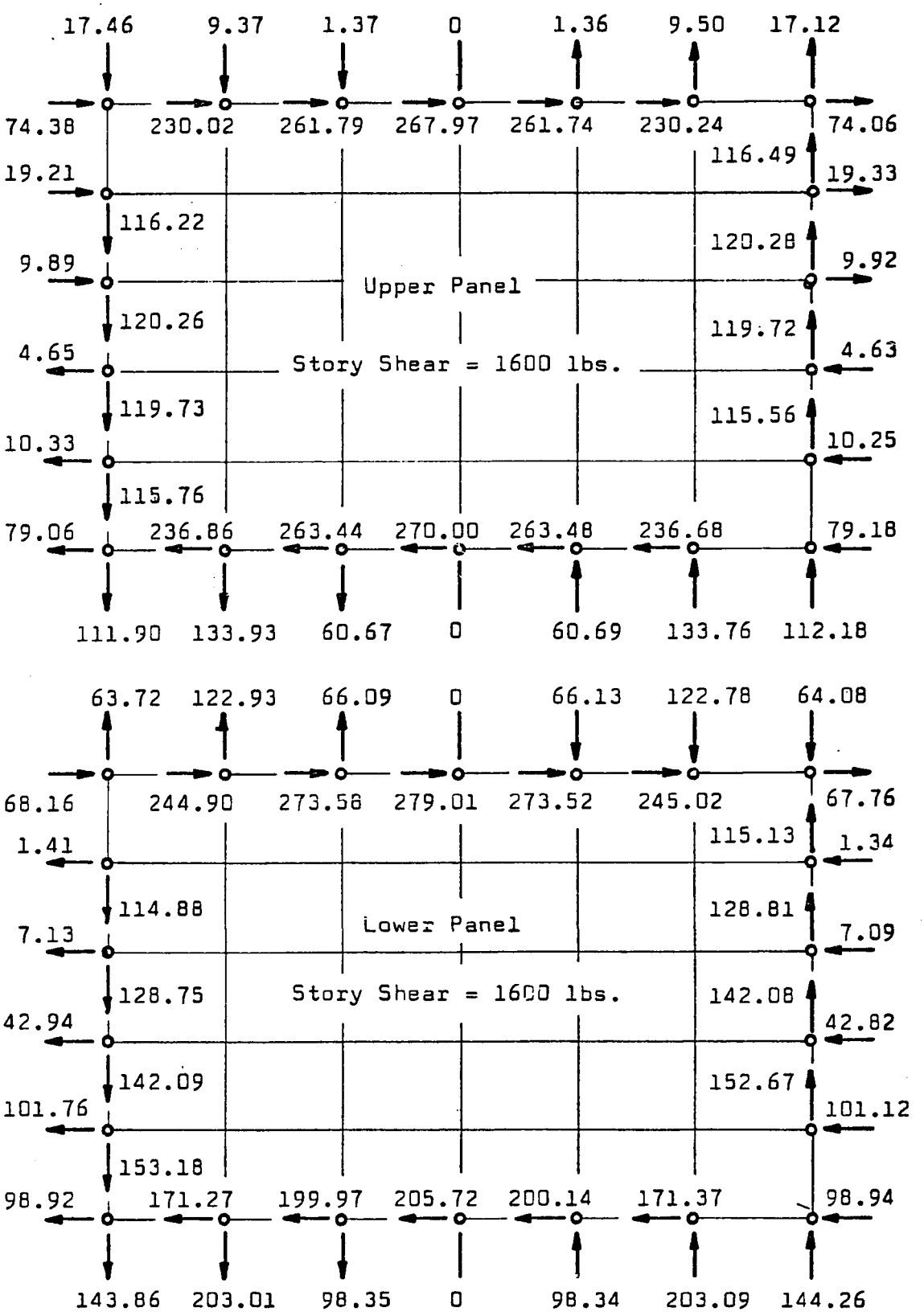

FIGURE 7.27 PANEL EDGE FORCES BEFORE CRACKING.

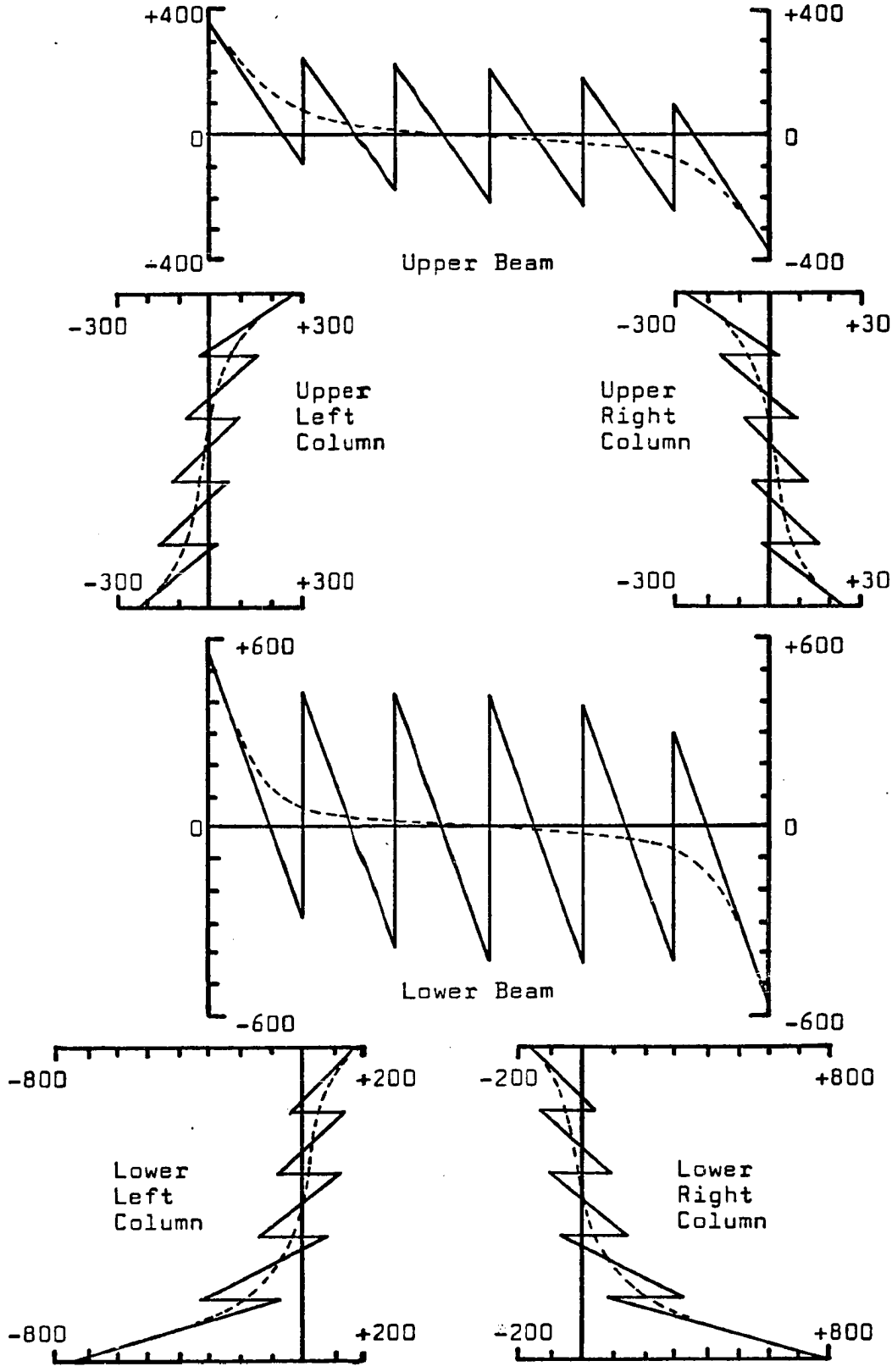

(Moments given in inch-lbs.)

Applied Load = 1600 lbs.

FIGURE 7.28(A) FRAME MOMENTS BEFORE CRACKING.

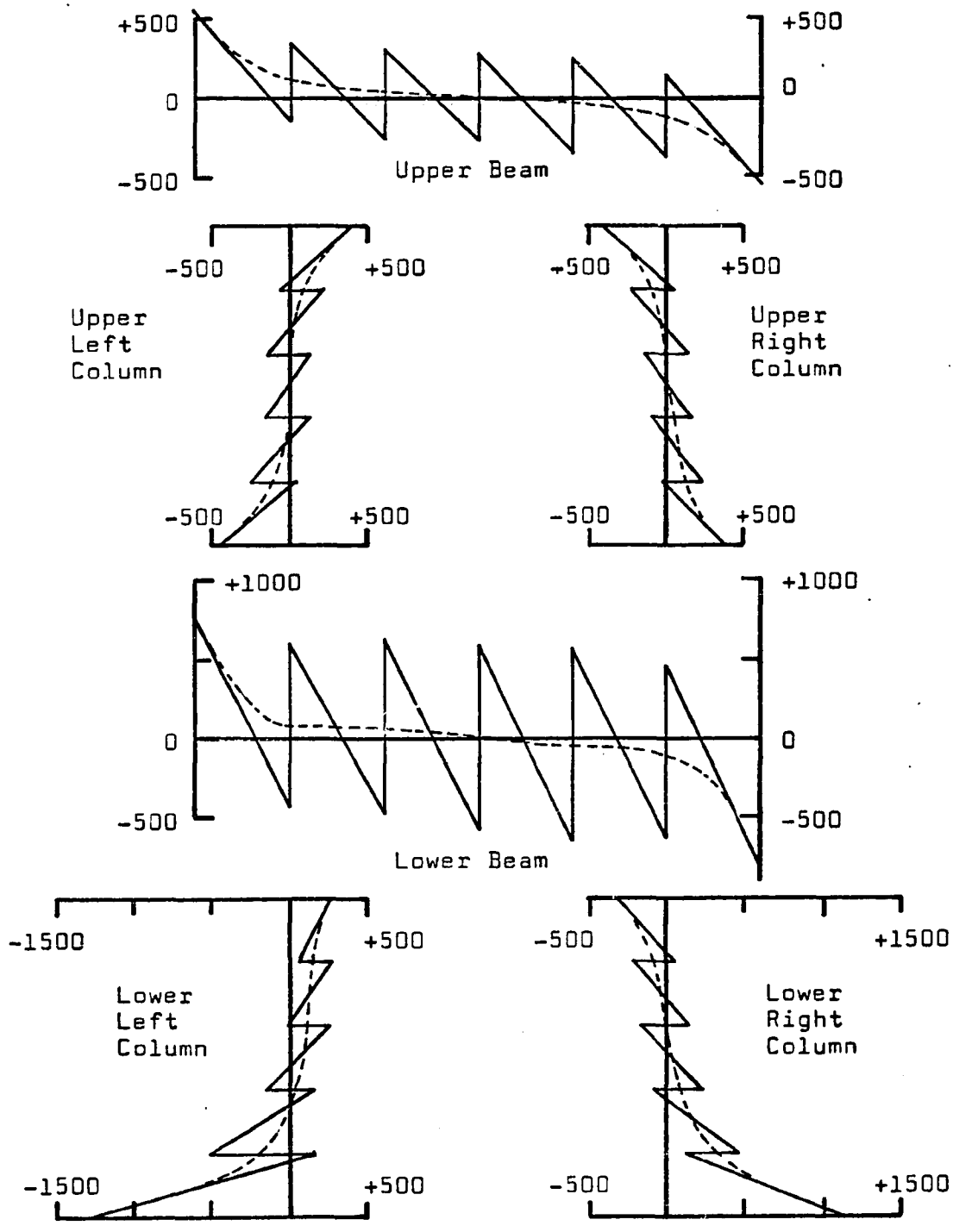

(Moments given in inch-lbs.)

Applied Load = 2300 lbs.

FIGURE 7.28(B) FRAME MOMENTS BEFORE FAILURE.

the average frame moments considerably so that even just before failure the frame was lightly loaded.

The results for all of the preceding structures will be discussed further in the next section.

7.3 Review And Summary

It is first necessary to consider some basic characteristics of the frame members before giving interpretation to the behavior of these systems.

Figure 7.3 shows that the beams and columns have approximately the same cross-section details so that a single ultimate strength envelope (relating axial force and section moment) can be used. This means that plastic moments at hinge locations of the yielding frames should converge to similar values except for the influence of axial forces. Since only small axial forces were generated in these frames (dead loads were not included for the frames or for tributary floor systems) then only a small portion of the ultimate strength envelope need for used. The complete envelope was computed for a typical beam section, using the Whitney stress block and the ACI method, assuming a steel yield stress of 40000 psi. The complete curve is plotted in Figure 7.29(A) and the portion that is relevant to the present analyses is re-plotted in Figure 7.29(B). Since all sections are under-reinforced, with a tensile steel ratio of only 0.55%, then yielding of the tension steel was expected to be the governing condition for ultimate strength. The ultimate strength of these doubly-reinforced sections was further explored by computing equilibrium forces on the cross-section for selected plane

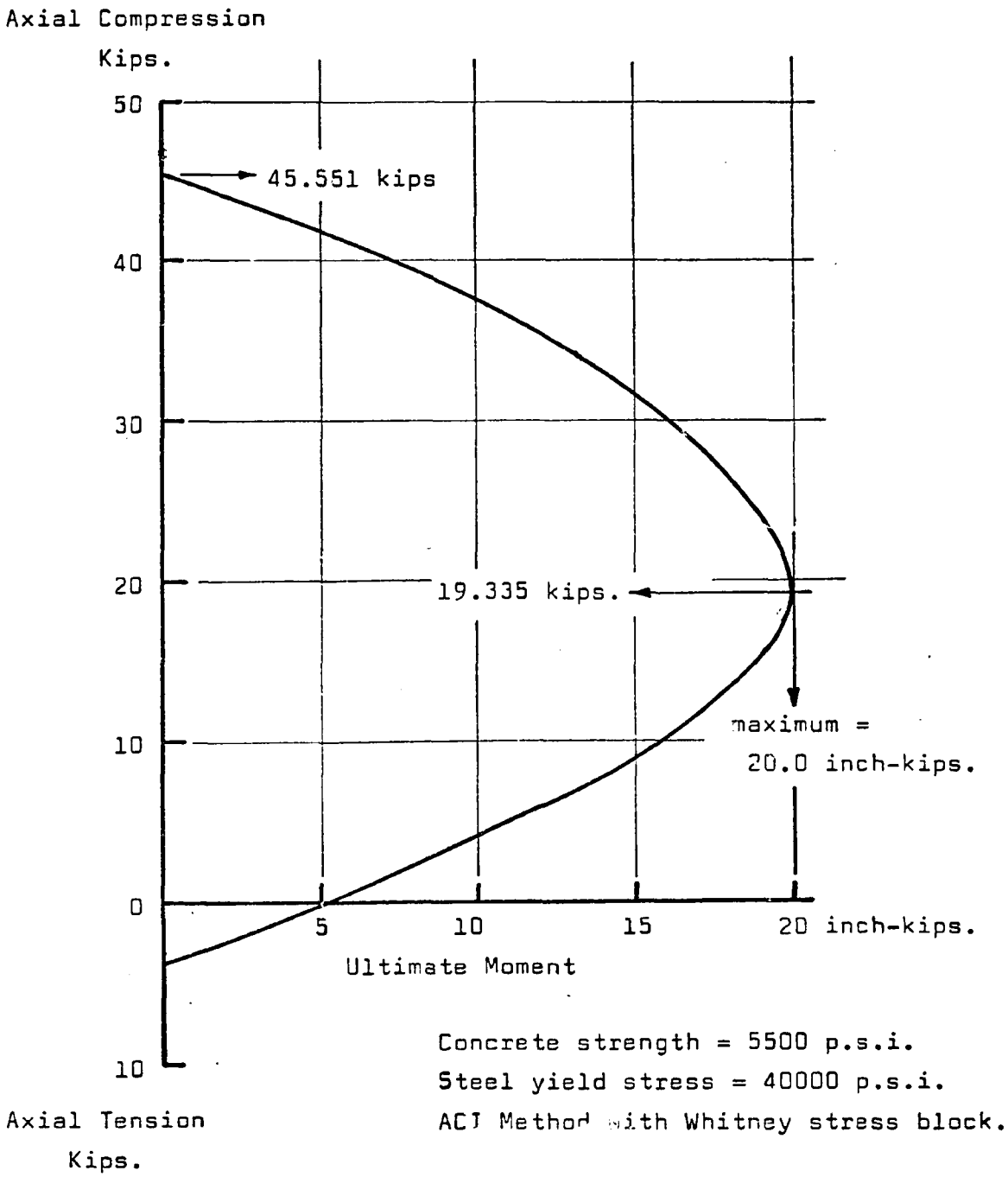

FIGURE 7.29(A) ULTIMATE CAPACITY ENVELOPE.

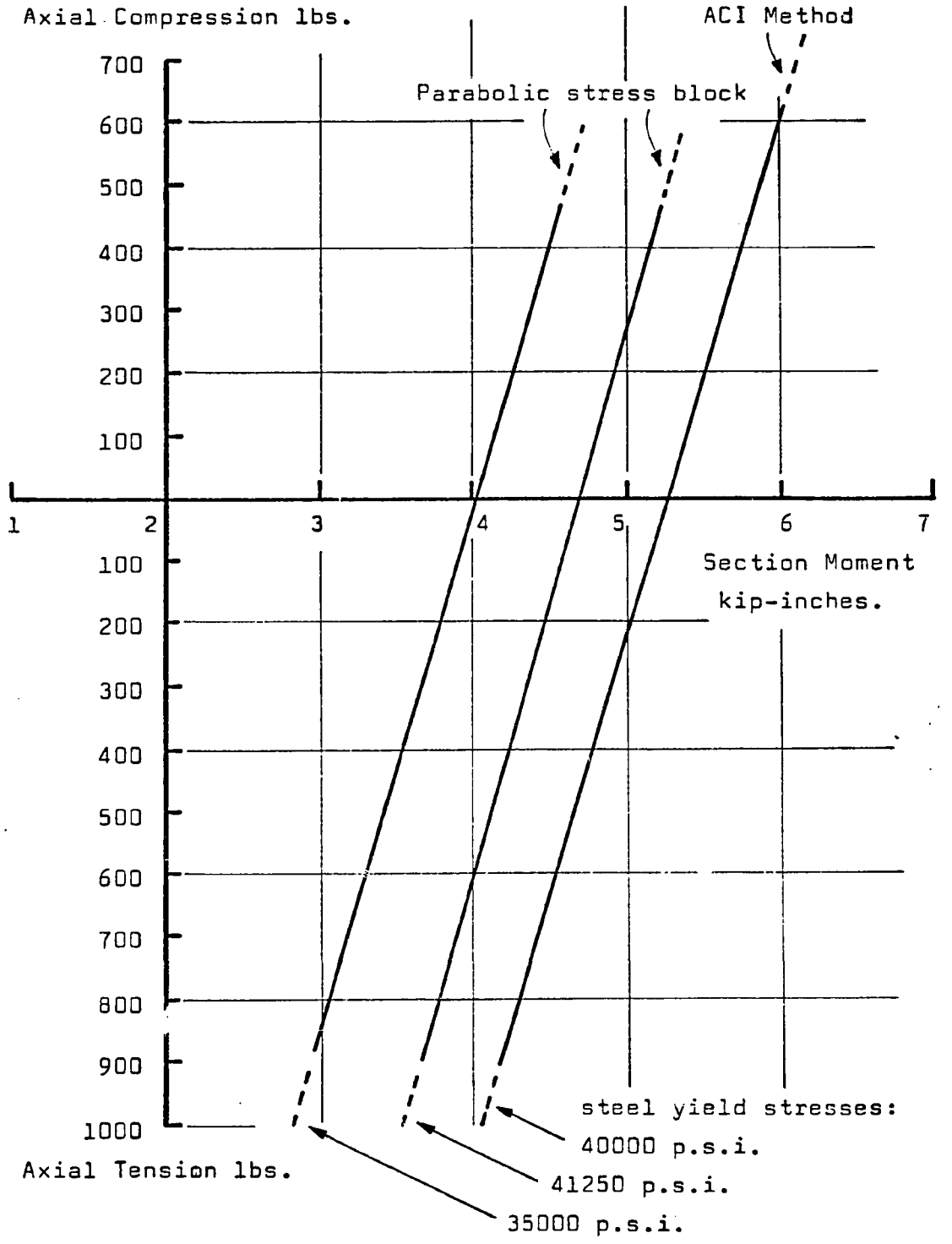

FIGURE 7.29(B) DETAIL OF ULTIMATE CAPACITY ENVELOPES.

deformations of the section, assuming a parabolic stress-strain curve for the compression concrete, using various values of steel yield stress and tensile steel strain. These results were added to Figure 7.29(B).

Cracking started at the base of the tension column in both frames and agreed with predicted values. Computing M_{cr} at mid-height of the outer slice, and allowing for axial tension (about 26 psi for 23A and 60 psi for 23B) then predicted values were given thus:

for 23A, $M_{cr} = 714 \times 7.79/1.35 = 4110$ inch lbs.,

for 23B, $M_{cr} = 680 \times 7.79/1.35 = 3920$ inch lbs.

Analytic cracking was actually given for these locations at average moment magnitudes of

4009 inch lbs. for 23A,

3856 inch lbs. for 23B (averaged at mid-length of the element).

Referring now to Figure 7.29(B), it is important to note that the values of M_{cr} and M_{ult} for these sections are about the same magnitude. This fact is basic to understanding the behavior of these frames to yielding. Several hypothetical M - φ diagrams are presented in Figure 7.30 for cross-sections whose different reinforcement details cause different ratios between their M_{cr} and M_{ult} values. Each of these diagrams has gradients plotted which relate the section behavior to different amounts of cracking. For a well reinforced, ductile section, such as in example (A), the change in section stiffness while cracking progresses is much less than the stiffness degradation that can be expected with cracking of a lightly reinforced

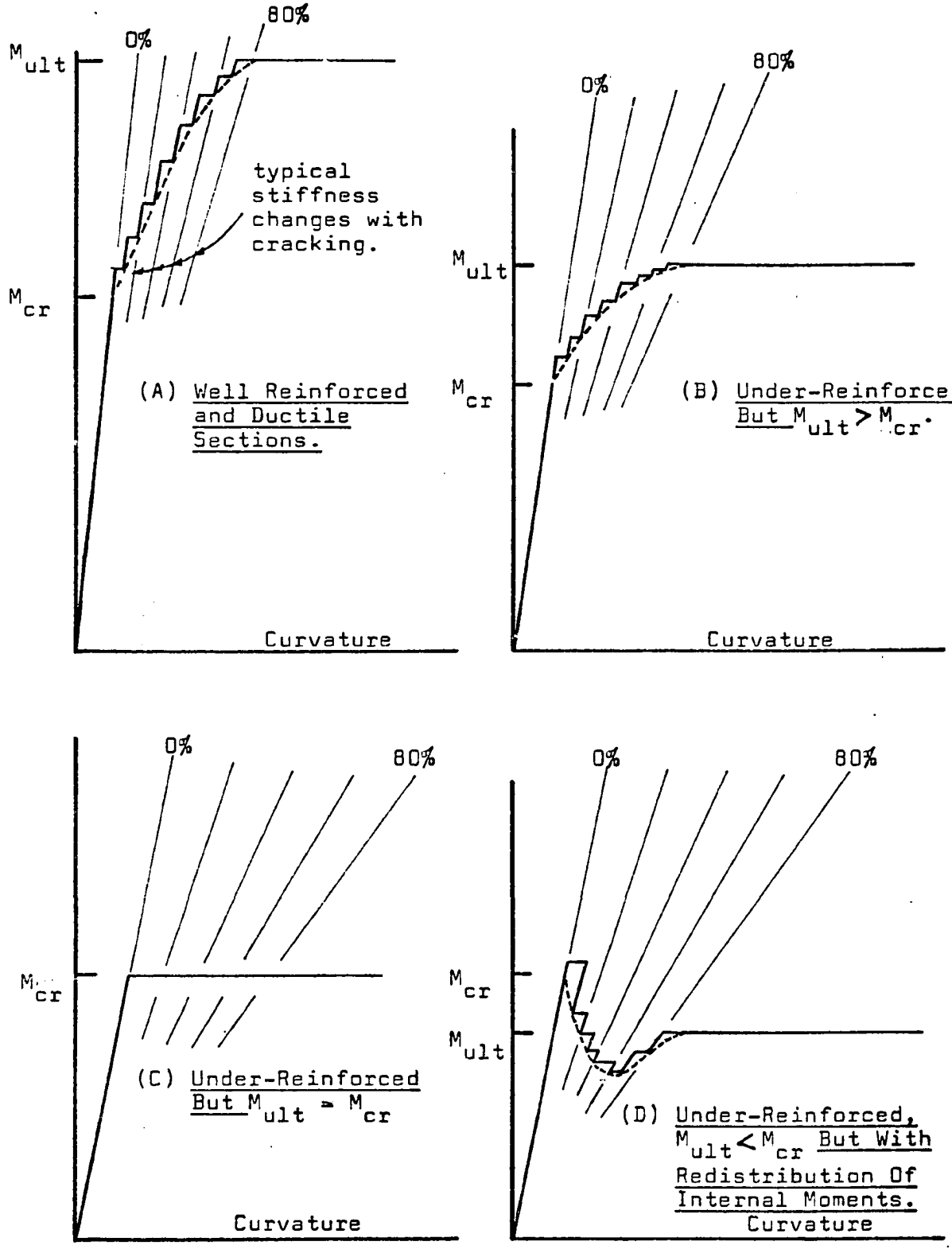

FIGURE 7.30 MOMENT-CURVATURE BEHAVIOR PATTERNS.

section, such as examples (C) and (D). Each of these diagrams also suggests that ultimate moment is achieved with about 80% cracking of the concrete. Examples (A) and (B) represent section behavior that is usually observed in laboratory testing and published results. M_{ult} is clearly greater than M_{cr} and there is a steady progression to the ultimate cracked state after cracking begins. Discretized structures analyzed by the procedures of this research would tend to exhibit the stepped path to the ultimate state; each vertical moment increment may be achieved over several load increments, or one load increment may encompass several moment increments. But in each case, this program reports the progress of cracking in discrete jumps, slice by slice. The rate at which the moment increases in any section with increase of external loading depends on whether the structure is determinate. Further load capacity after cracking is proportional to the extra moment capacity after cracking $(M_{ult} - M_{cr})$ only for the determinate case. In the indeterminate structure the increase, or decrease, of local moment depends on the relative distributions of stiffness throughout the entire structure. This is particularly relevant to examples (C) and (D) of Figure 7.30. When M_{cr} and M_{ult} coincide then the onset of cracking leads directly to yield and a plastic hinge for the determinate structure. But for the indeterminate structure there is always the possibility that the hinge not be immediately formed. By the earlier discussion, progressive cracking causes a local decrease of stiffness and this can lead to a decrease in the section moment. This is illustrated for the more drastic case when M_{ult} is less than M_{cr}, example (D). As

long as moment reductions can occur with curvature increases after cracking then it may be possible to achieve a new moment equilibrium at some value less than ultimate. If stiffness degradation occurs elsewhere then a further increase in moment can be absorbed by the section until the ultimate is reached and a plastic hinge forms. This type of action was observed at the base of the tension column, element 11, in frame 23B. The M - φ data is plotted in Figure 7.31 and shows how 60% cracking was achieved over 7 iterations of the solution with redistribution of the moments in the system. However, over the last 5 iterations, cracking occurred in other beams and columns which forced a new redistribution of moments. This caused an increase in section moment to a value not much below the ultimate moment of the section.

Examination of Table 7.4 (frame 23A) and Table 7.8 (frame 23B) shows the moment redistributions that occurred after cracking began. The tendency for M_{cr} and M_{ult} to be so similar for these members caused the frames to have little load capacity after cracking and before yield mechanisms were fully established. The load-deflection plots of Figure 7.7 (frame 23A) and Figure 7.9 (frame 23B) illustrate this clearly. In fact, after cracking in frame 23B, 4 cracked locations showed tensile steel stresses between 28000 and 33000 psi, while just before ultimate these locations all averaged 35000 psi (see Section 7.1.2). Frame 23A cracked at 83% of the yield load, and frame 23B at 97% of yield; as seen in their load-deflection diagrams. These facts are presented to emphasize the dependence of the total structural behavior on the phenomenon of having frame sections whose

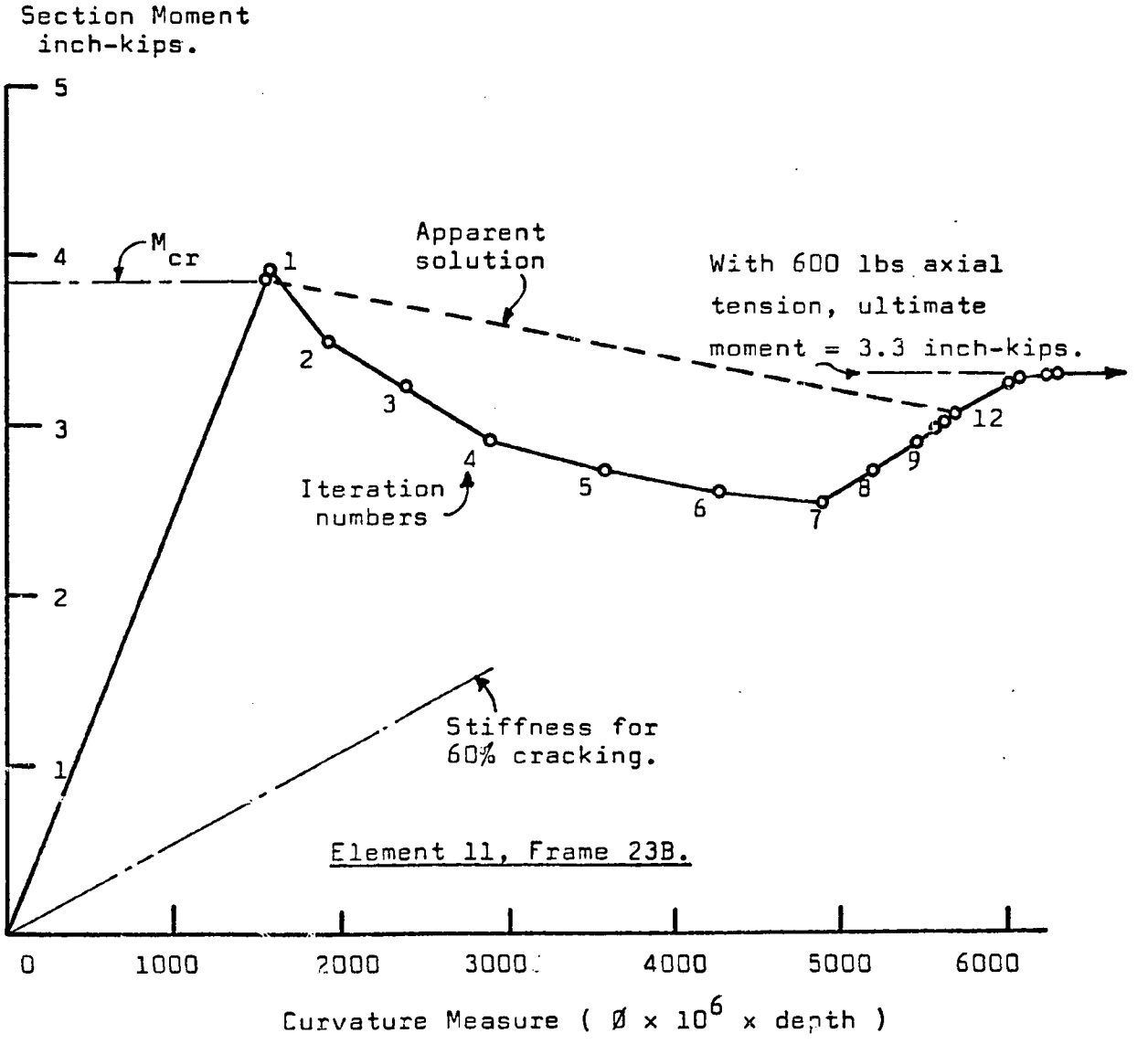

FIGURE 7.31

EXAMPLE OF COMPUTED MOMENT-CURVATURE BEHAVIOR.

uncracked capacity was little different than their ultimate moment capacity.

A further aspect of the load capacity of these frames at yield can be derived from a limit analysis using approximate values of yield moments from Figure 7.29(B) in the virtual work equations.

If a steel yield stress of 41250 psi is used, ± 300 lbs. in the columns and ± 250 lbs. in the upper columns of frame 23B, and zero axial force assumed for the beams, then the hinge moment values may be as shown in the Figure 7.32 layouts. For frame 23A, this gives

$$15\ R = 4300 + 5000 + 2(4700)$$

$$R = 18700/15 = 1240 \text{ lbs.}$$

Actual yield load derived from the computer analysis was about 1225 lbs. For frame 23B, the equation is

$$33\ R = 3(9400)$$

$$R = 9400/11 = 855 \text{ lbs.}$$

Actual yield load derived from the computer analysis was about 854 lbs.

It is clear that the analytical procedure of this research has successfully predicted the complete structural behavior of these frames through cracking to yield, based upon the actual stress-strain response of the materials, without assumptions of elasto-plastic behavior for the reinforcement, and giving a realistic description of the formation of yield mechanisms in the process.

When weak shear panels were added to each of these frames the behavior changed completely. The ductile, yielding response of the frames alone now vanished and a considerable increase in strength and stiffness was added. The failure process for these models was

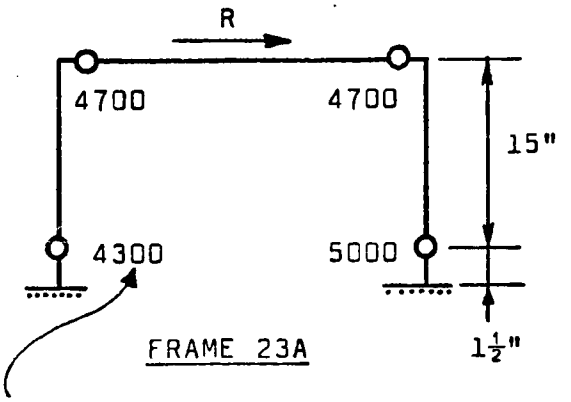

FRAME 23A

Yield moment estimates, typical. (inch-lbs.)

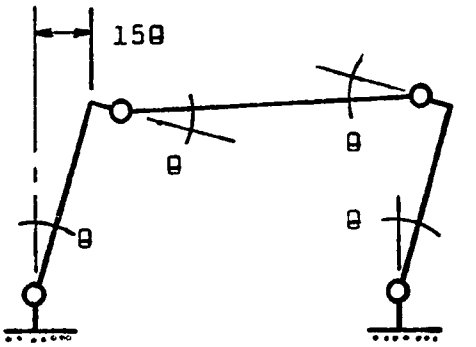

Virtual work deformations.

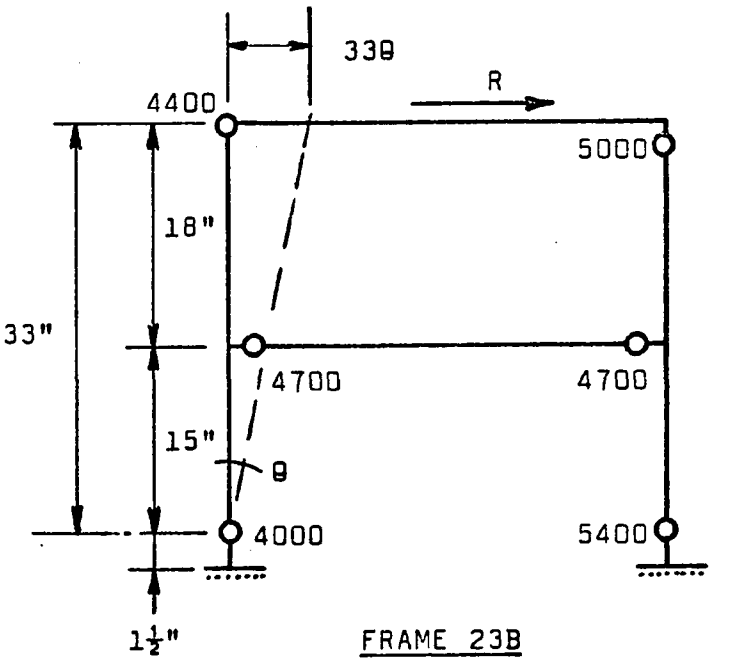

FRAME 23B

FIGURE 7.32 LIMIT ANALYSIS OF FRAMES.

confined to the panels but their deterioration made little difference to the overall stiffness near maximum loads. Thus the failure was abrupt, of a brittle nature. Table 7.14 shows the changes

TABLE 7.14
SUMMARY OF RESULTS

	Maximum Loads Lbs.		Energy Capacity, Inch Lbs.	
	1-Story	2-Story	1-Story	2-Story
Frame alone	1225	854	39.32	61.77
With panels	2450	2300	2.41	5.82

in load capacity for the 4 structures analyzed. Even though strength increased greatly by adding even weak panels, the energy absorptions up to failure were much decreased in comparison with energy absorptions up to yield of the frames alone. Furthermore, since maximum load for the frames was at the formation of a yield mechanism, then a yield-type plateau of deflection with no increase of load was feasible (but not attainable by this type of analysis) and so further energy capacity could be expected for the frames. But in the case of failure by panel deterioration, the applied load had risen to levels well above the fully-yielded frame capacity and, without a load reduction, collapse would ensue and no further energy capacity could be expected. On the other hand, if deflection-controlled test or analysis was performed then failure of the panels would cause an immediate drop in applied load to the value that could be sustained by the frame at that deflection. These situations, and

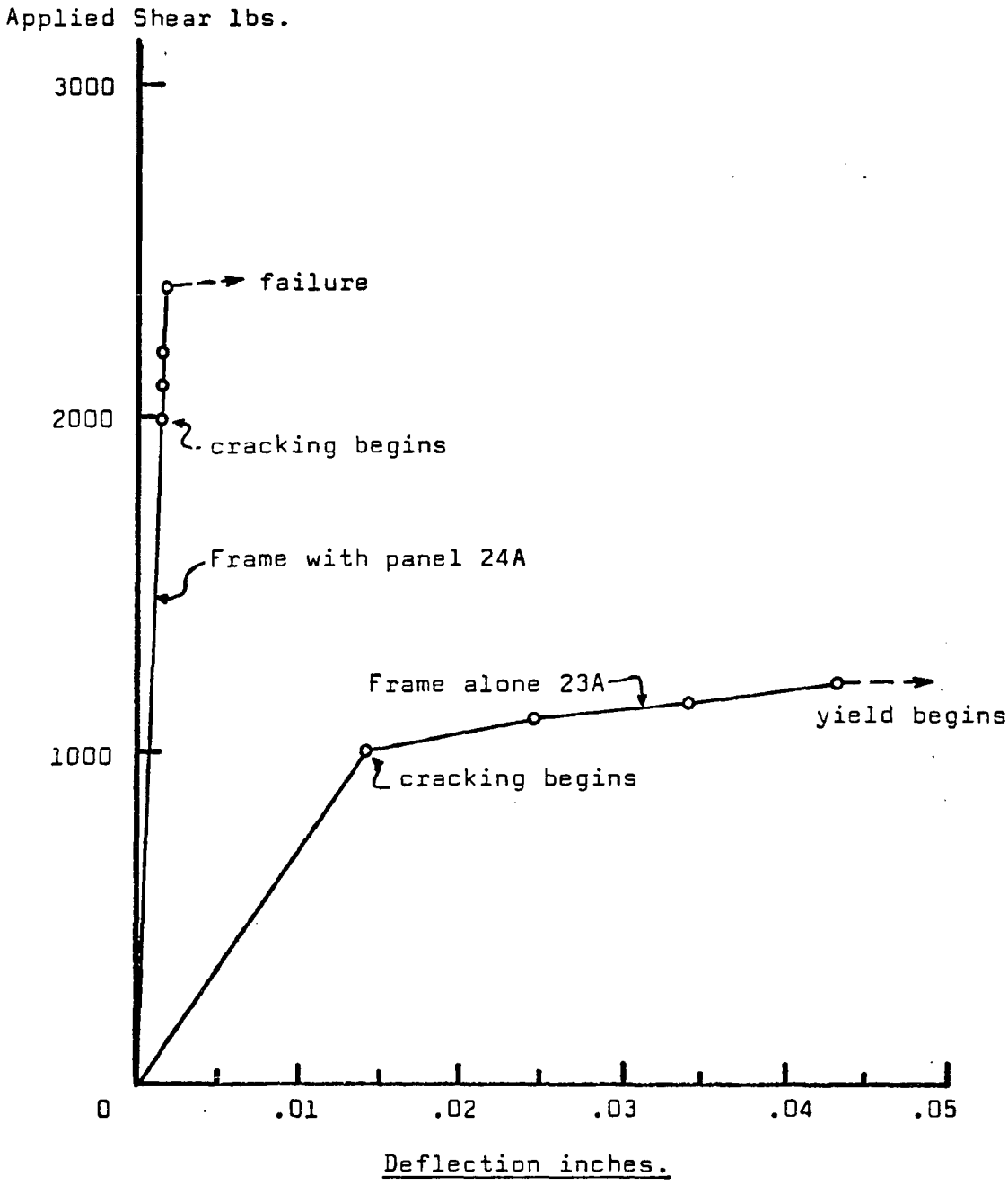

FIGURE 7.33(A)

LOAD-DEFLECTION COMPARISON FOR 1-STORY MODELS.

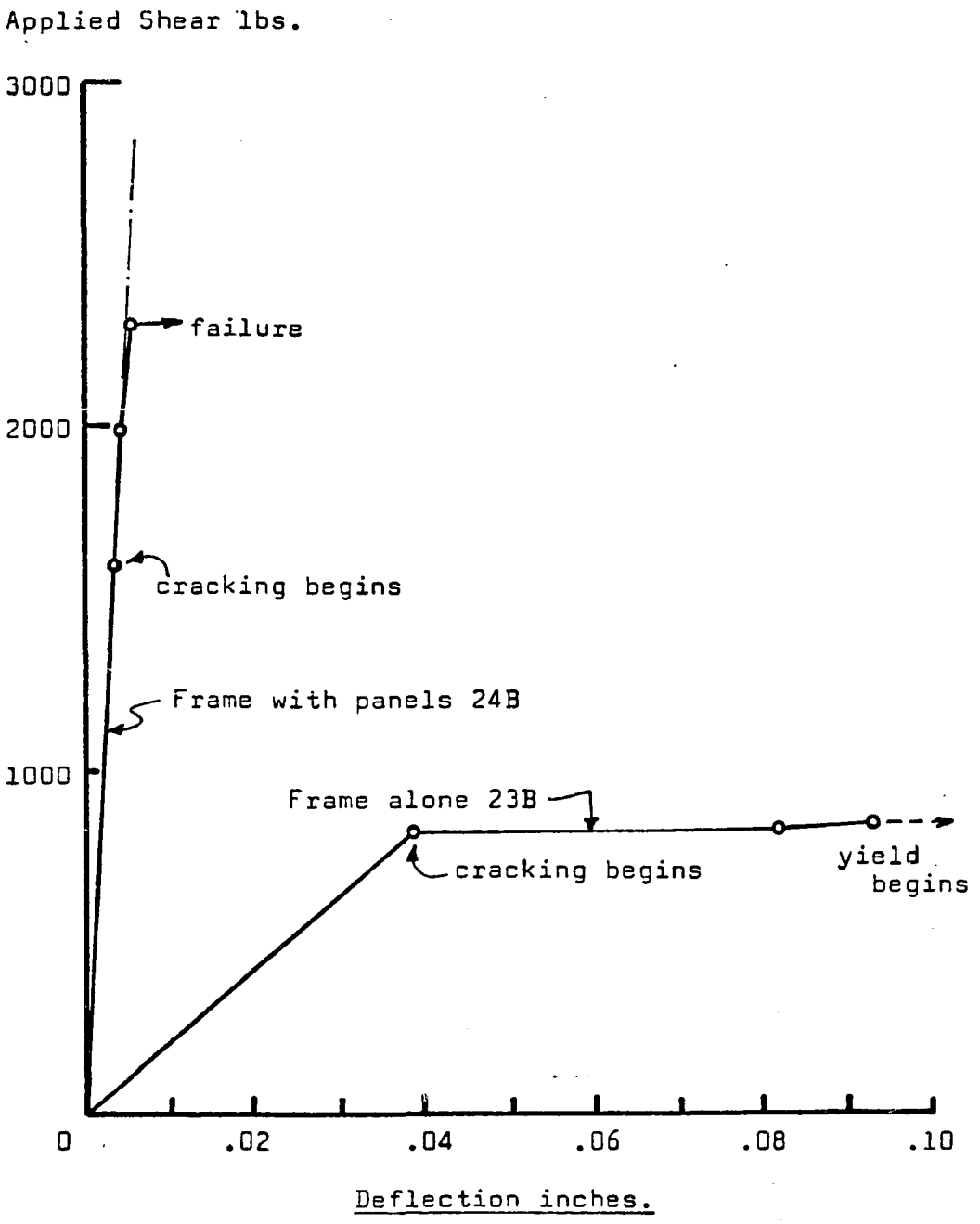

FIGURE 7.33(B)

LOAD-DEFLECTION COMPARISON FOR 2-STORY MODELS.

others are shown on the diagram of Figure 7.34.

The situation of wind or gust loadings gives an example where a loading could cause panel failures and be sustained, or later repeated without reduction. System collapse would be probable, depending on direction and time of application of such loads, of course. But seismic loads are created by the dynamic response of the structure (a function of overall stiffness and inertia distributions) to ground accelerations. When stiffness deteriorates due to panel failures then relative deflections can increase, generated story shears may decrease, depending on the nature of the ground accelerations at that time and on the new stiffness distribution of the structure. It is possible that if a sufficiently large decrease of applied shear occurs with the increase in deflections that the structural frame may indeed be able to carry the loads. Some of these possibilities are shown in Figure 7.34. Thus the analytical procedure of this work has been demonstrated able to provide the designer and analyst with information about structural behavior to failure or yield which can involve actual design details and material properties, and which can be used in more complex, dynamic analyses.

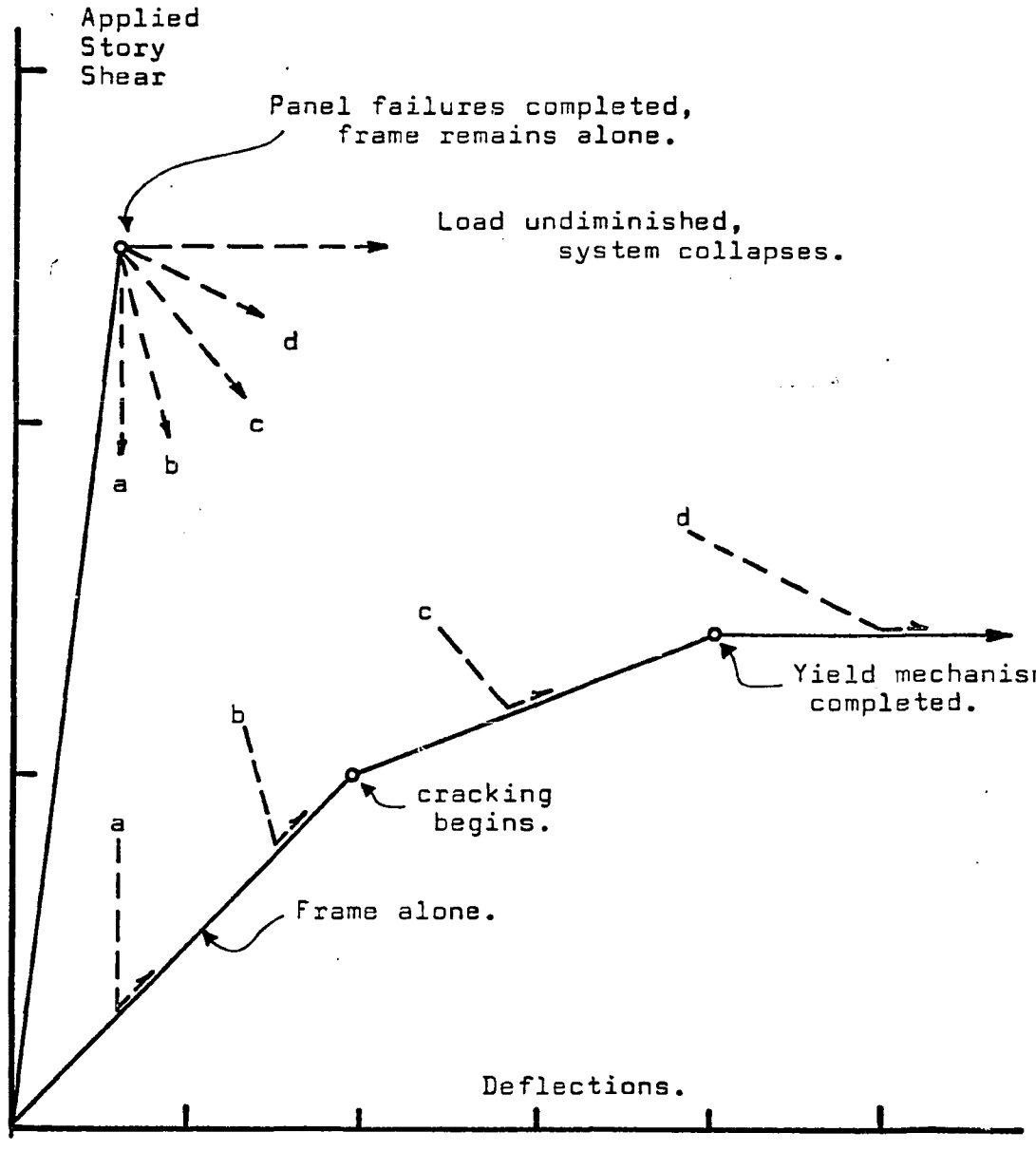

Path a. Deflection controlled, load adjusts.
Path b. System load carried by uncracked frame.
Path c. System load carried by cracked frame.
Path d. System load carried by fully hinged frame.

FIGURE 7.34 RESPONSE CHANGES WHEN PANELS FAIL.

8. CONCLUSIONS

An analytical method involving load incrementing and solution iterations has been developed and applied to the analysis of nonlinear, failing, planar structures with various combinations of structural elements and materials. The various elements available in this program were demonstrated either separately or in some combinations, to illustrate their applications in nonlinear analysis. Quadrilateral plane stress finite elements were used to model reinforced concrete beams and unreinforced, weak shear panels in frame structures; special frame elements were used to model reinforced concrete beams and frames; one-dimensional rods were used for either nonlinear, planar trusses, or reinforcing rods in a plane continuum; special two-dimensional tielinks were used to attach shear panels to frame members so that releases could occur between members, if required. These examples demonstrated analytic behavior of various structures under increasing loads using the actual stress-strain laws of the various materials. The analytic results compared well with available laboratory tests and agreed with theoretical expectations in other instances.

The procedure applies selected increments of in-plane loads, in specified patterns, to the discretized structure. If fracturing or crushing of materials or separation of elements occurs then the system stiffness is adjusted and the solution is iterated before the next load increment is applied. The complete structural behavior can be followed by means of node deflections and element stresses that are printed after each iteration. The process halts

either when the specified load increments have all been applied or when the structural deterioration has become sufficiently extensive (such as when very large deflections are generated).

Since stress-strain curves were not specified with unloading paths for this program then the generation of hysteresis loops cannot be obtained by using cyclic load increments. However, the program gives extensive and accurate insight into the process of deterioration and force (or stress) redistributions that occur in structures loaded to failure, and may provide a valuable adjunct to laboratory testing of some structures.

The program was finally applied to the study of two simple reinforced concrete frames to exhibit their change in behavior when shear panels were added. Parameter studies are required in this area of structural research which would be too extensive for this dissertation. However, the program developed here could be usefully applied to further studies. Some further improvements could be incorporated, such as varying the uniaxial stress-strain curves for biaxial conditions, improving the failure criterion for biaxial elements and tie-links, and including nonlinear, fracturing bandlinks. The latter addition would permit this program to be usefully applied to the study of shear failure in reinforced concrete beams. This program has demonstrated a capability for determining yield loads in a structure that fails by yielding. Ultimate deflections cannot be attained beyond yield by this process. Of some interest in seismic analysis would be a version of this program that increments

deflections rather than loads. Such a program would allow the analytic determination of ductility factors for structural assemblages and would help define ultimate failure states for the yielding structure.

9. REFERENCES

1. Przemieniecki, J.S., "Theory of Matrix Structural Analysis," McGraw-Hill, New York, 1968.

2. Clough, R.W., "Structural Analysis By Means of A Matrix Algebra Program," Proc. 1st. Conf. Electronic Computation, ASCE, Kansas City, Mo., Nov. 1958.

3. Clough, R.W., "The Finite Element Method In Plane Stress Analysis," Proc. 2nd Conf. Electronic Computation, ASCE, Pittsburgh, Pa., Sept. 1960.

4. Clough, R.W., Wilson, E.L., King, I.P., "Large Capacity Multistory Frame Analysis Program," J. Struct. Div. ASCE, v. 89, no. ST4, 1963, pp. 179-204.

5. Felippa, C.A., "Refined Finite Element Analysis of Linear And Nonlinear Two-Dimensional Structures," SESM Report, no. 66-22, Univ. of California, Berkeley, Oct. 1966.

6. Selna, L.G., "Time-Dependent Behavior of Reinforced Concrete Structures," SESM Report No. 67-19, Univ. of California, Berkeley, Aug. 1967.

7. Wilson, E.L., "Finite Element Analysis of Two-Dimensional Structures," SESM Report No. 63-2, Univ. of California, Berkeley, June 1963.

8. Ngo, D., Scordelis, A.C., "Finite Element Analysis of Reinforced Concrete Beams," ACI Journal, v. 64, no. 3, March 1967.

9. Nilson, A.H., "Nonlinear Analysis of Reinforced Concrete By The Finite Element Method," ACI Journal, v. 65, no. 9, Sept. 1968.

10. Sandhu, R.S., Wilson, E.L., Raphael, J.M., "Two-Dimensional Stress Analysis With Incremental Construction And Creep," SESM Report No. 67-34, Univ. of California, Berkeley, December 1967.

11. Argyris, J.H., "Energy Theorems And Structural Analysis," Aircraft Engineering, v. 26-27, Oct. 1954-May 1955.

12. Clough, R.W., King, I.P., Wilson, E.L., Structural Analysis Of Multistory Buildings," J. Struct. Div. ASCE, v. 90, no. ST3, June 1964.

13. Fox, L., "An Introduction To Numerical Linear Algebra," Oxford University Press, New York, 1964.

14. Gallagher, R.H., Padlog, J., Bijlaard, P.P., "Stress Analysis Of Heated Complex Shapes," J. Am. Rocket Soc., v. 32, May 1962.

15. Turner, M.J., Dill, E.H., Martin, H.C., Melosh, R.J., "Large Deflections Of Structures Subjected To Heating And External Loads," J. Aero. Science, v. 27, 1960.

16. Murray, "Large Deflection Analysis of Plates," SESM Report No. 67-44, Univ. of California, Berkeley, September 1967.

17. Brebbia, C., Connor, J., "Geometrically Nonlinear Finite Element Analysis," J. Eng. Mech. Div. ASCE, v. 95, no. EM2, April 1969.

18. Hognestad, E., Hanson, N.W., McHenry, D., "Concrete Stress Distribution In Ultimate Strength Design," ACI Journal, v. 27, no. 4, Dec. 1955.

19. Parme, A.L., Discussion of a paper by Seiss, C.P., "Review Of Research On Ultimate Strength Of Reinforced Concrete Members," ACI Journal, Proc. v. 48, June 1952.

20. Hajnal-Konyi, K., "The Modular Ratio - A New Method Of Design Omitting m," Concrete And Construction Engineering (London), v. 32, no. 1 to 3, Jan-March 1937.

21. ACI Committee 335 Draft Report "Deflection Of Concrete Beams," April 1963.

22. Steinbacher, F.R., Gaylord, C.N., Rey, W.K., "Method For Analyzing Indeterminate Structures Stressed Above The Proportional Limit," NACA Tech. Note 2376, June 1951.

23. Borg, S.F., Gennaro, J.J., "Advanced Structural Analysis," Van Nostrand, New York, 1959.

24. Kalian, C.G., "Short Time Deflections Of Reinforced Concrete Beams," SESM Graduate Student Report No. 186, University of California, Berkeley, May 1965.

25. Bresler, B., Scordelis, A.C., "Shear Strength of Reinforced Concrete Beams - Series II," SESM Report No. 64-2, Univ. of California, Berkeley, December 1964.

26. Saenz, L.P., Discussion of "Equation For The Stress-Strain Curve of Concrete," by P. Desayi and S. Krishnan, ACI Journal, v. 61, no. 9, Sept. 1964.

27. Fioratio, A.E., Sozen, M.A., Gamble, W.L., "Behavior Of Five-Story Reinforced Concrete Frames With Filler Walls," Interim Report, Univ. of Illinois, Urbana, Illinois, Jan. 1968.

28. Blume, J.A., Newmark, N.M., Corning, L.H., "Design Of Multistory Reinforced Concrete Buildings For Earthquake Motions," Portland Cement Association, Chicago, 1961.

29. Ferguson, P.M., "Reinforced Concrete Fundamentals," J. Wiley & Sons, New York, 1961.

30. Clough, R.W., Benuska, K.L., "FHA Study Of Seismic Design Criteria For High Rise Buildings," U.S. Dept. of Housing and Urban Development, Report HUD TS-3, August, 1966.

31. Degenkolb, H.J., "Structural Observations Of The Kern County Earthquake," Trans. ASCE, v. 120, paper no. 2777, 1955.

32. Whetstone, W.D., Jones, C.E., "Vibrational Characteristics Of Linear Space Frames," J. Struct. Div. ASCE, vol. 95, no. ST10, October, 1969.

33. Muto, K., "Earthquake Resistant Design Of 36-Storied Kasumigaseki Building," Special Report for IV WCEE, Muto Institute of Structural Mechanics, Tokyo, August 1968.

34. Walpole, W.R., Shepherd, R., "Elasto-Plastic Seismic Response Of Reinforced Concrete Frame," J. Struct. Div. ASCE, vol. 95, no. ST10, October, 1969.

35. Blume, J.A., "Structural Dynamics In Earthquake-Resistant Design," J. Struct. Div. ASCE, vol. 84, no. ST4, July, 1958.

36. Clough, R.W., "Effect of Stiffness Degradation On Earthquake Ductility Requirements," SESM Report No. 66-16, Univ. of California, Berkeley, Oct. 1966.

37. Selna, L.G., "Creep, Cracking, And Shrinkage In Concrete Frame Structures," J. Struct. Div. ASCE, vol. 95, no. ST12, December, 1969.

38. Tomii, M., "Studies On Shearing Resistance Of Reinforced Concrete Plates," Report Of The Inst. Of Industrial Science, Univ. of Tokyo, vol. 6, no. 3, January, 1957.

39. Benjamin, J.R., Williams, H.A., "The Behavior Of One-Story Brick Shear Walls," J. Struct. Div. ASCE, vol. 84, no. ST4, July 1958.

40. Benjamin, J.R., Williams, H.A., "Behavior Of Reinforced Concrete Shear Walls," Trans. ASCE, vol. 124, paper no. 2998, 1959.

41. Tomii, M., "Tests Of Quake Resisting Walls By Shear Force Distributed Along The Boundary," Trans. Architectural Inst. of Japan, no. 89, Sept., 1963.

42. Umemura, H., Aoyama, H., Liao, H.M., "Studies On Reinforced Concrete Shear Walls And Framed Masonry Shear Walls," Report of The Structural Testing Laboratory, Univ. of Tokyo,

43. Tomii, M., "Design Procedures Of Concrete Shear Walls," Report of Dept. of Architecture, Kyushu University, Japan, April 1966.

44. Rashid, Y.R., "Ultimate Strength Analysis Of Prestressed Concrete Pressure Vessels," Nucl. Eng. Design, vol. 7, pp. 334-344, 1968.

45. Rashid, Y.R., Rockenhauser, W., "Pressure Vessel Analysis By Finite Element Techniques," Conf. on Prestressed Concrete Pressure Vessels, March 1967, The Institution of Civil Engineers, London, 1968.

46. Zienkiewicz, O.C., Valliappan, S., King, I.P., "Stress Analysis Of Rock As A 'No Tension' Material," Geotechnique, March 1968.

47. Zienkiewicz, O.C., "The Finite Element Method In Structural And Continuum Mechanics," McGraw-Hill Publishing Co., Ltd., London, 1967.

48. Valliappan, S., Nath, B., "Tensile Crack Propagation In Reinforced Concrete Beams - Finite Element Technique," Int. Conf. On Shear, Torsion And Bond In Reinforced And Prestressed Concrete, Coimbatore, India, January 1969.

49. MacLeod, I.A., "New Rectangular Finite Element For Shear Wall Analysis," J. Struct. Div. ASCE, vol. 95, no. ST3, March 1969.

50. Popov, E.P., Pinkney, R.B., "Cyclic Yield Reversal In Steel Building Connections," J. Struct. Div. ASCE, vol. 95, no. ST3, March 1969.

51. Karsan, I.D., Jirsa, J.O., "Behavior Of Concrete Under Compressive Loadings," J. Struct. Div. ASCE, vol. 95, no. ST12, December 1969.

52. Pope, G.G., "A Discrete Element Method For The Analysis Of Plane Elasto-Plastic Stress Problems," The Aeronautical Quarterly, February 1966.

53. Robinson, G.S., "Behavior Of Concrete Under Biaxial Compression," J. Struct. Div. ASCE, vol. 93, no. ST1, February 1967.

54. Kupfer, H., Hilsdorf, H.K., Rusch, H., "Behavior Of Concrete Under Biaxial Stresses," ACI Journal, v. 66, no. 8, August 1969, pp. 656-666.

APPENDIX A

Description of the Input Sequence

To the CDC-6400 Computer Program

For the Nonlinear Analysis of

Reinforced Concrete Frames and Panels.

Program Version QBLX-141.

APPENDIX A. COMPUTER PROGRAM INPUT

Identification

A general two-dimensional structural analysis program which may be used to determine stresses and deflections in a plane reinforced concrete structure with optional plane-stress shear panels. The basic assumptions are that the frame members have rectangular sections and are symmetric about their plane of bending. Displacements and stresses are determined along frame members and over the shear panels due to the exterior live loads (lateral and vertical) and member dead loads. The live loads may be applied in various patterns and are superimposed in the sequence of their input. Hysteretic behavior for unloading is not included. The materials of the structure are described by multilinear stress-strain curves. Axial deformations are included in the frame members.

Machine Dependence

The program is written in FORTRAN IV for the CDC-6400 and uses tapes 1 and 2 for temporary storage.

Use Restrictions

In this presentation the program is restricted to the following maximum values of certain input parameters

200 nodes and 150 elements,

12 materials and 5 stress-strain curves,

5 different load patterns with no restriction on the number of increments per pattern,

50 nodes loaded in each pattern

These restrictions can be varied by suitable programming to new capacities

Input

The following sequences of punched cards define the problem to be analyzed and are described separately thus:

1. General control cards:

1.a DATA DECK LEAD CARD (6H)

Cols 1 - 6 *DATA* begins each data deck.

1.b TITLE CARD (72H)

Cols 1 - 72 title of problem.

1.c CONTROL CARD (4I5,2F10.0,1I5)

Cols 1 - 5	No. of nodes	
6 - 10	No. of elements	
11 - 15	No. of materials	
16 - 45	Leave Blank	

1.d CONTROL CARD (4I5)

Cols 1 - 5	No. of Quad materials	NQD
6 - 10	No. of Frame materials	NBD
11 - 15	No. of Rod materials	NØD
16 - 20	No. of Link materials	NLK

Material descriptions need not be in numerical sequence within each group, however the major material classifications must be in the following sequence:

first, quadrilateral elements;

second, frame elements;

third, rod and truss elements;

fourth, linkage elements.

2. Materials Descriptions:

2.a INPUT FOR QUAD MATERIALS IF NQD $\neq$ 0. Input consists of two cards per material, no. of pairs = NQD as follows:

(i) Cols 1 - 10 Material identity number

11 - 20 Mass density of the material

(ii) 1 - 10 Initial concrete modulus E_c

11 - 20 Poisson ratio nu (assumed constant)

21 - 30 Element thickness

31 - 40 Initial X-stress

41 - 50 Initial Y-stress

2.b INPUT FOR FRAME MATERIALS IF NBD $\neq$ 0. Input consists of three cards per material, no. of triples = NBD as follows:

(i) 1 - 5 Material identity number

6 - 10 No. of layers of reinforcement

11 - 20 Mass density of the main section material

(ii) 1 - 10 Initial concrete modulus E_c

11 - 20 Initial reinforcement modulus E_s

21 - 30 Beam thickness (into the plane)

31 - 40 Blank

41 - 50 % tolerance for convergence of moduli

(iii) 1 - 10 Area of bottom reinforcement

11 - 20 Area of next higher layer

21 - 30 Area of next higher layer

31 - 40 Area of uppermost layer

41 - 45 Distance to bottom reinforcement from base

46 - 50 Distance to next higher layer

51 - 55 Distance to next higher layer

56 - 60 Distance to uppermost layer

2.c INPUT FOR ROD MATERIALS IF NØD $\neq$ 0. Input consists of two cards per material, no. of pairs = NØD as follows:

(i) Cols 1 - 10 Material identity number

11 - 20 Mass density of the material

(ii) 1 - 10 Initial modulus E_s

11 - 20 Blank

21 - 30 Rod cross-section area

31 - 40 Initial axial stress

41 - 50 % tolerance for convergence of modulus

2.d INPUT FOR LINK MATERIALS IF NLK $\neq$ 0. Input consists of two cards per material, no. of pairs = NLK as follows:

(i) Cols 1 - 10 Material identity number

11 - 20 Blank

(ii) 1 - 10 Rigid stiffness value

11 - 20 Friction stiffness value

21 - 30 Link slope, degrees

31 - 40 Shear strength of link, force units

41 - 50 Tensile strength of link, force units

3. Material stress-strain relations:

In this version of the program up to 5 stress-strain relations may be input. Each group of ordinates (a 'curve') carries a code number automatically assigned by the sequence of its input in Section 3.c, i.e. the first stress-strain group is curve no. 1

(has curve code 1); the second is curve no. 2 (has curve code 2), etc. Each stress-strain curve can be associated with any of the material descriptions previously input by using these code number identities, as in Section 3.a that follows.

3.a ASSIGNMENT CARDS (3I5), one card for each of the previous materials to relate that material and any corresponding stress-strain curve which follows.

Cols 1 - 5 Previous material identity number

6 - 10 Curve code no. for Quads, Rods, Links, and main material of Frame elements

11 - 15 Curve code for Frame reinforcement

3.b CONTROL CARD (1I5)

Cols 1 - 5 No. of stress-strain curves to follow (maximum of 5)

3.c STRESS-STRAIN CURVES, one set of 4 cards corresponds to each curve to be input, no. of sets described by the previous control card.

(i) Cols 1 - 10 Stress ordinates 1, ult. tensile stress

11 - 20 " " 2

21 - 30 " " 3

31 - 40 " " 4

41 - 50 " " 5

51 - 60 " " 6

(ii) 1 - 10 " " 7

11 - 20 " " 8

21 - 30 " " 9, ult. comp. stress

(iii)	1 - 10	Strain abscissa	1,	max. tensile strain
	11 - 20	"	"	2
	21 - 30	"	"	3
	31 - 40	"	"	4
	41 - 50	"	"	5
	51 - 60	"	"	6
(iv)	1 - 10	"	"	7
	11 - 20	"	"	8
	21 - 30	"	"	9, max. comp. strain

4. NODE POINT GEOMETRY CARDS (2I5, 4F10.0). A mesh generator is included so that first and last cards of an equally spaced set will define the set, but each boundary code is automatically set to zero. The boundary codes govern the interpretation of input data for nodes as either displacements or forces. Assuming a global Cartesian coordinate system, and calling node forces R_i and node displacements V_i, then the boundary condition codes for any node give the following interpretations:

0 Assign R_x and R_y; solve for V_x and V_y.

1 Assign V_x and R_y; solve for V_y (often a vertical roller).

2 Assign V_y and R_x; solve for V_x (often a horizontal roller).

3 Assign V_x and V_y; (often a fixed node).

Node load values R_i are left zero at this stage and are actually input in Section 5 following.

Cols	1 - 5	Node number
	6 - 10	Boundary code
	11 - 20	X-coordinate

21 - 30 Y-coordinate

31 - 40 Boundary X-displacement

41 - 50 Boundary Y-displacement

5. Load Pattern Descriptions.

5.a CONTROL CARD (1I5)

Cols 1 - 5 No. of load patterns for input

5.b LOAD PATTERN DESCRIPTION. Two types per load pattern.

(i) Cols 1 - 5 Pattern identity number

6 - 10 No. of nodes involved with loads

11 - 15 No. of increments required for this pattern

(ii) A group of cards follows, one card for each node that has a loading applied to it.

1 - 5 Node number

6 - 15 X-load increment

16 - 25 Y-load increment

6. ELEMENT DESCRIPTION CARDS (7I5). One card for each element, but a mesh generator is included that accepts the first and last element of a row of equally spaced element numbers and fills in the missing elements with material codes and failure codes according to the first element listed. Failure codes are all = 1 except for Frame elements which are zero.

Cols 1 - 5 Element number

6 - 10 I-node number (put negative for Frames)

11 - 15 J-node number

16 - 20 K-node number (zero for Rods & Links)

21 - 25 L-node number (zero for Rods,
Links = -1)

26 - 30 Material type code

31 - 35 Failure status code (see above)

7. DEAD LOAD CONTROL (1I5)

Cols 1 - 5 Set = zero to exclude dead loading
Set = 1 to include dead loading

8. CONTROL CARD (6H). Required at the end of all the data sets, one card only, to indicate no further problems.

Cols 1 - 6 *STOP*